Includes Online Access to Fully Searchable Text and Images

CT and MRI of the Abdomen and Pelvis

A TEACHING FILE

THIRD EDITION

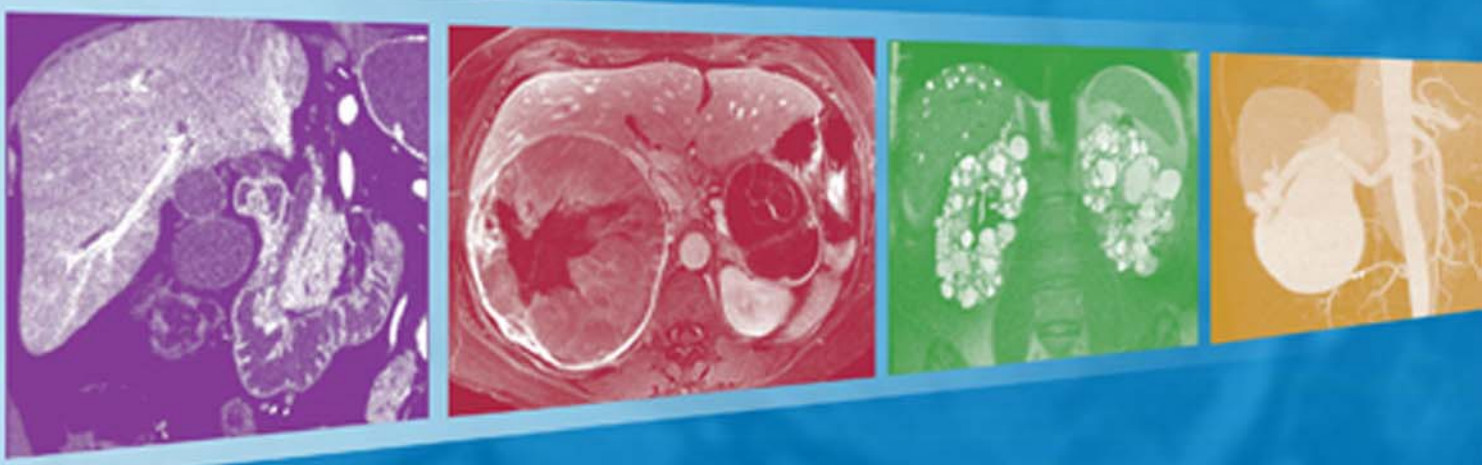

EDITORS

Pablo R. Ros

Koenraad J. Mortele

ASSOCIATE EDITORS

Vincent Pelsser

Smitha Thomas

Wolters Kluwer Health | Lippincott Williams & Wilkins

CT and MRI of the Abdomen and Pelvis

A Teaching File

THIRD EDITION

CT and MRI of the Abdomen and Pelvis

A Teaching File

THIRD EDITION

Editors

Pablo R. Ros, MD, MPH, FACR
Theodore J. Castele University
Professor and Chair
Department of Radiology
University Hospitals Case Medical Center
Case Western Reserve University
Radiologist-in-Chief
University Hospitals Health System
Cleveland, Ohio

Koenraad J. Mortele, MD
Associate Professor of Radiology
Harvard Medical School
Director, Division of Clinical MRI
Staff Radiologist, Divisions of Abdominal Imaging and Body MRI
Department of Radiology
Beth Israel Deaconess Medical Center
Boston, Massachusetts

Associate Editors

Vincent Pelsser, MD
Assistant Professor of Radiology
McGill University
Staff Radiologist
Jewish General Hospital
Montreal, Quebec, Canada

Smitha Thomas, MD
Clinical Instructor, Abdominal Imaging
University Hospitals Case Medical Center
Case Western Reserve University
Cleveland, Ohio

Wolters Kluwer Health | Lippincott Williams & Wilkins

Philadelphia • Baltimore • New York • London
Buenos Aires • Hong Kong • Sydney • Tokyo

Senior Executive Editor: Jonathan W. Pine, Jr.
Product Manager: Amy G. Dinkel
Vendor Manager: Bridgett Dougherty
Senior Manufacturing Coordinator: Beth Welsh
Senior Marketing Manager: Kimberly Schonberger
Senior Designer: Stephen Druding
Production Service: Integra Software Services Pvt. Ltd.

Two Commerce Square
2001 Market Street
Philadelphia, PA 19103 USA
LWW.com

Printed in China

Library of Congress Cataloging-in-Publication Data
CT and MRI of the abdomen and pelvis : a teaching file / editors, Pablo R. Ros, Koenraad J. Mortele; associate editors, Vincent Pelsser, Smitha Thomas. — Third edition.
p. ; cm.
Includes bibliographical references and index.
ISBN-13: 978-1-4511-1352-5
ISBN-10: 1-4511-1352-8
I. Ros, Pablo R., editor of compilation. II. Mortele, Koenraad J., editor of compilation. III. Pelsser, Vincent, editor of compilation. IV. Thomas, Smitha, editor of compilation.
[DNLM: 1. Abdomen—pathology—Atlases. 2. Diagnosis, Differential—Atlases. 3. Digestive System Diseases—diagnosis—Atlases. 4. Magnetic Resonance Imaging—Atlases. 5. Pelvis—pathology—Atlases. 6. Tomography, X-Ray Computed—Atlases. WI 17]
RC944
617.5'507548—dc23

2013030751

---

10 9 8 7 6 5 4 3 2 1

To all the residents I had the opportunity to show cases to during my career. They are the inspiration for this book.

Pablo Ros, MD

To Dejana, for her bottomless love.
To Charlotte, Christophe, Mabel and Mila—my four extraordinary children—for the joy they give me every day.
To my family and friends, for all their help and support over the years.
To my mentors, colleagues and trainees, for keeping abdominal imaging exciting and fun to practice!

Koenraad J. Mortele, MD

To my parents, Albert and Odile, for instilling in me their values.
To my brother Bernard, for his invaluable advice.
To Chantal, for her love and unconditional support.

Vincent Pelsser, MD

To Binu, Matthew, and Irene, for your support and understanding.

Smitha Thomas, MD

PUBLISHER'S FOREWORD

Teaching Files are one of the hallmarks of education in radiology. When there was a need for a comprehensive series of books to provide the resident and practicing radiologist with the kind of personal consultation with the experts normally found only in the setting of a teaching hospital, Lippincott Williams & Wilkins is proud to have created a series that answers this need.

Actual cases have been culled from extensive teaching files in major medical centers. The discussions presented mimic those performed on a daily basis between residents and faculty members in all radiology departments.

This series is designed so that each case can be studied as an unknown. A consistent format is used to present each case. A brief clinical history is given, followed by several images. Then, relevant findings, differential diagnosis, and final diagnosis are given, followed by a discussion of the case. The authors thereby guide the reader through the interpretation of each case.

This year we have made additional changes to the series. Cases have been randomized to better prepare the reader for the challenges of the clinical setting. In addition, to answer the growing demand for Web-based product, we have included more cases online, which has left us, in turn, able to offer a more cost-effective product.

We hope that this series will continue to be a trusted teaching tool for radiologists at any stage of training or practice, and that it will also be a benefit to clinicians whose patients undergo these imaging studies.

The Publisher

PREFACE TO THE THIRD EDITION

As the saying goes, the only constant in life is change. Obviously, we are delighted that the Third Edition of *CT and MRI of the Abdomen and Pelvis: A Teaching File* is seeing the light in its third incarnation.

This book, which started as a collection of interesting cases in the First Edition, became a more robust textbook in the Second Edition with 470 cases and almost 2,000 illustrations in a 500-page hard-cover volume. Fortunately, the Second Edition did well, and as with the First Edition, our publishers started to lobby for a new edition. However, as mentioned, things had changed. The changes were obvious, both in our team and in the publishing world. In the time that since the Second Edition (2007), the publishing environment has changed. Radiologists throughout the world, like any other walk of life, are living not only in the world of hard copy material but also in the world of digital and Web-based media. This is an incredibly attractive alternative for a specialty such as ours that is primarily based on images. The possibilities of Web-based publications are endless. Therefore, the Third Edition of *CT and MRI of the Abdomen and Pelvis: A Teaching File* is a hybrid publication. The hard copy version is limited to 150 cases, and it has a soft cover for better ease of transportation and immediate access for consultation. Of interest is that the 150 cases contain completely new material either with totally new cases not presented in the previous editions or with completely new and current images of well-established and classic entities. Our beloved textbook is becoming a leaner, meaner textbook.

The beauty of the hybrid approach is that the publishers have made available to all of the patrons of this Third Edition 416 cases that can be accessed on the Web.

Our team also has undergone changes. What was originally the effort of a small team of two people in the late 1990s, became a larger team for the Second Edition but still primarily based in a single center where Vincent, Koenraad, and Pablo were working in the mid-2000s. The Third Edition is now based in three different centers in two countries. Vincent returned to his native Canada and therefore his contributions are cases from McGill University in Montreal; Koenraad moved into town to the Beth Israel-Deaconess Medical Center; and Pablo moved to Case Western Reserve and therefore enlisted the help of Smitha. In short, we are delighted that the Third Edition is now a reality, despite publication and personnel changes.

This volume is faithful to its basic principles: it is composed of great clinical cases with exquisite illustrations of the highest quality. Another change from prior editions is that all the cases are now randomized and not presented by chapters following organ/system divisions.

We hope our readers will also have fun with the Third Edition of *CT and MRI of the Abdomen and Pelvis: A Teaching File* and will be infected by the enthusiasm of the authors for teaching Abdominal Imaging using a case format. We will be looking forward to receiving feedback regarding this hybrid publication combining hard copy printed material and access to hundreds of Abdominal Imaging cases on the Web.

Pablo R. Ros, MD, MPH, FACR

Koenraad J. Mortele, MD

Vincent Pelsser, MD

Smitha Thomas, MD

Although it is said that sequels rarely improve on the original movie, we hope our readers will agree that this Second Edition of our book, *CT and MRI of the Abdomen and Pelvis: A Teaching File*, is clearly better than its predecessor. The images are technically better; there is an increased number of cases illustrating more entities; it includes advanced technology, such as three-dimensional reformatted images; and it has more collaborators with specialized expertise than the First Edition.

This project started a few years ago when we kept receiving emails and verbal comments from radiologists asking if they could get a copy of the First Edition since it was out of print. Because we did not have additional copies of the book on hand, we started to think about writing a Second Edition. Because we had a professional relationship of over 10 years and understood each other very well, it was natural to decide to pool our efforts and talents to tackle this Second Edition.

We initially thought we could keep 80% of the old cases, add 20% of new ones, and update a few of the older images. Doing that would have taken only a few months. We really underestimated the amount of work to be done. Because we wanted to offer to our readers a complete, modern collection of outstanding cases, we ended up adding many more cases, changing almost all of the images, and making this Second Edition a more robust and complete teaching atlas. We selected the best possible cases out of our daily practice at the Brigham and Women's Hospital and Dana-Farber Cancer Institute in Boston, Massachusetts, and put them in an unknown case format, as we would present them in our routine case conferences. We also tried to incorporate cases that one of us has had the chance to see during our visits to other departments, particularly the Armed Forces Institute of Pathology in Washington, DC, and the University Hospital in Ghent, Belgium, or received in consultation from the United States and abroad. We have kept the best material from the First Edition because we realized that some cases were so unique that we could not replace them.

At the end, we had trouble limiting the number of cases we wanted to include from our pool and staying within the space allowed by this single volume. We enjoyed meeting weekly with Vincent and

trying to convince each other to include "just one more case" in a particular section, constantly updating differential diagnoses and making sure we had the best and most updated discussions and references for each case.

The structure of the book is similar to the First Edition. We have divided the cases according to the traditional abdominal sections: Liver and Biliary System; Pancreas; Gastrointestinal Tract; Spleen; Mesentery, Omentum, and Peritoneum; Kidney, Ureter, and Bladder; Pelvis; Retroperitoneum and Adrenal Glands; and Abdominal Wall. For each case, after a brief history, up to four images follow, which by definition are CT and/or MRI. A brief description of the findings, the differential diagnosis, the final diagnosis, and a short discussion complete the case. This format allows the readers to take these cases as unknowns, thereby simulating the daily clinical practice of a radiologist.

We hope our readers will have fun with the Second Edition of *CT and MRI of the Abdomen and Pelvis: A Teaching File* and sense the enthusiasm of the authors for teaching abdominal imaging using a case format. If our readers gain even a small nugget of additional knowledge, we will feel satisfied that the educational goal of this book has been achieved.

Pablo R. Ros, MD, MPH, FACR

Koenraad J. Mortele, MD

PREFACE TO THE FIRST EDITION

This book is the fruit of our collaboration that spans at least 6 years, when both of us were in the Department of Radiology at the University of Florida College of Medicine, Gainesville. Although the point of view of one of us (Sly) changed from medical student to radiology resident, fellow, and finally attending, we tried to duplicate the experience of reviewing interesting cases presented in the Abdominal Imaging divisional conferences, in "hot seat" sessions for the senior residents, and most importantly, in daily read-out sessions.

Our goal was to select the "best in show" material out of an archive of over 5,000 teaching file cases and put it in book format. The Abdominal Imaging teaching file at the University of Florida College of Medicine contains primarily cases that have been performed at Shands Hospital at the University of Florida and also cases originating from the Armed Forces Institute of Pathology, Washington, DC. It also includes cases collected in visiting professorships in the United States and Canada, as well as other countries in Europe, Central and South America, and Asia, cases that have been presented in film-reading panels in national and international meetings, and cases that have been brought by visitors to the department. All cases entered into the teaching file have to be proven by either surgery, biopsy, laboratory data, or clinical and/or radiologic follow-up. Cases with an obvious pathognomonic imaging diagnosis (e.g., pneumoperitoneum) are also included. From this pool, we selected the best ones and divided them into chapters according to the traditional abdominal sections: liver and biliary tree, pancreas, spleen, gastrointestinal tract, kidney, retroperitoneum and adrenal, mesentery and omentum, and pelvis. We also added a chapter called "Unknowns and Aunt Minnies," which contains a potpourri of cases with a short differential diagnosis.

The format for each case is the same. A brief clinical history is followed by two to four images, which by definition are either computed tomography, magnetic resonance imaging scans, or a combination of both. Then, pertinent findings, differential diagnosis, final diagnosis, and a brief discussion follow.

This format is designed so that cases can be taken as unknowns. A simple piece of paper will cover the entire information given on each case. If the reader wants to know the findings or the differential diagnosis before knowing the final diagnosis, this can be easily accomplished by removing the paper.

To make this book reflect real life, we took actual cases from an extensive teaching file and recreated the discussions performed on a daily basis in hundreds of departments of radiology between residents and faculty members. We duplicated our discussions at the viewbox, emphasizing a practical approach. The cases in each chapter are not presented with traditional divisions (congenital, inflammatory, neoplastic, vascular, etc.), but are all mixed up, again mimicking real life. The end result, we hope, is that radiologists at any stage in their training or careers will benefit from reading this book.

We had fun selecting the cases, going over differential diagnosis lists, and trying to summarize a pertinent discussion for each case. We hope the reader will also enjoy going over them and learning more about diseases of the abdomen and pelvis using computed tomography and magnetic resonance imaging as diagnostic tools.

Pablo R. Ros, MD, MPH, FACR

Sylvester Lee, MD

ACKNOWLEDGMENTS

The Publication of any book is possible with the efforts of many contributors. The same happened with this Third Edition of our book.

Like in prior editions, we like to acknowledge the residents, fellows, and supporting staff of the division of Abdominal Imaging at Case Western reserve University/University Hospitals Case Medical Center and the Divisions of Body MRI and Abdominal Imaging of Beth Israel/Deaconess Medical Center/Harvard Medical School. All of our trainees and support staff directly and indirectly contributed to this book by either donating cases, presenting differential diagnosis when the cases were originally read, or producing the images that now constitute this volume. We also wish to extend our gratitude to many clinical colleagues around the world who also provided cases.

A special thanks goes to the staff of Wolters Kluwer-Lippincott Williams and Wilkins. Without the help of Jonathan Pine, Sarah Granlund, Amy Dinkel, and Jeffrey Gunning, this edition would not have come to fruition.

Special appreciation also goes to our Administrative and Executive Assistants, Molly McGinnis and Marianne Chaloupek from University Hospitals Case Medical Center, and Lois Gilden from Beth Israel Deaconess Medical Center who helped us prepare and send materials to the publisher and also made our days go smoothly so we could dedicate time to the preparations of the materials.

Pablo R. Ros, MD, MPH, FACR

Koenraad J. Mortele, MD

Vincent Pelsser, MD

Smitha Thomas, MD

CASE 1

CLINICAL HISTORY *28-year-old man presenting with persistently elevated liver function tests post-ERCP for stone extraction.*

FIGURE 1A

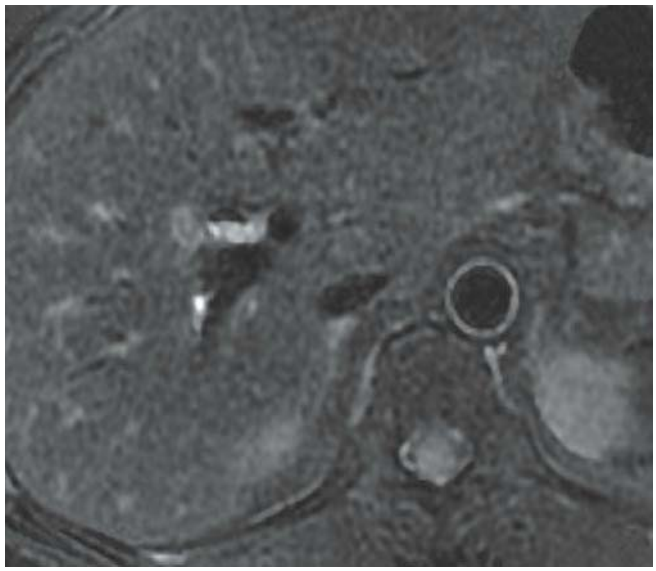

FIGURE 1B

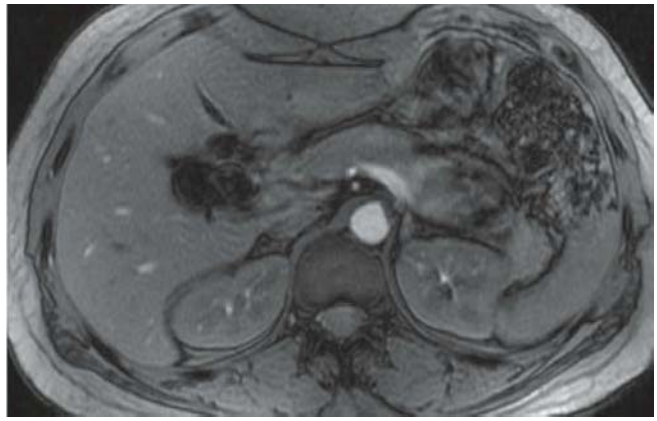

FIGURE 1C

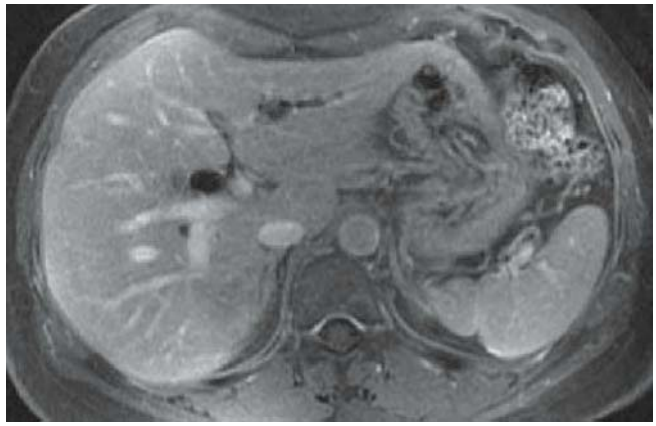

FIGURE 1D

FINDINGS Thick-slab MRCP image (A) demonstrates absence of fluid signal in the common hepatic duct (CHD) and apparent strictures of left-sided intrahepatic bile ducts. Note the mild bile duct dilatation. Axial fat-suppressed T2-WI (B) shows nondependent dark signal in the CHD with dependent layering fluid. Out-of-phase T1-WI (C) and gadolinium-enhanced, fat-suppressed axial T1-WI (D) demonstrate a larger signal "void" in the central bile ducts and in the intrahepatic ducts.

DIFFERENTIAL DIAGNOSIS Retained stones, flow artifact.

DIAGNOSIS Pneumobilia.

DISCUSSION Pneumobilia or gas in the bile ducts is usually the result of a previous ERCP or choledocho-enteric anastomosis. Rare causes include fistulas with bowel due to stone disease, or from tumor eroding into bowel. As gas is less dense than fluid, it forms a nondependent layer above the fluid in the bile ducts, and during an MRI examination, it will shift preferentially in the left-sided intrahepatic bile ducts, as they are the most nondependent ducts in the supine position. On the gradient echo sequences with longer echo times, due to magnetic susceptibility, gas tends cause blooming artifacts and may even obscure residual bile signal, as seen in this case. Other causes of filling defect in the bile ducts are stones, but these are usually in the extrahepatic ducts, and will be dependent as they are denser than bile. Flow artifact can also be seen in the extrahepatic bile ducts, in the form of a dark signal, but this signal is centrally located and entirely surrounded by fluid signal, allowing distinction from a true filling defect.

CASE 2

CLINICAL HISTORY *22-year-old female presenting with fever.*

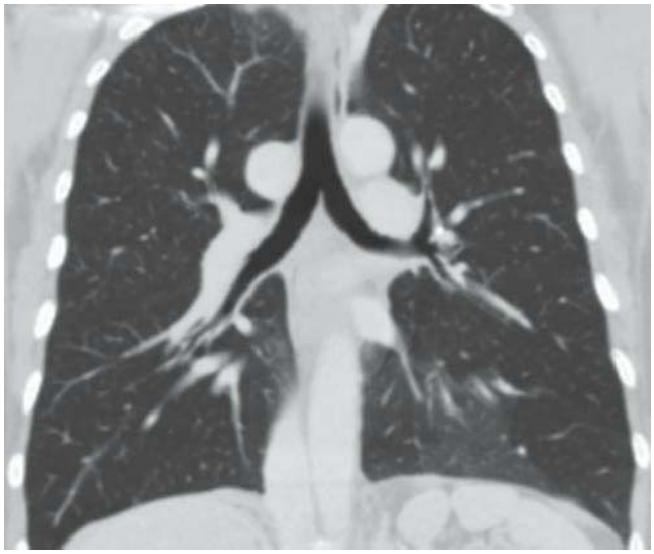

FIGURE 2A

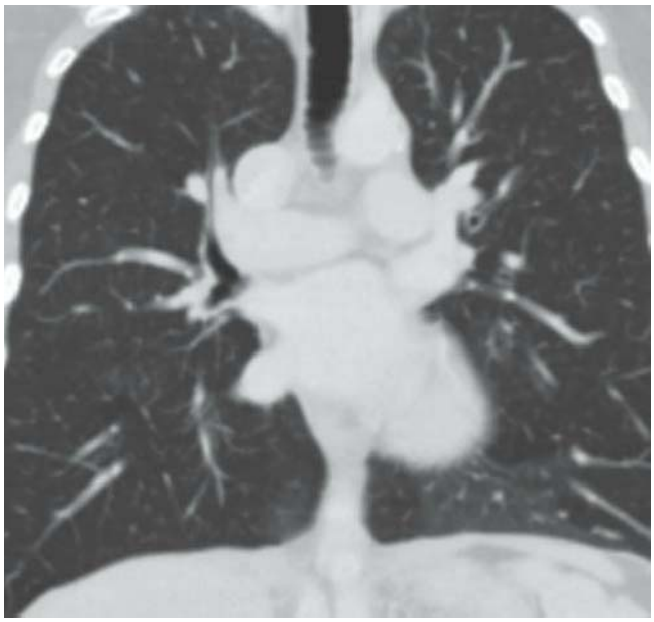

FIGURE 2B

FIGURE 2C

FIGURE 2D

FINDINGS Coronal (A and B) CECT images of the lung demonstrates hypoarterial branching pattern of bilateral bronchi and bilobar lungs. Axial CECT images (C and D) demonstrate centrally located liver and stomach, polysplenia and interrupted IVC with azygous continuation.

DIFFERENTIAL DIAGNOSIS None.

DIAGNOSIS Heterotaxy syndrome.

DISCUSSION Heterotaxy is defined as an abnormality where the internal thoracoabdominal organs demonstrate abnormal arrangement across the left–right axis of the body. They can be divided into two subgroups: asplenia syndrome and polysplenia syndrome. Polysplenia is more common in females. In general, cardiac anomalies are less common in this subgroup. The critical structures evaluated with imaging in determining situs include position of atria, position of venous drainage below the diaphragm, position of liver and gallbladder, presence, appearance, and number of spleen, and presence of bi- or trilobed lungs. Malrotation of the bowel is a frequent finding in heterotaxy syndrome. The common findings in polysplenia syndrome include bilateral bilobar lungs and IVC interruption. The spleen or spleens are always on the same side of the stomach, typically along the greater curvature. The splenic function may be abnormal and patients can even present with biliary atresia. The mortality rate in the first year of life is about 60% in polysplenia and 85% in asplenia syndrome.

CASE 3

CLINICAL HISTORY *64-year-old man presenting with left lower quadrant pain.*

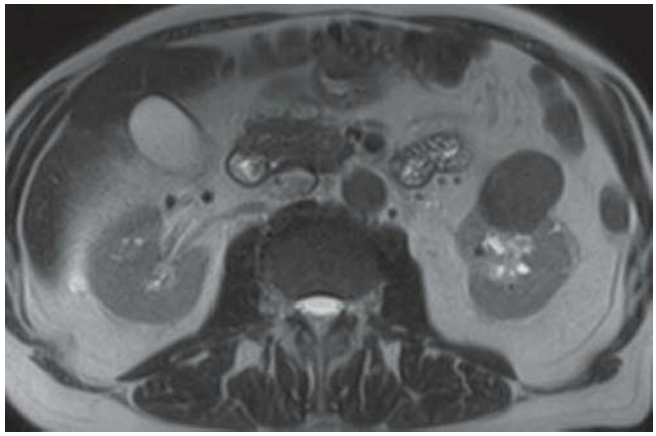

FIGURE 3A

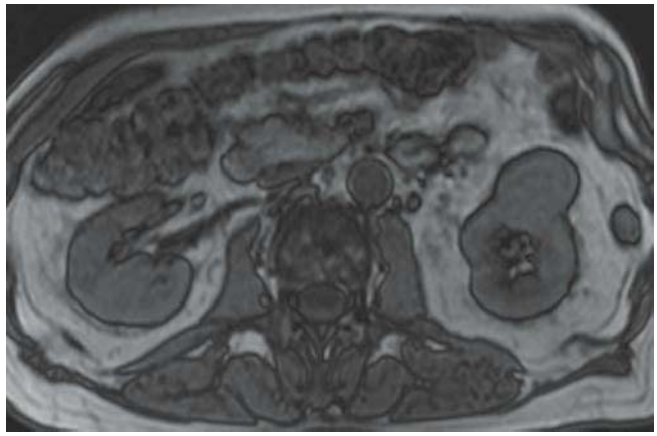

FIGURE 3C

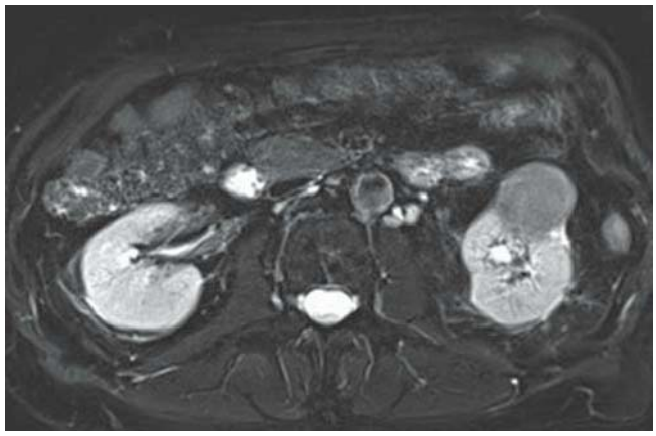

FIGURE 3B

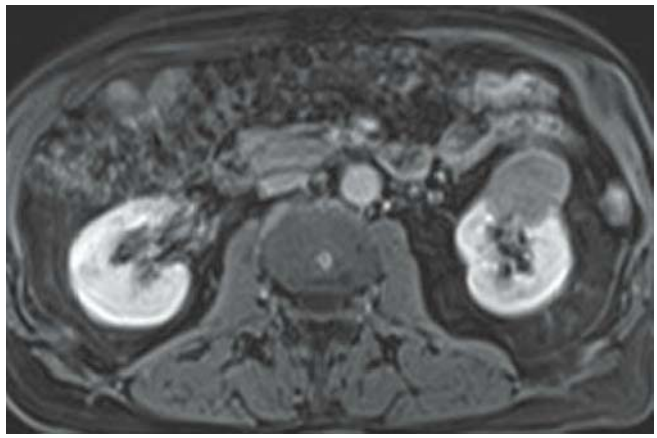

FIGURE 3D

FINDINGS Axial T2-WI (A) and fat-suppressed T2-WI (B) show a 3.5-cm hypointense exophytic renal mass. It is isointense to the renal cortex on the out-of-phase T1-WI (C). Gadolinium-enhanced, fat-suppressed axial T1-WI (D) shows only mild enhancement of the mass.

DIFFERENTIAL DIAGNOSIS Clear cell renal carcinoma, angiomyolipoma with minimal fat, oncocytoma.

DIAGNOSIS Papillary renal cell carcinoma.

DISCUSSION Papillary renal carcinoma is the second most common (15% to 20%) pathologic subtype of primary renal neoplasm, clear cell (conventional) being the most common (70%). The 5-year survival rate is also much better with the papillary subtype (80% to 90%) when compared to the conventional type (55% to 60%). Although papillary renal cell cancer may be hyperdense on NECT, the attenuation value of the mass on NECT is not a reliable differentiating factor. However, on CECT, papillary renal carcinoma enhances less than the clear cell subtype. Tumors that enhance more than 84 HU in the corticomedullary phase are more likely to be of the clear cell variant. Papillary renal carcinomas are considered hypovascular, as seen in this case. Calcifications in a renal mass are also more common in the papillary variant (32%), than in the conventional type (11%). On T2-WI, the signal intensity of the papillary subtype tends to be less than that of the renal parenchyma. On the gadolinium-enhanced gradient echo sequence, the papillary tumors may appear hypointense, as seen in this case, likely due to artifacts caused by hemosiderin within the mass. This subtype of renal cell carcinoma can be suggested based on imaging characteristics, but histologic confirmation is often needed to differentiate the lesion for an angiomyolipoma with minimal fat or an oncocytoma. Both may be hyperdense on NECT and hypointense on T2-WI, but are expected to enhance more vividly following contrast administration.

Case images courtesy of Dr. Dejana Radulovic, St-Boniface Hospital, University of Manitoba, Winnipeg, Canada.

CASE 4

CLINICAL HISTORY *46-year-old woman presenting with acute right upper quadrant pain and fever.*

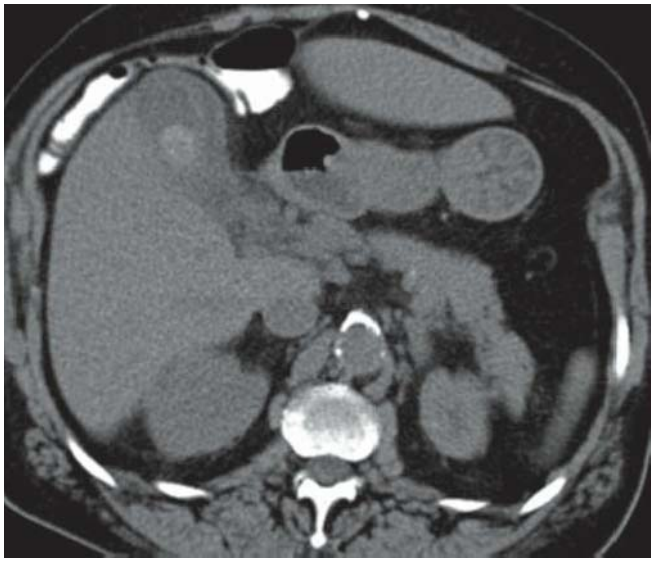

FIGURE 4A

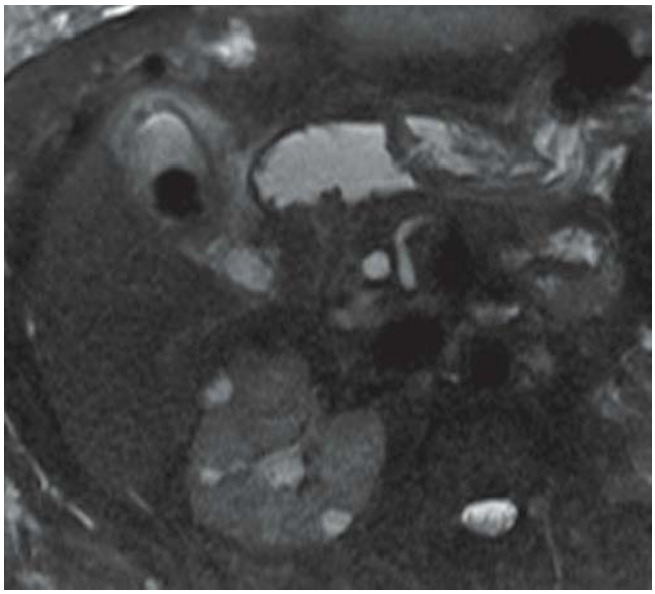

FIGURE 4C

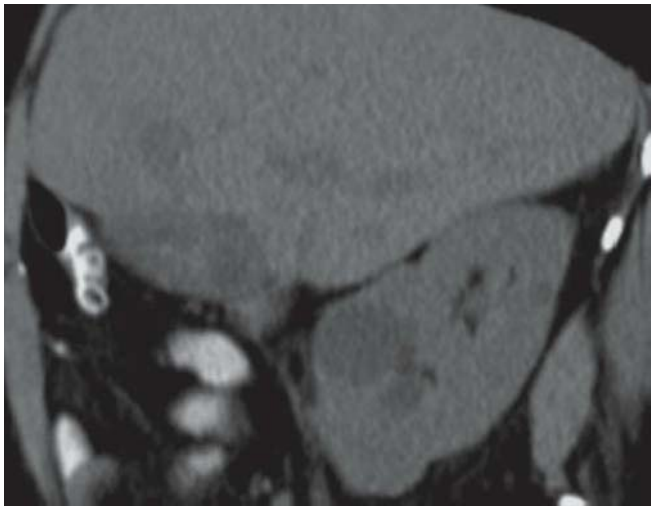

FIGURE 4B

FIGURE 4D

FINDINGS Axial CECT (A) and axial T2-weighted MRI (C) demonstrate the dilated gallbladder, thickened gallbladder wall, pericholecystic fat stranding, and a large gallstone. Reformatted sagittal CECT image (B) demonstrates an ill-defined hypodensity adjacent to the gall bladder, which could represent an abscess. Post-gadolinium reformatted sagittal image (D) indicates the presence of tract between the collection and the gallbladder.

DIFFERENTIAL DIAGNOSIS None.

DIAGNOSIS Acute cholecystitis with gallbladder perforation and abscess formation.

DISCUSSION Acute cholecystitis is the fourth most common cause of hospital admissions for patients with acute abdomen pain. It typically results from obstruction of the cystic duct or gallbladder (GB) neck due to cholelithiasis with resulting inflammation of the gallbladder wall. Acute cholecystitis is caused by gallstones in most patients, with acalculous cholecystitis occurring in approximately 5% to

10%. In a patient with suspected acute cholecystitis, ultrasonography is typically the imaging procedure of choice. The typical CT findings in acute cholecystitis include gallstones, gallbladder distention (>5 cm in anteroposterior diameter), mural thickening (>3 mm), pericholecystic fluid, poor definition of the gallbladder wall at the interface with the liver, inflammatory stranding in the pericholecystic fat, and hyperemia of the adjacent liver parenchyma. Of all these findings, the presence of pericholecystic inflammatory change is assumed to be the most specific because other findings, such as gallbladder wall thickening and distention, do not necessarily indicate cholecystitis. The complications of acute cholecystitis include massive dilation of the gallbladder, rupture, and abscess formation as in this case. This case also illustrates the important role of MRI in evaluating complications of cholecystitis.

CASE 5

CLINICAL HISTORY *32-year-old man with a history of ulcerative colitis presenting with increased liver function tests.*

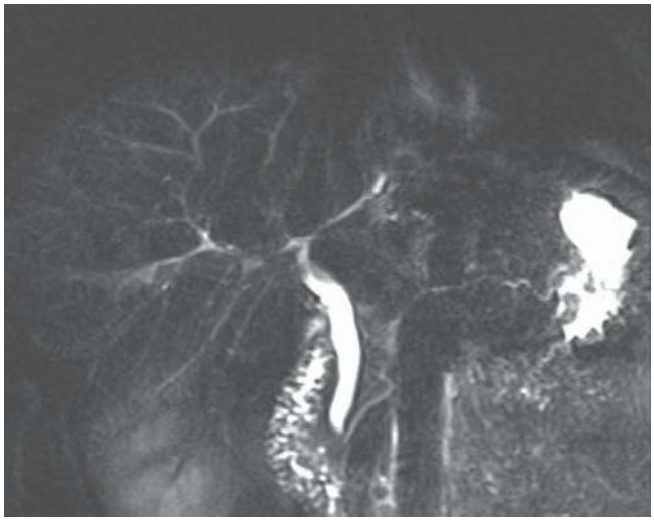

FIGURE 5A

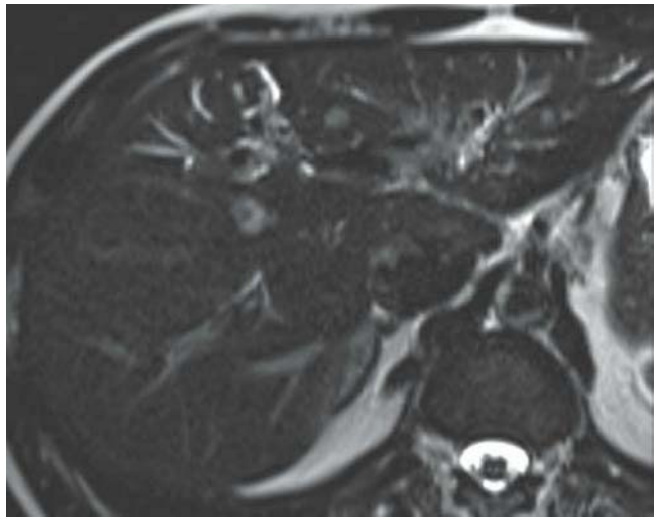

FIGURE 5C

FIGURE 5B

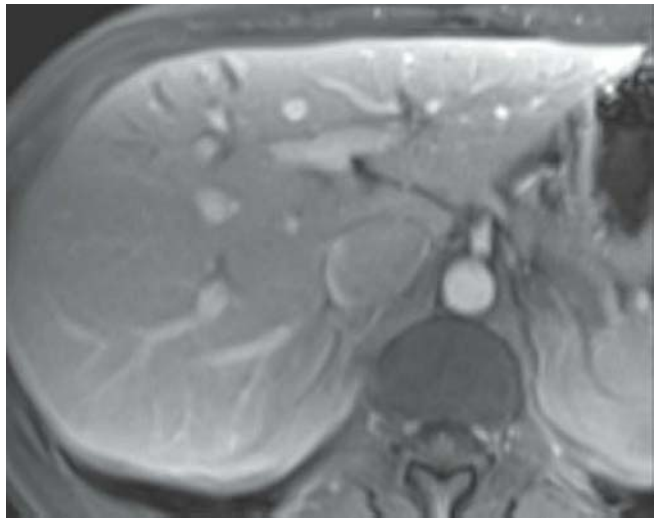

FIGURE 5D

FINDINGS Thick-slab MRCP images (A and B) demonstrate alternating strictures-narrowing and dilatation of the intrahepatic and upstream extrahepatic bile ducts. Heavily weighted axial T2-WI (C) and gadolinium-enhanced, fat-suppressed axial T1-WI (D) demonstrate focally dilated peripheral intrahepatic bile ducts without abnormal enhancement.

DIFFERENTIAL DIAGNOSIS Recurrent pyogenic cholangitis (oriental cholangiohepatitis), acute cholangitis.

DIAGNOSIS Primary sclerosing cholangitis (PSC).

DISCUSSION Primary sclerosing cholangitis is an autoimmune disorder characterized by obliterative fibrotic inflammation of the bile ducts that eventually leads to cholestasis, and biliary cirrhosis. It usually presents in patients younger than 40 years and is more common in males. Typically, intra- and extrahepatic bile ducts are involved simultaneously (80%). A strong association with inflammatory bowel disease, especially ulcerative colitis, is noted (70%). Although patients may be asymptomatic, 75% have progressive fatigue, intermittent obstructive jaundice, and pruritus. On MRI, the characteristic appearance of the disease is multiple stenoses, minor dilatations (because of the periductal fibrosis), and beaded appearance of the bile ducts. In patients with cirrhosis, associated imaging findings, such as splenomegaly, confluent hepatic fibrosis, and especially caudate lobe hypertrophy, are present. On MRCP, by using heavily T2-WI sequences, the signal of static or slow-moving fluid-filled structures, such as the bile ducts, is greatly increased, resulting in increased duct-to-background contrast and confidence in diagnosis.

CASE 6

CLINICAL HISTORY *50-year-old woman presenting with pulmonary embolism.*

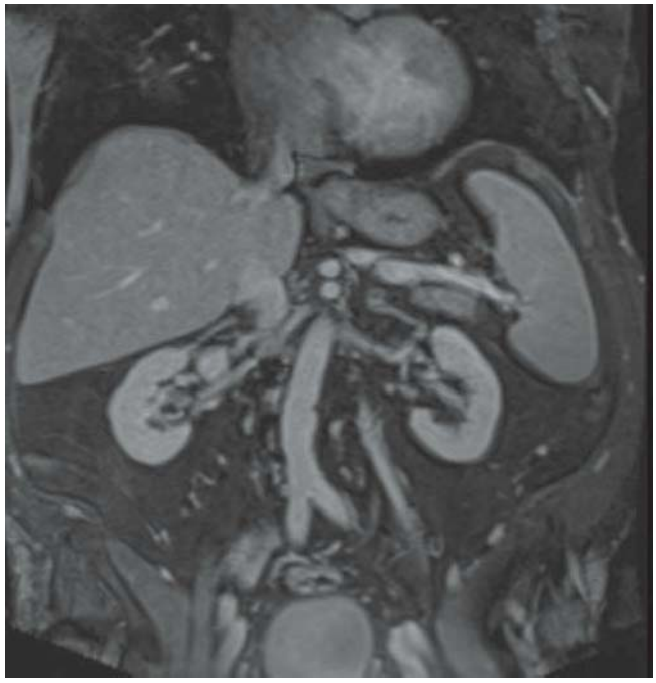

FIGURE 6A

FIGURE 6C

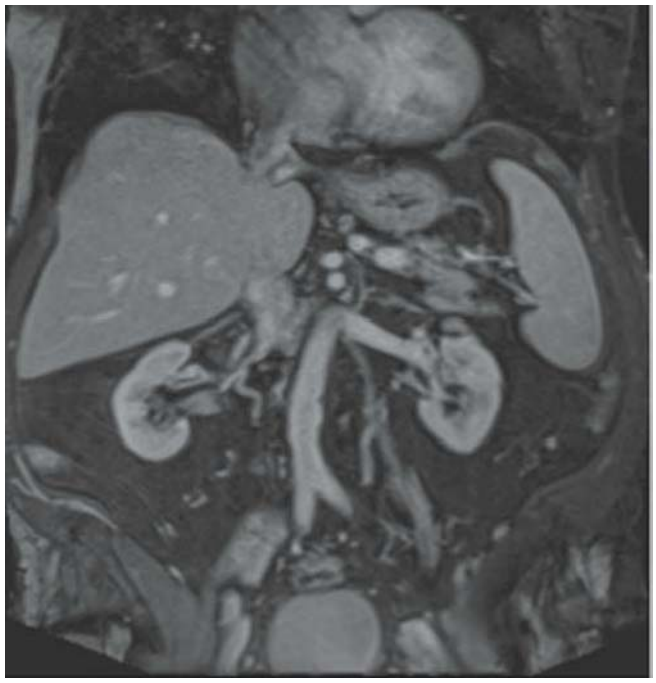

FIGURE 6B

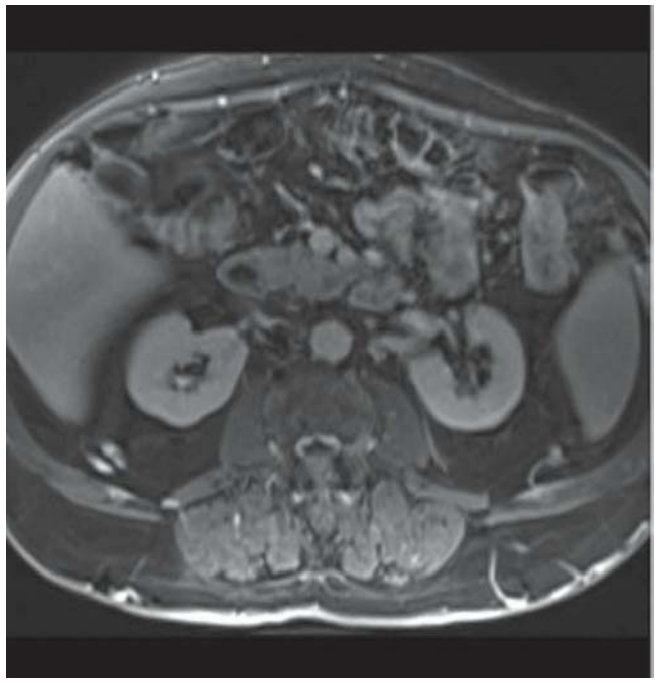

FIGURE 6D

FINDINGS Coronal post-gadolinium MRI sequences (A–C) through the retroperitoneum demonstrate the confluence of bilateral common iliac veins to form the IVC in the lower abdomen. The IVC is not visualized in the mid-abdomen and is reconstituted by multiple collateral vessels as depicted on axial sequence (D). There is reformation of the suprarenal IVC by the collaterals.

DIFFERENTIAL DIAGNOSIS IVC tumor.

DIAGNOSIS IVC thrombosis.

DISCUSSION Predisposing factors for thrombus formation include alterations in blood flow (stasis), injury to the vascular endothelium, and abnormalities in the constitution

of blood hypercoagulability (Virchow's Triad). Endothelial damage is invariably an acquired phenomenon whereas hypercoagulability may result from both congenital and acquired risk factors (especially in the perioperative period). The classical presentation of IVC thrombus varies according to the level of the thrombosis with up to 50% of patients presenting with bilateral lower extremity swelling and dilatation of superficial abdominal vessels. Duplex ultrasound scanning has become an accurate noninvasive method of diagnosing IVC thrombosis, but is operator dependent and can be limited by body habitus or the presence of bowel gas CT imaging is a rapid noninvasive method which can accurately diagnose and assess the extent of thrombus as well as delineate any associated abdominal or pelvic abnormality. MRI is now replacing CT as the optimal investigative tool avoiding radiation and giving more accurate delineation of thrombus as well as any IVC anomaly. MRI is also used to follow-up patients to determine morphologic changes in the thrombus following therapy.

CASE 7

CLINICAL HISTORY *45-year-old man presenting with acute left lower quadrant pain.*

FIGURE 7A

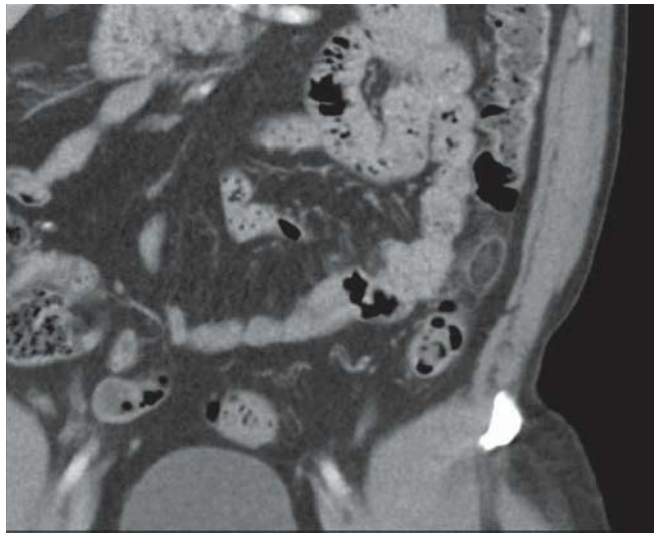

FIGURE 7C

FIGURE 7B

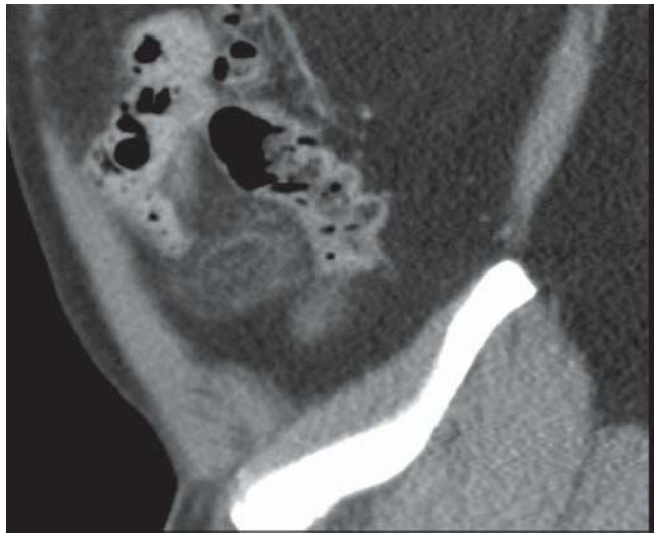

FIGURE 7D

FINDINGS Axial (A and B), coronal reformatted (C), and sagittal reformatted (D) CECT images demonstrate a fat-containing lesion on the anti-mesenteric side of the distal descending colon, with a hyperdense surrounding rim and adjacent fat stranding. A central hyperdense dot (B) is present. The adjacent colonic wall is not thickened.

DIFFERENTIAL DIAGNOSIS Omental infarct, acute diverticulitis, liposarcoma.

DIAGNOSIS Epiploic appendagitis.

DISCUSSION Epiploic appendages are fat-containing outpouchings arising from the anti-mesenteric side of the colon. They can measure up to 5 cm. Acute inflammation of one of them, called epiploic appendagitis, results either from torsion or venous occlusion. Patients present acutely with abdominal pain. Classically, appendagitis occurs either in the sigmoid or descending colon, but can be found in any colonic segment. The lesion has a central fatty core, with a surrounding hyperdense rim and a central dot representing the occluded central vessel. This central dot is only seen in 54% of cases, however. The adjacent colonic wall is rarely thickened; this is a useful differentiating factor as the colonic wall is almost invariably thickened in acute diverticulitis. A hyperdense rim is also not seen in cases of omental torsion, which excludes this diagnosis. Liposarcomas are exceedingly rare intraperitoneally and occur in the retroperitoneum. The imaging findings typically resolve completely after 6 months.

CASE 8

CLINICAL HISTORY *46-year-old man presenting with abdominal pain and constipation.*

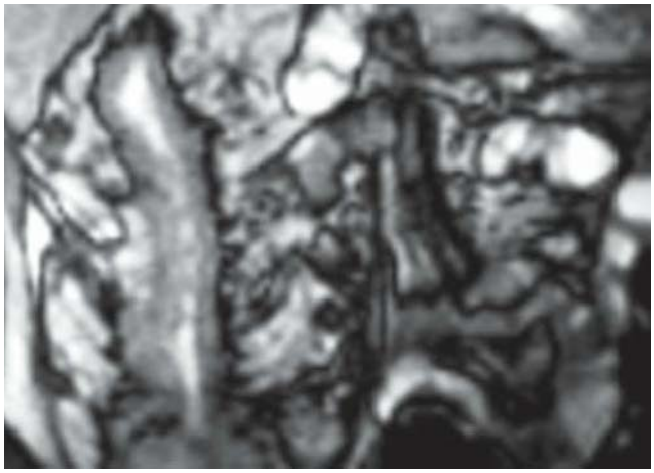

FIGURE 8A

FIGURE 8B

FIGURE 8C

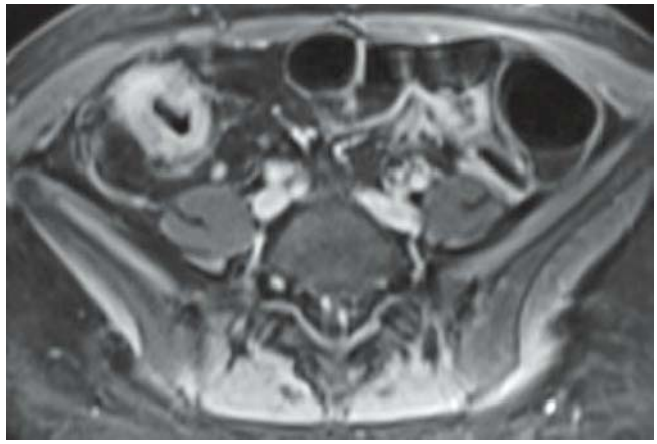

FIGURE 8D

FINDINGS Coronal T2-weighted MRI (A) demonstrates diffuse segmental wall thickening of the ascending colon. There is a small focal area of narrowing involving the mid-ascending colon. There is increased fat proliferation within the right pericolic region. Post-gadolinium sagittal (B) and coronal (C) sequences demonstrate diffuse mural enhancement. Note the relative sparing of the left hemicolon. There is thickening of the ileocecal valve and terminal ileum. An additional small bowel segment is involved on the left. Axial post-gadolinium sequences (D) demonstrate the concentric mural thickening and pericolonic fat stranding.

DIFFERENTIAL DIAGNOSIS Ulcerative colitis, pseudomembranous colitis.

DIAGNOSIS Crohn colitis.

DISCUSSION Crohn disease is of unknown etiology and characterized by transmural inflammation in a discontinuous fashion (skip lesions) usually involving the terminal ileum. Involvement of the colon and terminal ileum is seen in approximately 40% to 45% of patients, and colonic involvement alone is seen in 30% of patients. Complications include fistula and abscess formation and adenocarcinoma. Changes of Crohn colitis include aphthous ulcers, thickening of the bowel wall, deep ulcers, rigidity of the bowel wall, and a "cobblestone" appearance of the mucosa. The cobblestone appearance is due to linear ulcers separated by areas of edematous mucosa. Finally, there is stricture formation of the bowel. "Creeping fat" represents fibrofatty proliferation typically seen in patients with Crohn disease, as demonstrated in this case. It is thought to occur as a response to repeated episodes of inflammation resulting in separation of loops of bowel; it is most frequently seen in the small bowel mesentery but can occur in the colon as well. Pseudomembranous colitis typically involves the entire colon, and there is a greater degree of bowel wall thickening. Ulcerative colitis begins in the rectum, progresses proximally without skip lesions, and does not involve the terminal ileum.

CASE 9

CLINICAL HISTORY *32-year-old woman presenting with acute recurrent pancreatitis.*

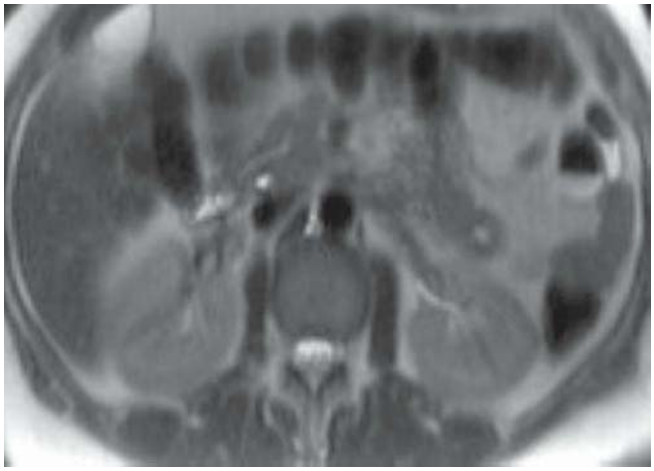

FIGURE 9A

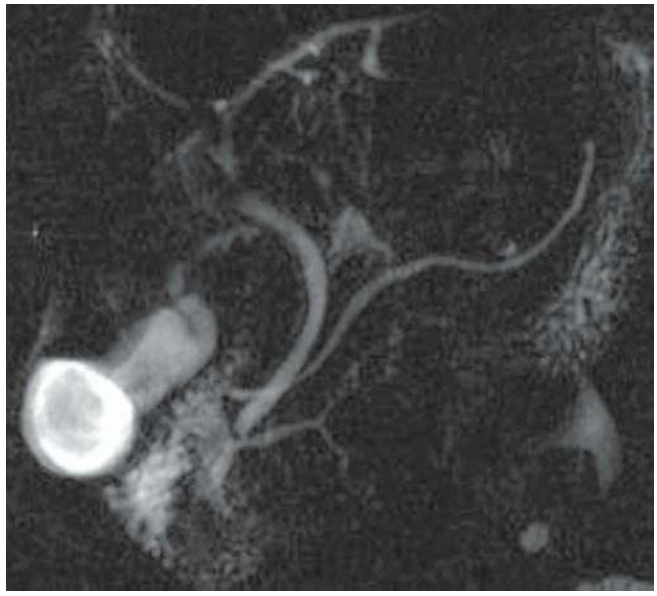

FIGURE 9B

FINDINGS Axial T2-WI (A) at the level of the pancreatic head shows drainage of the pancreatic duct in the minor papilla and drainage of the CBD through the major papilla. Projective coronal oblique thick-slab MRCP image (B) shows the lack of fusion between the main pancreatic duct and the duct of Wirsung (ventral duct). Note that the main pancreatic duct drains via the duct of Santorini into the minor papilla.

DIFFERENTIAL DIAGNOSIS Dorsal dominant duct syndrome.

DIAGNOSIS Pancreas divisum.

DISCUSSION Pancreas divisum (PD) is the most common congenital anomaly of the pancreatic ductal system, being reported in 4% to 10% of the population. This anomaly results when the ventral and dorsal pancreatic ducts fail to fuse. The ventral duct (duct of Wirsung) drains only into the ventral pancreatic anlage, while the majority of the gland empties into the minor papilla through the dorsal duct or duct of Santorini. Focal dilatation of the terminal portion of the dorsal duct, coined santorinicele, is described in association with PD and relative obstruction at the minor papilla. PD usually causes no symptoms, but it is found more frequently in patients with chronic abdominal pain and idiopathic pancreatitis than in the general population. The definitive diagnosis of PD is made with endoscopic retrograde pancreatography (ERP). MRCP has been shown to be highly sensitive and specific for depicting PD. MRCP with secretin stimulation helps in identifying PD and santorinicele. In dorsal dominant duct syndrome, the majority of the gland drains through the dorsal duct, but there is still a connection with the duct of Wirsung.

CASE 10

CLINICAL HISTORY *30-year-old man with acute lymphocytic leukemia presenting with fever after bone marrow transplantation.*

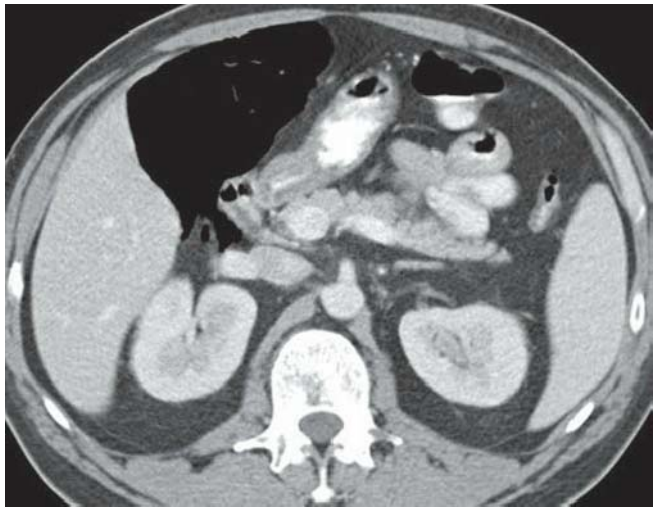

FIGURE 10A

FIGURE 10C

FIGURE 10B

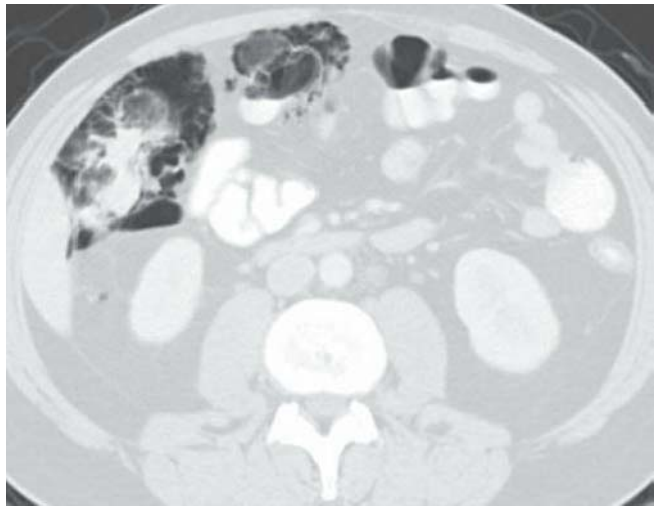

FIGURE 10D

FINDINGS Axial CECT images displayed in soft tissue (A and C) and lung (B and D) windows demonstrate extensive accumulation of air in the colonic wall at the level of the hepatic flexure.

DIFFERENTIAL DIAGNOSIS Pneumatosis intestinalis due to ischemia, pneumatosis cystoides.

DIAGNOSIS Benign colonic pneumatosis due to mucosal denudation (chemotherapy effect).

DISCUSSION It is generally accepted that bowel ischemia and bowel infarction are the most common causes of pneumatosis and that this constellation is associated with a bad prognosis and a high mortality rate. However, pneumatosis may occur in certain nonischemic conditions as well, where it is not automatically associated with an unfavorable outcome. The pathogenesis of pneumatosis following intestinal mucosal injury is obvious since mucosal and submucosal bowel wall damage may allow some intraluminal air to enter the damaged or dissected bowel wall; therefore, it is not surprising that pneumatosis may be associated with bone marrow transplantation, where it may be related, at least partially, to GI mucosal damage caused by the chemotherapeutic agents themselves. Pneumatosis has also been reported to occur secondary to diverticulitis, graft-versus-host disease, ulcerative colitis, Crohn disease, and gastric and colon cancers. Pneumatosis cystoides intestinalis, also known as primary pneumatosis, is characterized by bubble-like gas collections along the bowel wall and only involves the colon.

CASE 11

CLINICAL HISTORY *63-year-old man presenting with abdominal mass.*

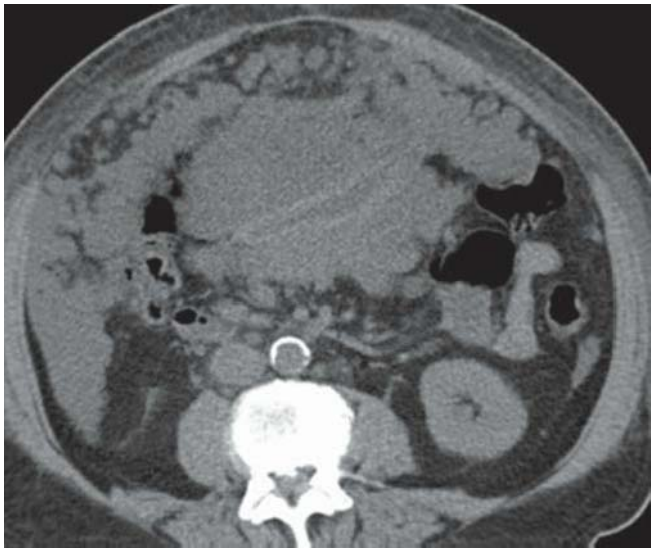

FIGURE 11A

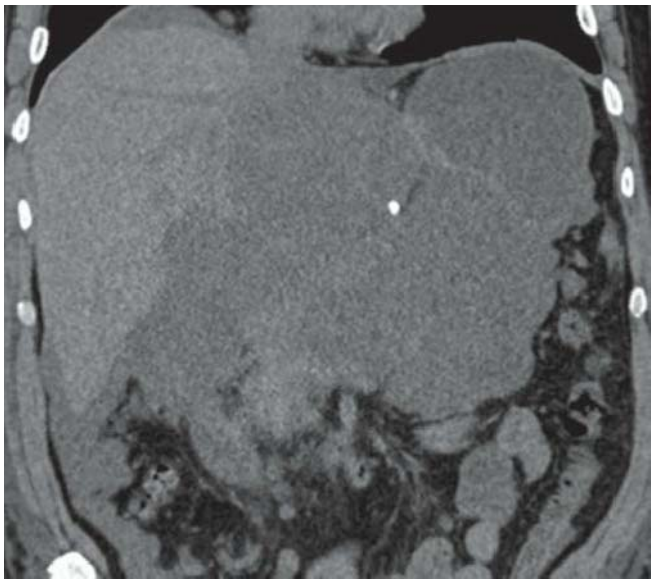

FIGURE 11B

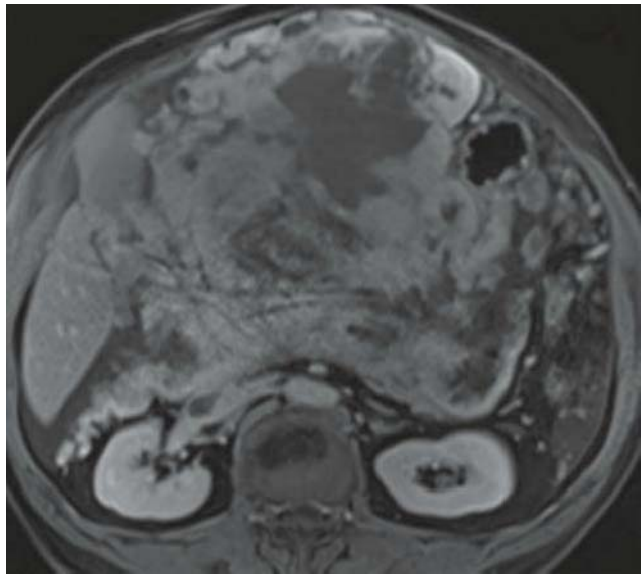

FIGURE 11C

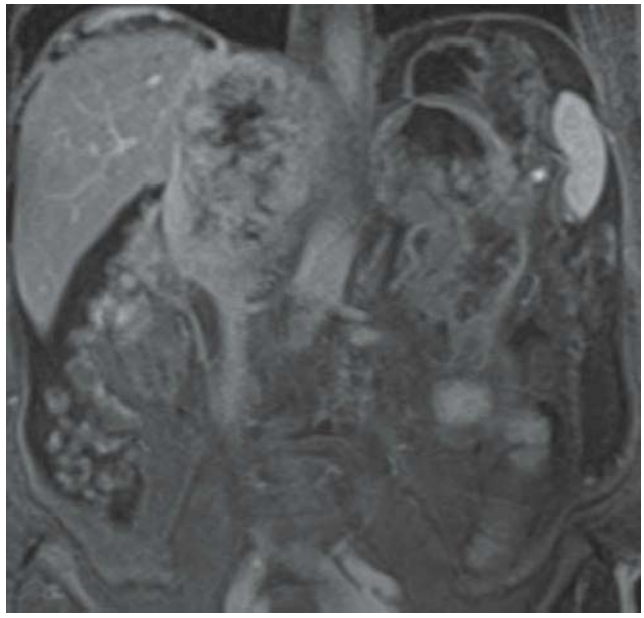

FIGURE 11D

FINDINGS Axial (A) and coronal NECT images (B) demonstrate large confluent omental and mesenteric masses. Nodular thickening of peritoneal surfaces and ascites are also noted. Post-gadolinium axial (C) and coronal (D) T1-WI demonstrate heterogeneous contrast enhancement of the omental mass with central necrosis. There is encasement of the mesenteric vessels and adherent small bowel loops.

DIFFERENTIAL DIAGNOSIS Tuberculosis, mesothelioma, lymphoma.

DIAGNOSIS Peritoneal and metastatic "omental caking" in a patient with colon cancer.

DISCUSSION Omental caking is a term used to describe peritoneal metastases or other processes, such as tuberculosis, that replace the normal fat of the greater omentum. The greater omentum extends caudally from the transverse colon and is located just deep to the anterior abdominal wall. Metastases in this fat plane can thicken or replace the fatty density of the omentum with soft tissue density mass as seen in this case. The most common primary neoplasms presenting with peritoneal metastases include GI tract and ovarian malignancies. Other entities that can simulate peritoneal metastases are lymphoma, tuberculosis, and mesothelioma. Image-guided biopsy can easily be performed through the anterior abdominal wall, if necessary.

CASE 12

CLINICAL HISTORY *40-year-old woman presenting with menometrorrhagia and dysmenorrhea.*

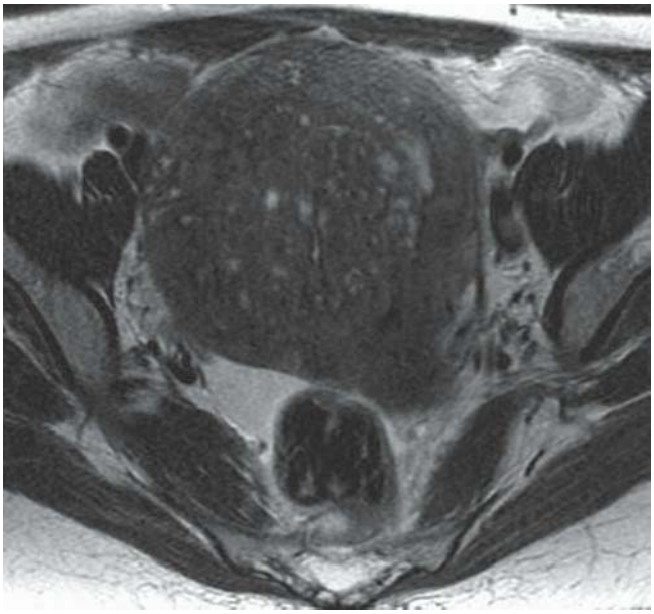

FIGURE 12A

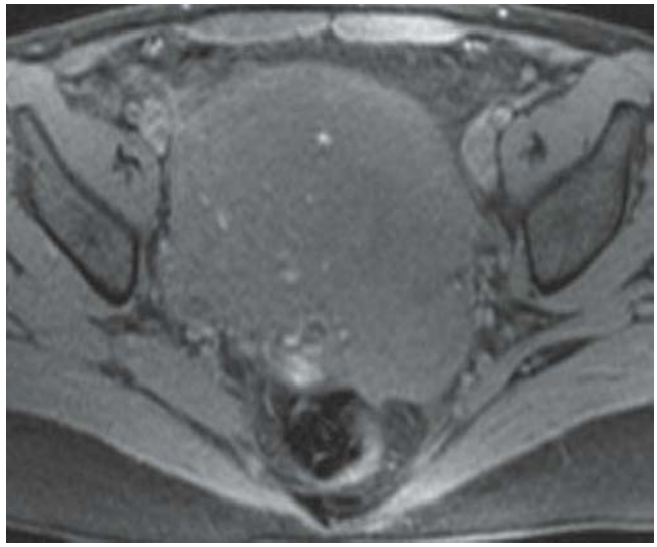

FIGURE 12C

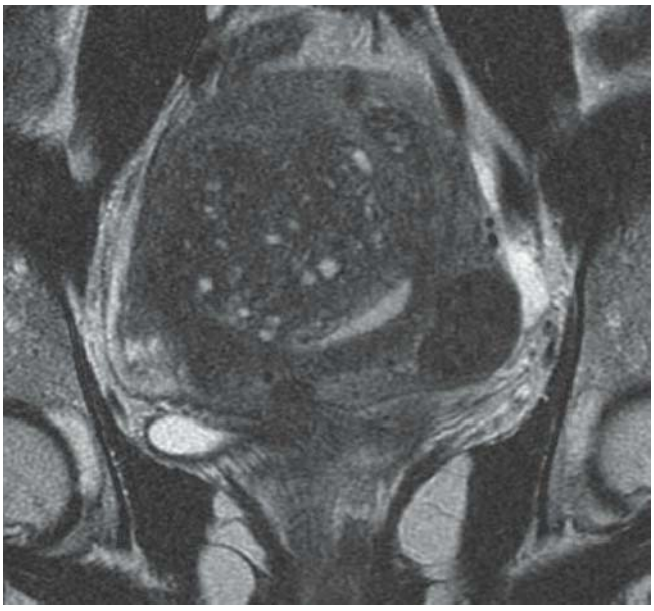

FIGURE 12B

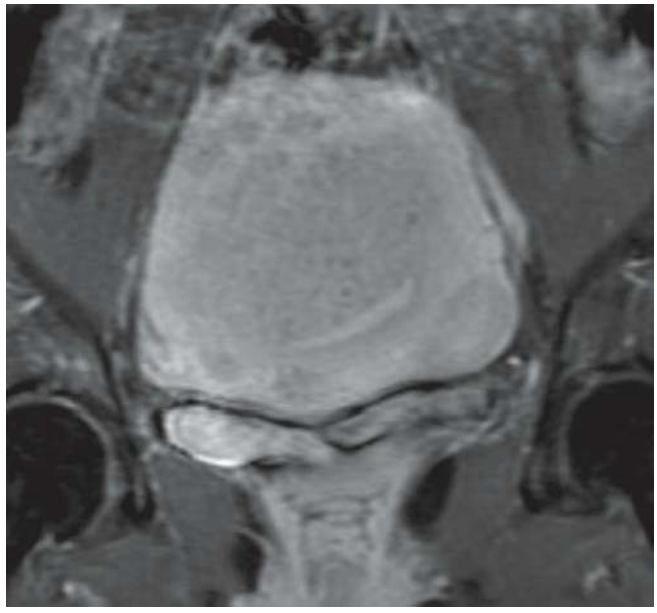

FIGURE 12D

FINDINGS Axial (A) and coronal (B) T2-WIs, fat-suppressed axial T1-WI (C), and gadolinium-enhanced, fat-suppressed axial T1-WI (D) demonstrate an ill-defined, Swiss cheese-like (hyperintense foci on T1-WI and T2-WI) mass in the uterine wall with loss of the zonal anatomy; the mass shows moderate enhancement compared to the normal myometrium. Note also two well-delineated T2 hypointense, T1 isointense, subserosal minimally enhancing nodules.

DIFFERENTIAL DIAGNOSIS Myometrial contraction, muscular hypertrophy.

DIAGNOSIS Adenomyosis and two uterine leiomyomas.

DISCUSSION Adenomyosis is due to the presence of ectopic endometrial glands and stroma within the myometrium, often accompanied by myometrial hyperplasia. It affects

women during their reproductive and perimenopausal years (40 to 60 years old). Symptoms include pelvic pain, menorrhagia, and dysmenorrhea. Two morphologic forms are described: diffuse and, less frequently, local adenomyosis (so-called adenomyoma). Due to the predominance of endometrial zona basilaris, which is relatively refractive to the cyclic hormonal changes, adenomyosis does not typically undergo bleeding. MRI features characteristic for adenomyosis are focal or diffuse widening (>12 mm) of the low-signal-intensity junctional zone, ill-defined margins, normal aspect of the endometrium, and high-signal-intensity foci on T1-WI or T2-WI within a T2-WI hypointense mass (due to associated smooth muscle hyperplasia). The hyperintense foci represent small areas of hemorrhage, ectopic endometrium, and/or cystically dilated endometrial glands. Differentiation with diffuse muscular hypertrophy can be challenging; muscular hypertrophy also causes widening of the junctional zone, although milder, and is well defined compared to diffuse adenomyosis.

CASE 13

CLINICAL HISTORY *43-year-old man presenting with pain and jaundice.*

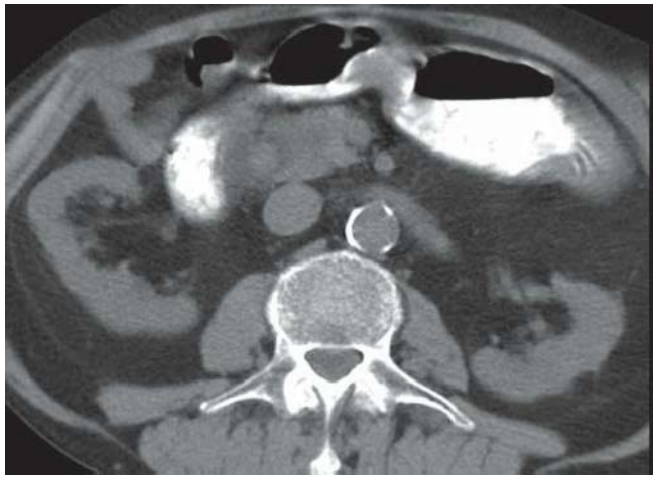

FIGURE 13A

FIGURE 13C

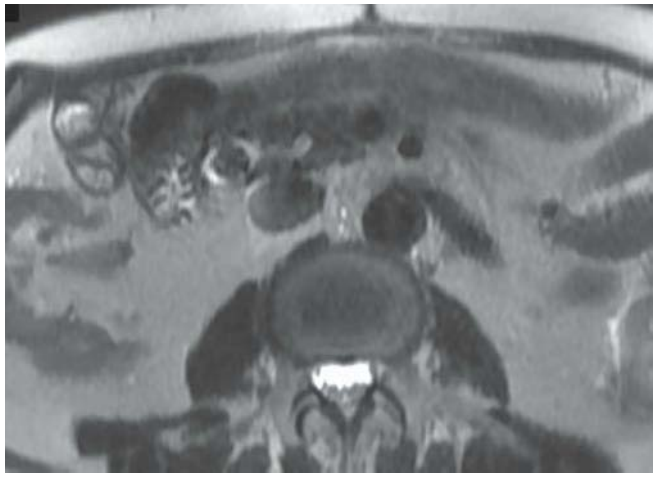

FIGURE 13B

FIGURE 13D

FINDINGS Axial NECT image (A) demonstrates a rounded density surrounded by fluid between the pancreatic head and the second duodenum. Axial T2-WI (B) shows the abnormality has dark signal. Thin- (C) and thick- (D) slab MRCP images show the filling defect is in the distal CBD, with moderate upstream bile duct dilation.

DIFFERENTIAL DIAGNOSIS Blood clot, cholangiocarcinoma, pneumobilia.

DIAGNOSIS Choledocholithiasis.

DISCUSSION Gallstones in the common bile duct are the most common cause of biliary obstruction. They are found in approximately 15% of patients undergoing cholecystectomy; they typically result from the migration of the gallbladder into the CBD. Clinical symptoms include right upper quadrant pain, obstructive jaundice, and fever (in the presence of ascending cholangitis). MRI is highly accurate in the detection of common bile duct stones, with a reported accuracy up to 97%. CBD stones are typically hypointense on both T1- and T2-WIs and surrounded by bile. On axial images, the stone is typically located in a dependent position in the duct. This position differentiates CBD stones from pneumobilia (filling defect in the nondependent position) and bile flow artifacts (typically central in location). MRCP is the imaging test of choice to evaluate patients who have a low to moderate probability of having a CBD stone. In patients with a high probability, ERCP is recommended as the latter technique allows immediate therapeutic intervention.

CASE 14

CLINICAL HISTORY *47-year-old man known to have chronic pancreatitis presenting with upper abdominal pain.*

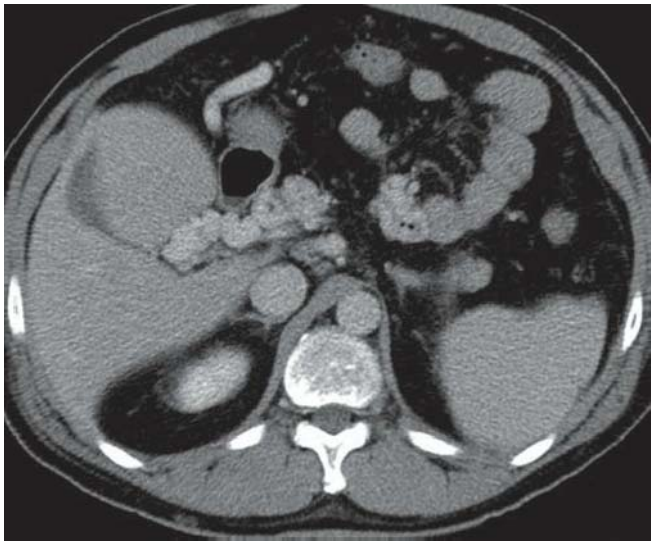

FIGURE 14A

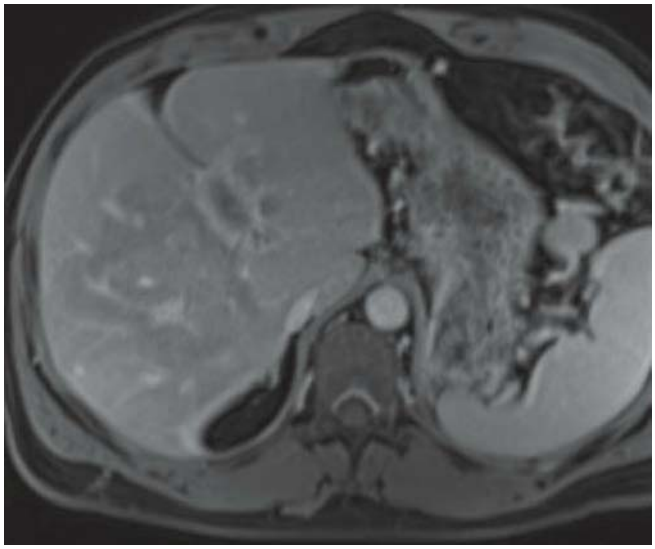

FIGURE 14C

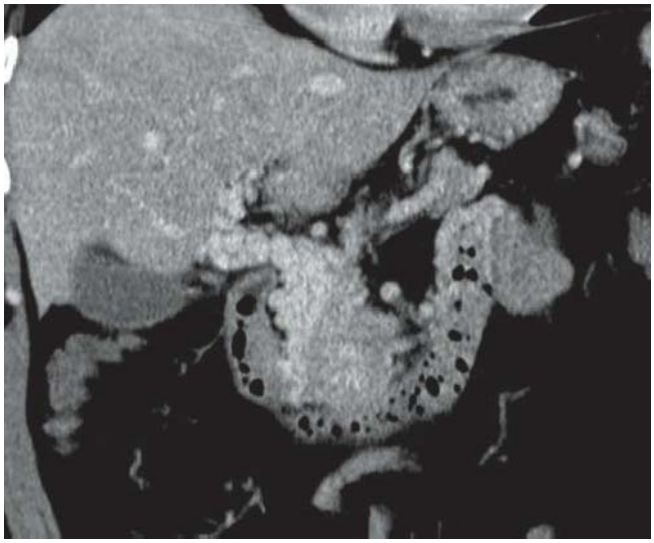

FIGURE 14B

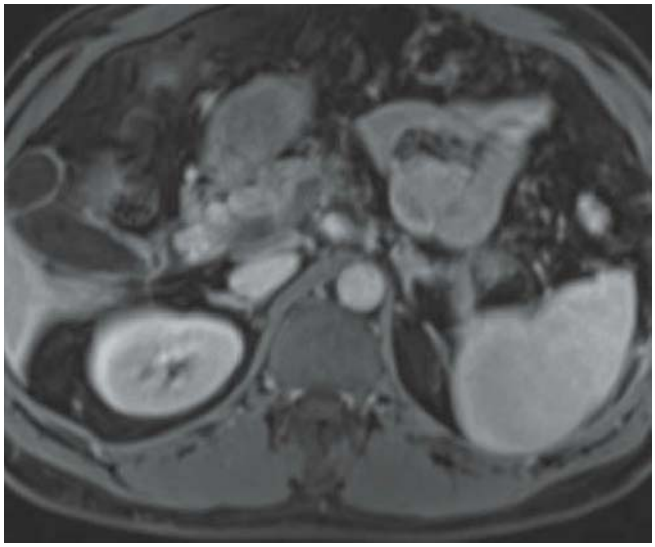

FIGURE 14D

FINDINGS Axial (A) and coronal reformatted (B) CECT images demonstrate serpiginous vessels along the expected course of the extrahepatic bile ducts. Gadolinium-enhanced, fat-suppressed axial T1-WI shows thrombus in the left portal vein branch (C) and pericholedochal varices (D).

DIFFERENTIAL DIAGNOSIS Extrahepatic cholangiocarcinoma, perihilar lymphadenopathy.

DIAGNOSIS Cavernous transformation of the portal vein with pericholedochal varices.

DISCUSSION Portal vein thrombosis can be secondary to multiple causes including malignancies (HCC, cholangiocarcinoma, metastases, pancreatic neoplasms), trauma, hematologic disorders, pancreatitis, and thrombophlebitis from sepsis, diverticulitis, or appendicitis. In up to 50% of the cases, however, the etiology is unknown. Portal vein thrombosis can either be intrahepatic or extrahepatic with cirrhosis being the most common cause for intrahepatic thrombosis. Cavernous transformation of the portal vein is the formation of multiple periportal or intramural collaterals in the expected location of the portal vein. This can often alter the enhancement pattern of the liver because of compensatory arterial blood flow to the liver. The collateral vessels are thought to represent the hypertrophic vasa vasorum in the wall of the portal vein rather than true recanalization of the thrombosed portal vein. Other collateral vessels can often extend to the wall of the gallbladder and bile ducts, as seen in this example.

CASE 15

CLINICAL HISTORY *48-year-old man presenting with pulmonary nodule.*

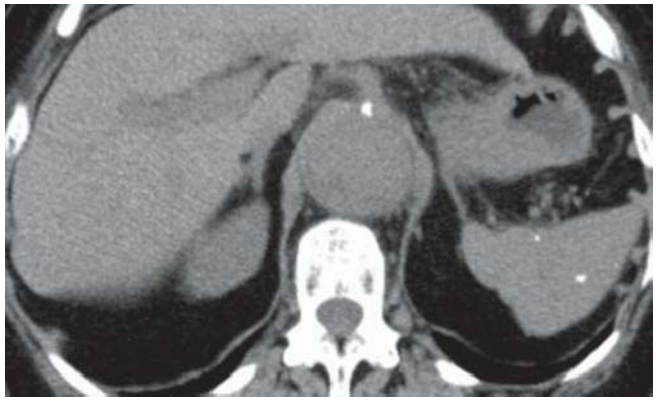

FIGURE 15A

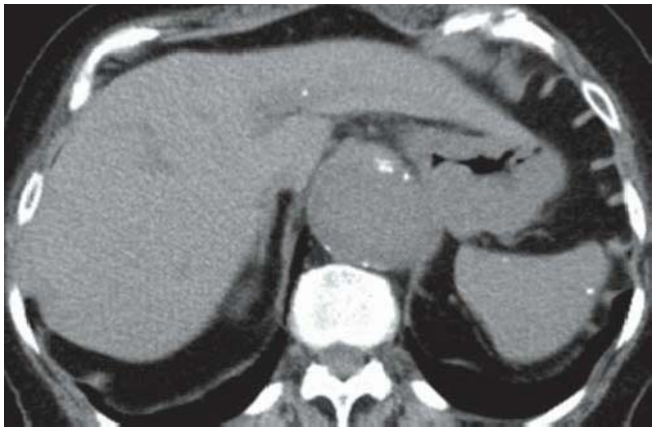

FIGURE 15B

FIGURE 15C

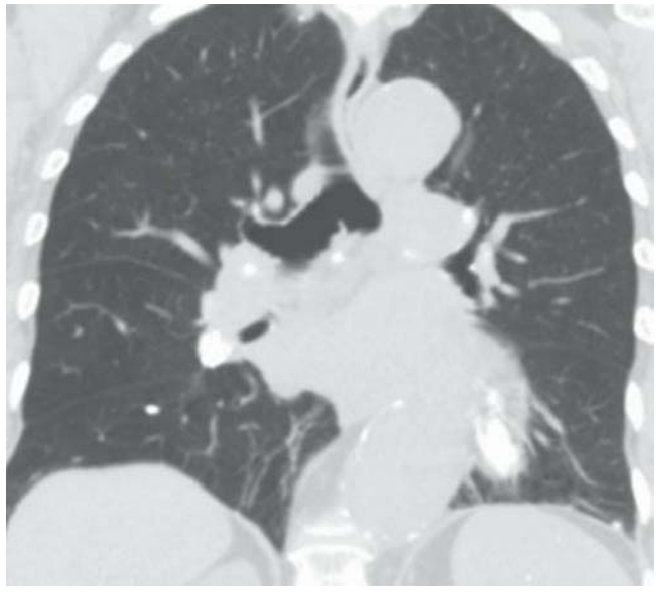

FIGURE 15D

FINDINGS Axial NECT (A and B) images demonstrate multiple calcifications of varying sizes in the spleen and liver. The spleen and liver are within normal limits of size. Coronal reformatted (C and D) images in mediastinal and lung windows, respectively, demonstrate mediastinal and hilar calcified lymphadenopathy and calcified pulmonary nodules. Incidental finding is of an aortic aneurysm.

DIFFERENTIAL DIAGNOSIS Tuberculosis, treated fungal micro abscesses.

DIAGNOSIS Splenic histoplasmosis.

DISCUSSION The central United States is an area where histoplasmosis is endemic. Since the onset of the AIDS epidemic, disseminated *Histoplasma capsulatum* infection has been reported with much greater frequency in both endemic and nonendemic areas. Most cases of histoplasmosis are associated with enlargement of mediastinal lymph nodes, which can calcify as in this case and cause mediastinal obstructive symptoms. Abdominal CT findings in patients with disseminated histoplasmosis include hepatomegaly (63%), splenomegaly (38%), diffuse splenic hypoattenuation (19%), bilateral adrenal enlargement, and enlarged lymph nodes (44%). Healed *Histoplasma capsulatum* infection is the most common cause of diffuse splenic calcification in the United States. Other causes of multiple splenic calcifications are healed tuberculosis, brucellosis, or *Pneumocystis* infections, hemangiomas, phleboliths, hemosiderosis, sickle cell anemia, and Gamna-Gandy bodies.

CASE 16

CLINICAL HISTORY *48-year-old man presenting with rectal bleeding.*

FIGURE 16A

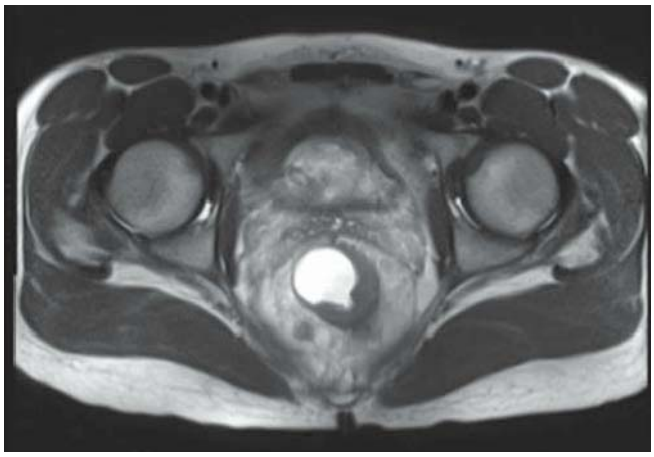

FIGURE 16B

FIGURE 16C

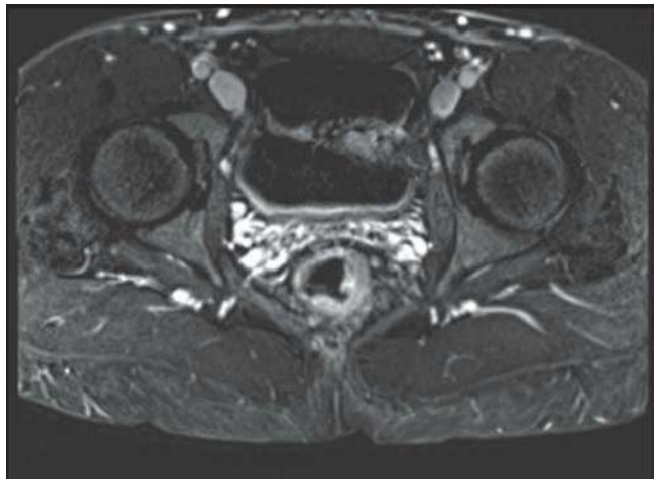

FIGURE 16D

FINDINGS Axial CECT (A) images demonstrate a large circumferential mass in the rectum. A 1-cm perirectal lymph node is seen to the right. The rectal lumen appears to be slightly narrowed. Axial (B) and sagittal (C) T2-WI demonstrate the rectal mass to be more focal involving the posterior and left lateral walls. The post-gadolinium fat-suppressed axial image (D) demonstrates the perirectal invasion and enhancing perirectal lymph node.

DIFFERENTIAL DIAGNOSIS Lymphoma, metastasis, ulcerative colitis.

DIAGNOSIS Adenocarcinoma of the rectum.

DISCUSSION Colon cancer is the most common malignancy of the GI tract. More than 50% of the cases occur in the rectosigmoid. Metastases to the liver via the portal venous system occur in lesions located in the proximal two-thirds of the rectum. The lesions in the distal one-third of the rectum metastasize to the lung via the hemorrhoidal plexus. Rectosigmoid lesions demonstrate spread to lymph nodes in the mesorectal fat, inferior mesenteric chains, external iliac chain, and para-aortic chain. CT is good at detecting gross extension of the tumor outside the colonic wall, but microscopic invasion is often missed. The size of the lesion (>1 cm) and extension outside the wall into the mesorectal fat suggest malignancy. These lesions can present as annular constricting, polypoid, or infiltrating. The most common lesion is the annular constricting lesion. The lumen is almost obliterated by the tumor. Both lymphoma and metastases could have this appearance, although they much less commonly involve the rectum. Ulcerative colitis does not produce localized bowel wall thickening with mesorectal extension, as seen in this case.

CASE 17

CLINICAL HISTORY *35-year-old man presenting with right adrenal mass.*

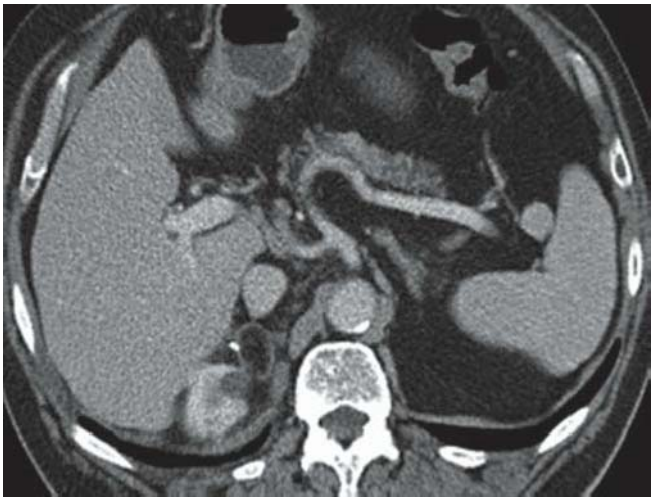

FIGURE 17A

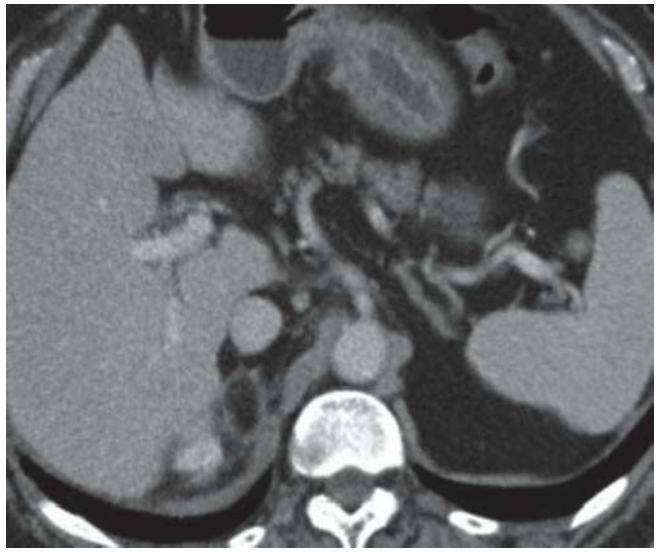

FIGURE 17C

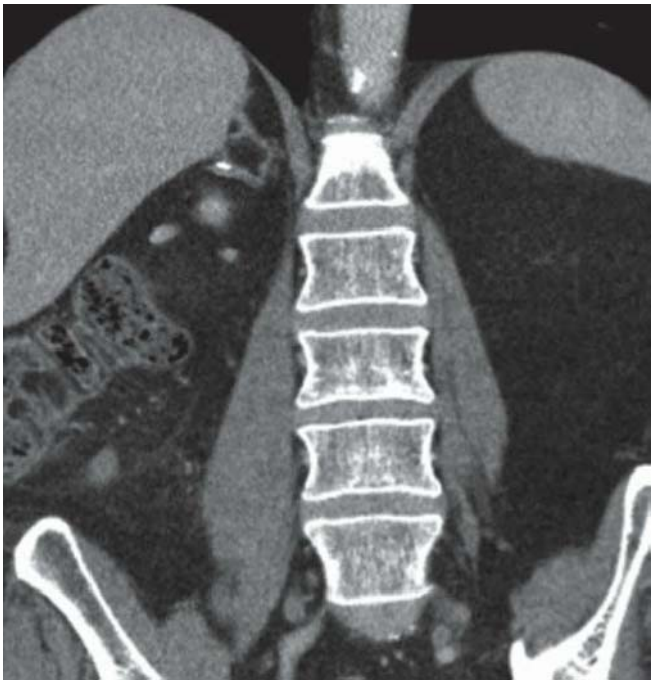

FIGURE 17B

FIGURE 17D

FINDINGS Axial CECT (A and C), coronal (B), and sagittal (D) images demonstrate a 2.0-cm fat attenuation lesion with a peripheral rim of soft tissue attenuation in the posterior aspect of the right adrenal gland. A small focus of peripheral calcification is seen in the lateral aspect of the lesion.

DIFFERENTIAL DIAGNOSIS Liposarcoma, teratoma.

DIAGNOSIS Adrenal myelolipoma.

DISCUSSION Myelolipoma is a benign tumor arising from the adrenal cortex. It is composed of mature fat and cells similar to those found in the bone marrow, such as myelocytes, megakaryocytes, erythrocytes, and lymphocytes. Myelolipomas are typically asymptomatic and found

incidentally on imaging. Adrenal myelolipomas can have a variable amount of fat present within the lesion. The presence of fat in an adrenal lesion is diagnostic of a myelolipoma. Myelolipomas can also hemorrhage and calcify, which can give the lesion a heterogeneous appearance. This can mimic other adrenal masses, such as adrenal carcinomas and metastases. CT is useful in detecting myelolipomas due to the characteristic low density of fat present in the mass. With MRI, fat-suppression sequences can be used to identify fat within an adrenal lesion. Adrenal liposarcomas and teratomas are other fat-containing adrenal tumors, but they are exceedingly rare.

CASE 18

CLINICAL HISTORY *79-year-old woman presenting with right upper quadrant pain.*

FIGURE 18A

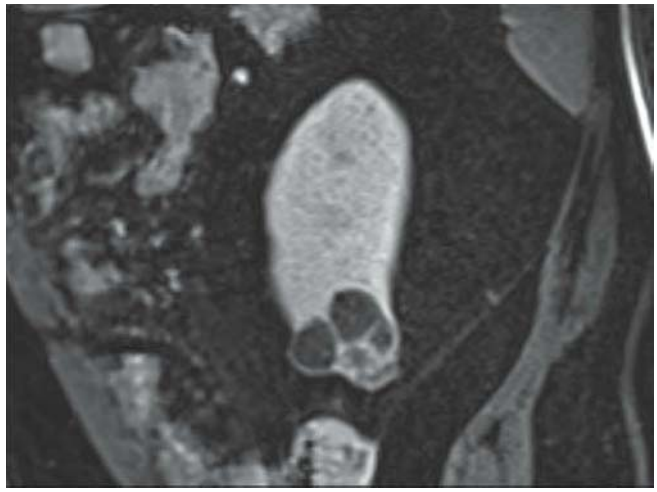

FIGURE 18C

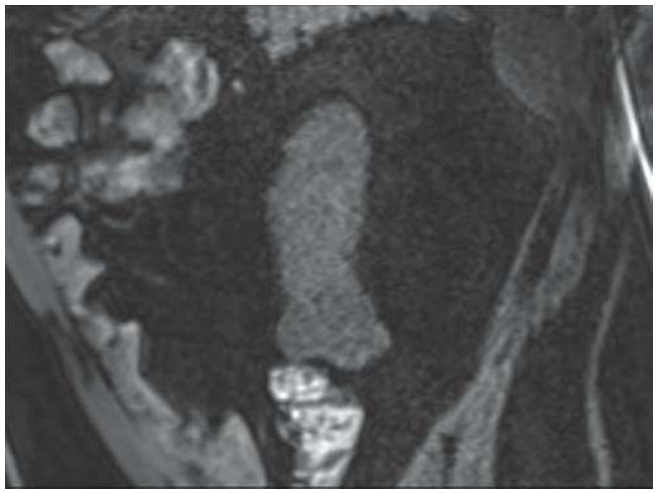

FIGURE 18B

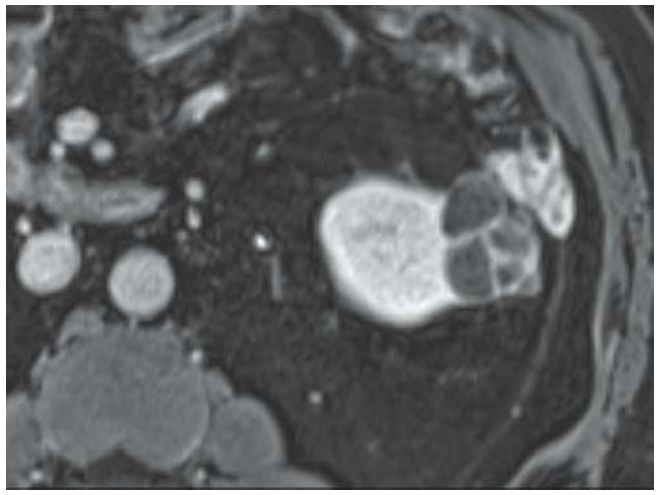

FIGURE 18D

FINDINGS Coronal T2-WI (A) demonstrates an exophytic 3.5-cm cystic lesion in the lower pole of the left kidney with thickened septations. Sagittal (B and C) and axial (D) fat-suppressed T1-WI pre- (B) and post-gadolinium (C and D) injections (D) show measurable enhancement of the thickened slightly irregular septations.

DIFFERENTIAL DIAGNOSIS Complex multilocular cyst, cystic nephroma, mixed epithelial stromal tumor (MEST).

DIAGNOSIS Cystic renal cell carcinoma.

DISCUSSION Renal cell carcinoma can be primarily cystic, as in this case, or have central necrosis, resulting in a cystic, complex lesion. It is critical to closely evaluate a cystic lesion for signs of malignancy. A simple cyst should be round, well defined, with an imperceptible wall. The fluid should be of water density and should not enhance with contrast. Thin septations or thin peripheral calcifications can also be seen in benign cysts. Thick and irregular walls or septations, thick calcifications, and a tumor nodule are possibly suggestive of a malignancy. The lesion in this case demonstrates measurable enhancement of thickened septations (Bosniak category III). Approximately 50% of Bosniak III cysts are malignant. In this case, a cystic renal cell carcinoma was found at surgery. A cystic nephroma or MEST may be indistinguishable from a cystic RCC by imaging but typically occur in perimenopausal women and frequently the lesion extends into the renal pelvis, a feature not seen in this case.

CASE 19

CLINICAL HISTORY *31-year-old woman presenting with pelvic pain and constipation.*

FIGURE 19A

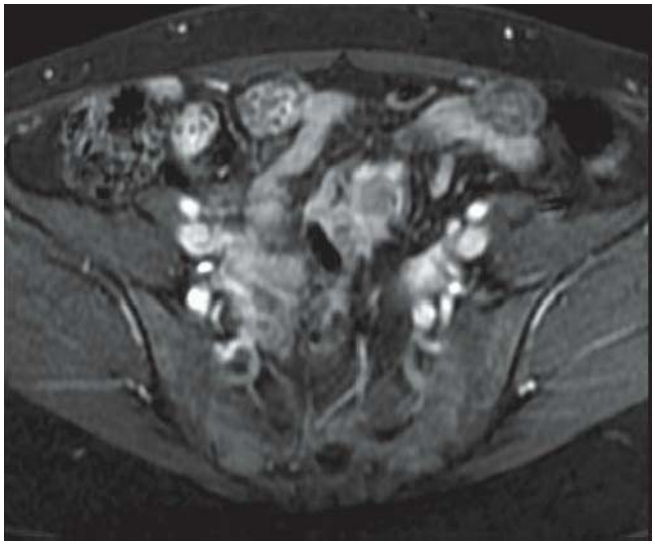

FIGURE 19C

FIGURE 19B

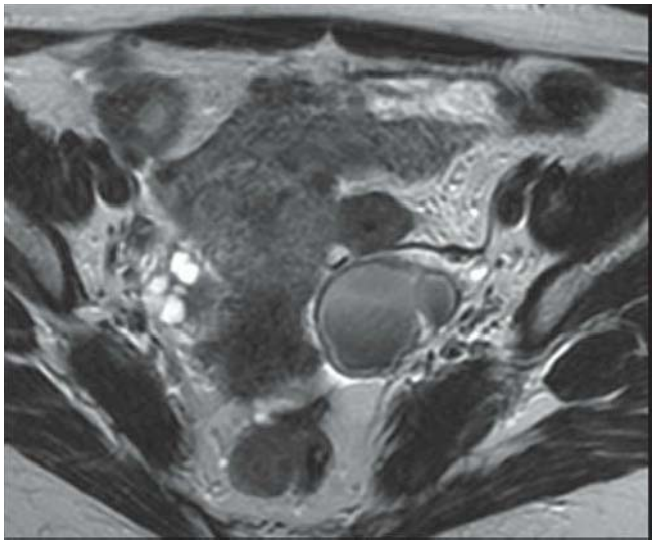

FIGURE 19D

FINDINGS Axial CECT image (A) demonstrates a soft tissue mass along the mid-sigmoid colon. Axial T2-WI (B) shows the mass is hypointense, with heterogeneous enhancement on the axial fat-suppressed, gadolinium-enhanced T1-WI (C). Note enhancing spiculations in the adjacent fat. A more inferior axial T2-WI (D) shows two left adnexal cysts with shading.

DIFFERENTIAL DIAGNOSIS Sigmoid adenocarcinoma, drop metastasis, GIST, carcinoid.

DIAGNOSIS Sigmoid endometriosis.

DISCUSSION Endometriosis is defined as the presence of endometrial tissue outside the endometrium. The most common locations of endometriosis are the ovaries and the pelvic peritoneum, followed in order of decreasing frequency by deep lesions of the pelvic subperitoneal space, the intestinal system, and the urinary system. Although peritoneal endometriosis can be asymptomatic, deep pelvic endometriosis is a cause of pelvic pain, dysmenorrhea, dyspareunia, dyschezia, and urinary symptoms and is associated with infertility. The histologic findings of deep pelvic endometriosis are mainly characterized by fibromuscular hyperplasia that surrounds foci of endometriosis, and the foci sometimes contain

small cavities. Between 7% and 35% of all women with endometriosis have been reported to have bowel involvement. Endometriosis of the rectum and/or sigmoid may be serosal or adventitial, in the muscle (muscularis), or full thickness involving both the muscularis and the lamina propria of the mucosa; the mucosal surface is rarely broken. The rectal lesions are anterior or lateral. Posterior wall endometriosis is a rarity but can form a "napkin ring" deformity. Fibrotic endometriosis nodules infiltrating the anterior rectal wall are the commonest and may be focal (cicatrical) or linear (a transverse bar often with associated stricture where the rectum is fused to the posterior vagina). The presence of gynecological endometriosis, as evidenced in this case by ovarian endometriomas, clinches the diagnosis.

CASE 20

CLINICAL HISTORY *55-year-old woman presenting with left lower quadrant pain.*

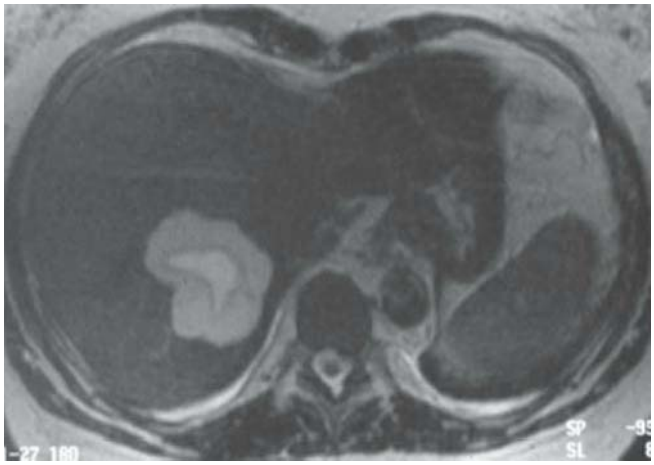

FIGURE 20A

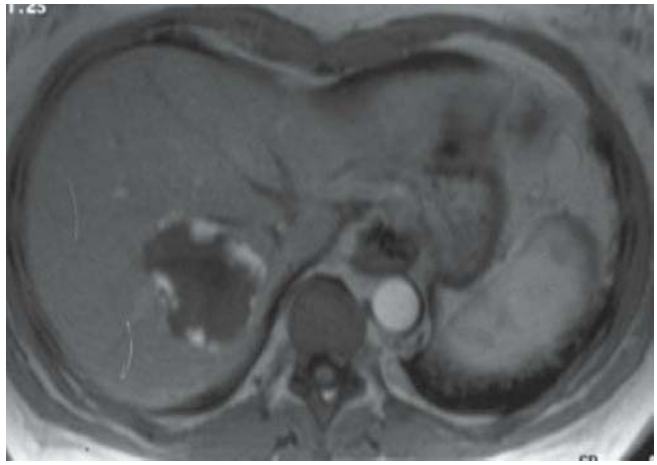

FIGURE 20C

FIGURE 20B

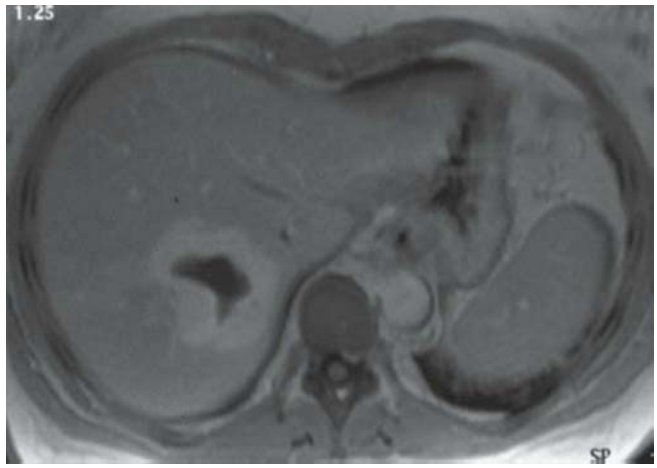

FIGURE 20D

FINDINGS Axial T2-WI (A) and heavily weighted T2-WI (B) show a large, hyperintense, well-defined lesion with a more hyperintense central area. On the early-phase, gadolinium-enhanced, fat-suppressed axial T1-WI (C), a peripheral, incomplete nodular enhancement pattern is seen. On the delayed-phase image (D), the central area of the lesion remains unenhanced.

DIFFERENTIAL DIAGNOSIS Metastasis, hepatocellular carcinoma.

DIAGNOSIS Atypical hemangioma with cystic degeneration.

DISCUSSION Large, heterogeneous hemangioma is a type of an atypical hemangioma, a category that consists of lesions, such as rapidly filling hemangiomas, calcified hemangiomas, hyalinized hemangiomas, cystic or multilocular hemangiomas, hemangiomas with fluid–fluid levels, and pedunculated hemangiomas. Large hemangiomas are often heterogeneous, and they are termed giant hemangiomas when they exceed 10 cm in diameter. On unenhanced CT scans, large, heterogeneous hemangiomas appear hypodense and heterogeneous with marked central areas of lower density. After intravenous administration of contrast material, the typical peripheral nodular enhancement pattern is still observed. Nevertheless, the progressive central enhancement may not lead to complete filling on delayed images. At MRI, on T1-WI, hemangiomas with cystic degeneration appear sharply marginated and hypointense with a cleft-like area of lower intensity. Accordingly, T2-WI shows a markedly hyperintense cleft-like area. The enhancement pattern is similar to that seen on CT; the cleft-like area remains hypointense, and therefore, the lesion shows incomplete filling.

CASE 21

CLINICAL HISTORY *75-year-old woman with abdominal pain.*

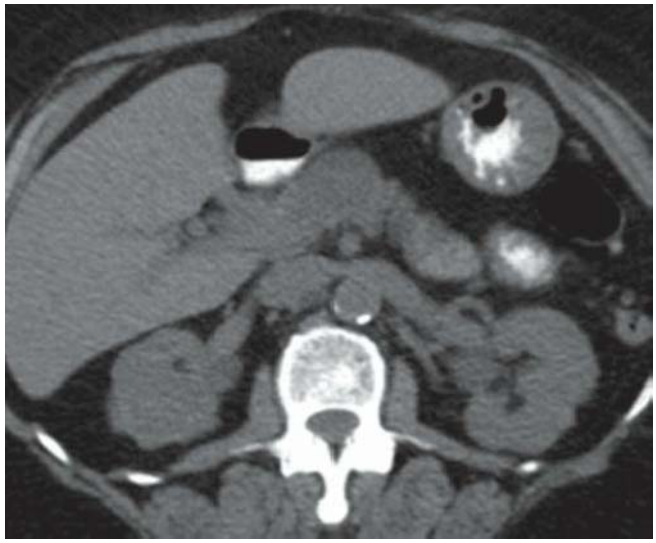

FIGURE 21A

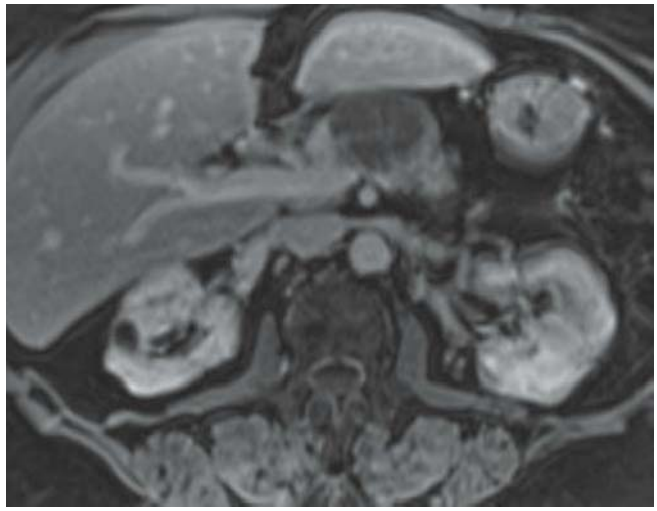

FIGURE 21C

FIGURE 21B

FIGURE 21D

FINDINGS NECT axial image (A) demonstrates a low-attenuation lesion in the head and neck of the pancreas. CECT image (B) demonstrates the same lesion to have enhancing septations separating multiple small cysts. Axial post-gadolinium fat-suppressed T1-WI (C) confirms the delayed enhancement of the internal septations and capsule. MRCP (D) confirms the microcystic mass with no communication with pancreatic duct. The CBD and MPD are of normal caliber.

DIFFERENTIAL DIAGNOSIS None.

DIAGNOSIS Microcystic serous pancreatic adenoma.

DISCUSSION Microcystic serous pancreatic adenoma is almost always a benign neoplasm of the pancreas arising from the duct cells. They typically occur in older women between the ages of 60 and 80 years ("grandmother tumor"). This lesion has been associated with von Hippel-Lindau disease. This lesion can occur anywhere within the pancreas, but there is a predilection for the pancreatic head. The cysts tend to be small, measuring less than 2 cm in size. Generally, there are more than six individual

cystic components. The septations separating the cysts can enhance after intravenous contrast administration, and if the cysts are very small, the lesion can appear solid, especially on sonography and CT. Punctate calcifications within a central stellate fibrotic scar are characteristic of this lesion. Other cystic neoplasms of the pancreas include a mucinous cystic neoplasm, which tends to have larger cysts; a solid and papillary epithelial neoplasm, which is seen in younger patients; an intraductal papillary mucinous neoplasm, which connects to the pancreatic duct; and a necrotic islet cell tumor, which would not have innumerable small cysts.

CASE 22

CLINICAL HISTORY *57-year-old man presenting with elevated PSA.*

FIGURE 22A

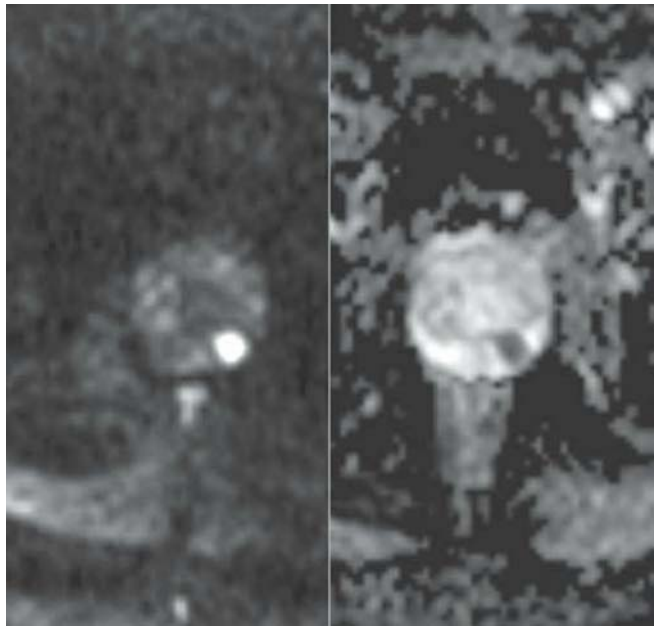

FIGURE 22C

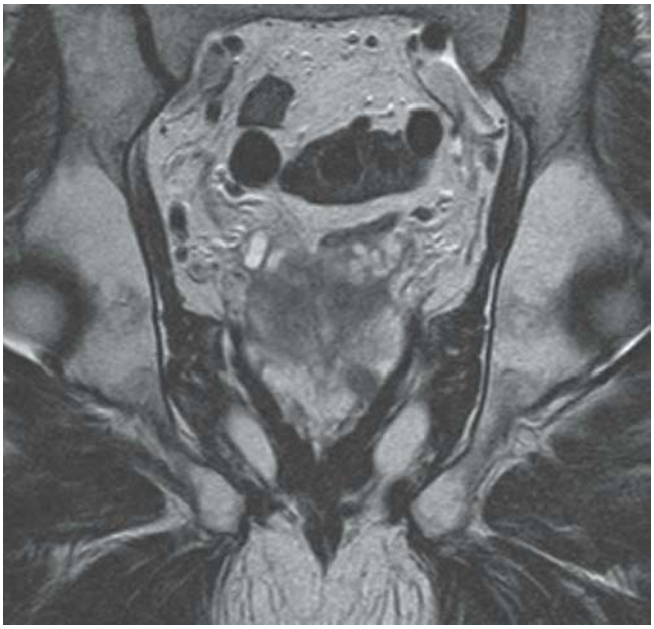

FIGURE 22B

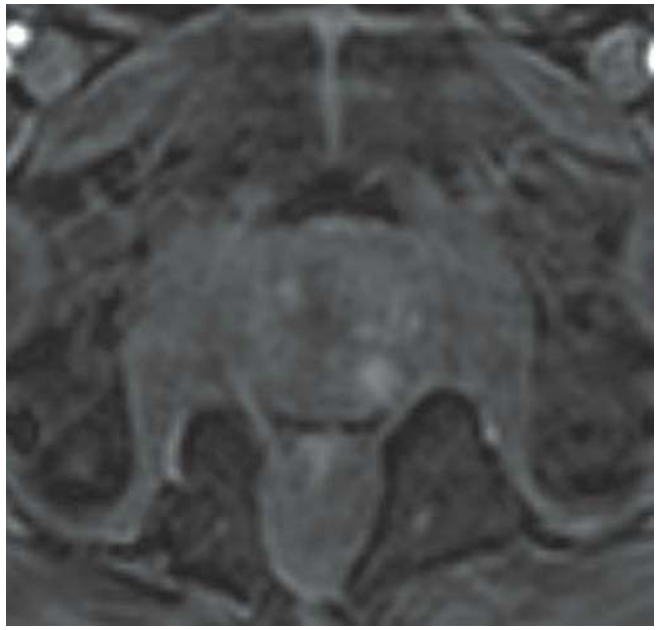

FIGURE 22D

FINDINGS Axial (A) and coronal (B) T2-WIs demonstrate a focal nodular area of hypointense signal in the posterior left side of the peripheral zone of the prostate. Marked restricted diffusion is present (C, left), with dark signal on the ADC (C, right). On the gadolinium-enhanced, fat-suppressed axial T1-WI (D) arterial enhancement is present.

DIFFERENTIAL DIAGNOSIS Hyperplasia (fibrous, fibromuscular, muscular, and atypical adenomatous types), prostatitis, infarction, scar, and hemorrhage after biopsy.

DIAGNOSIS Prostate cancer (adenocarcinoma).

DISCUSSION In the United States, prostate cancer is the most common malignancy in men, and the second most

common cause of cancer-related deaths after lung carcinoma. After the diagnosis of prostate cancer has been made (often after US-guided prostate biopsy), the staging of prostate cancer has important implications for treatment. The majority of prostate cancers arise from the peripheral zone (70%); a smaller number originates in the central gland. Tumors that are extending outside the gland (stage T3a) and invading surrounding tissues (stage T3b) have high rates of recurrence and morbidity. Therefore, an important staging threshold for treatment is between stages T2 (tumor confined to the prostate gland; treated with curative radical prostatectomy) and T3 (gross or bilateral extraglandular tumor; treated with external beam radiation, hormonal therapy, or both). Research on stage T3a suggests that patients with microscopic extraglandular tumor can still be candidates for surgery. Multiplanar MRI has a specificity of 90% to 95% in staging T2 and T3 prostate cancers.

The normal peripheral zone has a homogeneous bright signal on T2-WI, with a few hypointense internal radiating bands. Prostate cancer is hypointense on T2-WI, has restricted diffusion with hypointense ADC signal, and shows hyperenhancement with washout. If all findings are present, the likelihood of prostate cancer is very high. Diffusion imaging with high b values ($b = 1{,}400$ in this case) increases the accuracy of prostate cancer detection. It is crucial to perform very early acquisition following contrast administration to detect the early arterial enhancement of cancers.

CASE 23

CLINICAL HISTORY *9-year-old boy presenting with right upper quadrant pain and a palpable mass.*

FIGURE 23A

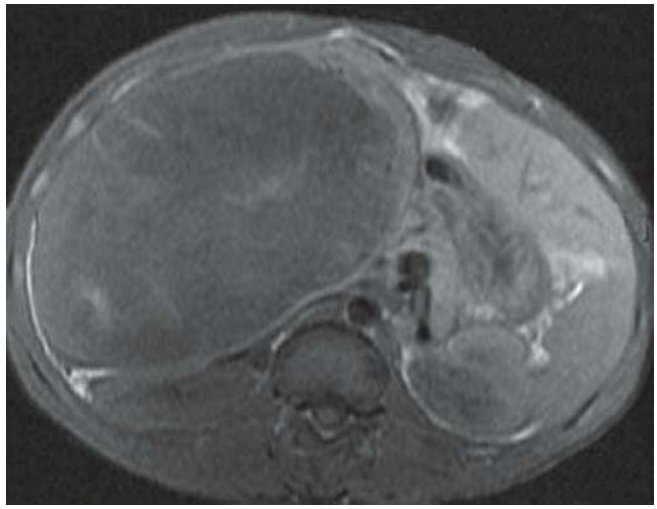

FIGURE 23C

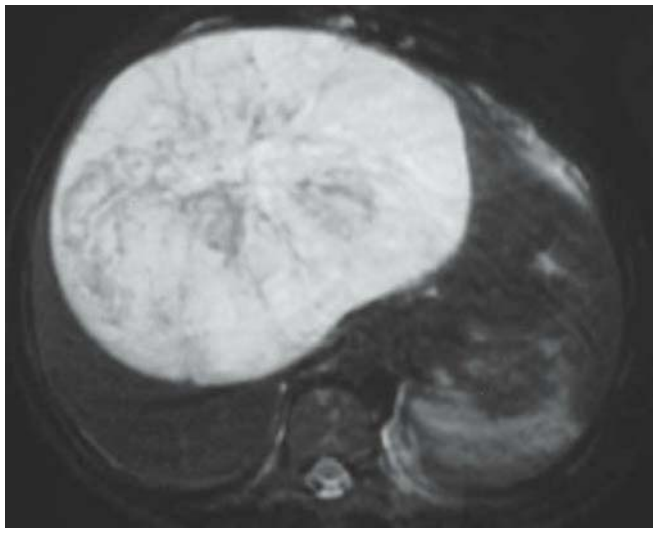

FIGURE 23B

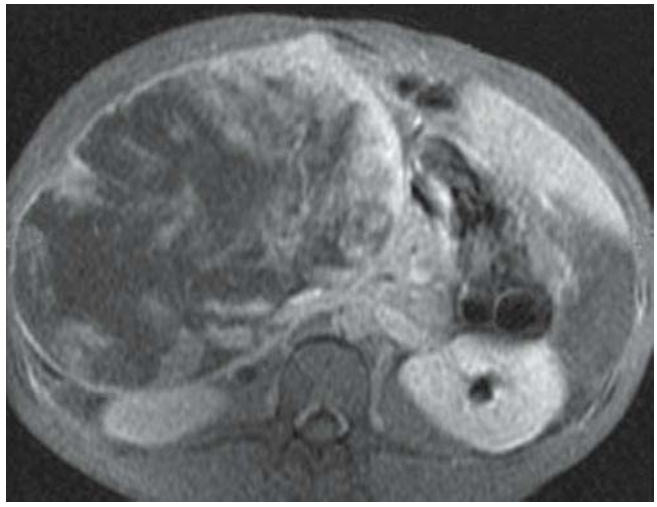

FIGURE 23D

FINDINGS Axial CECT image (A) demonstrates a large complex liver mass. This lesion is mostly hyperintense on the axial fat-suppressed T2-WI (B). Pre- (C) and post-gadolinium (D) fat-suppressed axial T1-WIs demonstrate the lesion to be hypointense with solid enhancing components and capsular enhancement. Note the areas of absent enhancement representing necrosis.

DIFFERENTIAL DIAGNOSIS Mesenchymal hamartoma, hepatocellular carcinoma, hepatic adenoma, necrotic metastasis.

DIAGNOSIS Undifferentiated embryonal sarcoma.

DISCUSSION Undifferentiated embryonal sarcoma (UES) is an uncommon malignant neoplasm of mesenchymal origin composed of spindle-shaped sarcomatous cells. About 90% of these lesions occur before the age of 15, with most occurring in older children (6 to 12 years). Even with surgery, chemotherapy, and radiotherapy, the prognosis is poor with life expectancy of less than 12 months. UES is typically a large encapsulated mass with areas of hemorrhage and necrosis. The lesion will, therefore, appear as a combination of large cystic and solid areas. The only good differential diagnosis for this appearance in the pediatric patient is the benign mesenchymal hamartoma. Other possibilities, such as a hepatocellular carcinoma and adenoma, are much less likely in the pediatric patient. UESs are typically hypointense on T1-WI and hyperintense on T2-WI with the areas of necrosis having the signal characteristics of water. The solid component of UES enhances after gadolinium administration.

CASE 24

CLINICAL HISTORY *66-year-old man presenting with bacteremia during the course of an acute pancreatitis attack.*

FIGURE 24A

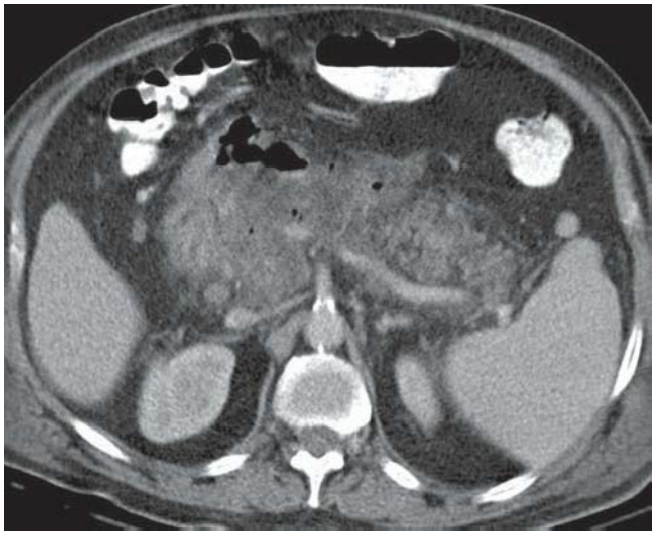

FIGURE 24C

FIGURE 24B

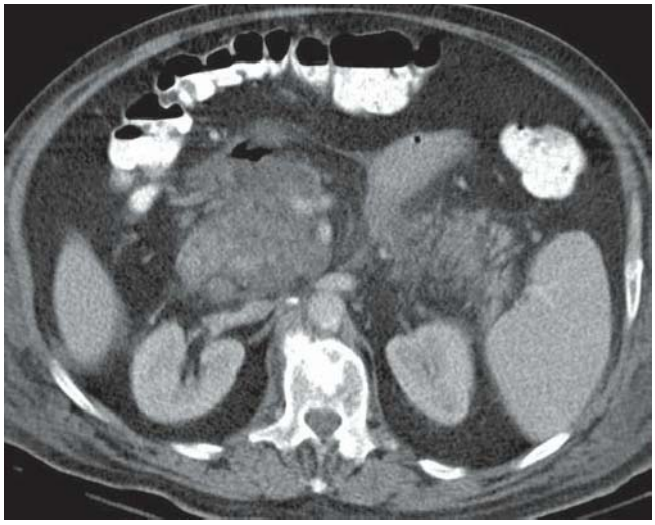

FIGURE 24D

FINDINGS Consecutive axial CECT images (A–D) demonstrate an edematous and swollen pancreas with peripancreatic inflammation and stranding. Note the air-fluid level in the lesser sac and the scattered mottled gas in the pancreatic bed.

DIFFERENTIAL DIAGNOSIS None.

DIAGNOSIS Infected pancreatic necrosis.

DISCUSSION Many complications can occur in acute pancreatitis. Necrotizing pancreatitis is one of the most worrisome. In necrotizing pancreatitis, there is destruction of the pancreatic parenchyma due to the pancreatic enzymes. This can lead to infection of the pancreas by gram-negative bacteria, typically due to translocation of microorganisms from the gut. Infected necrotizing pancreatitis carries a high mortality rate. CT findings include lack of enhancement of the normal pancreas after contrast administration and formation of a low-attenuation area in the pancreas region. The presence of gas bubbles within the pancreatic bed is highly suggestive of infected necrosis, but sterile necrosis cannot be excluded. Often percutaneous needle aspiration is needed to confirm the presence of infection. Treatment options for infected necrotizing pancreatitis include surgical debridement or aggressive percutaneous catheter drainage.

CASE 25

CLINICAL HISTORY *54-year-old man presenting with abdominal pain and low blood pressure.*

FIGURE 25A

FIGURE 25C

FIGURE 25B

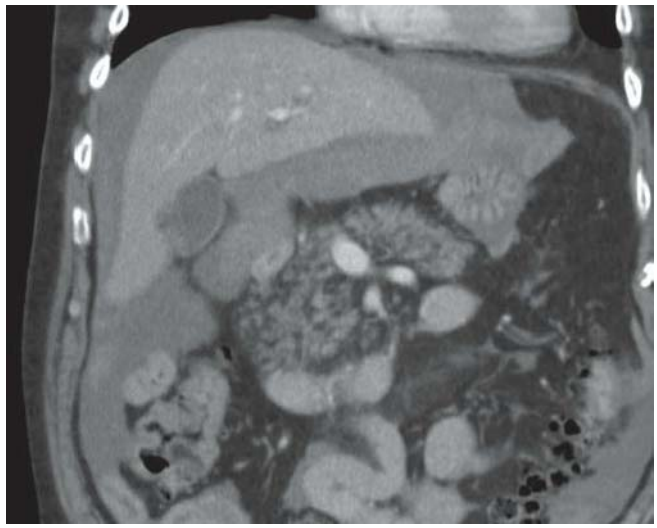

FIGURE 25D

FINDINGS Axial CECT image (A) shows a mushroom-shaped hyperdensity anterior to the left lobe of the liver. An underlying heterogeneous liver lesion is noted on the axial CECT images in the left lobe of the liver (B and C). The liver has a nodular contour and hyperdense ascites is seen to extend to the lower abdomen on the coronal reformatted CECT image (D).

DIFFERENTIAL DIAGNOSIS Bleeding hepatocellular adenoma, traumatic liver injury, hemorrhagic cyst with rupture.

DIAGNOSIS Hemoperitoneum due to ruptured hepatocellular carcinoma.

DISCUSSION Spontaneous hemoperitoneum usually originates from a parenchymal lesion rupturing in the peritoneal cavity. These lesions can be of hepatic origin (such as a simple biliary cyst, hepatocellular carcinoma, and adenoma) or of splenic origin (angiosarcoma). In women, gynecological pathologies are common culprits, such as a ruptured ovarian cyst and a ruptured ectopic pregnancy. Traumatic injuries or post-surgical complications account for a large proportion of intraperitoneal bleeds. Rarely, the source of bleeding cannot be identified on imaging and is therefore idiopathic if no blood dyscrasia or bleeding diathesis is identified. The presence of shock indicates a large amount of bleeding has occurred. When active contrast extravasation is identified on imaging, as evidenced

by a focus that is isodense to the bloodpool (aortic) density (the mushroom-shaped hyperdensity in this case), and the patient remains unstable, an angiogram with the intention of embolization is often performed. Obtaining delayed images in 2 minutes may sometimes help identify active bleeding if it is occurring at a slow rate. The attenuation of clotted blood is typically between 45 and 70 HU. As the highest attenuation hematoma, called the sentinel clot, is the closest to the site of bleeding, it is useful in identifying the source of bleeding.

CASE 26

CLINICAL HISTORY *45-year-old woman presenting with a prior history of melanoma with jaundice and weight loss.*

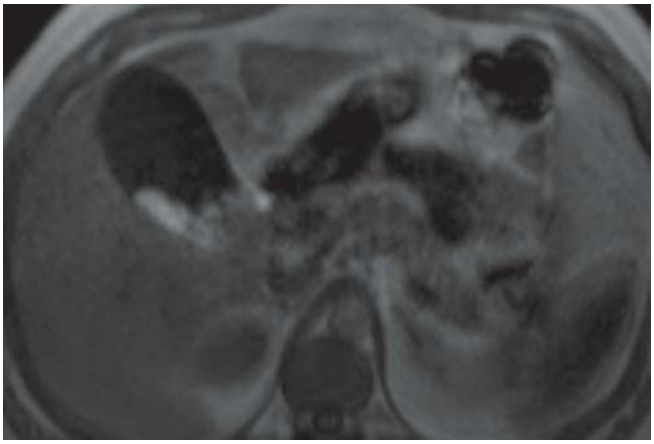

FIGURE 26A

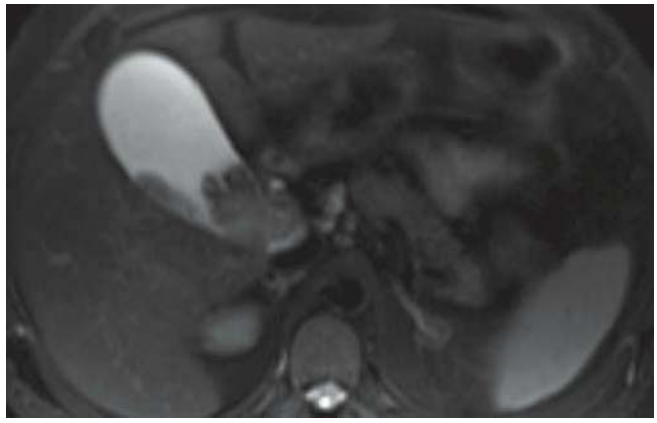

FIGURE 26C

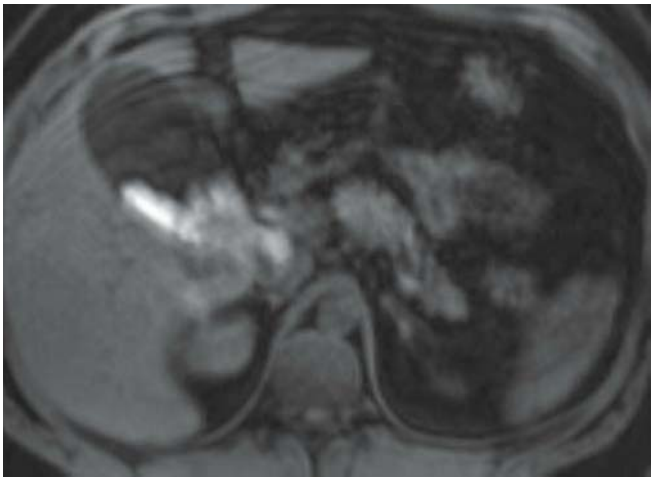

FIGURE 26B

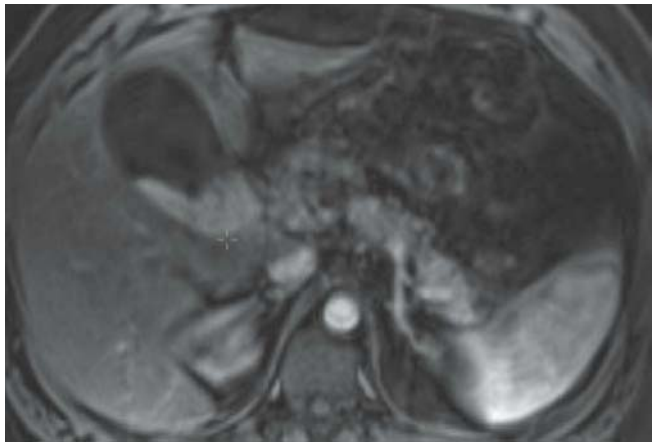

FIGURE 26D

FINDINGS Axial T1-WI (A) shows hyperintense focal mural thickening of the dependent wall, with no drop of signal on fat-suppressed image (B). The lesion appears hypointense on T2-WI (C). Post-gadolinium fat-suppressed T1-WI (D) demonstrates the enhancement of the lesion of the T1 hypointense lesion. There is extension of the tumor into the common hepatic duct.

DIFFERENTIAL DIAGNOSIS Gallbladder carcinoma with bleed, metastasis.

DIAGNOSIS Gallbladder melanoma.

DISCUSSION Both primary and metastatic melanomas of the gallbladder are rare. Involvement of the gallbladder occurs in about 15% of all gastrointestinal metastatic localizations in postmortem case. It is difficult to differentiate between primary and metastatic melanoma based on imaging. The tissue components that appear bright on T1-WI include fat, glycogen, blood, protein, and melanin. The absence of drop in signal on fat-suppressed image excludes fat as the tissue component. Melanin can appear bright on T1-WI and iso- to hypointense on T2-WI. Melanomas are prone to hemorrhage and can present with variable signal based on the stage of hemorrhage.

CASE 27

CLINICAL HISTORY *38-year-old woman presenting with constipation and sensation of incomplete stool evacuation.*

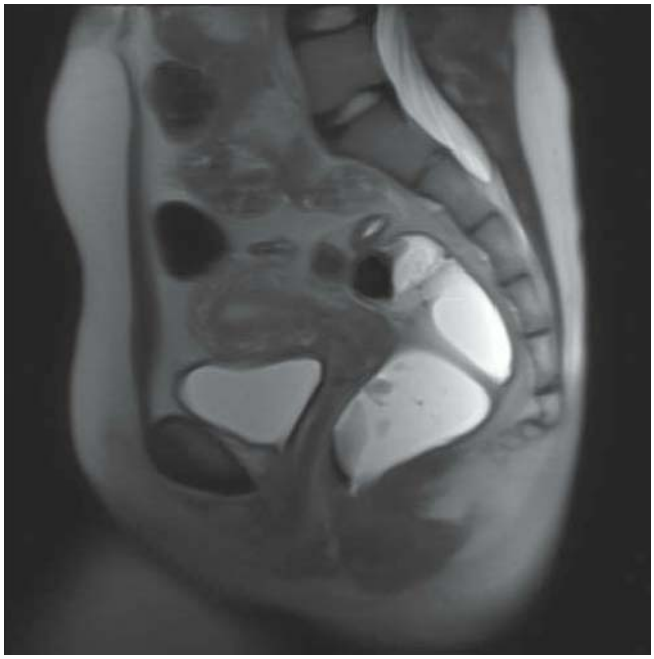

FIGURE 27A

FIGURE 27C

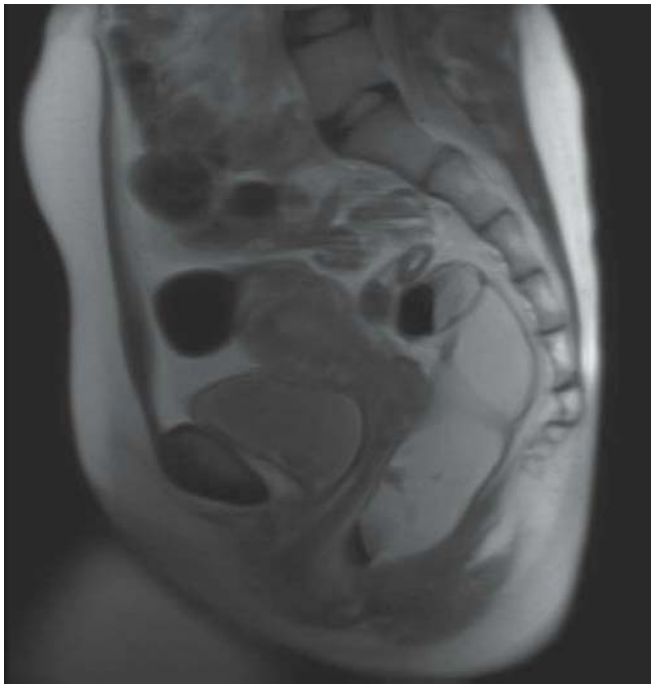

FIGURE 27B

FIGURE 27D

FINDINGS Sagittal heavily T2-WI (A) obtained after administration of rectal contrast and during relaxation shows a normal position of the bladder, vagina, and anorectal junction in relation to the pubococcygeal line. Sagittal T2-WI (B) obtained during contraction of the sphincter shows motion of all three compartments suggestive of competence of the pelvic floor muscles; there is normal sharpening of the anorectal angle. Sagittal T2-WI (C) obtained during straining shows

descent of the anorectal junction with widening of the anorectal angle. Sagittal T2-WI (D) obtained during defecation shows that the anterior wall of the rectum projects approximately 4 cm more anteriorly than expected.

DIFFERENTIAL DIAGNOSIS None.

DIAGNOSIS Anterior rectocele.

DISCUSSION Pelvic organ prolapse is very common, and it is the indication for more than 300,000 surgeries in the United States annually. Rectocele is defined as herniation or bulging of the posterior vaginal wall, with the anterior wall of the rectum in direct apposition to the vaginal epithelium. Etiologically, most cases are the result of vaginal childbirth and chronic increases in intra-abdominal pressure. In some patients, rectocele is thought to develop as a result of congenital or inherited weaknesses within the pelvic support system. Rectocele is a defect of the rectovaginal septum, not the rectum. Rectoceles are commonly found on proctograms, and small bulges of the anterior rectal wall detected upon evacuation proctography might be normal findings. Rectoceles should be considered abnormal if contrast trapping (the rectocele does not completely empty upon evacuation) is noted.

CASE 28

CLINICAL HISTORY *55-year-old woman presenting with hematuria.*

FIGURE 28A

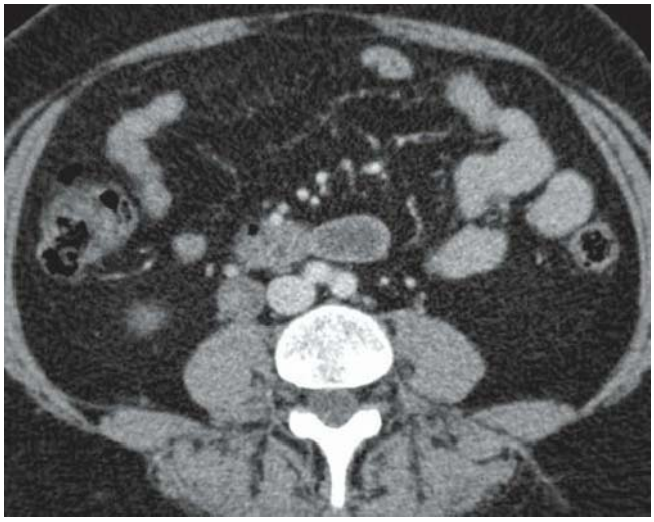

FIGURE 28B

FIGURE 28C

FIGURE 28D

FINDINGS Axial NECT image (A), axial CECT image in nephrographic (B) and excretory (C) phases, and coronal curved reformatted image (D) show a 7.2-cm-long enhancing mass in the proximal third of the right ureter. The more distal ureter is filled with nonenhancing material. Note the marked dilatation of the right ureter.

DIFFERENTIAL DIAGNOSIS Transitional cell carcinoma, hematoma.

DIAGNOSIS Fibroepithelial polyp.

DISCUSSION Primary neoplasms of the pelvicaliceal system are either of epithelial (the prototype being transitional cell carcinoma [TCC]) or of mesodermal origin. Mesodermal

tumors are rarely encountered entities in the urinary tract, and the most common lesion in this category is a fibroepithelial polyp. Other tumors of mesodermal origin are angiomatous polyps, hemangiomas, leiomyomas, neurofibromas, and lymphangiomas. Fibroepithelial polyp usually occurs in patients between 20 and 40 years of age. Presenting symptoms are typically hematuria or nonspecific flank pain. Because the fibrous stalk of the polyp is covered by normal urothelium, urine cytology analysis is of very limited value in the diagnosis. On CT, an enhancing mass in the collecting system will be seen. As for gastrointestinal polyps, peristalsis may elongate the lesion over many years. The major differential diagnosis is a TCC, and differentiation may be difficult. Both tumors enhance and are intraluminal masses with mural attachment. Identification of the pedunculated nature of the mass may be the only clue that the lesion is a polyp. Because treatment of a fibroepithelial polyp consists of simple excision, whereas nephroureterectomy is preferred for upper tract TCC, correct preoperative diagnosis, which is sometimes impossible to make by imaging, is crucial. As for a hematoma, it should not enhance. In this case, the nonenhancing material in the distal ureter proved to be a clot.

CASE 29

CLINICAL HISTORY *35-year-old woman presenting with a perineal mass.*

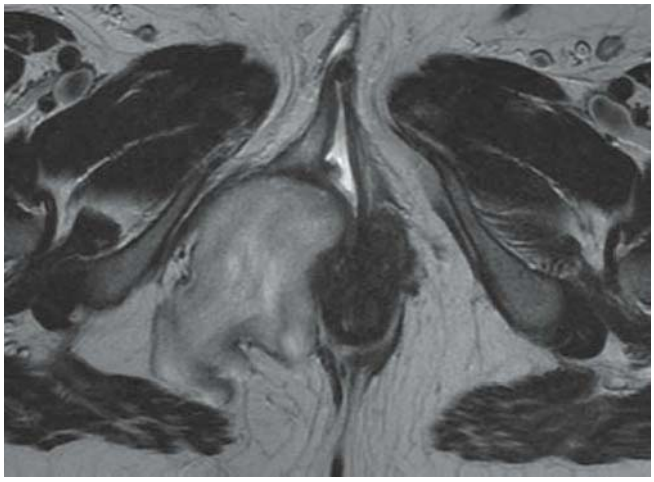

FIGURE 29A

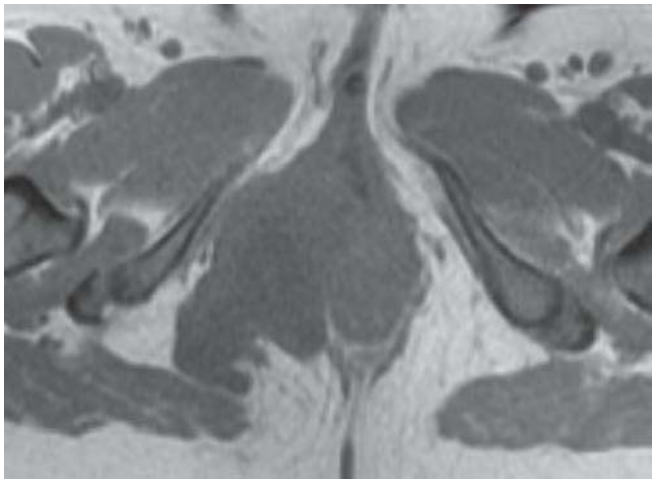

FIGURE 29C

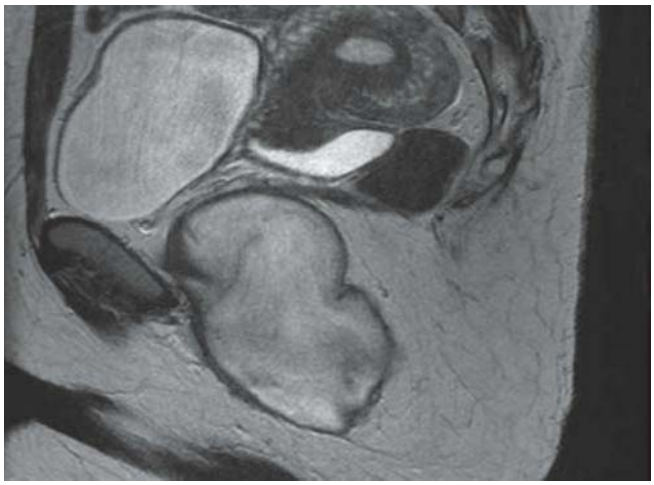

FIGURE 29B

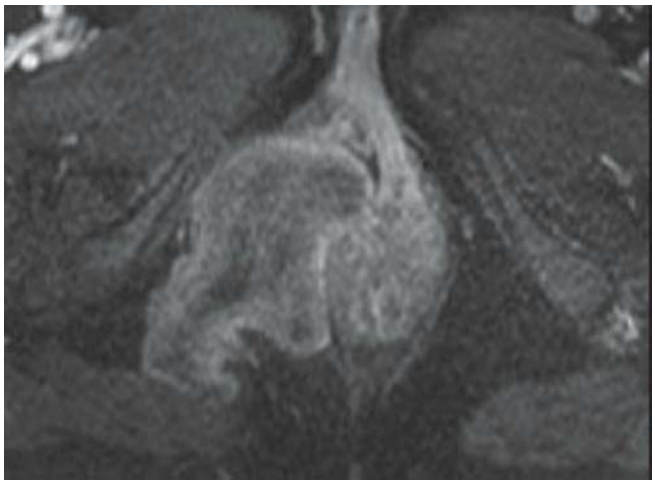

FIGURE 29D

FINDINGS Axial and sagittal T2-WIs (A and B) demonstrate a heterogeneous hyperintense mass in the right perineum extending to the right labia. Axial T1-WI (C) reveals near isointensity of the lesion with the surrounding musculature. Gadolinium-enhanced, fat-suppressed axial (D) T1-WI shows heterogeneous enhancement of the mass.

DIFFERENTIAL DIAGNOSIS Liposarcoma and infiltrating angiolipoma, myxoid peripheral nerve sheat tumor, myxoid smooth muscle tumor, angiomyofibroblastoma.

DIAGNOSIS Aggressive angiomyxoma.

DISCUSSION Aggressive angiomyxoma is a rare benign soft tissue tumor that contains myxoid and vascular components. It is predominantly seen in women of childbearing age. The slow-growing tumor has a propensity to reach large sizes within the pelvis, especially in the perineum. Although this tumor rarely shows mitotic activity, the term "aggressive" refers to the locally infiltrative growth pattern and the high recurrence rate (36% to 72%) after surgery. The typical imaging features include a vascular tumor with indolent growth and local infiltration but without invasion of adjacent organs. On MRI, the tumor is isointense to muscle on T1-WI, and after contrast administration, it shows moderate enhancement. On T2-WI, as in this case, the tumor has a swirled or layered appearance. The key features in differentiating aggressive angiomyxoma from the main differential considerations are the lack of fat content, the infiltrative but not invasive growth pattern and the heterogeneous enhancement of the soft tissue mass in women of childbearing age. Long-term MRI follow-up is recommended as recurrence occurring several years after the initial excision has been reported.

CASE 30

CLINICAL HISTORY *88-year-old man presenting with weight loss and right upper quadrant pain.*

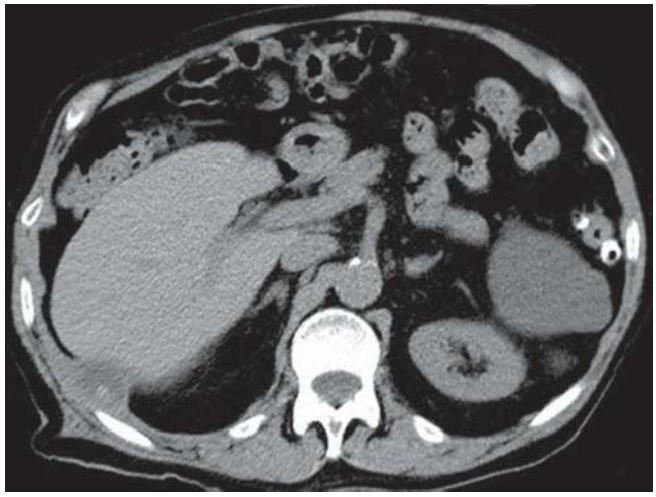

FIGURE 30A

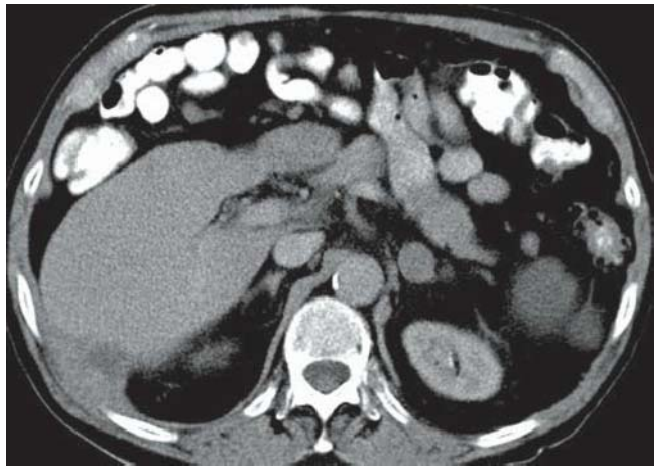

FIGURE 30C

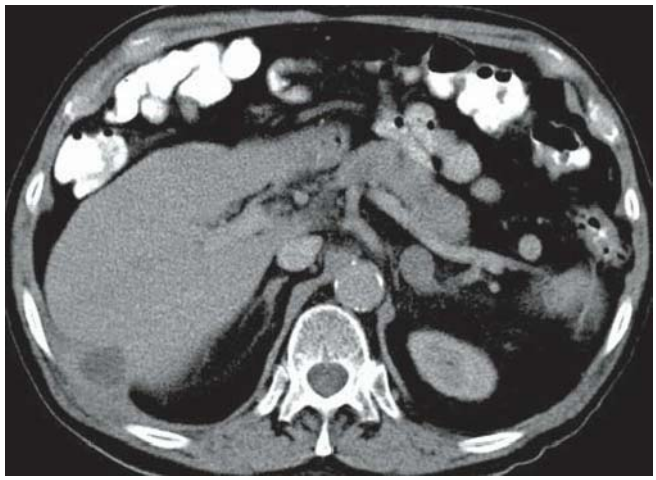

FIGURE 30B

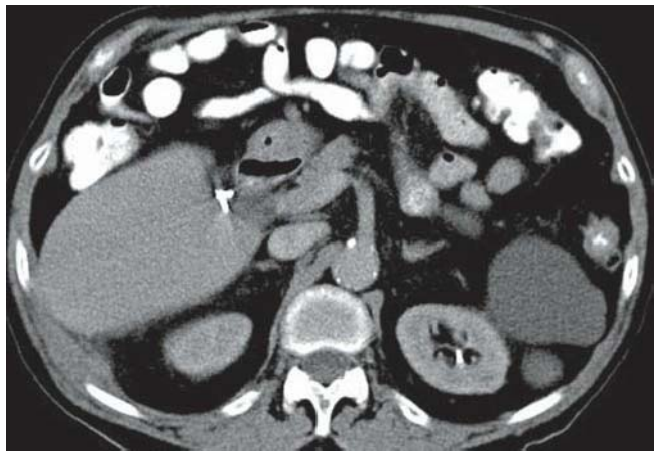

FIGURE 30D

FINDINGS Axial NECT (A) and CECT (B–D) images show a lesion with a hypodense center abutting the posterior aspect of the liver and the right chest wall, with surrounding soft tissue thickening. There is a small hyperdense structure within the collection (A).

DIFFERENTIAL DIAGNOSIS None.

DIAGNOSIS Dropped gallstone with abscess formation.

DISCUSSION Laparoscopy has become the procedure of choice for routine cholecystectomy. Despite the fact that the overall complication rate of the procedure is less than that observed with open cholecystectomy, there are two complications occurring more frequently at laparoscopy. One of them is bile duct injury or bile leakage, and the other is late infection due to dropped gallstones. If a spilled stone is retained in the abdominal cavity, recurrent intra-abdominal abscess may occur as a delayed complication. The diagnosis of dropped gallstone after laparoscopic cholecystectomy is important because simple abscess drainage or antibiotics therapy is typically not enough to treat such cases. In fact, surgical or percutaneous stone removal is essential for complete cure. In a patient with a recurrent intra-abdominal abscess, a history of laparoscopic cholecystectomy, and a hyperdense structure within a perihepatic collection on CT, the diagnosis of dropped gallstones should be rendered.

CASE 31

CLINICAL HISTORY *49-year-old man presenting with right upper quadrant pain.*

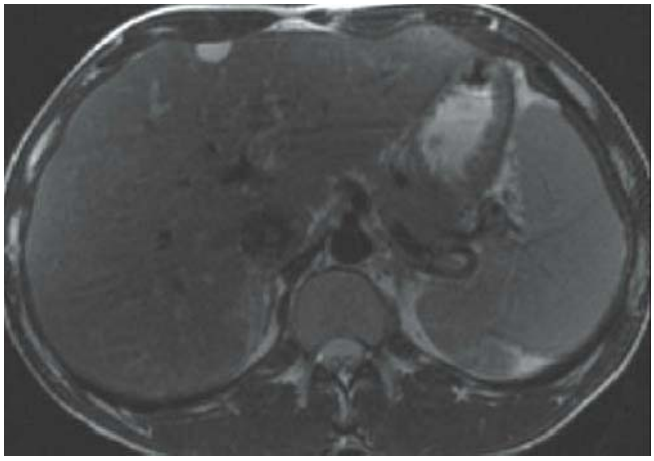

FIGURE 31A

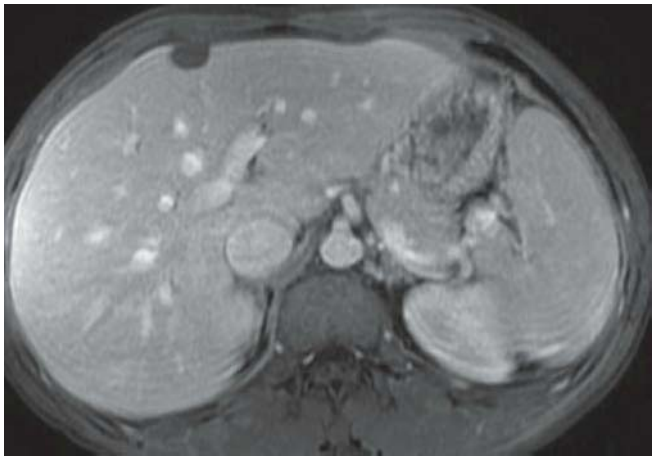

FIGURE 31C

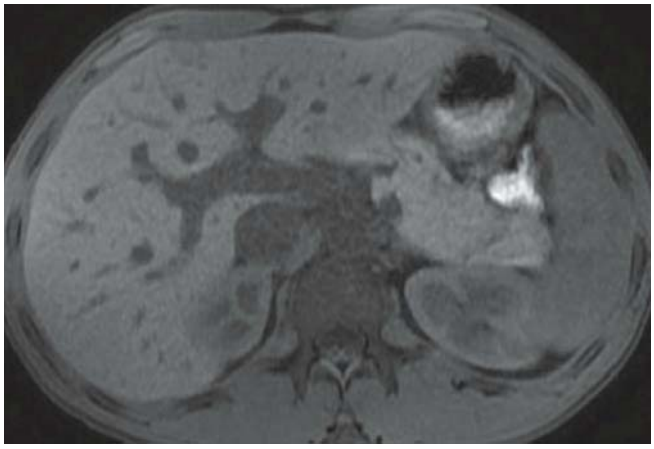

FIGURE 31B

FINDINGS Axial T2-WI (A) and fat-suppressed T1-WI (B) demonstrate a hyper- and slightly hypointense, respectively, lesion in segment 4a, beneath the hepatic capsule. The lesion shows no enhancement on gadolinium-enhanced, fat-suppressed axial T1-WI (C).

DIFFERENTIAL DIAGNOSIS Biliary cystadenoma, bile duct cyst, cystic metastasis.

DIAGNOSIS Ciliated hepatic foregut cyst.

DISCUSSION Ciliated hepatic foregut cyst is a rare cystic lesion of the liver; its histogenesis is still unclear but most authors consider that it arises from budding of the embryonic foregut in the liver. Ciliated hepatic foregut cyst is a benign, solitary cyst composed of a ciliated pseudostratified columnar epithelium, a subepithelial connective tissue layer, a smooth muscle layer, and an outer fibrous capsule. The lesion is almost always single and is situated in the medial segment of the left lobe (segment IV), beneath the Glisson capsule. On CT images, the density of ciliated hepatic foregut cyst may vary since it may contain various elements ranging from serous to mucoid material. Thus, on unenhanced CT, the lesion can be hypoattenuating or isoattenuating to normal liver parenchyma. On MR imaging, all ciliated hepatic foregut cysts are hyperintense on T2-WI. On T1-WI, on the other hand, the lesion may be hypo-, iso-, or hyperintense depending on its content. When a ciliated hepatic foregut cyst appears isodense relative to liver on CT images, it might be difficult to differentiate it from a solid hepatic lesion; in such cases, T2-WI is found to be useful to reach an accurate diagnosis.

CASE 32

CLINICAL HISTORY *50-year-old woman presenting with diffuse abdominal pain.*

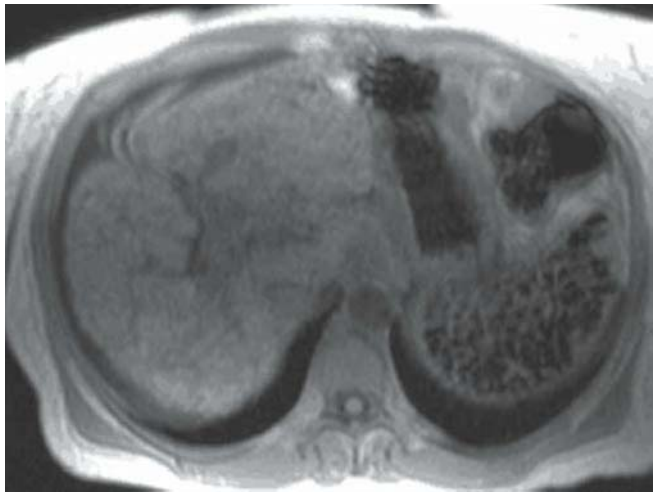

FIGURE 32A

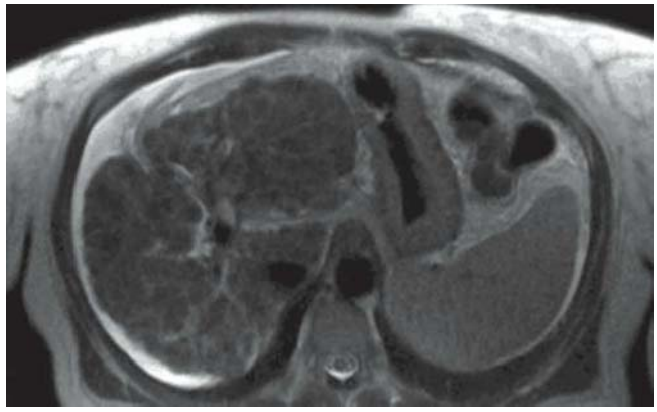

FIGURE 32C

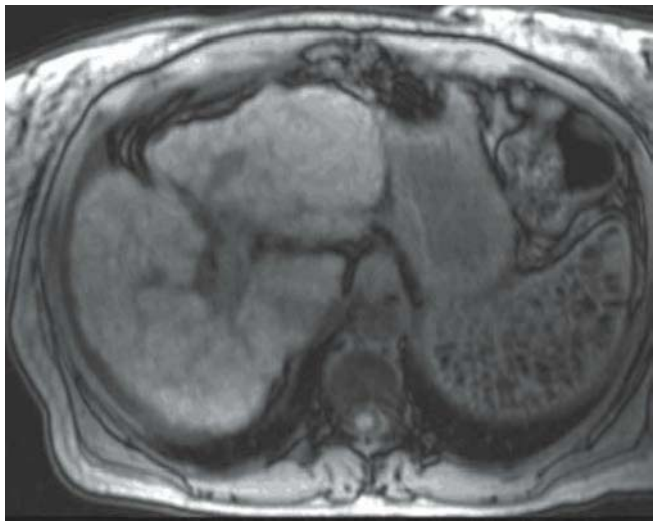

FIGURE 32B

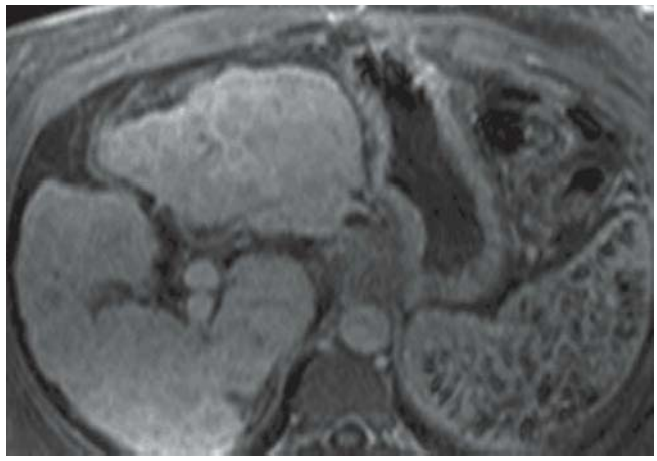

FIGURE 32D

FINDINGS Axial in-phase (A) and out-of-phase (B) T1-WIs demonstrate ill-defined small areas of signal void scattered within an enlarged spleen, with blooming on in-phase sequences reflecting iron deposition. These lesions are less evident on T2-WI axial (C) and demonstrate no enhancement on post-gadolinium image (D). Also note the presence of cirrhosis and portal vein thrombosis.

DIFFERENTIAL DIAGNOSIS Calcified granulomas (tuberculosis, histoplasmosis, brucellosis).

DIAGNOSIS Gamna-Gandy bodies.

DISCUSSION Portal hypertension causes enlargement of the splenic vein, formation of perisplenic collaterals and splenomegaly, and eventually, small areas of intrasplenic hemorrhage. The remnants of these tiny foci of hypertensive bleeding, which are composed of hemosiderin, fibrous tissue, and calcium, are referred to as siderotic nodules or Gamna-Gandy bodies. They vary in size but are usually less than 1 cm. On CT, noncalcified foci may appear as multiple, punctate, low-attenuation areas. Calcified foci may appear as multiple high-density lesions. On MRI, they can be seen as multiple, punctate, low-signal-intensity lesions on T1-WI, T2-WI, and gradient-echo sequences. The blooming artifact on gradient-echo images is pathognomonic for this entity because these sequences are more sensitive to detect the superparamagnetic effect of hemosiderin.

CASE 33

CLINICAL HISTORY *45-year-old woman presenting with left lower quadrant pain.*

FIGURE 33A

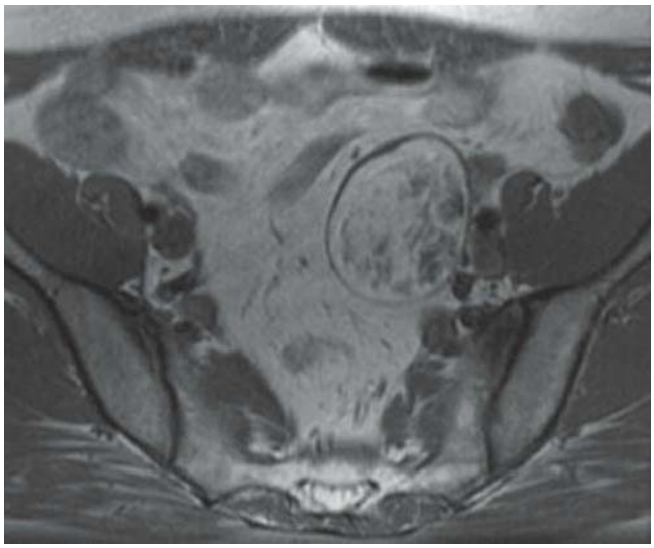

FIGURE 33B

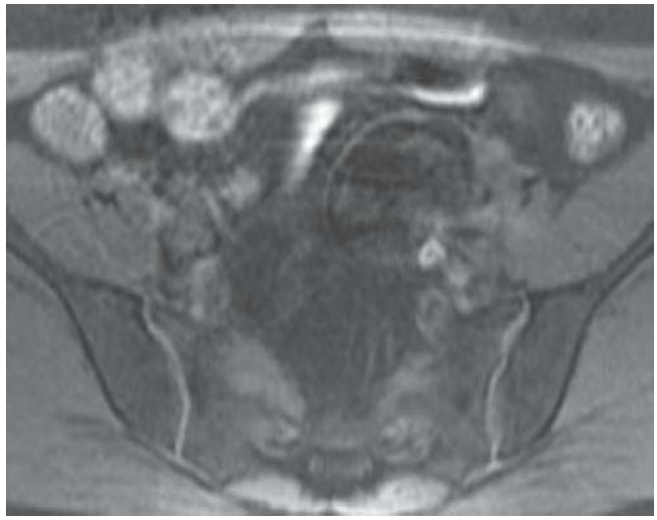

FIGURE 33C

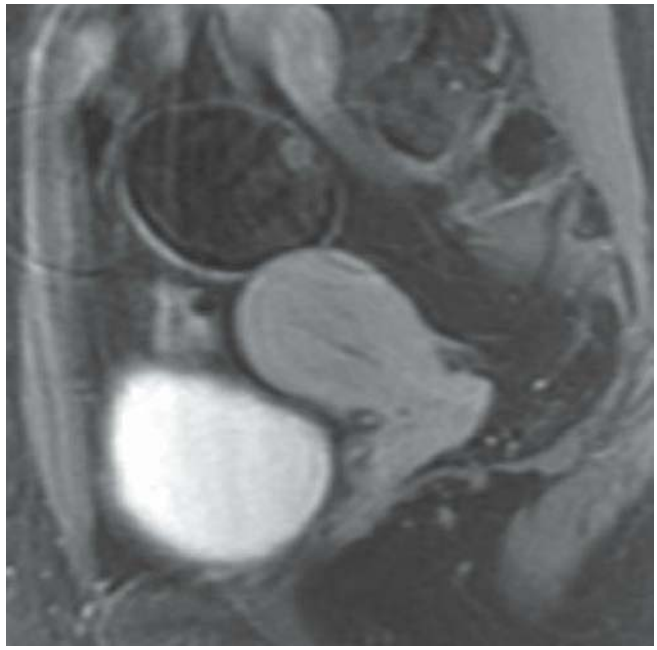

FIGURE 33D

FINDINGS Coronal T2-WI (A) and axial T1-WI (B) reveal a thin-walled, predominantly hyperintense, 5-cm left ovarian mass, with a small hypointense nodule adjacent to the wall. Unenhanced axial (C) and gadolinium-enhanced sagittal (D) fat-suppressed T1-WI show heterogeneous signal drop of the lesion and no internal enhancement.

DIFFERENTIAL DIAGNOSIS Hemorrhagic ovarian cyst.

DIAGNOSIS Mature ovarian teratoma.

DISCUSSION Fat-saturation MRI techniques are proven to be 100% specific and 96% accurate for the diagnosis of the most common germ cell tumor (99%), mature ovarian teratoma, due to depiction of the pathognomonic fat content of the lesion. Although hemorrhagic lesions can have T1 values similar to fat, they do not lose signal after fat suppression. Presence of a dermoid plug projecting from the wall is known as the Rokitansky nodule; it is a nonenhancing nodular component, which represents solid fat, hair, and/or teeth. The lack of enhancement of the dermoid enables the differentiation

from an ovarian carcinoma or the rare malignant transformation of a mature teratoma, also known as an immature teratoma. Immature teratoma occurs in the first two decades of life. It has a prominent solid component and may demonstrate hemorrhage and necrosis. Also in contrast with the mature teratoma, calcifications are rather scattered in immature teratoma. Immature teratoma is a rapidly growing tumor and frequently demonstrates local invasion. Elevated levels of serum CA 19-9 can be seen in all germ cell tumors; elevated alpha-fetoprotein is of concern for immature teratoma.

CASE 34

CLINICAL HISTORY *67-year-old man presenting with right inguinal pain.*

FIGURE 34A

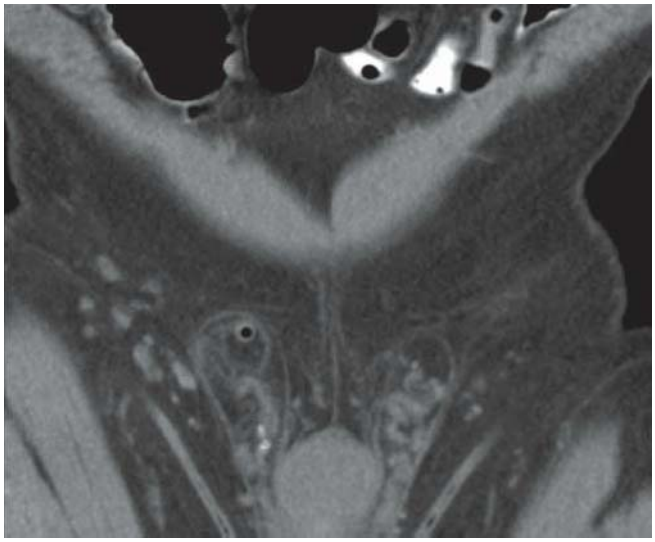

FIGURE 34C

FIGURE 34B

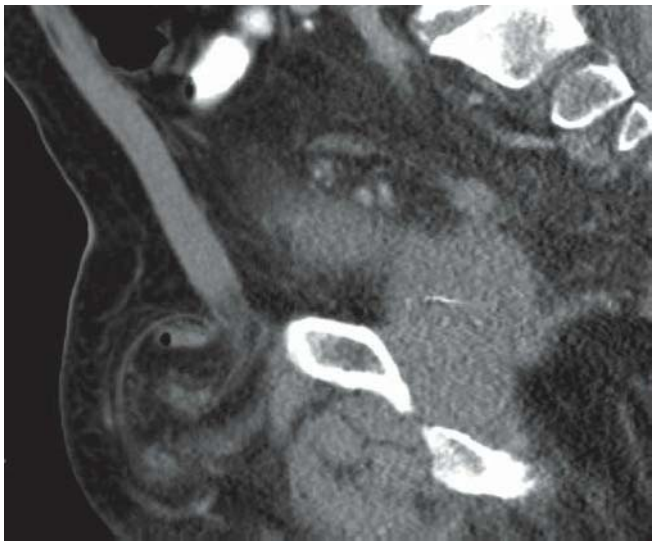

FIGURE 34D

FINDINGS Axial (A and B), coronal reformatted (C), and sagittal reformatted (D) CECT images demonstrate a right inguinal hernia-containing fat that is stranded by inflammation and a tubular blind-ending thin-walled gas-containing structure.

DIFFERENTIAL DIAGNOSIS De Garengeot's hernia.

DIAGNOSIS Amyand hernia.

DISCUSSION Spontaneous abdominal hernias occur in 5% of the population over their lifetime; 80% of these occur in the inguinal canal. Virtually any organ or structure can herniate through the inguinal canal: small or large bowel, fat, appendix, bladder, Meckel diverticulum, or gonads. When the appendix herniates through the inguinal canal, it is called Amyand hernia, and when it is a Meckel diverticulum, a Littré hernia. The presence of fat-stranding in the hernia sac may suggest strangulation, but can also be observed with back and forth motion of the herniated content through the hernia ring. Surgical repair of the abdominal wall defect, with or without associated appendectomy, is the treatment of choice.

De Garengeot's hernia is used to describe the incarceration of the vermiform appendix within a femoral hernia. The anatomic site of a femoral hernia is posterior to the inguinal ligament, medial to the femoral artery and vein, and inferior and lateral to the pubic tubercle. This is in contrast to inguinal hernias, which are located superior and medial to the pubic tubercle.

CASE 35

CLINICAL HISTORY *59-year-old man presenting with right upper quadrant pain and fever.*

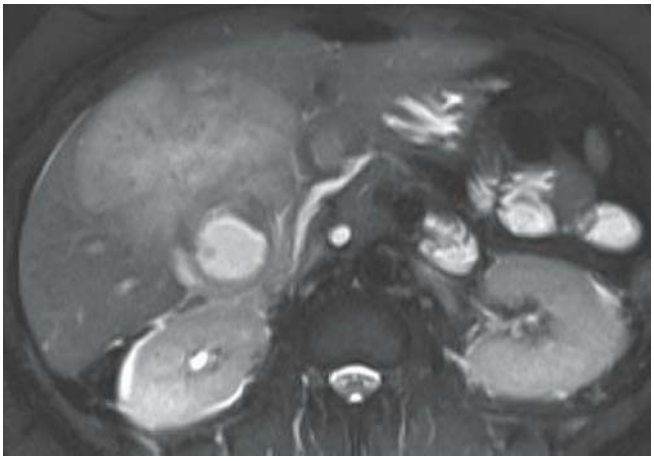

FIGURE 35A

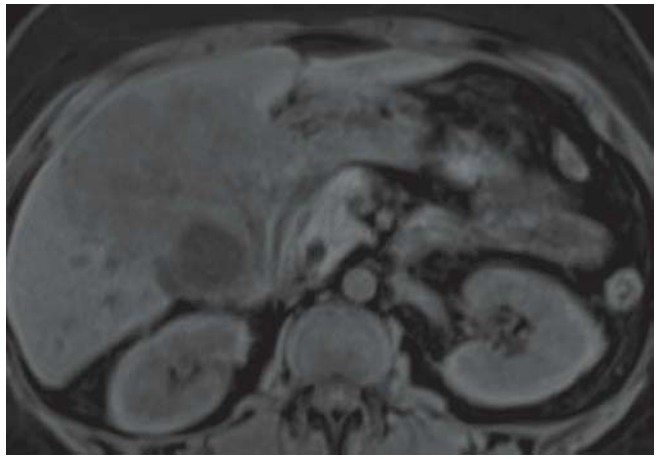

FIGURE 35C

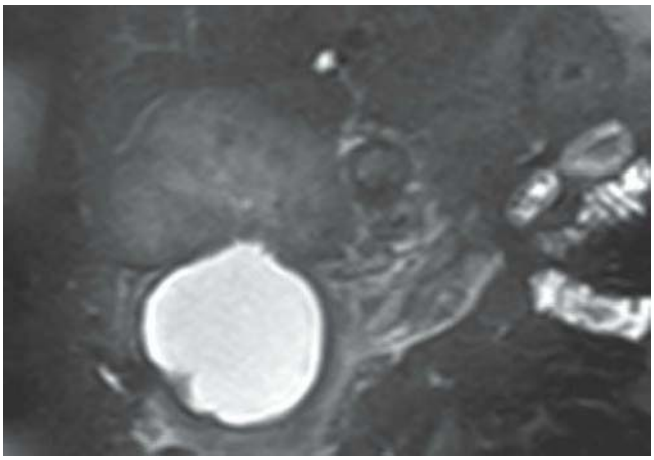

FIGURE 35B

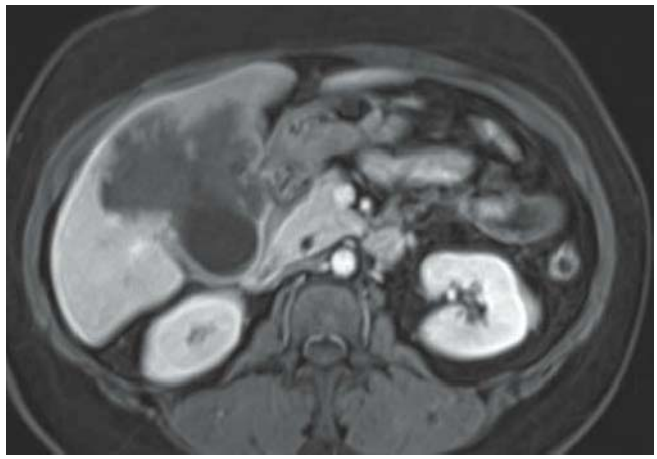

FIGURE 35D

FINDINGS Axial fat-suppressed T2-WI (A) and coronal MRCP (B) images demonstrate a large hyperintense lesion extending from the anterior gallbladder wall into the adjacent liver. Fat-suppressed, pre- (C) and post-gadolinium (D) axial T1-WIs demonstrate heterogeneous nodular enhancement of the mass, with breaches in the anterior gallbladder wall.

DIFFERENTIAL DIAGNOSIS Metastasis, acute cholecystitis.

DIAGNOSIS Gallbladder adenocarcinoma with liver invasion.

DISCUSSION Gallbladder cancer is an uncommon malignancy. Histologically, gallbladder cancer is usually an adenocarcinoma, although other cell types such as squamous cell carcinoma, anaplastic carcinoma, and sarcomas have been reported. Gallstones are present in more than 70% of the cases of gallbladder cancer; there is a slight female predominance. Gallbladder adenocarcinoma can present as a focal or diffuse thickening of the gallbladder wall, a polypoid lesion, or a mass replacing the gallbladder. Metastases are present at the time of diagnosis in approximately 75% of cases. This case demonstrates many findings of gallbladder carcinoma. There is typically an ill-defined low-attenuation mass involving the gallbladder wall and invading the liver parenchyma (segments IV and V). Although not seen in this case, multiple liver metastases are often present and account for the poor prognosis. Acute cholecystitis can also invade the liver; however, the wall is typically not irregularly thickened, and clinical symptoms are more severe.

CASE 36

CLINICAL HISTORY *57-year-old man presenting with crampy abdominal pain.*

FIGURE 36A

FIGURE 36C

FIGURE 36B

FIGURE 36D

FINDINGS Axial CECT images (A–D) demonstrate a circular mass in the proximal jejunum. This mass appears to be intraluminal and contains a crescent of fat at its periphery. Note the lack of obstruction of the proximal small bowel.

DIFFERENTIAL DIAGNOSIS Lymphoma, adenocarcinoma.

DIAGNOSIS Jejuno-jejunal intussusception.

DISCUSSION Intussusception represents invagination of a proximal segment of bowel (intussusceptum) into the lumen of a distal segment of bowel (intussuscipiens). It is typically seen in children (95%) and may be transient or persistent. Intussusceptions are easily identified on CT because there typically is a round soft tissue mass with concentric rings ("target" sign) made up of the walls of the small bowel. The peripheral fat attenuation layer represents herniated mesenteric fat, which has traveled with the loop of jejunum. Diagnosis is crucial because ischemia can occur if the intussusception should persist. Intussusception is classified into two types in adults: the more common short-segment intussusception, which typically is not obstructing and not caused by a lead mass; and long-segment intussusception, which is caused by a lead mass and is obstructing the proximal bowel. Most intussusceptions occur in the ileum; in the small bowel, benign tumors are more common causes than malignant neoplasms.

CASE 37

CLINICAL HISTORY *45-year-old woman presenting with left flank pain.*

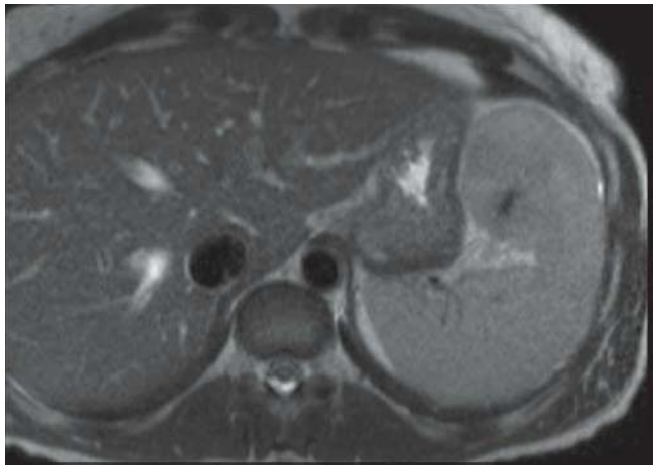

FIGURE 37A

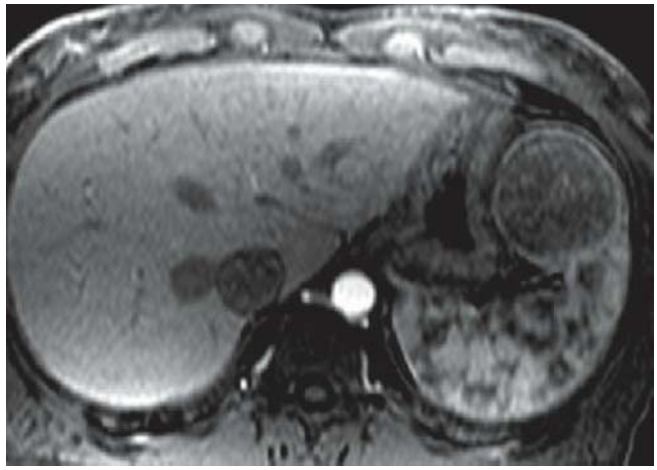

FIGURE 37C

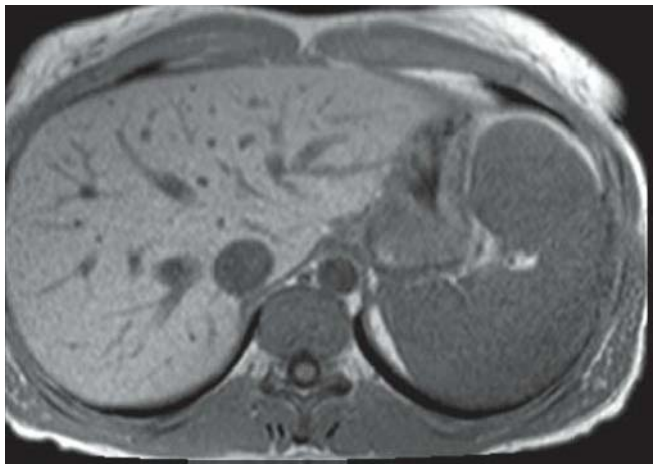

FIGURE 37B

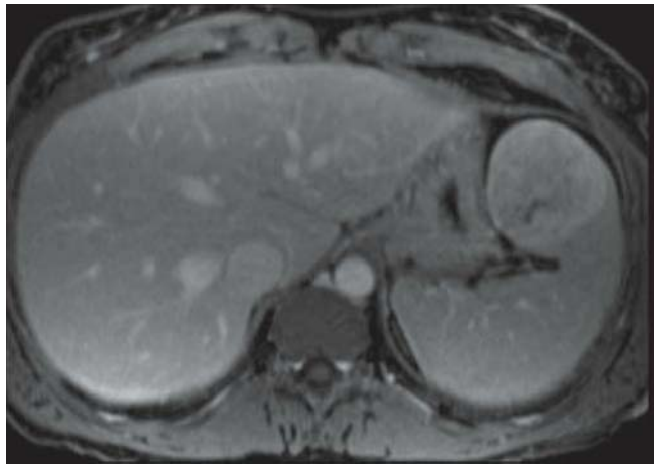

FIGURE 37D

FINDINGS Axial T2-WI (A) demonstrates a slightly heterogeneous, but mostly isointense mass in the anterior spleen with a hypointense central focus. The mass is isointense to the spleen on the T1-WI (B). The arterial phase gadolinium-enhanced, fat-suppressed axial T1-WI (C) shows speckled mostly peripheral heterogeneous enhancement of the lesion; the delayed gadolinium-enhanced, fat-suppressed axial T1-WI (D) shows more peripheral enhancement than the central stellate area.

DIFFERENTIAL DIAGNOSIS Hemangioma, hamartoma, extramedullary hematopoiesis.

DIAGNOSIS Sclerosing angiomatoid nodular transformation (SANT).

DISCUSSION SANT is a rare vascular benign tumor of the spleen. It is commonly encountered in middle-aged adults (mean age of 50), with a female predominance (2:1). Half of the patients are asymptomatic. Histologically, the mass is derived from red pulp, with central fibrous bands forming a stellate scar, explaining the imaging appearance. On non-contrast studies, the mass is hypodense on CT, and typically described as hypointense on T1-WI and T2-WI. Foci of internal hemorrhage may be more readily identifiable on MRI. Following contrast injection, the lesion demonstrates peripheral enhancement progressing centrally between the fibrous septae, accounting for the "spoke-wheel" appearance. Hemangiomas would not demonstrate a central scar. Hamartomas are typically hyperintense on T2-WI and have an early heterogeneous to uniform delayed enhancement. Extramedullary hematopoiesis would be positive on ^{99m}Tc-sulfur colloid SPECT, while SANT would not be.

CASE 38

CLINICAL HISTORY *38-year-old man presenting with an enlarging right upper quadrant mass.*

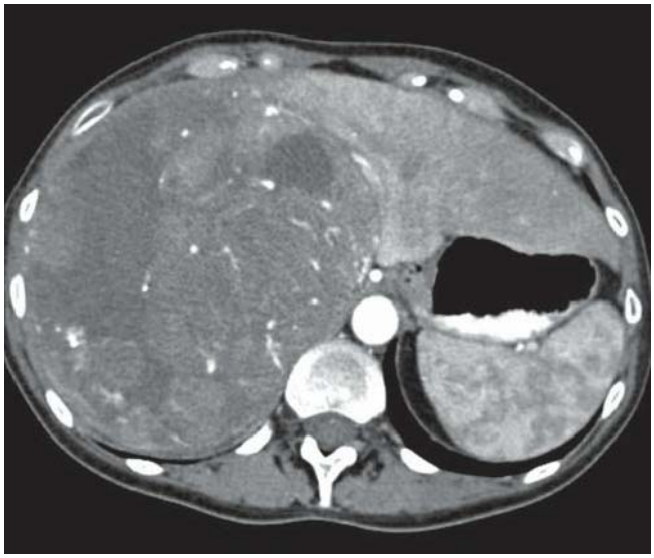

FIGURE 38A

FIGURE 38C

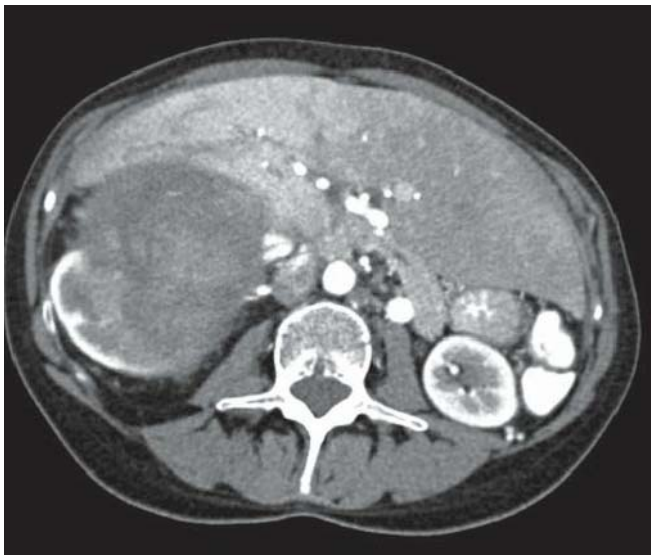

FIGURE 38B

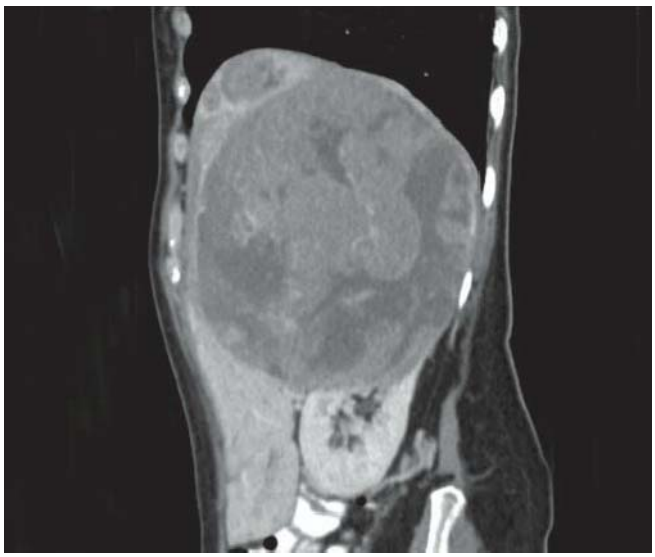

FIGURE 38D

FINDINGS Axial (A and B), coronal reformatted (C) arterial phase, and sagittal reformatted (D) portal venous phase CECT images demonstrate a 17-cm right heterogeneous suprarenal mass. The upper pole of the left kidney is involved by the mass, where a claw is seen. Note associated liver lesions (D).

DIFFERENTIAL DIAGNOSIS Renal cell carcinoma, hepatocellular carcinoma, pheochromocytoma, metastasis.

DIAGNOSIS Adrenocortical carcinoma.

DISCUSSION Adrenal carcinomas arise from the adrenal cortex, where hormones, such as cortisol, aldosterone, androgen, and estrogen, are produced. Most adrenal carcinomas produce hormones (most commonly cortisol) but the hormones produced are often not sufficient in number to cause symptoms. This accounts for the large size of these lesions before they become clinically symptomatic. The tumors are typically larger than 6 cm and can measure up to 20 cm. Adrenal carcinomas are easily seen on CT. They demonstrate enhancement with contrast, but this enhancement is often heterogeneous due to areas of necrosis. Calcifications may be present in 30% of

cases. Adrenal carcinomas can invade adjacent organs, such as the liver, spleen, and kidney, as seen in this case. Vascular invasion can also occur into the adrenal vein, which drains into the IVC. The differential diagnosis includes adrenal metastases, which are typically smaller, and pheochromocytomas, which are typically clinically symptomatic and thus present when the lesion is much smaller. As the renal and hepatic parenchyma can be involved, an exophytic primary renal or hepatic tumor should also be considered in the differential diagnosis. Biopsy of the adrenal gland can easily be performed in most situations to confirm the diagnosis. In this case, it would be preferable to biopsy a liver lesion, which represents a metastasis until proven otherwise, in order to stage and diagnose the tumor at the same time.

CASE 39

CLINICAL HISTORY *62-year-old man with acute episode of epigastric pain. He was admitted to the hospital and a day later developed acute drop in hematocrit.*

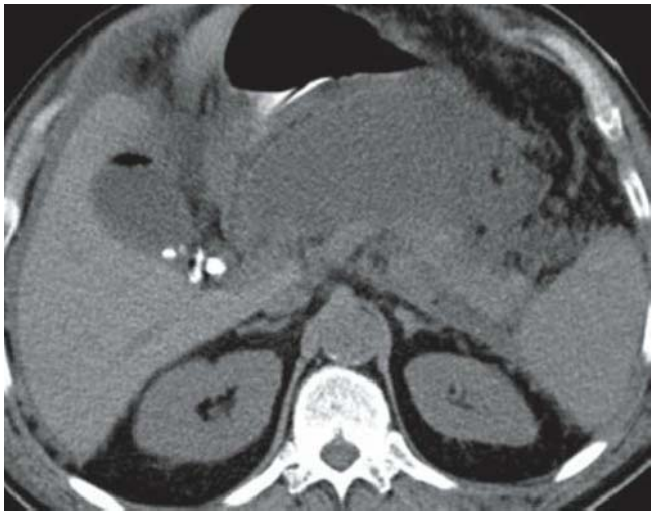

FIGURE 39A

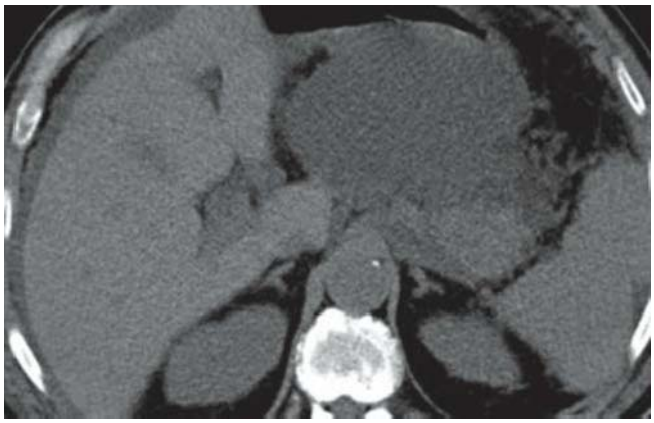

FIGURE 39B

FIGURE 39C

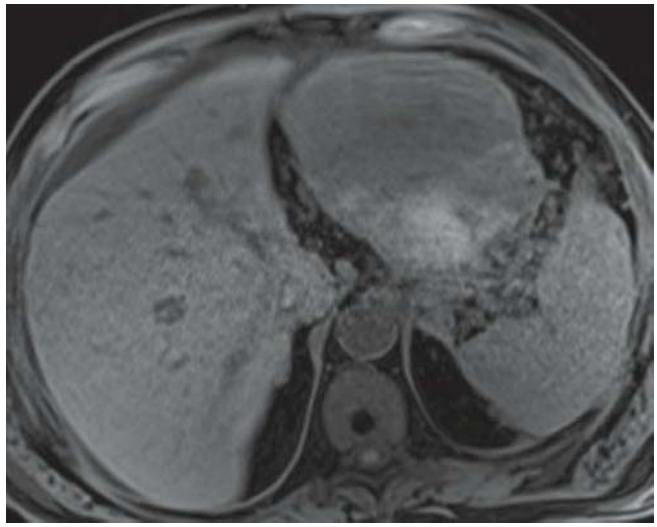

FIGURE 39D

FINDINGS Axial consecutive NECT images (A and B) obtained at the time of initial presentation demonstrate acute pancreatitis with cholelithiasis. A stent is seen within the pancreatic head and the air within the gallbladder is secondary to a common duct stent. Image (B) demonstrates a 9-cm, well-defined cystic lesion abutting the greater curvature of the stomach. Axial NECT image (C) obtained the next day demonstrates internal development of hyperattenuating debris in the dependent aspect of the cyst. Axial T1-WI MR Image (D) confirms the high T1 signal of the layering hyperattenuating material, compatible with interval bleeding into the walled off necrosis.

DIFFERENTIAL DIAGNOSIS Mucinous cystic neoplasm, necrotic tumor (metastasis, nonhyperfunctioning endocrine tumor).

DIAGNOSIS Pancreatic walled off necrosis with interval bleed.

DISCUSSION Pancreatic walled off necrosis and pseudo cyst formation are among the many complications of acute and chronic pancreatitis. The majority of peripancreatic fluid collections will resolve spontaneously without drainage. Approximately 10% of patients, however, will form a

pseudocyst. These cysts differ from true congenital cysts in that they do not have an inner epithelial lining. A fluid collection is not usually considered a true pseudocyst until it is approximately 6 weeks old and has developed a mature fibrotic wall. At that time, it is unlikely to resolve on its own. Drainage of noninfected pseudocysts is usually reserved for those larger than 5 cm, those that are enlarging, or those that are symptomatic for the patient. The main differential diagnosis for a pseudocyst is a mucinous cystic neoplasm. Patients with mucinous cystic neoplasms do not usually have a history of pancreatitis or demonstrate signs of chronic pancreatitis. If no history of pancreatitis can be elicited, then a mucinous cystic neoplasm must be considered, especially if the patient is a middle-aged woman.

CASE 40

CLINICAL HISTORY *50-year-old man presenting with a history of right renal mass.*

FIGURE 40A

FIGURE 40C

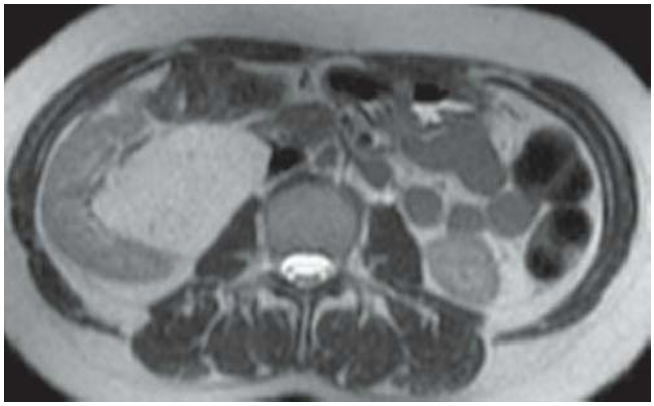

FIGURE 40B

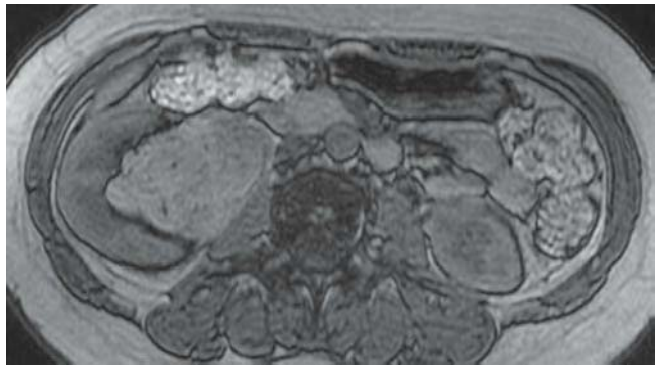

FIGURE 40D

FINDINGS Fat-suppressed post contrast coronal T1-WI image (A) demonstrates a large partially exophytic hypointense mass involving the right kidney. The lesion is mildly hyperintense on axial T2W1 (B). In-phase (C) and out-of-phase (D) T1-WIs demonstrates drop of signal on the out-of-phase image, consistent with a fat containing lesion.

DIFFERENTIAL DIAGNOSIS None.

DIAGNOSIS Angiomyolipoma.

DISCUSSION An angiomyolipoma (AML) is a benign renal mass that is composed of fat, smooth muscle, and abnormal blood vessels. Those tissues are present in variable quantity within the mass, such that approximately 95% of AMLs will have fat components detectable by imaging. CT and MRI are often diagnostic due to their ability to detect fat with high specificity. On CT, the fat-containing portions of the lesion will measure less than –10 Hounsfield units (HU) on both nonenhanced CT (NECT) and CECT, a threshold that is considered diagnostic for fat. On MRI, the fat in the lesion

will follow the signal intensity of the adjacent retroperitoneal subcutaneous fat. In addition, fat suppression techniques are required for absolute confirmation of fat within a lesion. However, the ability of MRI to detect fat within a lesion using either fat-suppression techniques or in- and out-of-phase images depends on the quantity of fat present within each voxel imaged. Enhancement is usually pronounced because of the abnormal vessels present in AML.

CASE 41

CLINICAL HISTORY *65-year-old woman presenting with a prior history of multiple abdominal surgery and pelvic radiation for uterine cancer presents with chronic abdominal pain.*

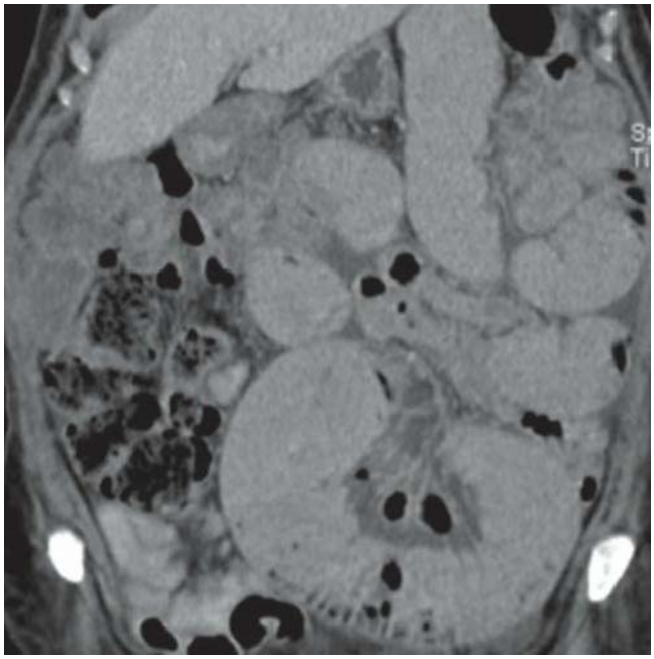

FIGURE 41A

FIGURE 41B

FINDINGS Axial (A and B) CECT images and reformatted images (B and D) reveal post-op changes consistent with right orchiectomy. There is a large wedge-shaped area of hypodensity within the left testes with edema of the adjacent structure, consistent with a testicular infarct.

DIFFERENTIAL DIAGNOSIS None.

DIAGNOSIS Small bowel obstruction secondary to an adhesion.

DISCUSSION CT has traditionally been used to reveal the site, level, and cause of obstruction and to display the signs of threatened bowel viability. Oral contrast agents may not be necessary because the fluid and gas in the dilated bowel provide sufficient contrast. Intravenous (IV) administration of contrast material is preferred for the evaluation of ischemia. The criterion of small bowel dilatation is defined as 2.5 cm calculated from outer wall to outer wall. The transition point is determined by identifying a caliber change between dilated proximal and collapsed distal small bowel

FIGURE 41C

FIGURE 41D

loops. Multiplanar reformations may aid in determining the site and level of obstruction. Complete versus partial obstruction of the small bowel is determined by the degree of distal collapse, proximal bowel dilatation, and transit of ingested contrast material. Adhesions are responsible for more than half of all small bowel obstructions, followed by hernias and extrinsic compression due to neoplastic growths. Radiation enteritis frequently involves loops of small bowel located within the radiation therapy port. The normal loops of small bowel in the pelvis make radiation enteritis unlikely.

CASE 42

CLINICAL HISTORY *53-year-old man presenting with elevated white blood count and serum bilirubin level post cholecystectomy.*

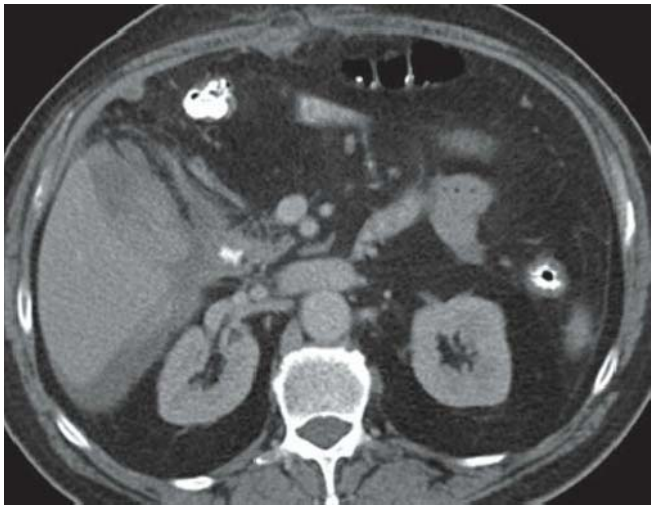

FIGURE 42A

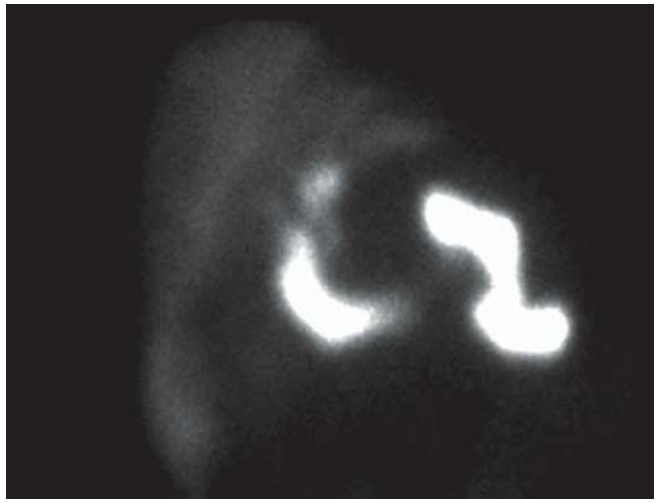

FIGURE 42C

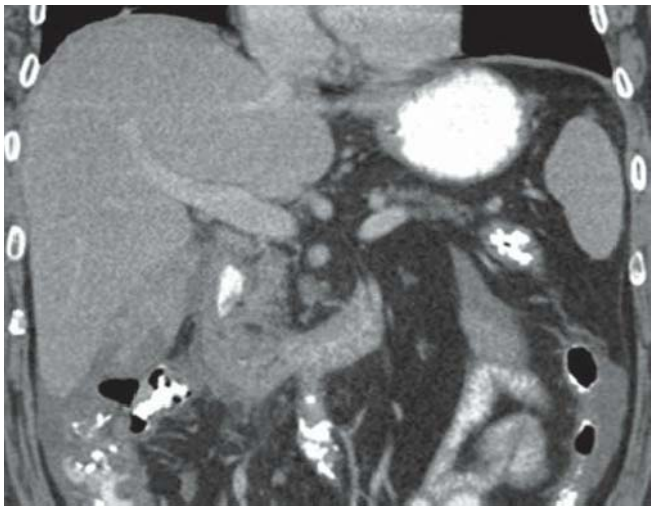

FIGURE 42B

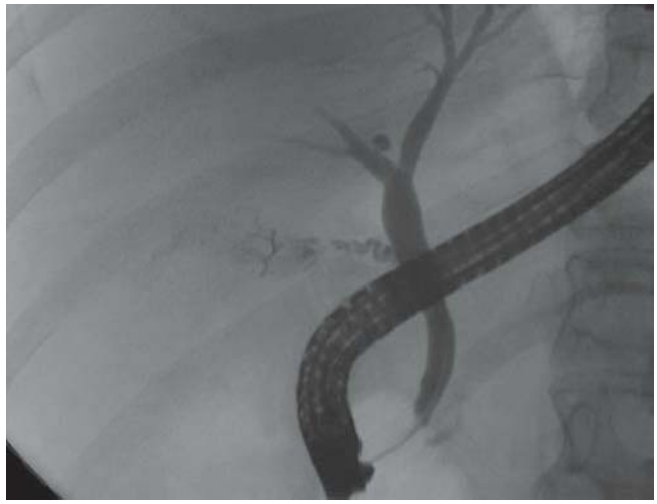

FIGURE 42D

FINDINGS Axial (A) and coronal reformatted (B) CECT images demonstrate increased density material in the gallbladder fossa and fluid in the right paracolic gutter. Hepatobiliary scintigraphy image (C) shows abnormal tracer accumulation in the same two locations. ERCP image (D) shows contrast extravasation from the cystic duct stump.

DIFFERENTIAL DIAGNOSIS Hematoma, abscess.

DIAGNOSIS Cystic duct stump leak.

DISCUSSION Cholecystectomies have a reported complication rate of approximately 2%. In this case, the hyperdense material in the gallbladder fossa could simply represent blood, and a high index of clinical suspicion for a bile duct leak is capital in establishing a diagnosis. Large quantities of bile in the abdominal cavity will form large bilomas, which very often exert significant mass effect on the liver surface. Percutaneous sampling can be performed and the aspirated fluid can be sent for bilirubin analysis to confirm a suspected bile leak. As in this case, hepatobiliary scintigraphy is useful to document small extravasation of the radio-tracer in the abdominal cavity. Eovist-enhanced MRI has also been utilized to detect bile leaks. Bilirubin is absorbed by the peritoneal surfaces, which explains the elevation of the serum bilirubin level in those patients. Bile duct leaks can originate from the cystic stump, as in this case, from a more catastrophic common bile duct or common hepatic duct injury, or from small ducts of Luschka, which are accessory ducts

draining directly from the liver parenchyma into the gallbladder fossa. Initial treatment of a confirmed bile leak is through insertion of a biliary stent, providing the injury is less than 5 mm, to preferentially redirect the bile into the duodenum. Other cholecystectomy complications include vascular injury—hematoma, abscess, seroma, bile duct obstruction, laparoscopy port hernia, retained stones, and dropped gallstones.

CASE 43

CLINICAL HISTORY *47-year-old woman presenting with chronic abdominal pain.*

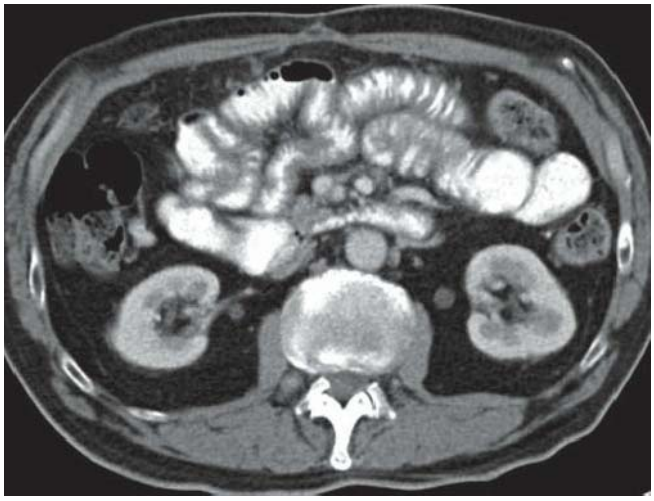

FIGURE 43A

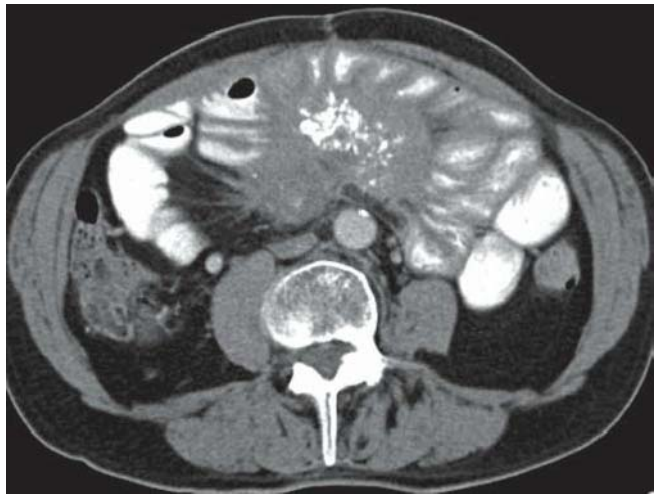

FIGURE 43C

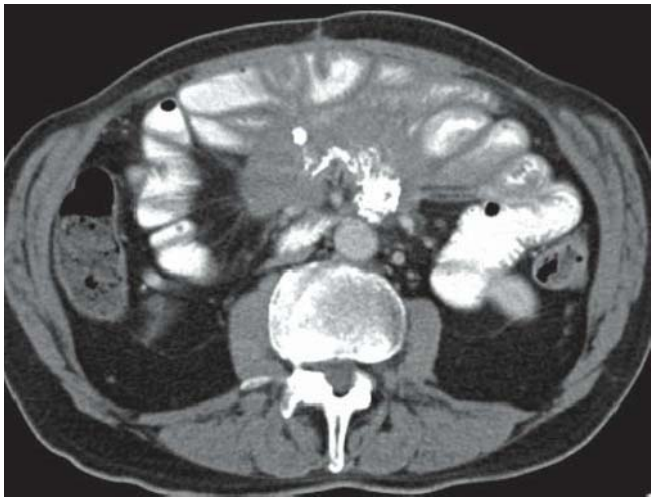

FIGURE 43B

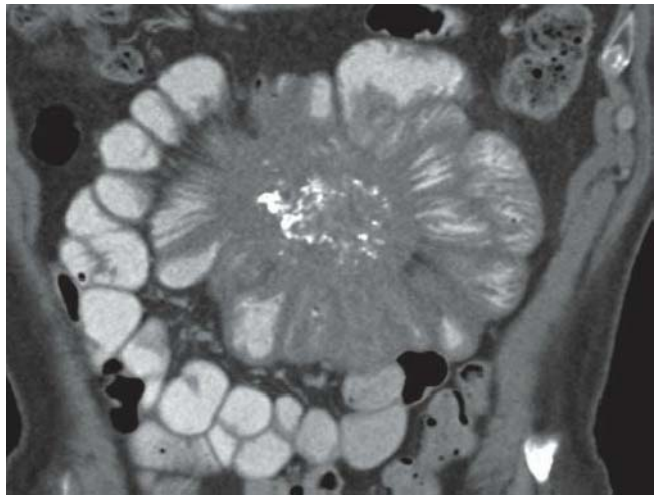

FIGURE 43D

FINDINGS Axial (A–C) and coronal reformatted (D) CECT images demonstrate a calcified soft tissue mass infiltrating the small bowel mesentery and causing engorgement of the mesenteric vessels. There is wall thickening of many small bowel loops anteriorly.

DIFFERENTIAL DIAGNOSIS Fibromatosis, metastasis, carcinoid, lymphoma, sarcoma.

DIAGNOSIS Slerosing mesenteritis (retractile mesenteritis).

DISCUSSION Sclerosing mesenteritis is a disorder of unknown etiology that results in chronic inflammation and fibrosis. Depending on the predominant tissue type within the mass, sclerosing mesenteritis can be subgrouped as (1) mesenteric panniculitis (inflammation), (2) mesenteric lipodystrophy (fat necrosis), and (3) retractile mesenteritis (fibrosis), as seen in this case. This disorder is usually confined to the mesentery and can occasionally calcify. By CT, retractile mesenteritis presents as a soft tissue mass that can contain fat and calcifications extending from the root of the mesentery toward the small bowel. This can lead to retraction and kinking of the bowel, resulting in crampy abdominal pain. The bowel wall thickening in this case is due to venous or lymphatic congestion. Carcinoid tumor arising in the small bowel can have mesenteric metastasis causing desmoplastic reaction, calcifications, and bowel kinking similar to retractile mesenteritis. This would be the best differential diagnosis in this example. Other entities that can involve the mesentery include lymphoma, metastases, and sarcomas. These do not usually calcify or cause bowel obstruction.

CASE 44

CLINICAL HISTORY *69-year-old woman presenting with an enlarging pelvic mass.*

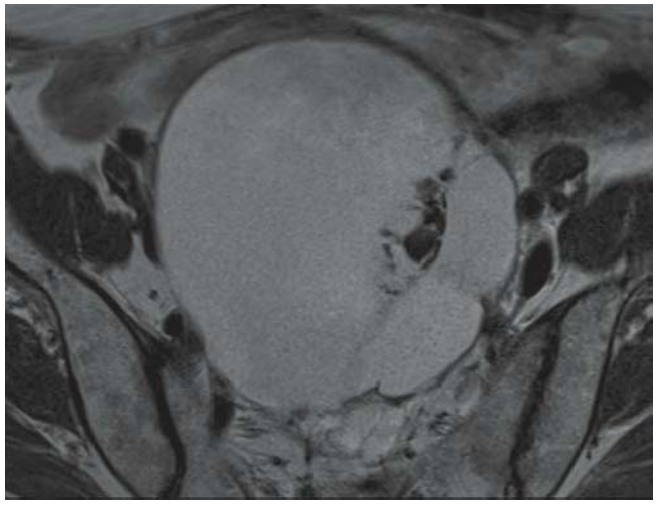

FIGURE 44A

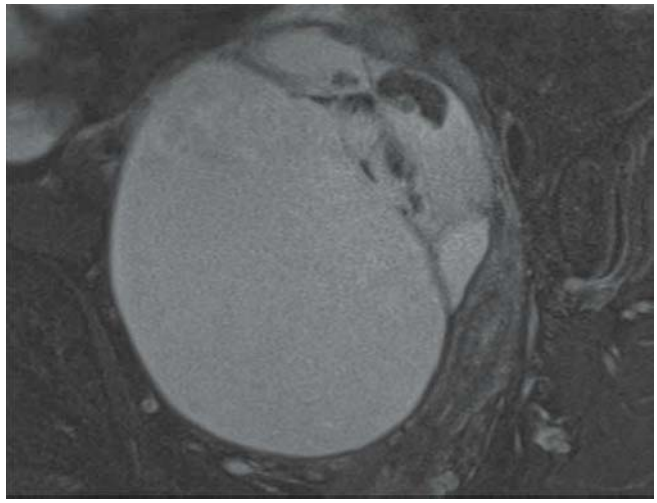

FIGURE 44C

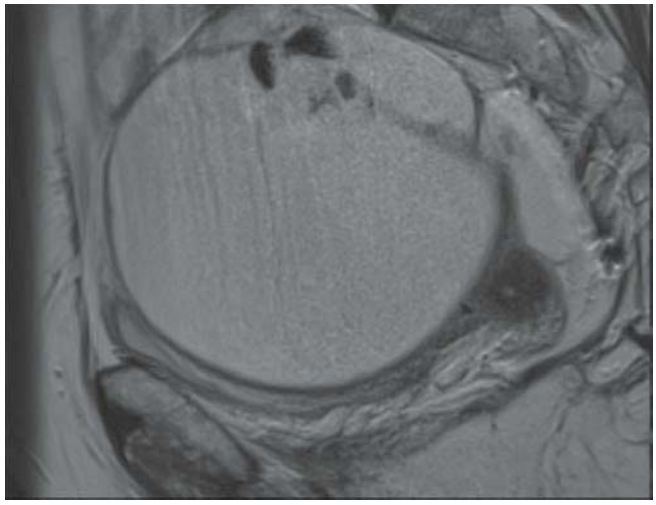

FIGURE 44B

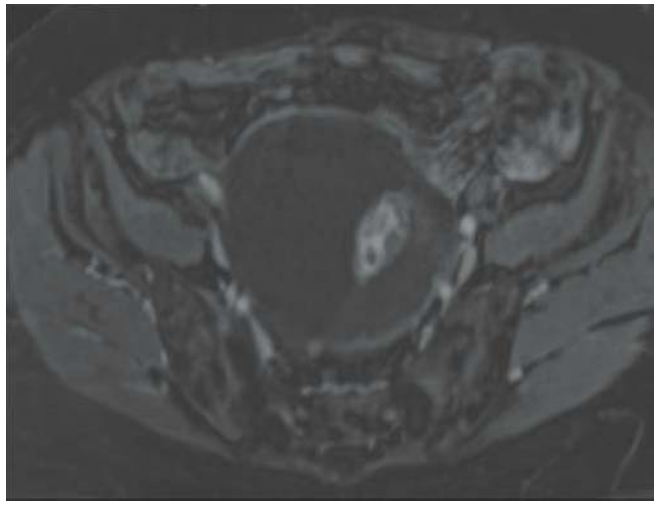

FIGURE 44D

FINDINGS Axial (A) and sagittal (B) T2-WIs and fat-suppressed axial T2-WI (C) demonstrate a multiloculated cystic pelvic mass with T2 dark nodular thickening of internal septations. The nodules and septations demonstrate enhancement on the gadolinium-enhanced, fat-suppressed axial T1-WI (D).

DIFFERENTIAL DIAGNOSIS Serous or mucinous cystadenoma or carcinoma, atypical mature teratoma, tubo-ovarian abscess, cystic metastasis.

DIAGNOSIS Serous cystadenofibroma.

DISCUSSION Serous cystadenofibromas are benign epithelial ovarian masses. They are defined as serous cystadenomas containing fibrous tissue. Epithelial ovarian tumors represent 85% of all ovarian tumors. About 60% of all the serous ovarian neoplasms are smooth-walled benign cystadenomas; 15% are of low malignant potential (borderline tumors). On imaging, the lesions present as a multilocular cystic mass with homogeneous CT attenuation or MRI signal intensity of the locules, a thin regular wall or septum, and no endocystic or exocystic vegetations. Different attenuation and signal intensity of the locules of a multilocular cystic mass are more typical of mucinous tumors. Serous cystadenomas can reach 30 cm in size with a mean diameter of 10 cm; mucinous cystadenomas tend to be larger (reaching 50 cm in size). Diagnosis of a benign ovarian neoplasm should only be made if the following features (accuracy of 84%) are present: entirely cystic mass, wall thickness less than 3 mm, lack of internal structure, and the absence of both ascites and invasive characteristics, such as peritoneal nodules or lymphadenopathy. After contrast administration, only the cyst wall and septations enhance.

CASE 45

CLINICAL HISTORY *36-year-old woman on oral contraceptives.*

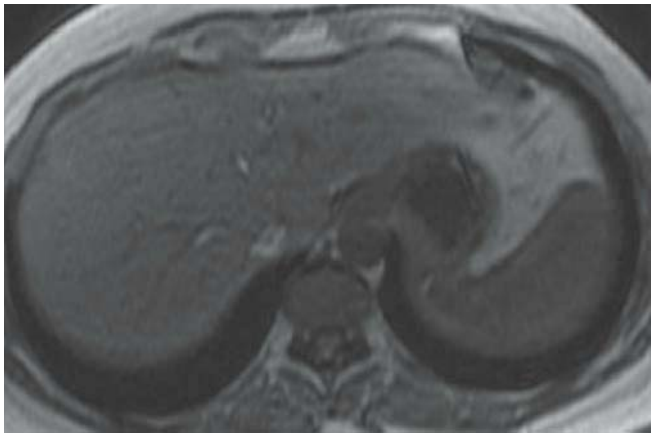

FIGURE 45A

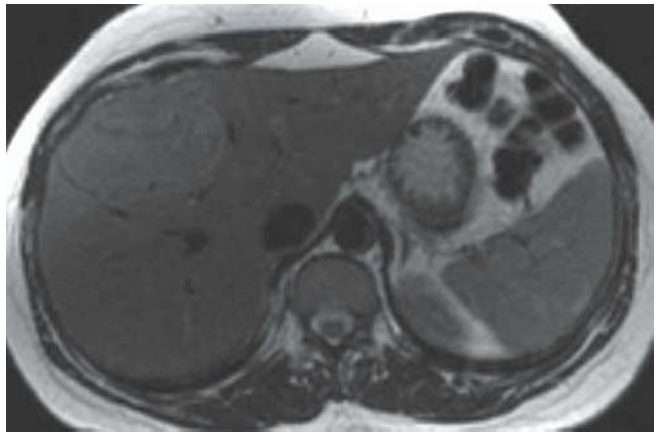

FIGURE 45C

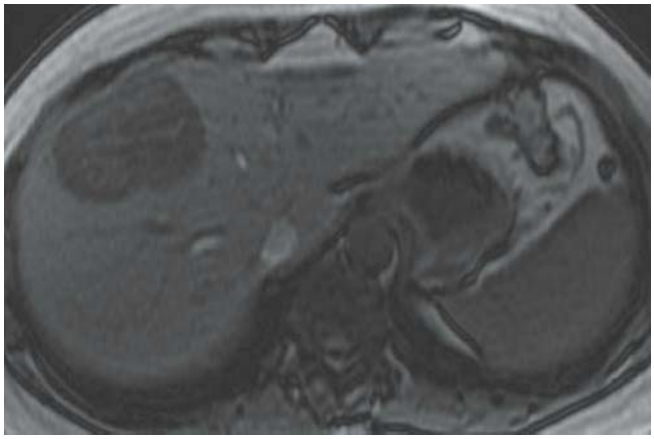

FIGURE 45B

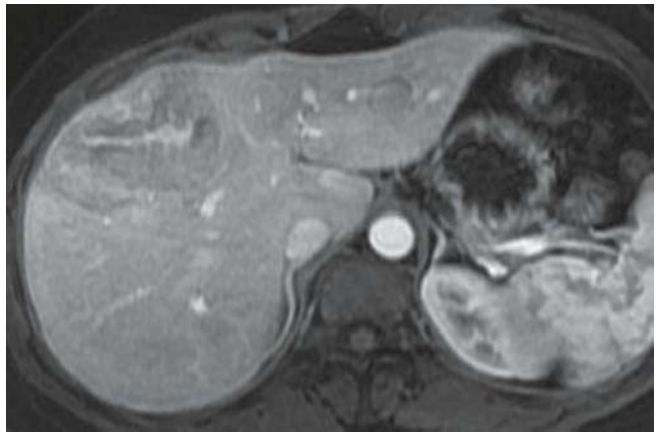

FIGURE 45D

FINDINGS Axial in-phase T1-WI (A) shows a subcapsular slightly hyperintense mass in right lobe of the liver, which demonstrates drop of the signal on the out-of-phase T1-WI (B). The mass is slightly hyperintense on the axial T2-WI (C). On gadolinium-enhanced, fat-suppressed axial T1-WI (D), the lesion shows heterogeneous enhancement, with some hyperenhancing central areas.

DIFFERENTIAL DIAGNOSIS Focal nodular hyperplasia, hepatocellular carcinoma, metastases.

DIAGNOSIS Hepatocellular adenoma.

DISCUSSION Hepatocellular adenoma is a benign neoplasm of the liver, composed of sheets of hepatocytes without veins or ducts. Typically, adenomas are solitary (80%). Oral contraceptive use is thought to lead to the development of adenomas as well as increase the risk of hemorrhage by the tumor. Although seen predominantly in females of childbearing age, males on anabolic steroids also have an increased risk. Type I glycogen storage disease is typically associated with multiple hepatocellular adenomas. Large adenomas are usually heterogeneous since they outgrow their blood supply and eventually hemorrhage or necrose. Up to 77% are found to contain fat when using chemical shift MR techniques. Hypervascular lesions could be focal nodular hyperplasia but FNH tend to enhance homogeneously and typically do not contain intracellular fat. A hepatocellular carcinoma would be less likely as no underlying cirrhosis is present. The age and sex of the patient, combined with the history of oral contraceptive use, make hepatocellular adenoma the best choice. Further differentiation between adenoma and FNH could be done with use of a hepato-specific MR contrast agent, such as gadobenate dimeglumine (MultiHance) or gadoxetic acid (Eovist–Primovist), since in FNH, there is delayed and persistent enhancement because of inadequate clearance of the agent.

CASE 46

CLINICAL HISTORY *34-year-old man presenting with persistent bloating after an episode of acute pancreatitis.*

FIGURE 46A

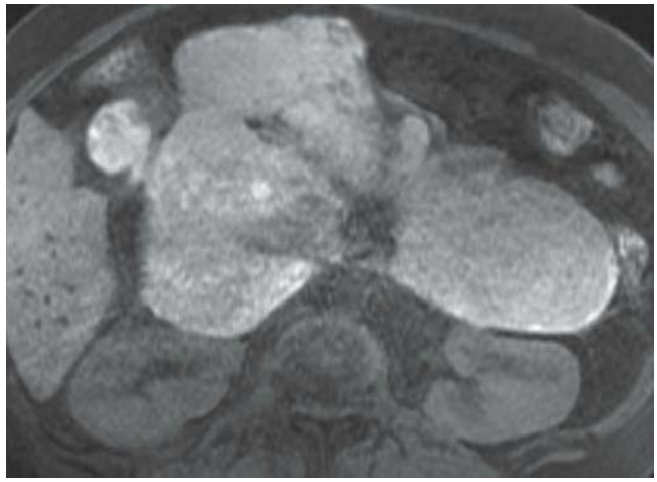

FIGURE 46C

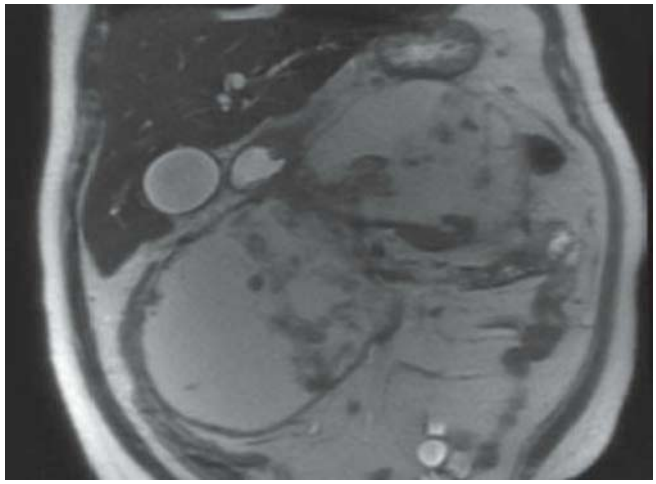

FIGURE 46B

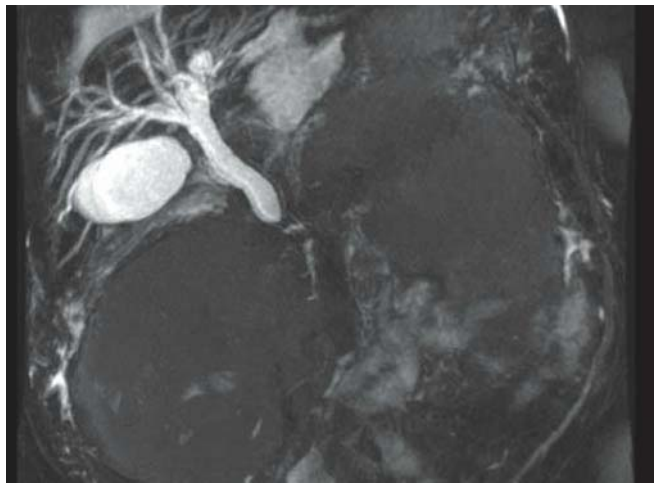

FIGURE 46D

FINDINGS Axial NECT image (A) demonstrates a large hypodense but heterogeneous collection occupying the entire pancreatic bed, with surrounding fat stranding. Axial T2-WI (B) shows the content is of bright fluid signal with internal hypointense debris. Fat-suppressed axial T1-WI (C) shows marked internal hyperintensity. Bile duct dilatation with distal CBD obstruction is visible on the thick-slab MRCP image (D). Hardly any normal pancreatic tissue is identifiable.

DIFFERENTIAL DIAGNOSIS None.

DIAGNOSIS Walled-off hemorrhagic pancreatic necrosis post acute necrotizing pancreatitis.

DISCUSSION In assessment of acute pancreatitis, MRI, as well as CT, can depict the presence and extent of necrosis and peripancreatic fluid collections. Several authors recommend intravenous gadolinium administration in imaging severe acute pancreatitis, particularly for the assessment of pancreatic parenchymal perfusion and presence of necrosis. The enlargement of the gland is well demonstrated on any sequence. Parenchymal edema is better shown on unenhanced T1-WI. Pancreatic enhancement is maximal within 20 to 40 seconds after gadolinium administration, and the extent of parenchymal necrosis is well demonstrated on sequential, multislice acquisition obtained during the first 1 to 2 minutes after injection. T2-WI sequences are the most sensitive in demonstrating fluid collections. Despite these results, CT retains several advantages: CT is widely accessible and less costly than MRI and is more sensitive in detecting small gas bubbles and calcifications. However, MRI combined with MRCP has become important in the evaluation of patients with suspected biliary pancreatitis, and MRI is superior to CT to detect hemorrhage and drainability of fluid collections. The hyperintense signal on T1-WI in this case is caused by hemorrhagic clot formation. The bile duct dilatation results acutely by swelling of the parenchyma, and later by compression from fluid collections or fibrosis.

CASE 47

CLINICAL HISTORY *60-year-old male who is status post-right orchiectomy for testicular carcinoma now presents with excruciating testicular pain.*

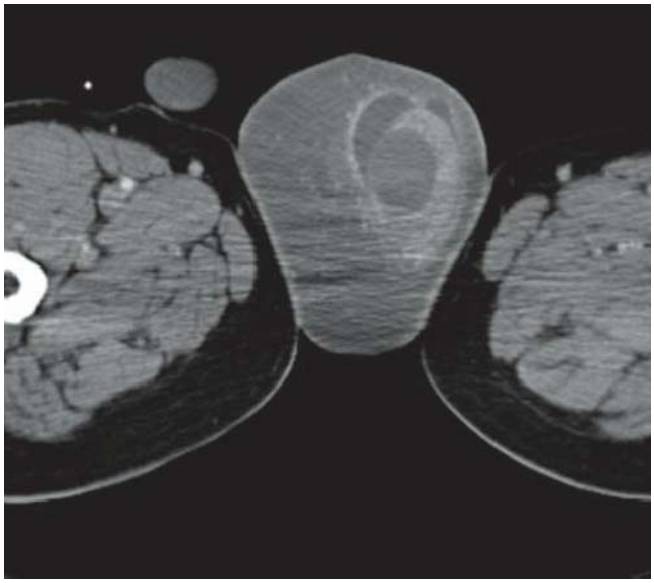

FIGURE 47A

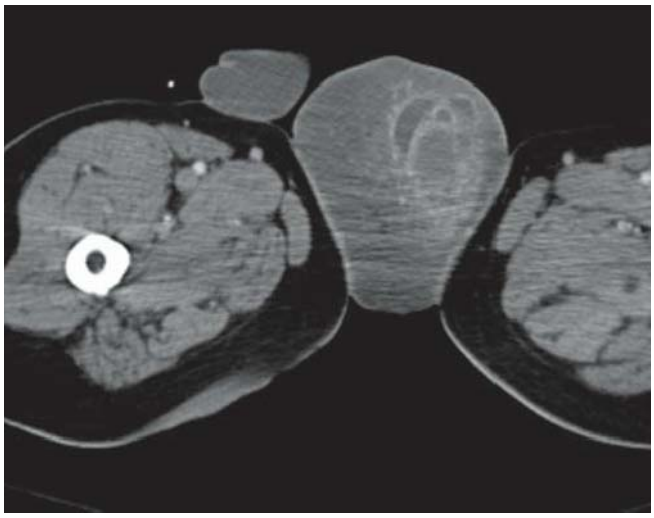

FIGURE 47B

FIGURE 47C

FIGURE 47D

FINDINGS Axial (A and C) CECT images and coronal reformatted images (B and D) reveal post-op changes consistent with right orchiectomy. There is a large wedge-shaped area of hypodensity within the left testes with edema of the adjacent structure, consistent with a testicular infarct.

DIFFERENTIAL DIAGNOSIS Testicular tumor.

DIAGNOSIS Testicular infarct.

DISCUSSION Testicular infarction is a partial ischemic process. Although mostly idiopathic, association with inflammatory events (epididymitis and orchitis), vasculitis, hematologic disorders (sickle cell and polycythemia vera), and bell-clapper anomaly have been described. This process usually affects men in the second through fourth decades of life. The upper pole of the testes is more prone to infarction secondary to the dual blood supply to the lower zone from the posterior epididymal artery. The first line in management is Doppler ultrasound, which demonstrates low flow and a segmental area of hypodensity within the testes. Differentiation from a low flow testicular tumor is difficult in some, in which case MRI would be of value in further evaluation as it easily shows the borders of the segmental testicular infarction on T2-WIs. Less frequently, CT is done as in our case due to history of prior surgery to evaluate for alternative pathology like bowel obstruction. An ultrasound was done at the same time, which demonstrated absent flow to the testes with increased flow to the epididymis, corresponding to testicular infarct and epididymitis and thereby confirmed the diagnosis.

CASE 48

CLINICAL HISTORY *50-year-old man presenting with fever, chills, and right upper quadrant pain.*

FIGURE 48A

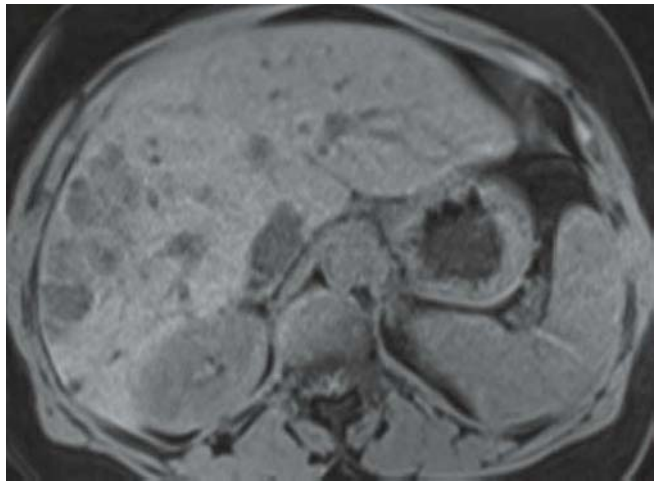

FIGURE 48C

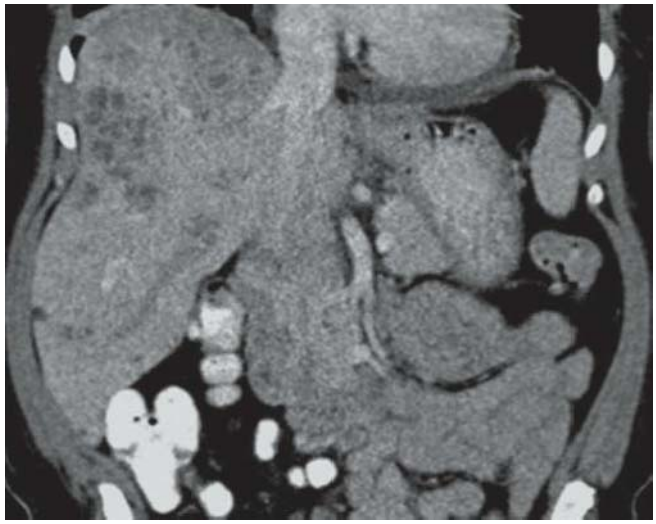

FIGURE 48B

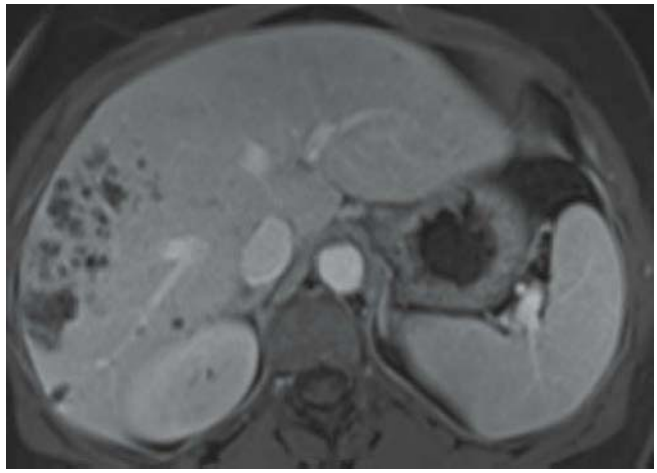

FIGURE 48D

FINDINGS Axial (A) and coronal reformatted (B) CECT images show nonenhancing right branch of the portal vein with scattered small hypodense hepatic lesions with rim enhancement. On pre– (C) and post– (D) gadolinium-enhanced, fat-suppressed axial T1-WIs, the lesions show rim enhancement, with the lack of signal in the portal main branches, predominantly the anterior division of the right portal branch.

DIFFERENTIAL DIAGNOSIS None.

DIAGNOSIS Portal vein thrombosis and hepatic abscesses.

DISCUSSION Portal vein thrombosis may be primary or secondary to other systemic or local disease. Liver cirrhosis is the most common cause of secondary portal vein thrombosis. Other secondary causes include tumor invasion (particularly hepatocellular carcinoma), trauma, blood dyscrasia, and intra-abdominal sepsis. Complete or partial obstruction of the regional portal vein branches is frequently observed around a hepatic abscess. Moreover, marked periportal inflammation and stenosis of the portal venules surrounding a hepatic abscess and associated thrombosis of the portal branches have also been reported. In this case, there is complete thrombosis of the anterior division of the right portal vein and its multiple branches. In the setting of hepatic lesions with portal vein thrombus, it is important to differentiate between a bland and tumor thrombus. The bland thrombus as in this case would not demonstrate any enhancement, whereas a tumor thrombus would demonstrate enhancement on post-gadolinium sequences.

CASE 49

CLINICAL HISTORY *49-year-old man presenting with fatigue and anemia.*

FIGURE 49A

FIGURE 49C

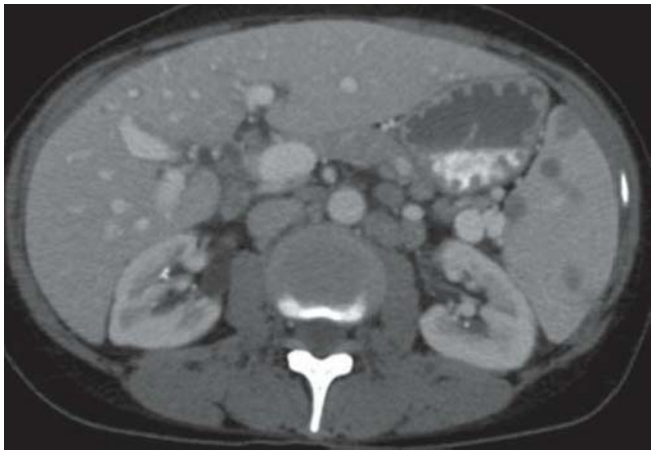

FIGURE 49B

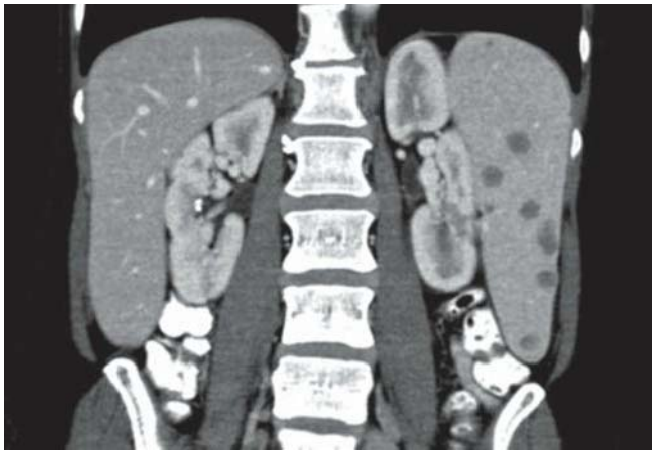

FIGURE 49D

FINDINGS Axial (A and B) and coronal reformatted (C and D) CECT images demonstrate several small hypodense splenic lesions in an enlarged spleen. Note the presence of retrocrural and retroperitoneal adenopathy.

DIFFERENTIAL DIAGNOSIS Abscesses, metastases.

DIAGNOSIS Splenic lymphoma.

DISCUSSION Lymphomatous involvement of the spleen is associated with nodal disease and systemic involvement is much more common than primary splenic lymphoma without nodal disease. Involvement of the spleen can be seen in both Hodgkin and non-Hodgkin lymphomas and occurs more commonly in an older population (older than 50 years of age). Patients typically have nonspecific symptoms of fever, night sweats, and left upper quadrant pain. These symptoms can mimic an abscess. CECT is accurate in detecting splenic lymphoma in its late stages but is less accurate in early stages when the lesions are small or diffusely infiltrating the spleen. In these cases, splenectomy is often necessary to confirm the diagnosis. Splenic lymphoma can present on CT imaging as diffuse splenic enlargement, multiple small masses (<2 cm), and one or multiple large masses. The presence of multiple hypodense lesions in the spleen is nonspecific and can be seen in metastases and abscesses. In selected cases, MRI can be performed to further characterize splenic lesions.

CASE 50

CLINICAL HISTORY *36-year-old woman presenting with pelvic pressure and urinary frequency.*

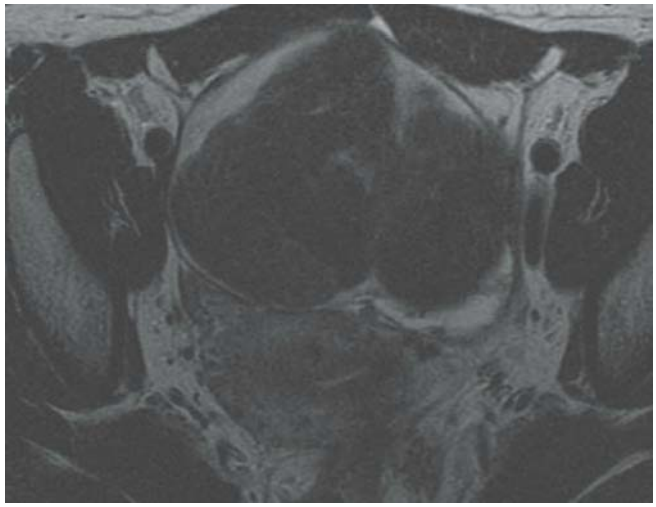

FIGURE 50A

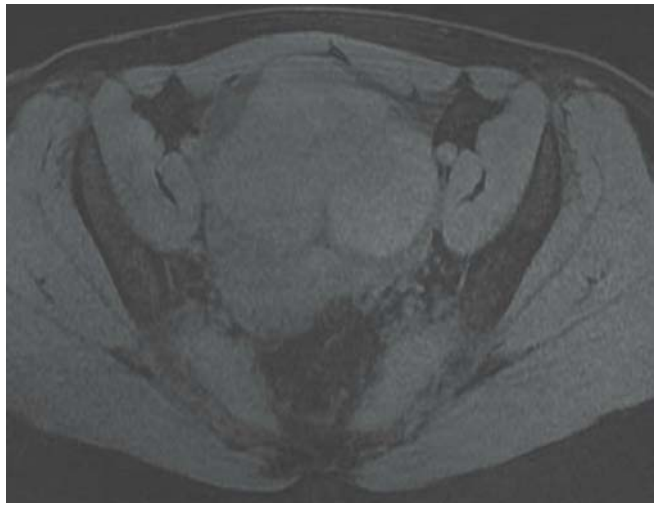

FIGURE 50C

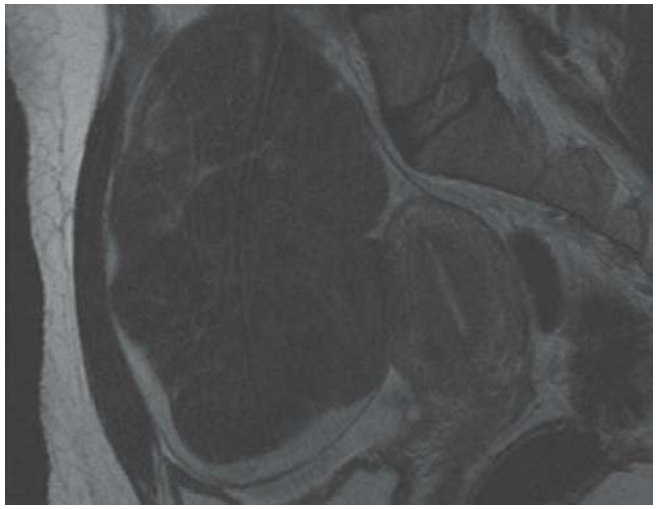

FIGURE 50B

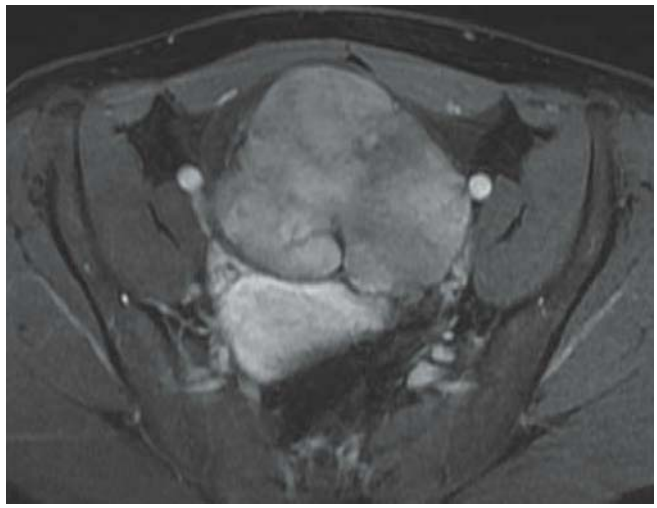

FIGURE 50D

FINDINGS Axial (A) and sagittal (B) T2-WIs demonstrate a multilobulated, heterogeneous, and hypointense mass anterior to the uterus, without clear communication with it. Unenhanced (C) and gadolinium-enhanced (D) fat-suppressed axial T1-WIs show heterogeneous and minimal enhancement of the mass.

DIFFERENTIAL DIAGNOSIS Pedunculated subserosal uterine or broad ligament leiomyoma, Brenner tumor.

DIAGNOSIS Ovarian fibroma/fibrothecoma.

DISCUSSION Fibromas, fibrothecomas, and thecomas represent approximately 4% of all ovarian tumors and 50% of sex cord stromal tumors. These benign tumors typically occur in the second and third decades of life. Fibromas are composed of collagen-producing spindle cells and are not hormonally active. They can be associated with two clinical syndromes. First, fibromas associated with ascites and pleural effusion are defined as Meigs' syndrome (1% of all fibromas). Even in the absence of the syndrome, ascites is commonly associated with all but small fibromas. Second, they can occur in the basal cell nevus syndrome and are typically bilateral, multinodular, and calcified. Fibrothecomas also contain a small amount of thecal cells, which have intracellular lipid and are often hormonally active. Thus, the latter can be associated with endometrial hyperplasia from hormonal stimulation. On MRI, fibromas and fibrothecomas are isointense on T1-WI and hypointense on T2-WI compared with skeletal muscle. In fibromas, edema and cystic

degeneration can be present (hyperintense on T2-WI), especially in large lesions. Unlike fibroids, they are frequently encapsulated and on gadolinium-enhanced images they only demonstrate mild enhancement. Calcifications (hypointense foci on T1- and T2-WI) may be present. In order to differentiate ovarian fibromas/-thecomas from uterine leiomyomas, the key feature is to depict "feeding vessels" from the uterus to the mass, which indicates the uterine origin of the lesion and thus suggests a uterine leiomyoma. Broad ligament fibroids and Brenner tumors may have a similar appearance.

CASE 51

CLINICAL HISTORY *57-year-old man presenting with epigastric pain and weight loss.*

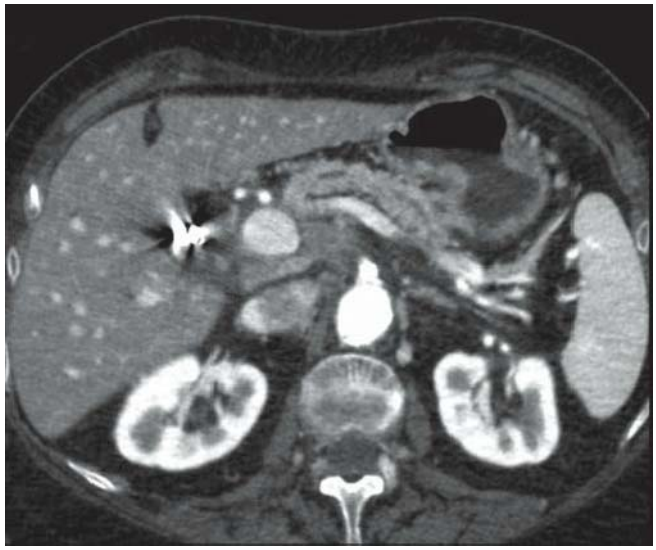

FIGURE 51A

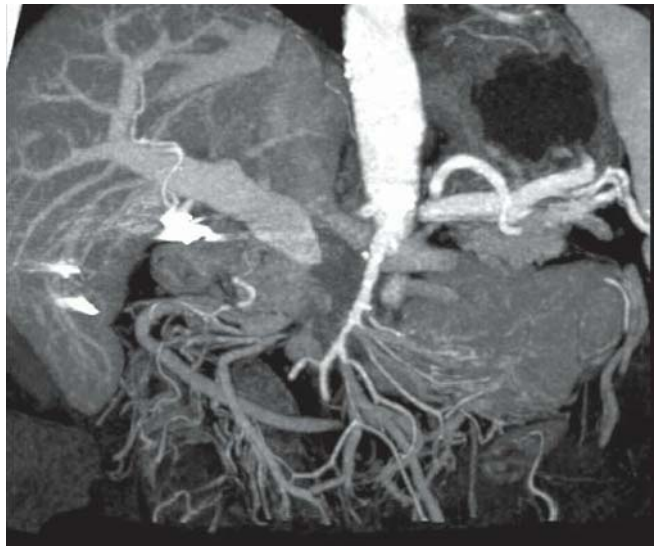

FIGURE 51C

FIGURE 51B

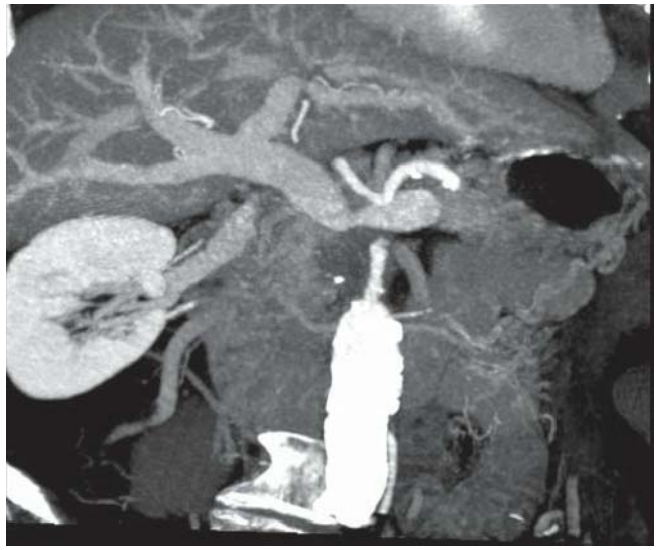

FIGURE 51D

FINDINGS Axial (A and B) and coronal MIP (C and D) CECT images demonstrate a low-attenuation ill-defined lesion in the head of the pancreas. It encases the superior mesenteric artery and obstructs the main pancreatic duct which is dilated. There is occlusion of the superior mesenteric vein. The portal confluence is narrowed, causing engorgement of the mesenteric veins.

DIFFERENTIAL DIAGNOSIS Pancreatitis.

DIAGNOSIS Pancreatic ductal adenocarcinoma with superior mesenteric vein occlusion.

DISCUSSION Key roles for CT in the evaluation of pancreatic ductal adenocarcinoma are to confirm the diagnosis and to determine the resectability. One of the most reliable staging criteria for resectability is the presence of vascular invasion. The fat plane between the pancreas and the superior mesenteric vein (SMV) can be obliterated normally. This does not necessarily indicate vascular invasion by the malignancy. However, if the SMV is obstructed by the mass then vascular invasion is likely present. In contradistinction, if the perivascular fat around the SMA is obliterated by the mass or there is thickening of the vessel wall, as seen in this case, then vascular invasion is suspected. Typically, encasement of more than 180 degrees of the circumference of the artery indicates vascular invasion. The presence of mesenteric, gastric, and omental collateral vessels should also suggest SMV or splenic vein thrombosis. These collaterals, typically the gastrocolic trunk entering the SMV, are usually seen well on CECT image.

CASE 52

CLINICAL HISTORY *31-year-old man presenting with fatigue.*

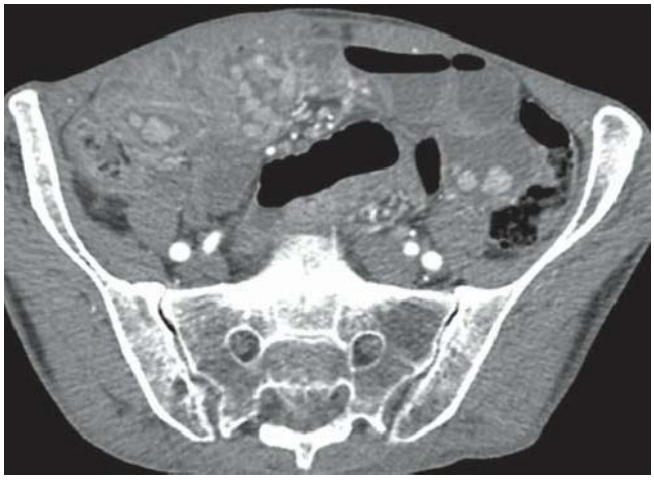

FIGURE 52A

FIGURE 52B

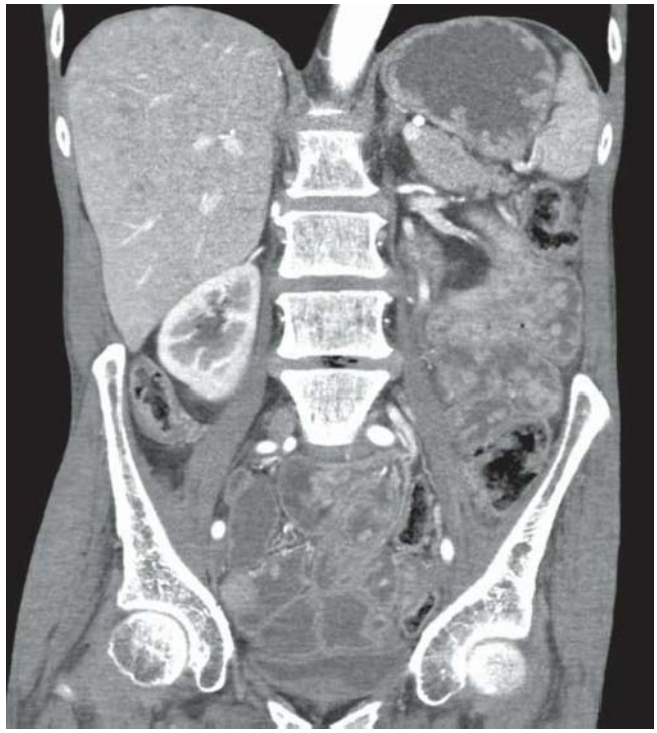

FIGURE 52C

FINDINGS Axial (A and B) and coronal reformatted (C) CECT images demonstrate several enhancing nodular lesions in the stomach and small bowel lumen.

DIFFERENTIAL DIAGNOSIS Cronkhite-Canada syndrome, Gardner variant of familial adenomatous polyposis, juvenile polyposis syndrome.

DIAGNOSIS Peutz-Jeghers syndrome.

DISCUSSION Peutz-Jeghers syndrome (PJS) is an autosomal dominant inherited disorder characterized by intestinal hamartomatous polyps in association with mucocutaneous melanocytic macules of the lips and other parts of the face, hands, and feet. PJS has been described in all races, the occurrence in males and females is about equal, and the average age of diagnosis is approximately 25 years. A 15-fold elevated relative risk of developing cancer exists in PJS over that of the general population; cancer primarily is of the GI tract and of the female and male reproductive tracts. The hamartomas in the small intestine have a low risk of becoming cancerous; however, polyps in the stomach and colon are more likely to do so and should be monitored endoscopically. The principal causes of morbidity in PJS stem from the intestinal location of the polyps (i.e., small intestine, colon, and stomach). Morbidity includes small intestinal obstruction and intussusception (43%), abdominal pain (23%), hematochezia (14%), and prolapse of a colonic polyp (7%). The polyposis syndromes may be classified as familial inherited (autosomal dominant) or nonfamilial. The inherited polyposis syndromes can be further subdivided into two groups depending on whether the polyps are adenomas or hamartomas. The adenomatous polyposis syndromes include the classic familial adenomatous polyposis (FAP), Gardner syndrome, and Turcot syndrome. Hamartomatous familial polyposis syndromes include PJS, juvenile polyposis syndrome, Cowden disease, and Ruval-Caba-Myhre-Smith syndrome. The non-inherited polyposis syndromes include Cronkhite-Canada syndrome and a variety of miscellaneous non-familial polyposis.

CASE 53

CLINICAL HISTORY *43-year-old Asian woman presenting with jaundice and fever.*

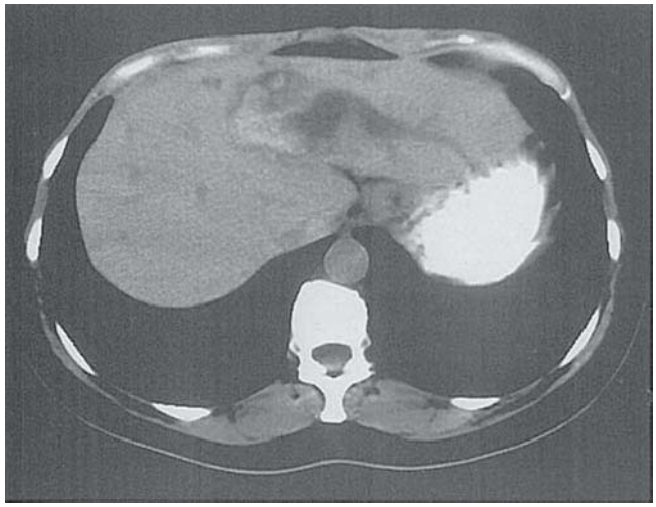

FIGURE 53A

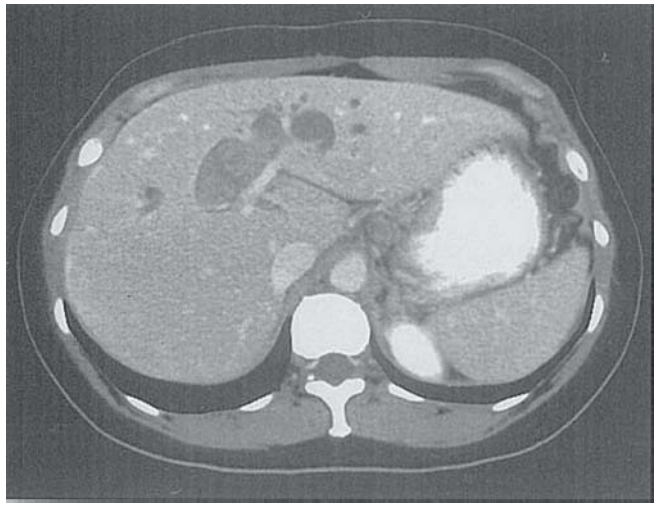

FIGURE 53C

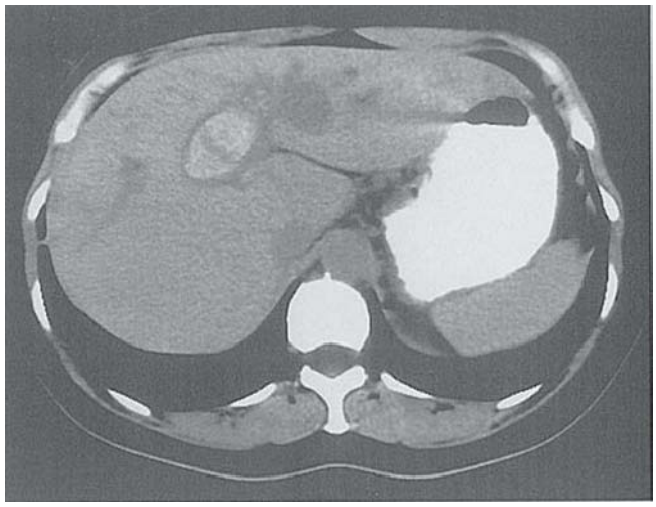

FIGURE 53B

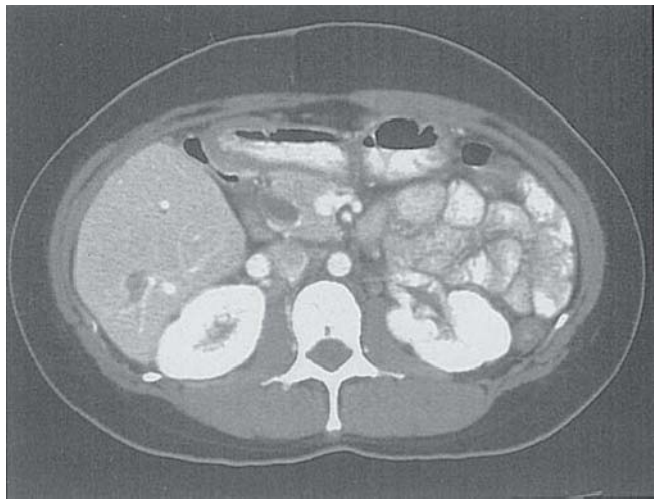

FIGURE 53D

FINDINGS Axial NECT images (A and B) demonstrate intrahepatic biliary dilatation with calcified foci within the dilated ducts. Axial CECT images (C and D) again demonstrate the dilated ducts and the calcified foci. Note the dilated common bile duct.

DIFFERENTIAL DIAGNOSIS Caroli disease.

DIAGNOSIS Oriental cholangiohepatitis (recurrent pyogenic cholangitis).

DISCUSSION Recurrent pyogenic cholangitis is a disease that is endemic to the Far East and is thought to be secondary to infestation by the parasite *Clonorchis sinensis* due to ingestion of raw fish. The parasite is thought to either cause direct damage to the biliary ducts or act as a focus for the formation of stones. This results in biliary dilatation and cholangitis. Patients present with intermittent bouts of jaundice, fever, and right upper quadrant pain. Radiologically, recurrent pyogenic cholangitis presents with intrahepatic and often extrahepatic biliary dilatation. The intrahepatic dilatation is often found centrally, and multiple areas of strictures are seen on cholangiograms. Stone formation and sludge is commonly seen in these patients. This case demonstrates intrahepatic and extrahepatic biliary dilatation, stone formation, and a clinical history that helps make the diagnosis almost certain. Caroli disease with abscess formation is another diagnostic possibility, but the extrahepatic biliary dilatation is not seen in Caroli disease.

CASE 54

CLINICAL HISTORY *57-year-old man presenting with symptoms of acute recurrent pancreatitis.*

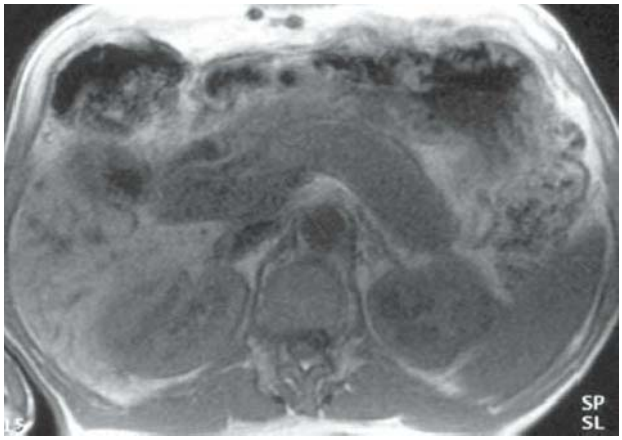

FIGURE 54A

FIGURE 54B

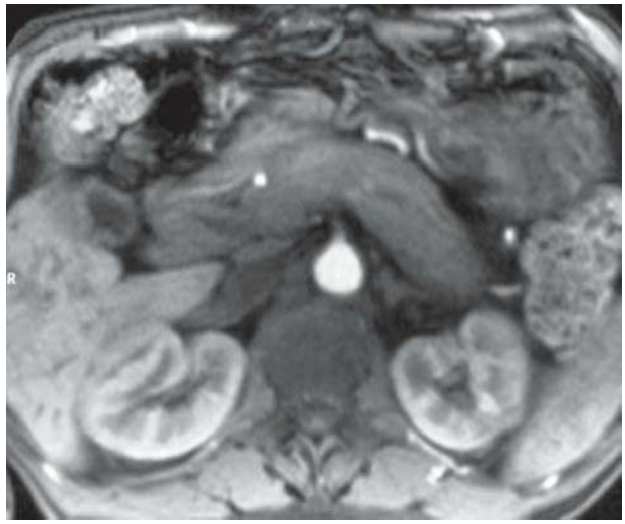

FIGURE 54C

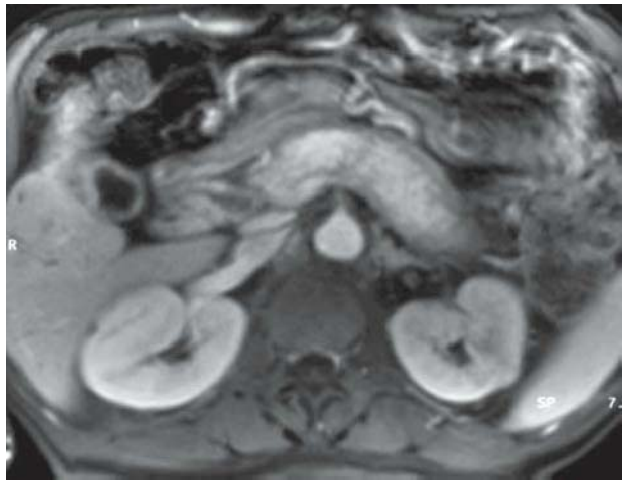

FIGURE 54D

FINDINGS Axial T1-WI (A) and T2-WI (B) show a swollen pancreas and abnormal low signal of the pancreas on T1-WI and increased signal intensity on T2-WI. Also note the peripheral hypointense rim surrounding the pancreas on T2-WI. After gadolinium administration, the pancreas shows a delayed enhancement on the pancreatic phase fat-saturated T1-WI (C) and shows lack of enhancement of the peripheral rim on the portal venous phase T1-WI (D). Also note the abnormal rim-like enhancement of the common bile duct (CBD).

DIFFERENTIAL DIAGNOSIS Diffuse pancreatic ductal adenocarcinoma, acute pancreatitis.

DIAGNOSIS Autoimmune pancreatitis.

DISCUSSION Autoimmune pancreatitis, also known as sclerosing or lymphoplasmacytic pancreatitis, is an increasingly recognized subtype of chronic pancreatitis. It is frequently associated with other autoimmune diseases, such as sclerosing cholangitis and retroperitoneal fibrosis. Immunoglobulin G4 levels are elevated in approximately 60% of cases. On contrast-enhanced CT (CECT), the pancreas is typically swollen and appears sausagelike in shape. The normal pancreatic lobulations are absent. The biliary duct is typically dilated due to the periductal fibrosis in the pancreatic head. The enhancement of the gland is heterogeneous and delayed after iodinated contrast administration. On MRI, the pancreas is abnormally hypointense on T1-WI and normal or mildly hyperintense on T2-WI. A rim of fibrosis, hypointense on both T1-WI and T2-WI, is sometimes seen encircling the gland. After gadolinium administration, the enhancement of the gland is delayed, and lack of enhancement of the peripheral fibrotic rim is typically detected. Enhancing periductal fibrosis around the CBD may also be present. Magnetic resonance cholangiopancreatography (MRCP) is helpful in diagnosing associated strictures in the intra- or extrahepatic bile ducts. Despite the fact that autoimmune pancreatitis can be treated noninvasively by steroids, it is currently the most common benign condition for which Whipple procedures are performed.

CASE 55

CLINICAL HISTORY *44-year-old woman with recent bone marrow transplantation for leukemia presenting with fever.*

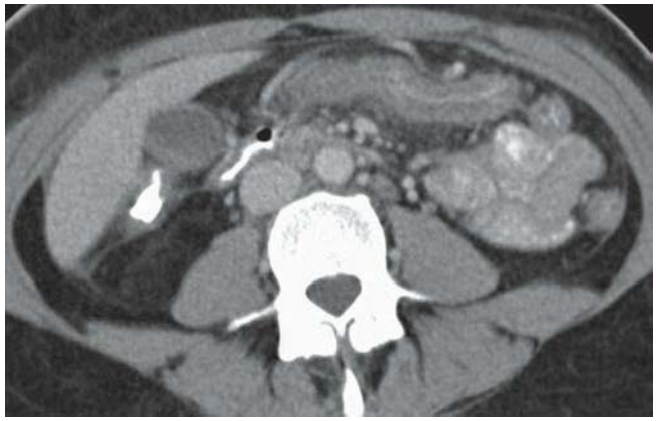

FIGURE 55A

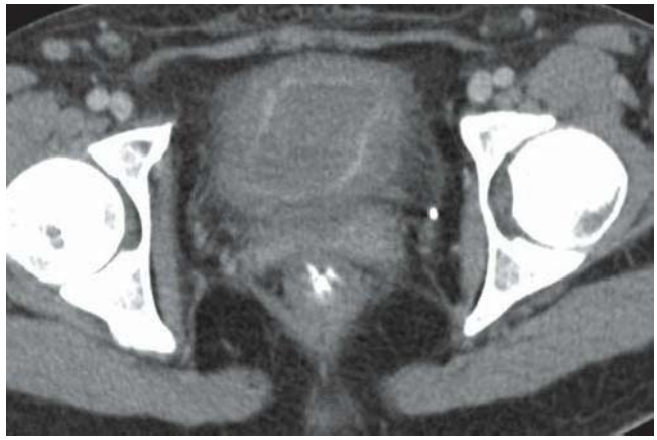

FIGURE 55C

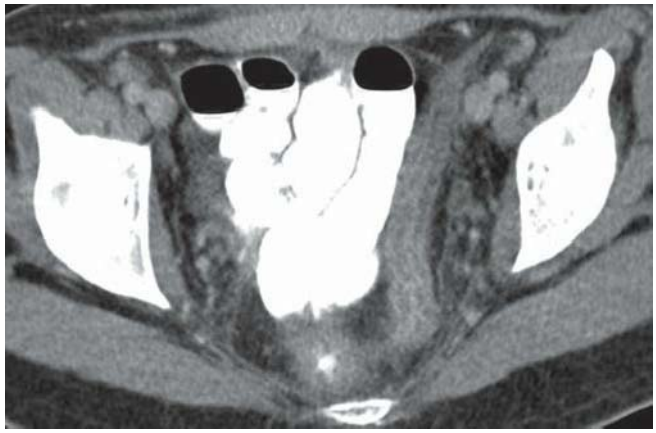

FIGURE 55B

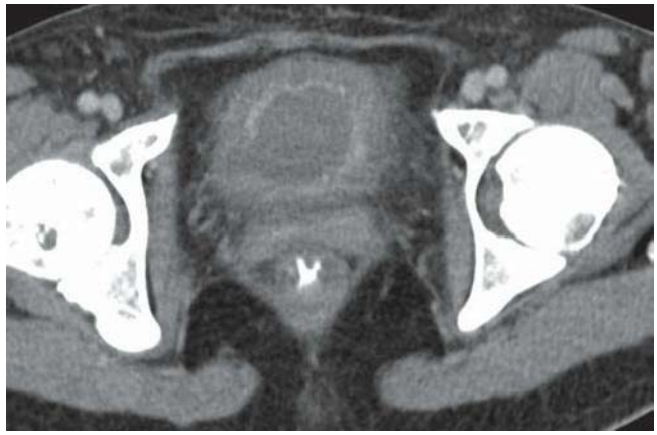

FIGURE 55D

FINDINGS Axial CECT images (A–D) show colonic and bladder wall thickening with mucosal hyperenhancement. Note the surrounding fat stranding, which is more pronounced around the bladder.

DIFFERENTIAL DIAGNOSIS Radiation cystitis, infectious cystitis, cyclophosphamide cystitis.

DIAGNOSIS Graft-versus-host disease of the bladder.

DISCUSSION Graft-versus-host disease (GVHD) occurs when the donor lymphoid cells damage organs of the recipient. Involvement occurs in 30% to 50% of allogeneic transplantation recipients within the first 100 days of the transplantation. The most commonly involved organs are the skin, liver, and bowel. In this case, the bladder mucosa was also involved. Gastrointestinal involvement is often nonspecific; bowel wall thickening is most commonly present. The bladder wall thickening in this case was also caused by GVHD. A biopsy of the involved organ is necessary to establish the diagnosis. Cancer patients receiving cyclophosphamide may develop hemorrhagic cystitis, but this drug would not directly cause bowel toxicity and bowel wall thickening observed in this case. The immunosuppressive regimen patients are exposed to prior to bone marrow transplantation puts them at increased risk for opportunistic infections, which should be excluded in this case. Exclusion of an infectious etiology is crucial because patients with GVHD are treated with immunosuppressive agents, which would be contraindicated in case of infectious enterocolitis. In the absence of small bowel pathology, radiation cystitis and colitis is unlikely because small bowel loops would have been included in the radiation field given the extent of colonic disease.

CASE 56

CLINICAL HISTORY *65-year-old man presenting with gross hematuria.*

FIGURE 56A

FIGURE 56B

FIGURE 56C

FIGURE 56D

FINDINGS Sequential images from a CT urogram. Axial NECT image (A) demonstrates a hyperdense mass involving the urinary bladder wall adjacent to the right UVJ with involvement of the distal right ureter. CECT axial (B), coronal (C), and sagittal (D) reformatted images reveal a hypodense mass relative to the opacified urinary bladder.

DIFFERENTIAL DIAGNOSIS Primary neoplasm of the bladder (squamous cell carcinoma, adenocarcinoma), schistosomiasis, tuberculosis, hematoma, metastasis.

DIAGNOSIS Transitional cell carcinoma.

DISCUSSION Transitional cell carcinoma of the bladder occurs most commonly in males in the sixth decade of life. These carcinomas make up 85% to 90% of bladder tumors, followed by squamous cell carcinoma and adenocarcinoma. Transitional cell carcinoma most commonly presents as an intraluminal mass with a broad base. They can be single or multiple and, although infrequent, may contain calcifications. Hydronephrosis is not frequently seen in transitional cell carcinoma of the bladder unless the ureteral orifice is obstructed, as in this case. An intraluminal mass is a nonspecific finding and can be due to any bladder neoplasm or, occasionally, due to an infection, such as tuberculosis or schistosomiasis. CT is excellent in evaluating for lymphadenopathy and invasion of adjacent organs. MRI is superior to evaluate the depth of wall invasion or extravesical extension by the tumor.

CASE 57

CLINICAL HISTORY *46-year-old man presenting with right upper quadrant pain.*

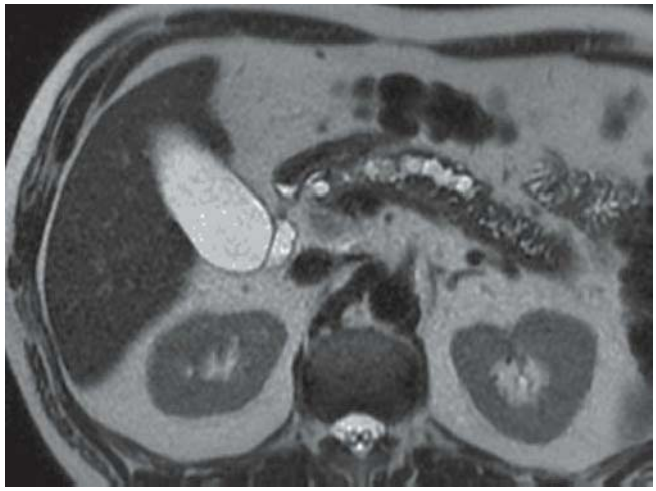

FIGURE 57A

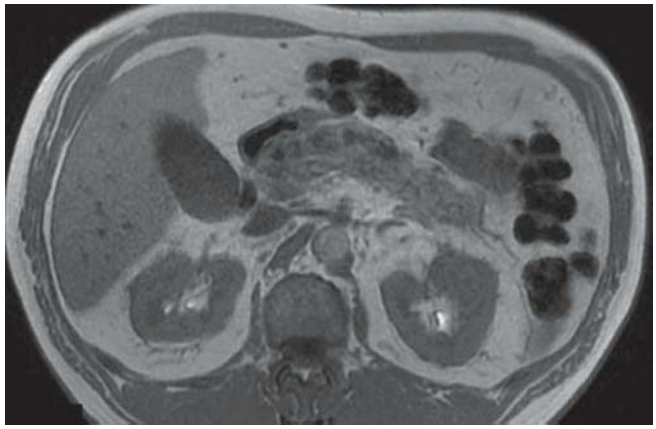

FIGURE 57B

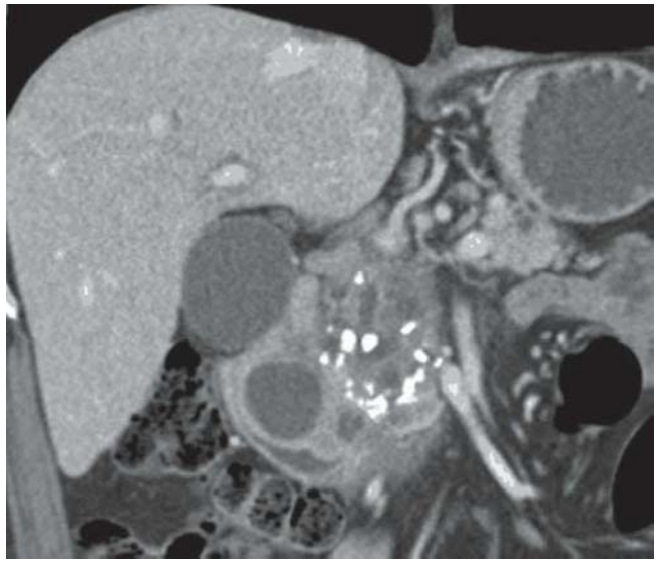

FIGURE 57C

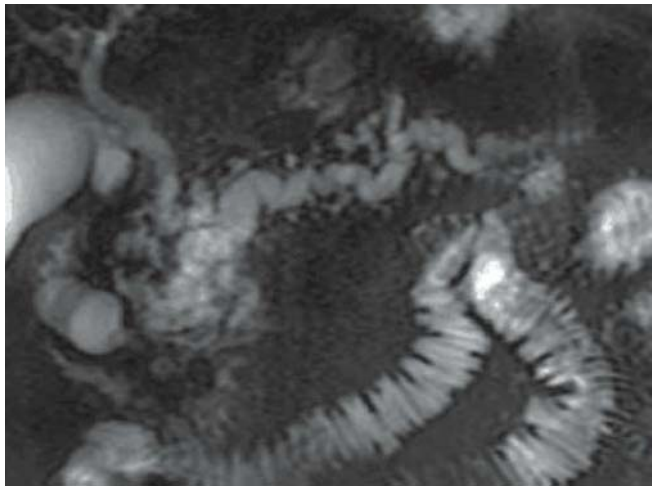

FIGURE 57D

FINDINGS Axial T2-WI (A) and T1-WI (B) at the level of the pancreatic body and tail demonstrate ductal dilatation, giving a beaded appearance. Coronal reformatted CECT (C) demonstrates normal enhancement of the pancreatic head demonstrates a dilated irregular pancreatic duct. Note the MRCP image (D) demonstrates irregularly dilated pancreatic duct with several dilated side branches, giving a beaded appearance.

DIFFERENTIAL DIAGNOSIS Polycystic liver disease, primary sclerosing cholangitis, recurrent pyogenic cholangitis.

DIAGNOSIS Caroli disease (diffuse form).

DISCUSSION Caroli disease is defined as congenital nonobstructive cystic dilatation of the intrahepatic biliary tree. It can be diffuse or localized. It is believed that Caroli disease is part of the spectrum of fibrocystic diseases that range from congenital hepatic fibrosis to choledochal cysts. Caroli disease can be associated with medullary sponge kidney and autosomal recessive polycystic kidney disease or present as an isolated phenomenon and not associated with other entities. The key to the diagnosis of Caroli disease is recognizing that the saccular dilatations are in communication with the biliary tree. The saccular dilatations in Caroli disease tend to radiate toward the porta hepatis following the path of the portal vein branches. This is in contradistinction to polycystic liver disease, which is randomly dispersed in the liver. The saccular dilatations in Caroli disease tend to be irregularly shaped, a feature that also helps to distinguish it from polycystic liver disease; the saccular dilatations in Caroli disease tend to be spherical and vary in size. Recurrent pyogenic cholangitis and primary sclerosing cholangitis usually do not produce saccular dilatation, as in this case, and involvement is frequently extrahepatic and characterized by the presence of strictures.

CASE 58

CLINICAL HISTORY *34-year-old woman presenting with chronic abdominal pain.*

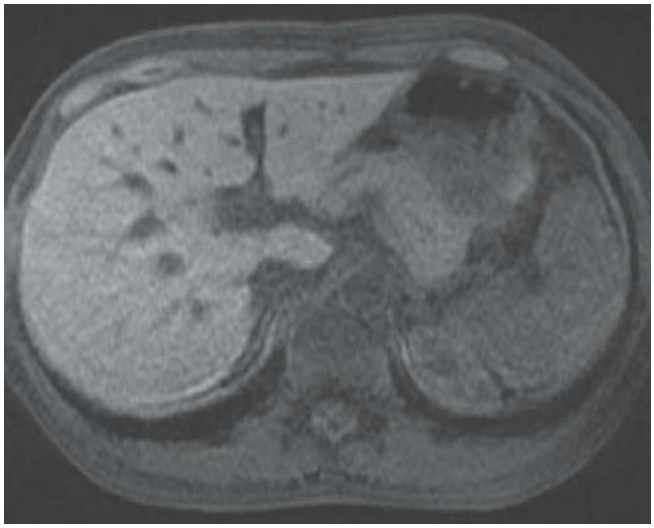

FIGURE 58A

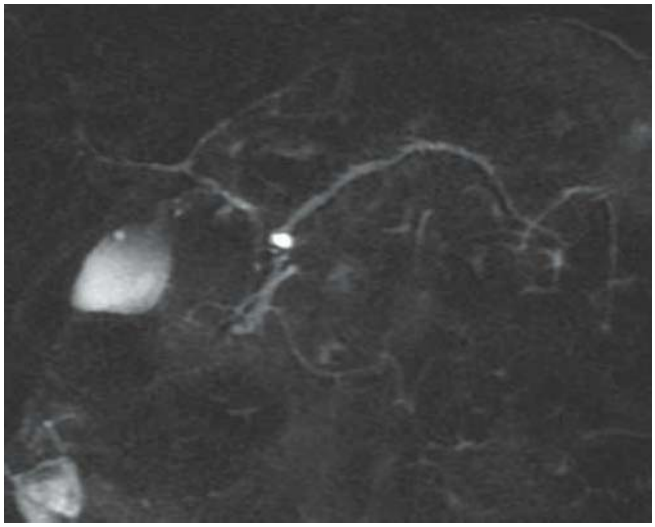

FIGURE 58C

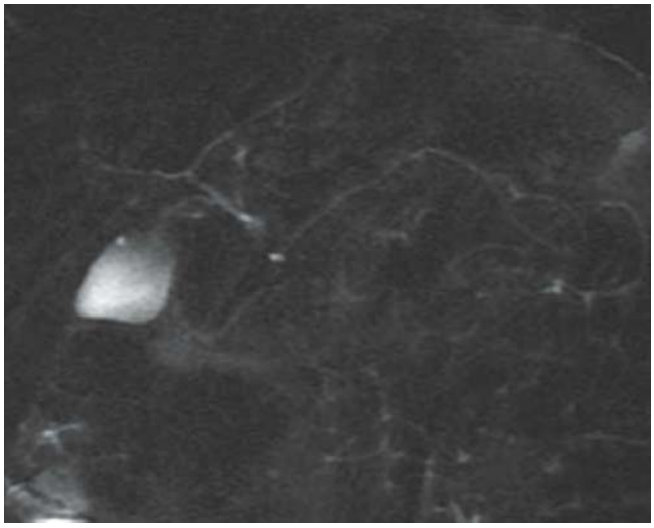

FIGURE 58B

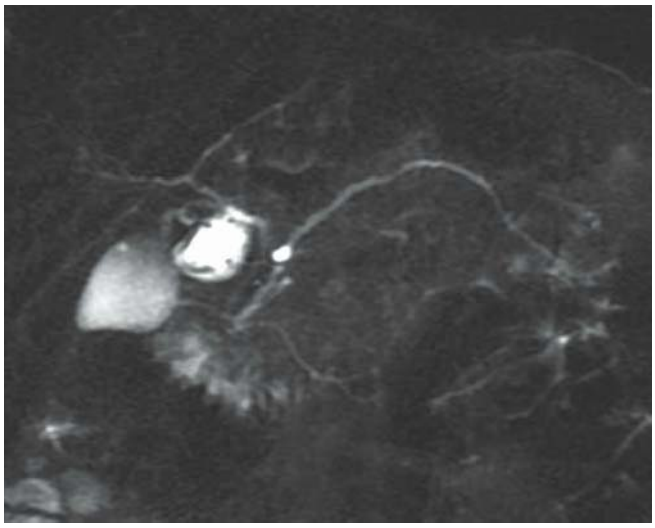

FIGURE 58D

FINDINGS Fat-suppressed axial T1-WI (A) demonstrates diffusely low pancreatic signal, lower than that of the liver. Thick-slab MRCP image (A) demonstrates a normal pancreatic duct. Thick-slab MRCP images obtained 3 (C) and 7 (D) minutes post-intravenous secretin injection demonstrate a stricture of the main pancreatic duct in the body with abnormally dilated side branches (C), and decreased duodenal excretion due to outflow obstruction at the ampulla with dilation of large side branches in the pancreatic head (D).

DIFFERENTIAL DIAGNOSIS Diffuse adenocarcinoma.

DIAGNOSIS Chronic pancreatitis.

DISCUSSION Secretin is a hormone secreted by the duodenum in response to luminal acidity. It stimulates secretion of pancreatic juice, and to a lesser extent secretion of bile. It also transiently increases the tone of the sphincter of Oddi for the first few minutes after its IV injection. Synthetic secretin (2 µg/kg) is injected over 1 minute followed by thick-slab MRCP acquisition every 30 seconds for 10 minutes. The normal response to secretin injection consists of dilatation of the main pancreatic duct due to exocrine stimulation accentuated by the increased tone of the sphincter of Oddi, followed by copious secretion of pancreatic juice in the duodenum once the sphincter relaxes. The diameter of the main pancreatic

duct typically returns to baseline after 10 minutes. In cases of chronic pancreatitis, side branches dilate and strictures of the main pancreatic duct may become apparent, both of these findings which are enhanced by secretin injection as seen in this case, allowing a noninvasive diagnosis. The exocrine function in cases of chronic pancreatitis is also reduced, explaining the decreased duodenal filling observed.

Finally, the pancreas normally demonstrates the brightest signal of all the abdominal organs on fat-suppressed T1-WI due to its high manganese and protein content, and most pathologies, either diffuse or focal, will cause a decrease in the pancreatic signal, as seen in this case. Diffuse tumoral infiltration of the pancreas is excluded in the present case, as the pancreatic duct branches would not dilate upon secretin injection if they were surrounded and constricted by tumor.

CASE 59

CLINICAL HISTORY *55-year-old man with a history of ruptured cerebral aneurysm presenting with increasing headaches and a palpable abdominal mass.*

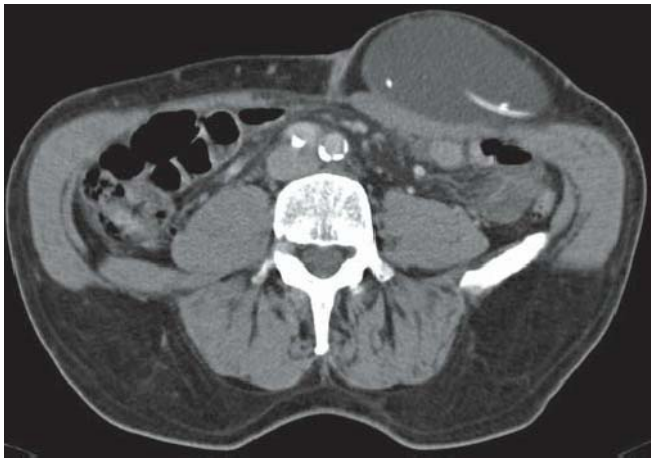

FIGURE 59A

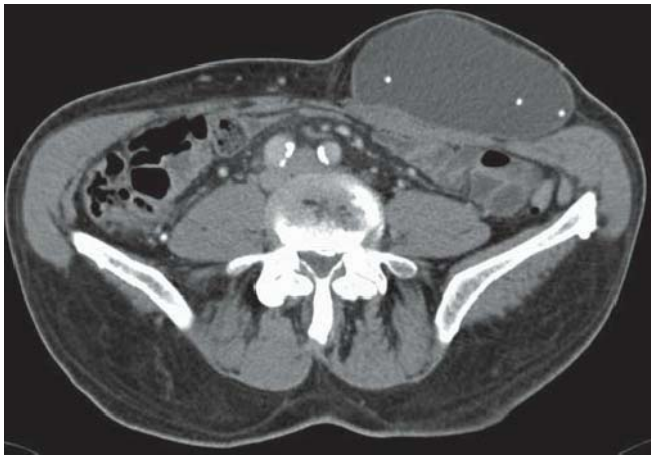

FIGURE 59B

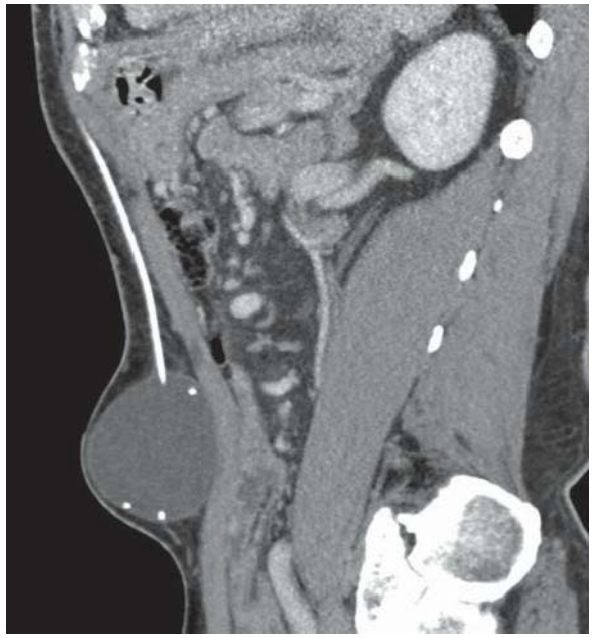

FIGURE 59C

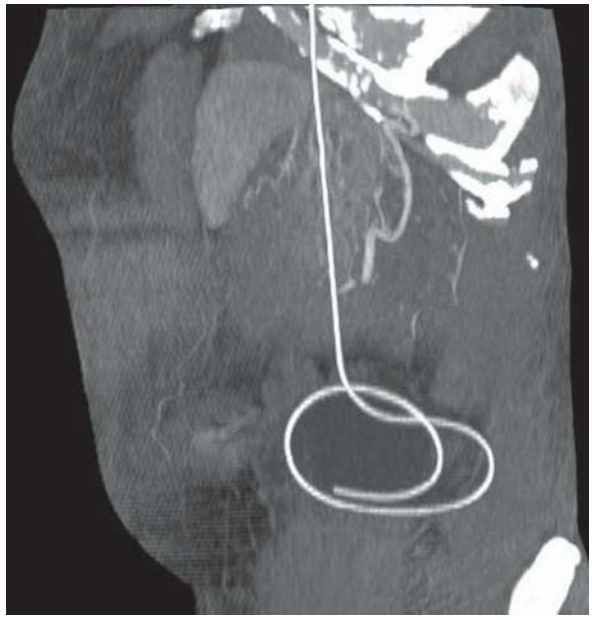

FIGURE 59D

FINDINGS Axial CECT (A and B), sagittal reformatted (C), and maximum-intensity projection (MIP) (D) images show an 11.3 cm × 5.7 cm fluid collection in the subcutaneous tissues. Note tube coiled within it.

DIFFERENTIAL DIAGNOSIS Seroma, hematoma, cystic metastasis.

DIAGNOSIS Ventriculoperitoneal shunt migration with cerebrospinal fluid pseudocyst formation.

DISCUSSION The primary treatment of hydrocephalus is through ventricular shunting. The most commonly used shunt is ventriculoperitoneal because the peritoneum is a very efficient site for fluid absorption. However, several complications may occur, leading to shunt malfunction and recurrent neurologic symptoms. The distal end of the shunt can migrate into the abdominal wall, thorax, or perforated viscus or can herniate in various locations, such as in the scrotum. When shunt migration occurs in the abdominal wall, where fluid absorption is less efficient, cerebrospinal fluid accumulation around the distal end of the shunt may develop, forming a cerebrospinal fluid pseudocyst. This gradually leads to shunt malfunction, increased central nervous system pressure, and recurrent symptoms, as in this case. Treatment consists of shunt revision with relocation of the distal end of the shunt in the peritoneal cavity. CT or ultrasound demonstrates the fluid composition of the abdominal wall mass and the abnormal position of the distal tip of the ventriculoperitoneal shunt. Other fluid collections that may occur in the abdominal wall include seroma, hematoma, abscess, and cystic metastasis. Identification of the shunt within the fluid collection is key to the correct diagnosis.

CASE 60

CLINICAL HISTORY *61-year-old woman presenting with painless jaundice and pruritus for 1 month.*

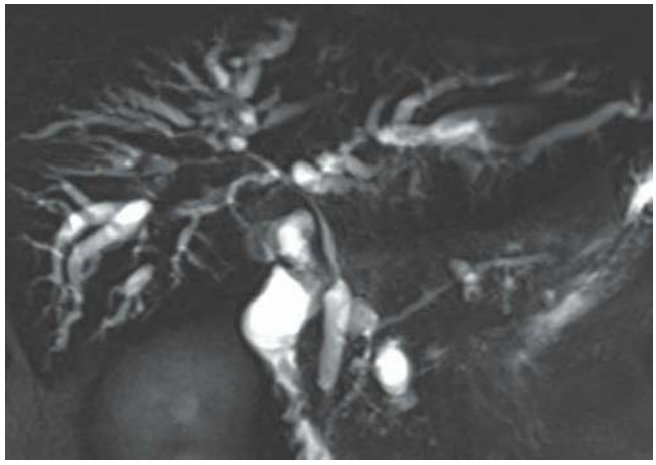

FIGURE 60A

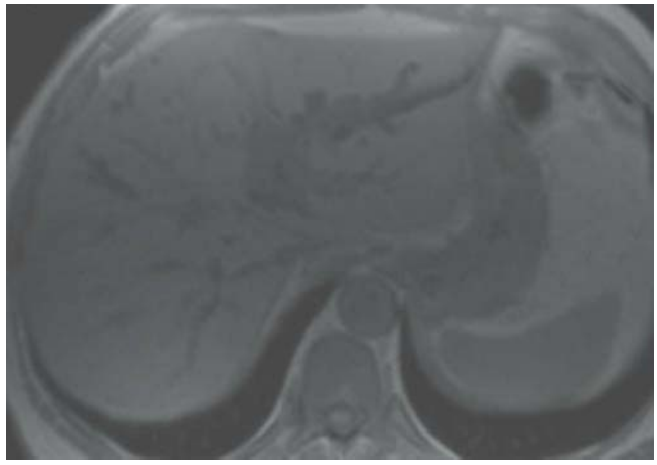

FIGURE 60C

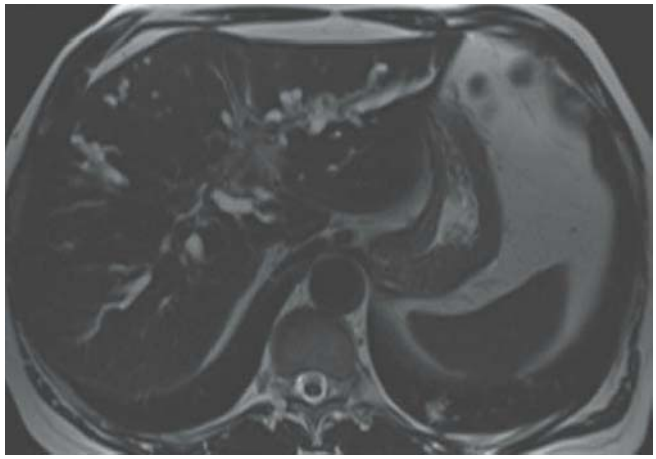

FIGURE 60B

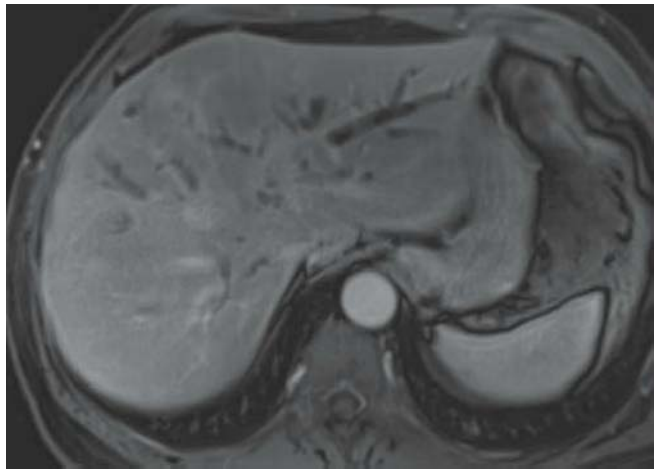

FIGURE 60D

FINDINGS Thick-slab MRCP image (A) demonstrates central bile duct cutoff and narrowing of the central intrahepatic bile ducts and of the common hepatic duct, with moderate upstream intrahepatic ductal dilatation. Axial T2-WI (B) demonstrates an ill-defined slightly hyperintense mass centrally in the liver, which is hypointense on the fat-suppressed axial T1-WI (C). The lesion shows hyperenhancement of the lesion on the delayed gadolinium-enhanced, fat-suppressed T1-WI (D).

DIFFERENTIAL DIAGNOSIS Hepatocellular carcinoma, metastasis.

DIAGNOSIS Cholangiocarcinoma (Klatskin tumor).

DISCUSSION Cholangiocarcinoma (CAC) is a malignant neoplasm of the bile ducts, which has an increased incidence in patients with sclerosing cholangitis, inflammatory bowel disease, Caroli disease, and gallstones. CACs occur most commonly in the larger extrahepatic ducts with more than 90% occurring at the confluence of the ducts or more distally. Although extrahepatic cholangiocarcinomas often present early with jaundice secondary to biliary obstruction, the prognosis is still very poor. A Klatskin tumor is a CAC at the bifurcation of the left and right hepatic ducts. This will cause biliary dilatation in both lobes of the liver. Because the bile ducts are small, a tumor mass is often not seen by imaging when the patients present with jaundice. This case, on the other hand, demonstrates the tumor mass invading into the liver. When a tumor mass is seen, it typically enhances late on CT and MRI and demonstrates mildly increased signal on T2-WI, as seen in this example. Neither HCC nor metastases frequently cause biliary dilatation or are associated with abnormal hyperenhancement of the bile duct wall.

CASE 61

CLINICAL HISTORY *63-year-old woman with hysterectomy and radiotherapy for cervical cancer presenting with weight loss.*

FIGURE 61A

FIGURE 61B

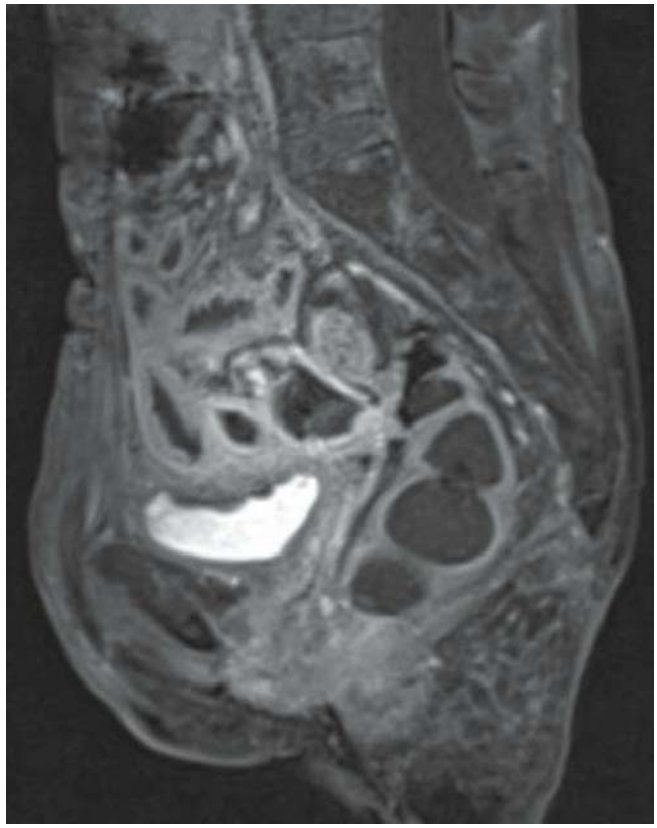

FIGURE 61C

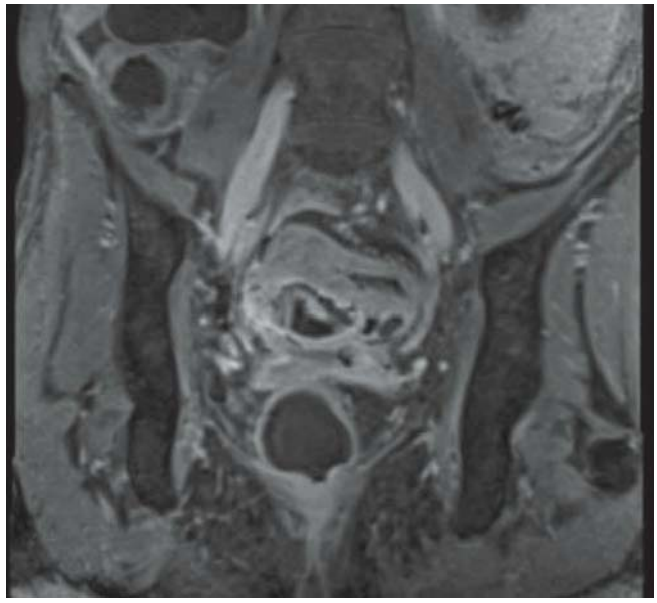

FIGURE 61D

FINDINGS Axial (A and B) CECT images demonstrate thickening of small bowel wall, rectosigmoid wall, and bladder wall in the pelvis. There is extensive mucosal hyperenhancement of the affected bowel segments and hyperemia of the mesenteric vessels. Sagittal T2-WI (C) and post-gadolinium coronal T1-WI (D) of the pelvis reveal evidence for fibrosis and demonstrate the increased hyperemia of the affected bowel segments.

DIFFERENTIAL DIAGNOSIS Ischemia, Crohn disease, lymphoma.

DIAGNOSIS Radiation enterocolitis.

DISCUSSION Radiation changes in the GI tract are commonly seen in the rectum, sigmoid, and small bowel with the use of external-beam radiation therapy for many pelvic malignancies. A good clinical history will suggest the diagnosis and often eliminate the need for a lengthy workup. Radiation enteritis and colitis can occur several years after radiation therapy. Most commonly, it is seen in women with cervical cancer who present with crampy abdominal pain and diarrhea. CT findings suggestive of radiation enteritis include bowel wall thickening of loops of bowel within the radiation port. Because of the

mesenteric edema, the loops of bowel are often separated in the pelvis. Mucosal hyperenhancement, as seen in this case, is suggestive of active inflammation. It is unusual to have involvement of both the sigmoid colon and the small bowel at the same time by the same disease process. This can occur in Crohn disease with skip lesions and ischemia with involvement of multiple branch vessels from vasculitis or emboli. Lymphoma, which is considered a systemic disease, can also affect various loops of bowel. Other CT findings in radiation disease include increased attenuation of the mesenteric fat and hyperemia of the mesenteric vessels supplying the involved bowel segments. MRI is much more sensitive for radiation-induced fibrosis, which appears hyperintense on T2-WI as in this case and demonstrates delayed but persistent enhancement on post-gadolinium sequences. Diffuse loss of the normal bone marrow signal within the pelvis, reflecting the radiation portal, can be seen on MRI.

CASE 62

CLINICAL HISTORY *25-year-old woman presenting with an enlarging abdominal mass.*

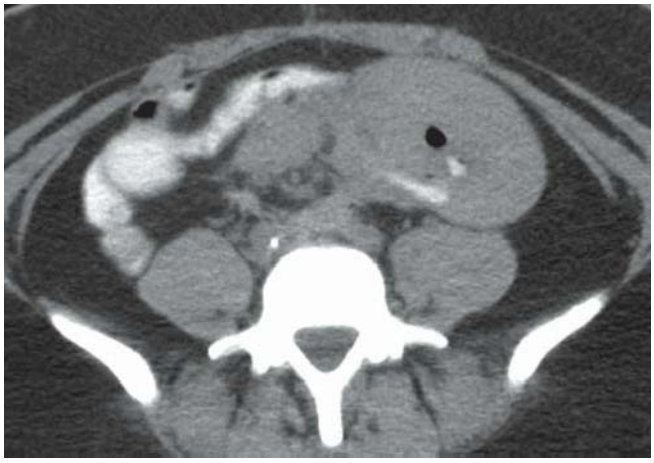

FIGURE 62A

FIGURE 62C

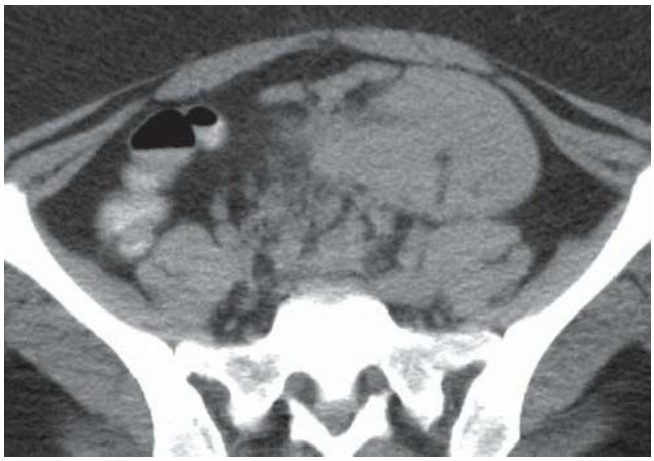

FIGURE 62B

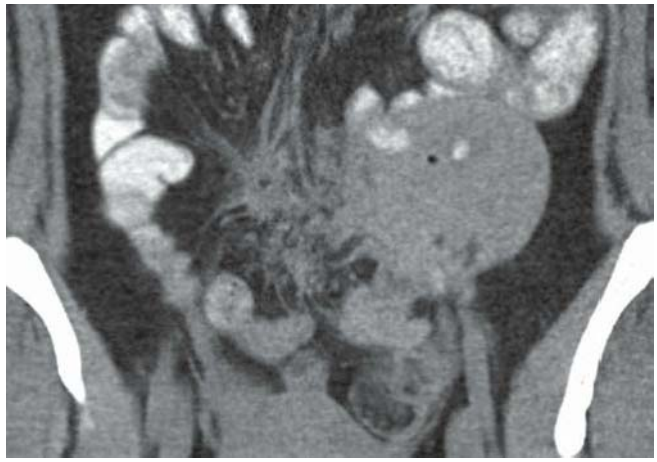

FIGURE 62D

FINDINGS Axial (A–C) and coronal reformatted (D) NECT images demonstrate a large, homogeneous mesenteric mass that contains a gas bubble and enteric contrast centrally. Smaller ill-defined satellite nodules are present in the mesentery at the midline. Note also the absence of the entire colon with pouch formation.

DIFFERENTIAL DIAGNOSIS Metastasis, sarcoma, gastrointestinal stromal tumor.

DIAGNOSIS Desmoid tumors in a patient with familial adenomatous polyposis syndrome.

DISCUSSION Familial adenomatous polyposis syndrome (FAPS) is an autosomal dominant disease in which hundreds of adenomatous polyps originate from the colonic mucosa. Colon cancers develop in virtually 100% of the affected patients and, therefore, prophylactic total colectomy at a young age is recommended. The absence of the colon in a young patient, such as in this case, is an important clue to the correct diagnosis. Desmoid tumors are common extracolonic abdominal findings in patients with FAPS and are among the leading cause of morbidity and mortality in these patients. Desmoid tumors typically present as well-circumscribed, homogeneous non-calcified masses, but infiltrative margins or heterogeneity may be seen. They can invade or cause compression on adjacent structures, such as the ureter or bowel. Medical therapy is initially favored as the recurrence rate after surgical resection is very high. Polyps involving the remainder of the gastrointestinal tract from the stomach to the ileum and carcinomas in the periampullary region, pancreas, gallbladder, and bile ducts are other abdominal manifestations of FAPS.

CASE 63

CLINICAL HISTORY *25-year-old woman presenting with chronic abdominal pain.*

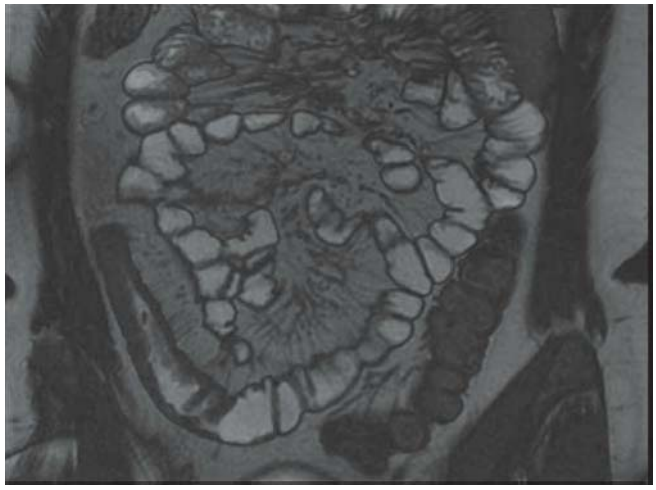

FIGURE 63A

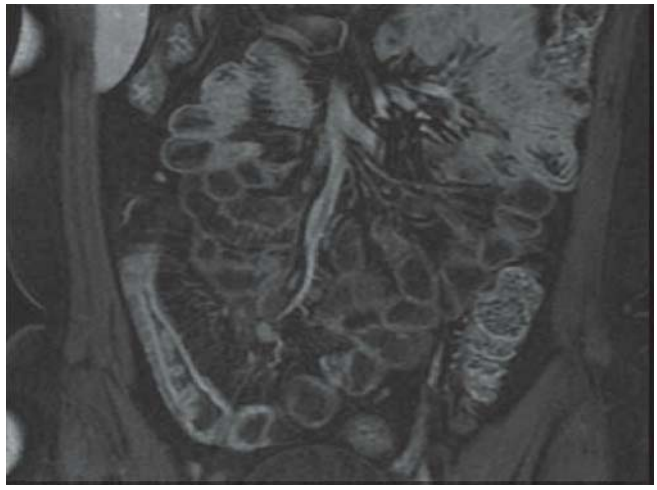

FIGURE 63C

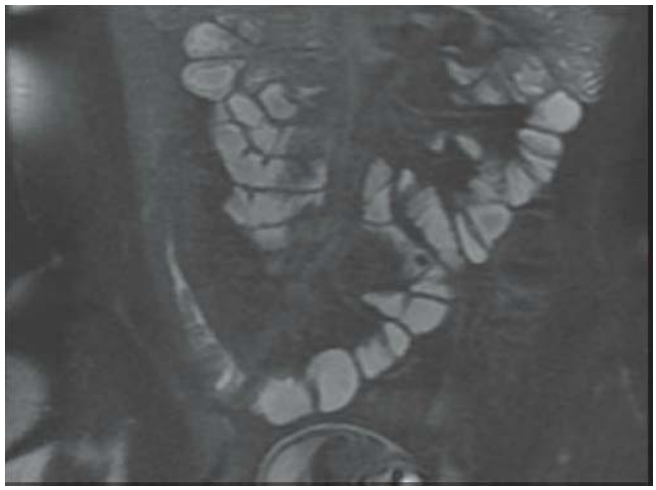

FIGURE 63B

FINDINGS Coronal FIESTA (A) and fat-suppressed T2-WI (B) demonstrate abnormal T2-dark wall thickening of a small bowel loop in the right lower quadrant. Coronal fat-suppressed, gadolinium-enhanced T1-WI (C) shows hyperenhancement of the mucosa, mesenteric hypervascularity, surrounding fat hypertrophy, and an enlarged mesenteric node. Note the narrowing of the lumen of the loop superiorly.

DIFFERENTIAL DIAGNOSIS Infectious enteritis, ischemic bowel, lymphoma.

DIAGNOSIS Terminal ileitis due to Crohn disease.

DISCUSSION Crohn disease is an idiopathic multifactorial chronic inflammatory disease of the GI tract. The age of onset is typically between the second and fourth decades of life. As the disease course is unpredictable with multiple recurrences and exacerbations, repetitive imaging is often performed. In order to minimize imaging with ionizing radiation, MR enterography has emerged as a technique of choice. After administration of oral contrast material, basic imaging sequences are acquired in the coronal plane, using T2-WI, rapid T2-WI sequences to allow kinetic assessment of the bowel, and dynamic gadolinium-enhanced, fat-suppressed T1-WI. Axial T2-WI is also obtained for anatomic correlation. Active disease is manifested on MRI by edematous (T2-bright) wall thickening, mucosal hyperenhancement, and surrounding edema in the fat and mesenteric hypervascularity. In the chronic phase, the wall becomes fibrosed and of darker T2 signal with stenosis formation. The surrounding fat hypertrophies due to chronic repetitive bouts of inflammation ("creeping fat"). In this case, most of the findings indicate the presence of chronic disease, with associated mild active inflammation. In infectious enteritis or ischemic bowel, the wall would be edematous, and therefore shows T2-bright signal. Mesenteric separation due to fat hypertrophy would not be seen in these two acute diseases, or in lymphoma.

CASE 64

CLINICAL HISTORY *45-year-old woman presenting with increased LFTs and epigastric pain.*

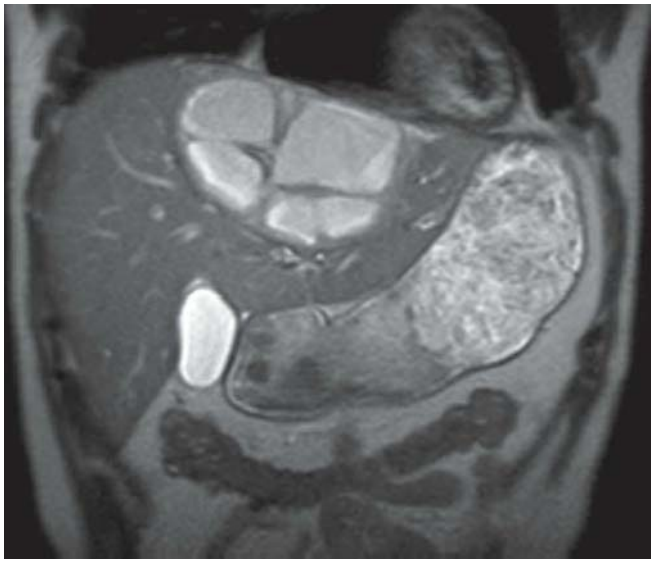

FIGURE 64A

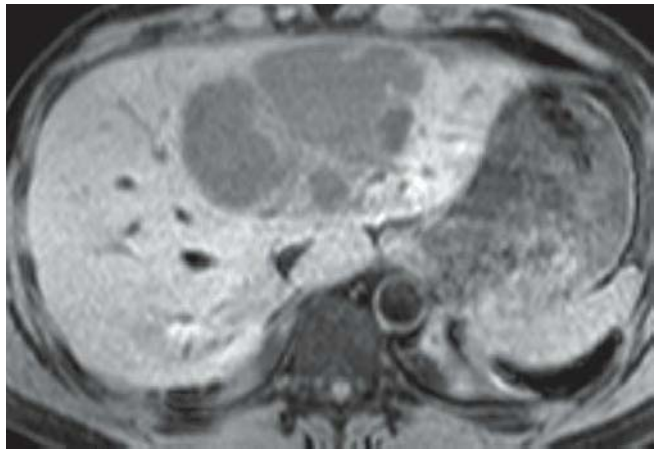

FIGURE 64C

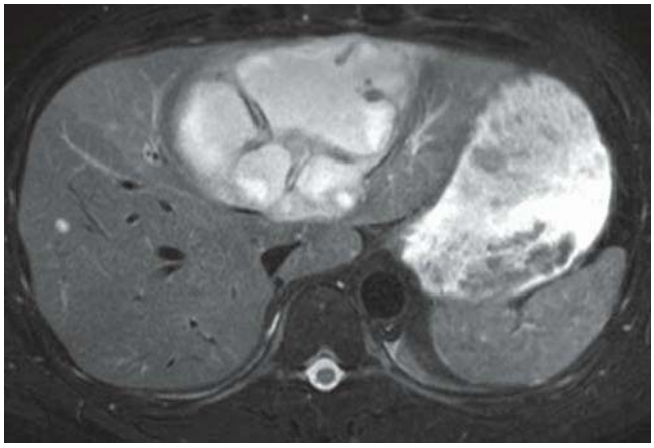

FIGURE 64B

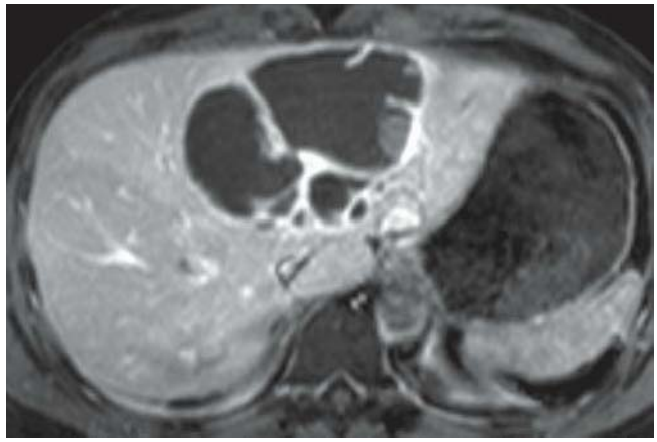

FIGURE 64D

FINDINGS Coronal (A) and axial fat-suppressed (B) T2-WIs show an encapsulated hyperintense lesion in segment 4 of the liver. The lesion is hypointense on the fat-suppressed axial T1-WI (C) and shows wall and septal enhancement on the gadolinium-enhanced, fat-suppressed axial T1-WI (D). There is T2 hyperintense signal in the lesion with edema and hyperenhancement of the liver parenchyma adjacent to the lesion.

DIFFERENTIAL DIAGNOSIS Cystic metastasis of the liver, amebic abscess, hydatid cyst.

DIAGNOSIS Pyogenic liver abscess.

DISCUSSION Hepatic abscesses, like most other focal hepatic processes, prolong T1 and T2 relaxation times and, therefore, appear hyperintense on T2-WI and hypointense on T1-WI. In one series, approximately 60% of the abscesses were hypointense on the T1-WIs and 72% were hyperintense on the T2-WI; 35% of the abscesses demonstrated increased signal intensity on the T2-WI around the lesion, which is thought to represent perilesional edema and inflammation, as seen in this case. After administration of gadolinium, abscesses typically show rim enhancement, which is secondary to increased capillary permeability in the surrounding liver parenchyma. Small lesions (<1 cm) may enhance homogeneously mimicking hemangiomas. The abscess wall enhancement on dynamic post-gadolinium images may be considered as a distinctive feature of pyogenic liver abscesses. Abscess wall shows a fast and intense enhancement that persists on portal venous and late-phase images. Some of the lesions may contain internal septations, which also reveal persistent enhancement on late-phase images. Although less likely, a solitary, infected, necrotic metastasis, or primary liver tumor could also have this appearance.

CASE 65

CLINICAL HISTORY *26-year-old woman presenting with repetitive lung infections.*

FIGURE 65A

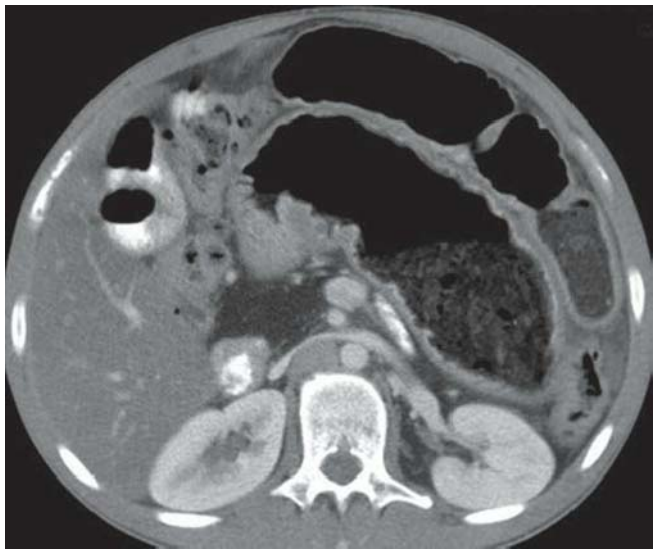

FIGURE 65B

FINDINGS Delayed image of a barium enema (A) shows dilated unopacified small bowel loops measuring up to 6.5 cm in diameter. Axial CECT images demonstrate complete fatty replacement of the pancreatic head (B) and dilated small bowel loops containing fecaloid "fatty" material (B and C).

FIGURE 65C

DIFFERENTIAL DIAGNOSIS Severe malnutrition, Shwachman-Diamond syndrome, diabetes, Cushing's syndrome.

DIAGNOSIS Cystic fibrosis with meconium ileus equivalent.

DISCUSSION Cystic fibrosis is characterized by the formation of thick secretions due to dysfunction of the exocrine glands, including pancreatic insufficiency. There is also dysfunction of the mucociliary transport system, which results in recurrent pulmonary infections; slow transit of GI content is also characteristic. A typical finding in cystic fibrosis is complete fatty replacement of the pancreas. Other CT and MRI features include pancreatic fibrosis, seen as hypointense signal on T1-WI, and the presence of retention cysts, which are caused by obstruction of sidebranches and appear hyperintense on T2-WI. The diagnosis is confirmed in this case by the age of the patient and the coexisting meconium ileus equivalent. The fatty replacement seen in elderly patients, obese patients, and patients with Cushing's syndrome tends to be marbled in appearance rather than diffuse replacement. Shwachman-Diamond syndrome is a rare disorder in the family of metaphyseal dysplasias that has coexisting fatty replacement of the pancreas.

CASE 66

CLINICAL HISTORY *47-year-old man presenting with repeated bouts of epigastric pain.*

FIGURE 66A

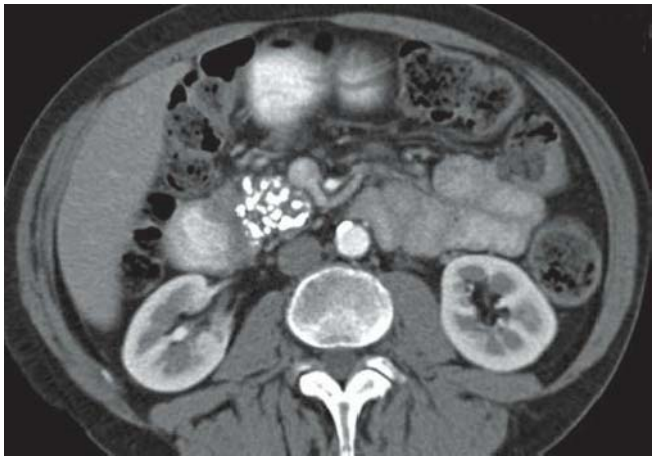

FIGURE 66C

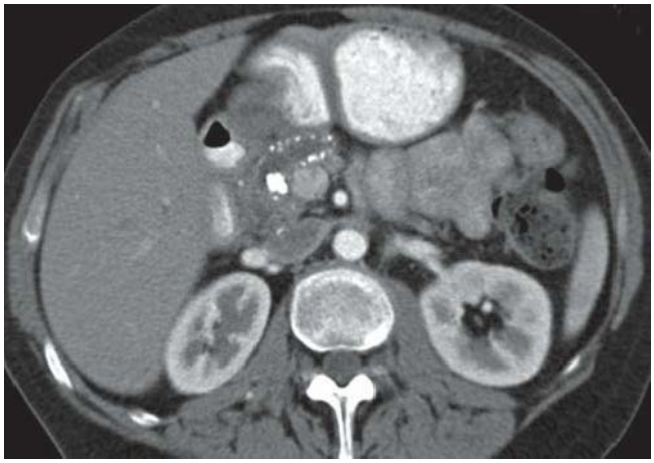

FIGURE 66B

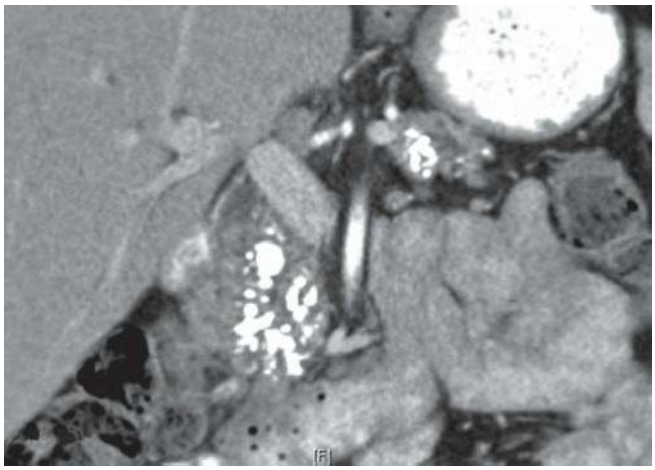

FIGURE 66D

FINDINGS Axial (A–C) and coronal reformatted (D) CECT images demonstrate multiple pancreatic calcifications scattered throughout the gland with an irregularly dilated pancreatic duct.

DIFFERENTIAL DIAGNOSIS None.

DIAGNOSIS Chronic pancreatitis.

DISCUSSION Chronic pancreatitis is most commonly secondary to underlying alcohol consumption. The alcohol alters the function of the acinar cells resulting in concentration of proteins in the ducts. This leads to stone formation, ductal stenosis and dilatation, and acinar atrophy. The ductal dilatation in chronic pancreatitis is most commonly irregular in appearance (73%), followed by smooth (15%), and beaded (12%). Pancreatic ductal dilatation is seen in 68% of patients with chronic pancreatitis, with glandular atrophy in 54%, and calcifications in 50%. This case demonstrates the typical findings of chronic pancreatitis with calcifications and ductal dilatation. There is always a concern for an underlying pancreatic adenocarcinoma in a patient with chronic pancreatitis causing pancreatic ductal dilatation. The head of the pancreas, however, is diffusely calcified with no focal low-attenuation mass present. Pancreatic adenocarcinomas rarely calcify. If there is continued concern for a malignancy, then MRI, EUS, ERCP, or biopsy is required. Correlation with serum CA 19-9 levels is also helpful because it is elevated in pancreatic adenocarcinoma.

CASE 67

CLINICAL HISTORY *37-year-old woman presenting with liver lesion detected on ultrasound.*

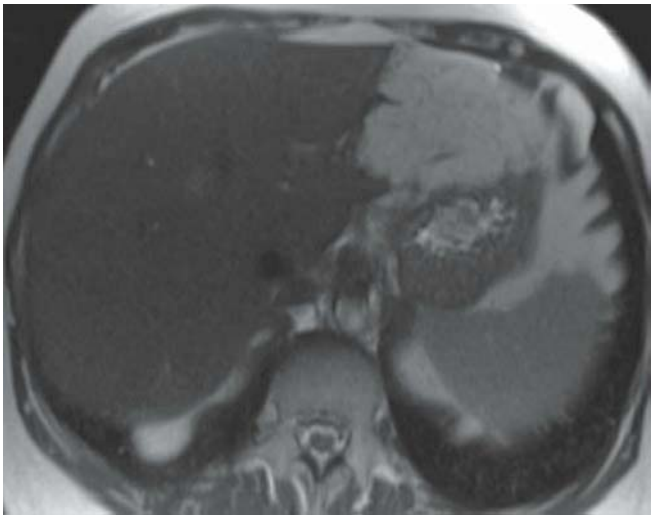

FIGURE 67A

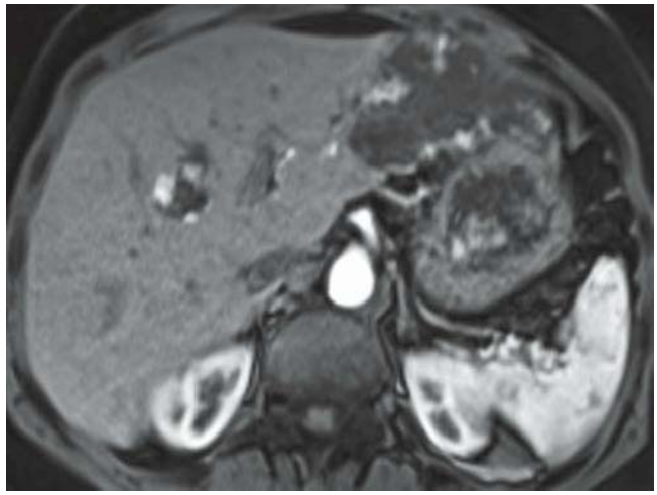

FIGURE 67C

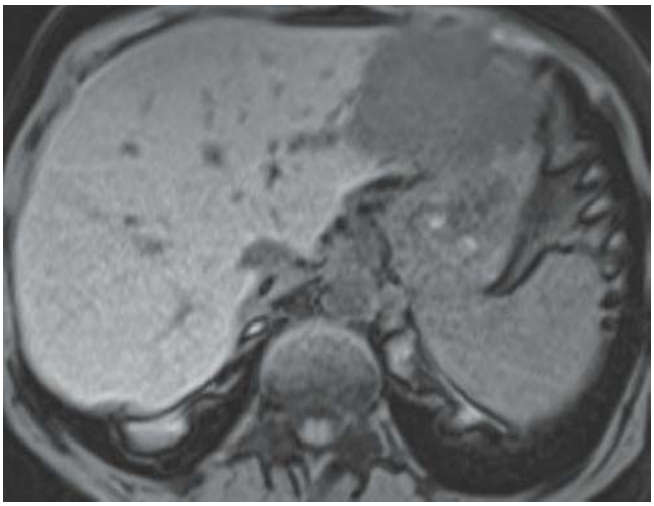

FIGURE 67B

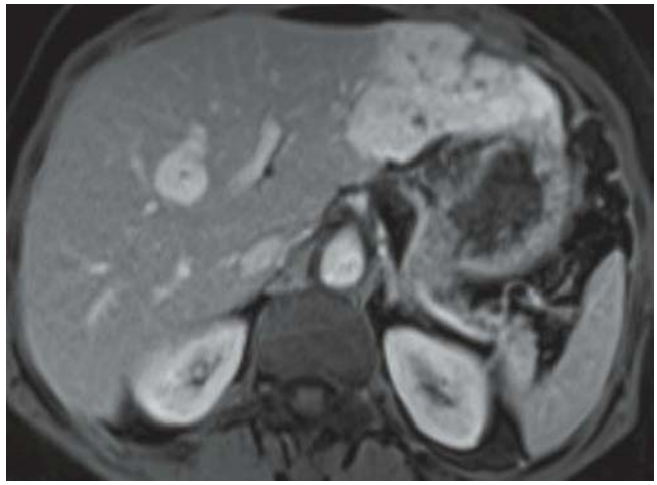

FIGURE 67D

FINDINGS Axial T2 WI (A) of the liver demonstrates a large lesion with homogenous high T2 signal within the left lobe of the liver. Pre– (B) and post–gadolinium-enhanced, fat-suppressed T1-W1 arterial (C) and delayed (D) phase MRI images show the early peripheral nodular of this lesion with delayed fill-in of the lesion.

DIFFERENTIAL DIAGNOSIS Metastasis.

DIAGNOSIS Hemangioma.

DISCUSSION Hemangiomas are the most common benign liver tumors. They are more commonly seen in women than men (5:1 ratio). They are typically asymptomatic and found incidentally. Hemangiomas tend to be stable lesions; however, growth of hemangiomas during pregnancy has been reported. They tend to be small and are multiple in about 10% of cases. Punctate and coarse calcifications, fibrosis, and central cystic degeneration can occur, especially in giant hemangiomas. Dynamic contrast administration demonstrates dense peripheral nodular incomplete enhancement of the lesion with sequential filling in of the lesion over time. This can take minutes to hours to occur. The contrast will wash out of the liver but at a much faster rate than the hemangioma, which will be of increased signal relative to the liver. The enhancement pattern of hypervascular metastasis tends to be ring-like rather than globular. Puddling of contrast in the periphery of the lesion is very characteristic for a hemangioma and is only seen in a minority of metastases, especially treated breast cancer metastases. Also, without a history of a primary malignancy, a solitary metastasis is unlikely in this case, making a hemangioma the best diagnosis.

CASE 68

CLINICAL HISTORY *42-year-old man, alcohol drinker, presenting with epigastric pain radiating to the back.*

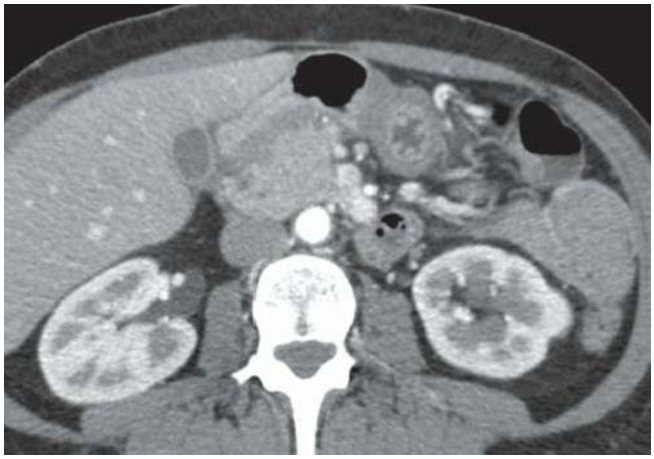

FIGURE 68A

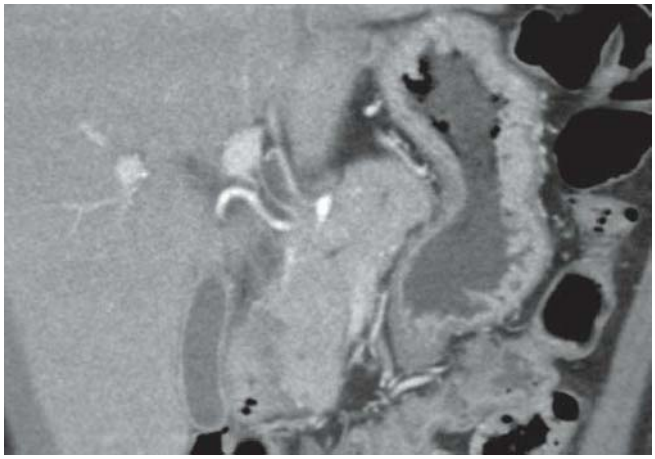

FIGURE 68C

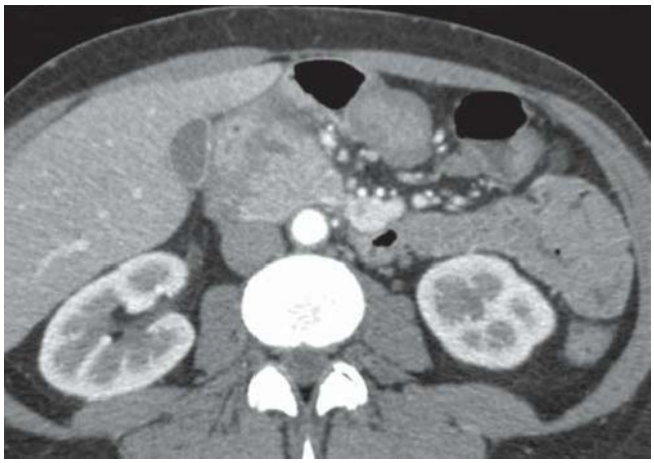

FIGURE 68B

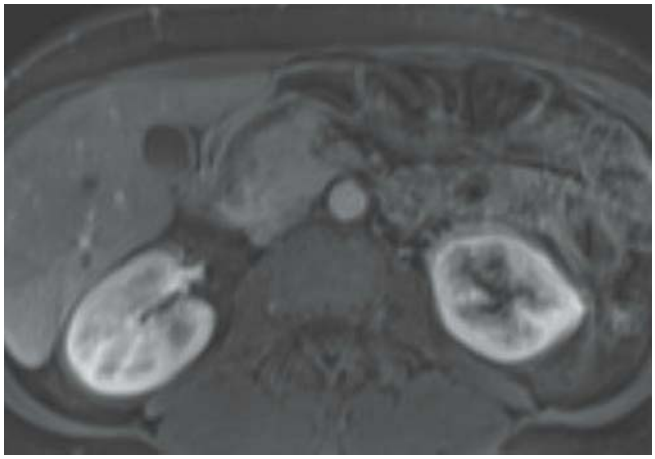

FIGURE 68D

FINDINGS Axial (A and B) and coronal reformatted (C) CECT images show an infiltrating density between the pancreatic head and the proximal duodenum. Note the absence of ductal or gastric dilatation. Gadolinium-enhanced, fat-suppressed axial T1-WI (D) shows the lack of enhancement of this abnormality.

DIFFERENTIAL DIAGNOSIS Pancreatic adenocarcinoma.

DIAGNOSIS Groove pancreatitis.

DISCUSSION Groove pancreatitis is a subtype of chronic pancreatitis that is poorly understood. It has also been referred to as cystic dystrophy of the duodenal wall. Alcohol has been recognized as an important risk factor, but abnormal dorsal duct drainage or ectopic pancreatic tissue may also play a role. The inflammation is typically restricted to the groove between the duodenal sweep and the pancreatic head. In the pure form, there is no involvement of the pancreatic duct or CBD, as in this case. In the segmental form, there is displacement of the CBD medially and segmental involvement of the pancreatic parenchyma. Associated changes of chronic pancreatitis can be present with pancreatic duct dilatation. A pancreatic adenocarcinoma in this location would cause bile duct and quite likely gastric obstruction and dilatation.

CASE 69

CLINICAL HISTORY *43-year-old woman presenting with crampy abdominal pain.*

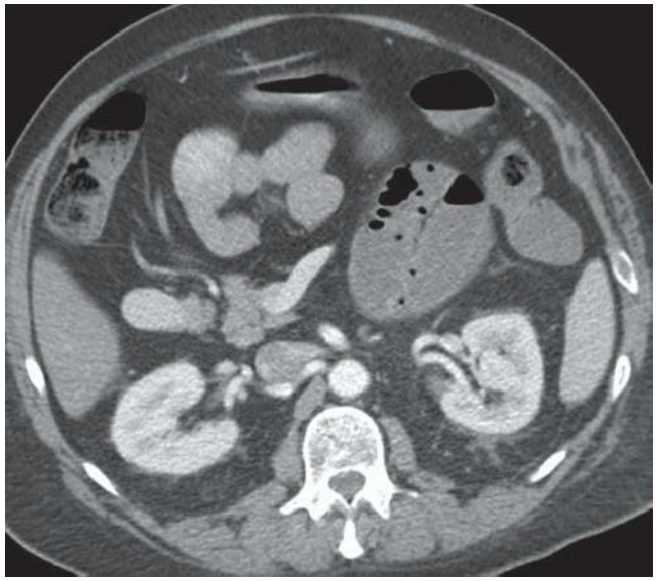

FIGURE 69A

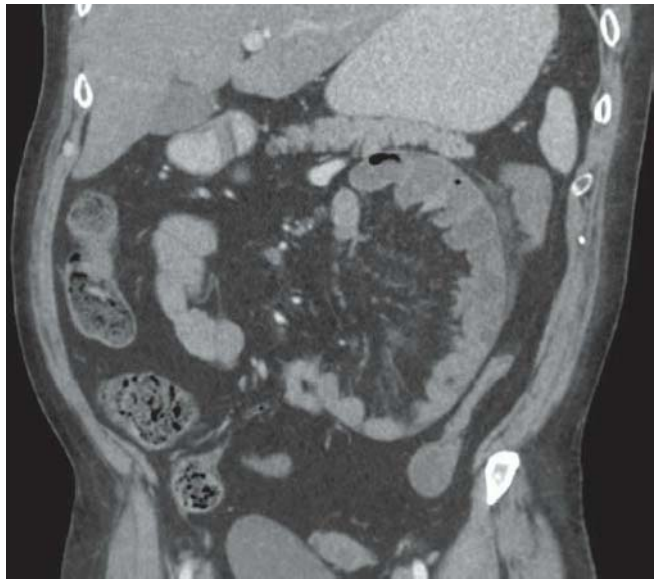

FIGURE 69C

FIGURE 69B

FIGURE 69D

FINDINGS Axial (A and B), coronal reformatted (C), and sagittal reformatted (D) CECT images demonstrate several small bowel loops grouped together in the left mid-abdomen. A layer of peritoneum that separates them from other small and large bowel segments surrounds the loops. Mesenteric stranding is seen within the enclosed area and laterally to it. Few loops with enteric stasis are mildly dilated superiorly.

DIFFERENTIAL DIAGNOSIS Small bowel obstruction due to adhesions.

DIAGNOSIS Internal small bowel hernia.

DISCUSSION Internal hernias are defined by the protrusion of a viscus through a normal or abnormal peritoneal or mesenteric aperture within the confines of the peritoneal cavity. The orifice can be either acquired, such as a post-surgical, traumatic, or post-inflammatory defect, or congenital, including both normal apertures, such as the foramen of Winslow, and abnormal apertures arising from anomalies of internal rotation and peritoneal attachment. Internal hernias, including paraduodenal

(traditionally the most common), pericecal, foramen of Winslow, and intersigmoid hernias, account for approximately 0.5% to 5.8% of all cases of intestinal obstruction and are associated with a high mortality rate, exceeding 50% in some series. Also, the incidence of internal hernias is increasing because of a number of relatively new surgical procedures now being performed. General CT features include apparent encapsulation of distended bowel loops with an abnormal location, "C" or "O" arrangement or crowding of small-bowel loops within the hernial sac, evidence of obstruction with segmental dilatation and stasis, with additional features of apparent fixation. Additional findings include mesenteric vessel abnormalities, with engorgement, crowding, twisting, and stretching of these vessels commonly found.

CASE 70

CLINICAL HISTORY *78-year-old woman presenting with a rapidly enlarging pelvic mass.*

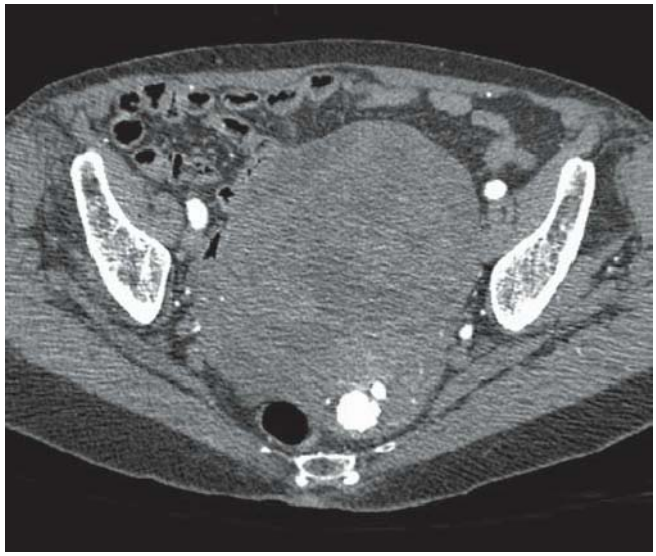

FIGURE 70A

FIGURE 70C

FIGURE 70B

FIGURE 70D

FINDINGS Axial (A) and sagittal reformatted (B) CECT images demonstrate a large heterogeneous uterine mass. Axial CECT (C and D) images obtained 9 months later show marked enlargement of the mass, which is now more necrotic.

DIFFERENTIAL DIAGNOSIS Endometrial carcinoma, lymphoma, metastasis.

DIAGNOSIS Uterine carcinosarcoma.

DISCUSSION Uterine sarcoma is a rare (2% to 3%) uterine neoplasm and is classified into four subtypes (malignant mesodermal tumor, endometrial stromal sarcoma, carcinosarcoma, and leiomyosarcoma). Most of these tumors are diagnosed histologically after hysterectomy due to insufficient tissue sampling during endometrial biopsy. On imaging, an ill-defined infiltrative lesion, extending beyond the contours of the normal uterus, is suggestive for malignancy. Although gadolinium-enhanced dynamic study appears to be able to differentiate uterine sarcoma (significant enhancement) from endometrial carcinoma (no or minimally enhancement), the main purpose of MRI is to determine the local extent of the mass. Rarely, the uterus and cervix are involved by leukemia or lymphoma; the most common manifestation of uterine lymphoma is diffuse, homogeneous enlargement of the uterus. Metastases to the uterus can occur in advanced stage malignancies, most commonly from breast and stomach cancers.

CASE 71

CLINICAL HISTORY *32-year-old man presenting with rectal discomfort.*

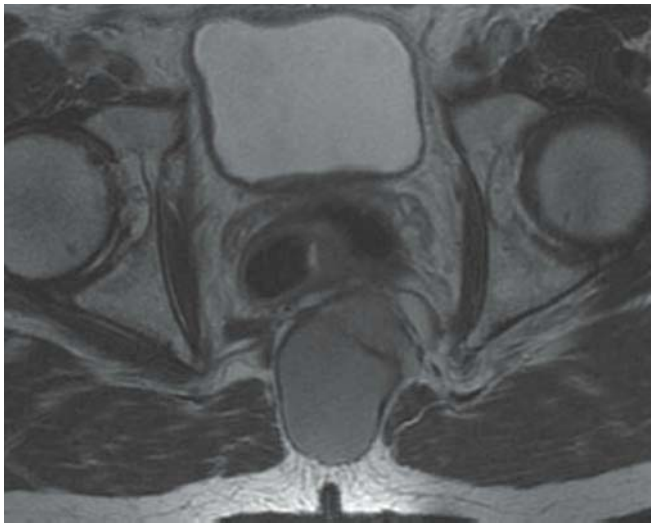

FIGURE 71A

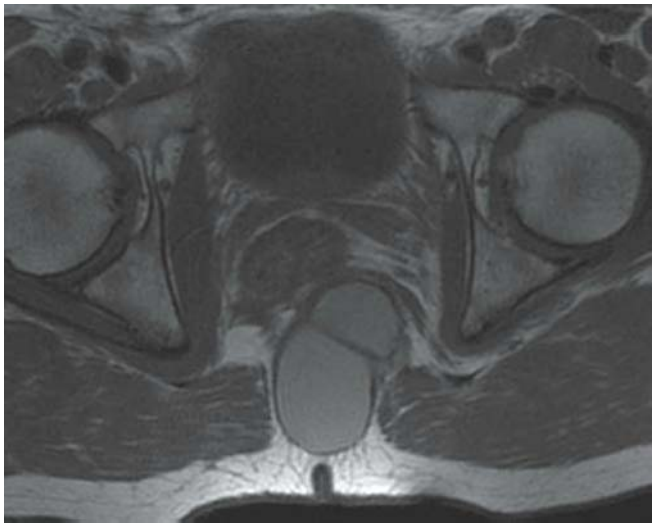

FIGURE 71C

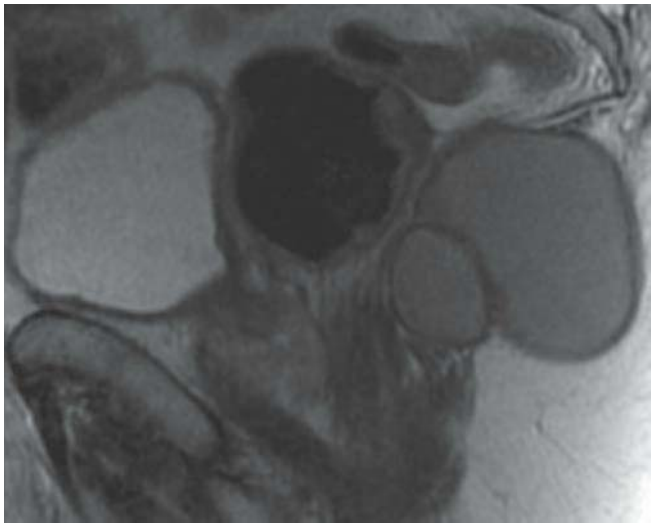

FIGURE 71B

FIGURE 71D

FINDINGS Axial and coronal T2-WIs (A and B) demonstrate a 4.5-cm bilocular retrorectal cyst. Its content is hyperintense on the axial T1-WI (C). Only enhancement of the cyst wall is perceptible on the gadolinium-enhanced, fat-suppressed T1-WI (D).

DIFFERENTIAL DIAGNOSIS Enteric cyst, dermoid cyst, neurenteric cyst.

DIAGNOSIS Epidermoid cyst.

DISCUSSION Retrorectal developmental cysts in adults are usually congenital and occur most commonly in middle-aged females. There are four types: epidermoid cysts, dermoid cysts, enteric cysts (which include tailgut cysts and cystic rectal duplication), and neurenteric cysts. They are typically asymptomatic, but patients may present with pressure symptoms or dysuria, or because of complications. At imaging, they are difficult to distinguish from each other; they present as unilocular or multilocular thin-walled cysts. Rarely, calcifications (seen with tailgut or dermoid cysts) or sacral bone defects may be encountered. When the cysts become complicated, they may contain gas (anorectal fistulization), blood products (bleeding), and soft tissue components (malignant degeneration, in up to 7%), or have thick walls and surrounding fat stranding (infection seen in 30% to 50% of cases). In cases of neurenteric cysts, a communication with the subarachnoid space may be demonstrated. Treatment consists of surgical excision to establish a definitive diagnosis and prevent complications. Other retrorectal cystic lesions include lymphangiomas, sacrococcygeal teratomas (seen in the pediatric population), anterior sacral meningoceles, and abscesses.

CASE 72

CLINICAL HISTORY *47-year-old man presenting with right flank pain.*

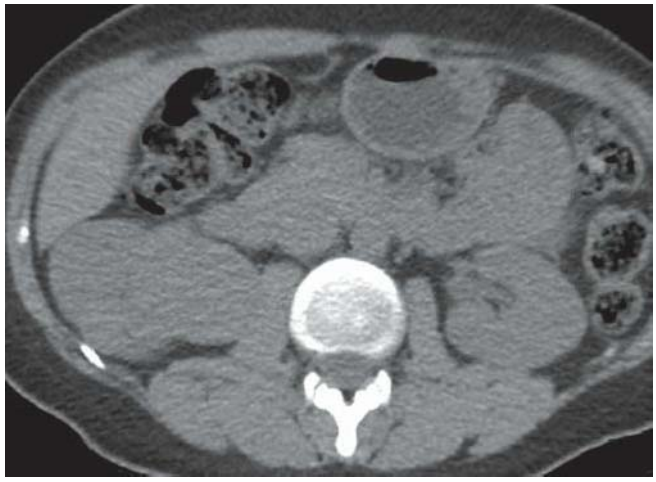

FIGURE 72A

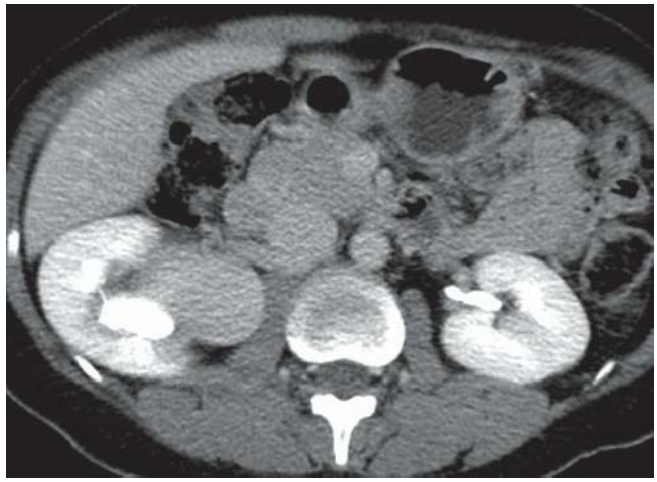

FIGURE 72C

FIGURE 72B

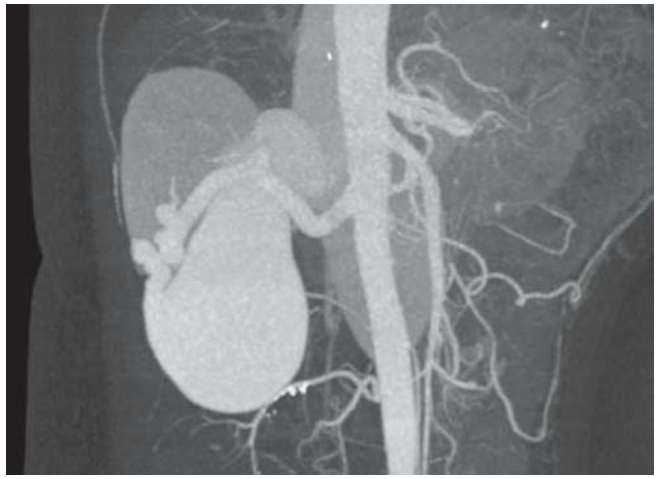

FIGURE 72D

FINDINGS Axial NECT image (A) demonstrates a 4.5 cm × 3.8 cm homogeneous ovoid mass in the right renal sinus. On the arterial phase (B) and portal venous phase (C) CECT images, the enhancement of the lesion follows that of the aorta. The coronal MIP image (D) shows enlargement of the right renal artery and vein. Additional abnormally enlarged vessels are seen deep in the renal sinus (B and D).

DIFFERENTIAL DIAGNOSIS Renal artery aneurysm.

DIAGNOSIS Arteriovenous malformation.

DISCUSSION Arteriovenous communications are of two types: arteriovenous malformations (AVMs) and arteriovenous fistulas (AVFs). AVMs can either be congenital or acquired, be secondary to trauma, result from rupture of an aneurysm, or result from a very vascular tumor. They are often asymptomatic and are more common in men. AVMs consist of multiple communications between segmental of interlobar arteries and veins, usually of normal caliber. AVMs are typically located adjacent to the renal collecting system, as seen in this case. AVFs are more common than AVMs, representing 70% to 80% of arteriovenous communications; they can result from trauma, surgery, tumors, or rupture of an aneurysm into a vein. AVFs typically have a single feeding artery and draining vein, which are usually enlarged. Most of them close on their own. Fifty percent of symptomatic AVFs will cause high-output heart failure. On imaging, arteriovenous communications will demonstrate prompt early filling of the draining vein. In case of an AVM, a vascular mass and curvilinear calcifications may be seen. Therapy consists of percutaneous intravascular treatment, surgery, or a combination of these two. This case does not represent a simple renal artery aneurysm because multiple abnormal surrounding vessels are present, indicating a more complex vascular anomaly.

CASE 73

CLINICAL HISTORY *27-year-old man presenting with shortness of breath and cough.*

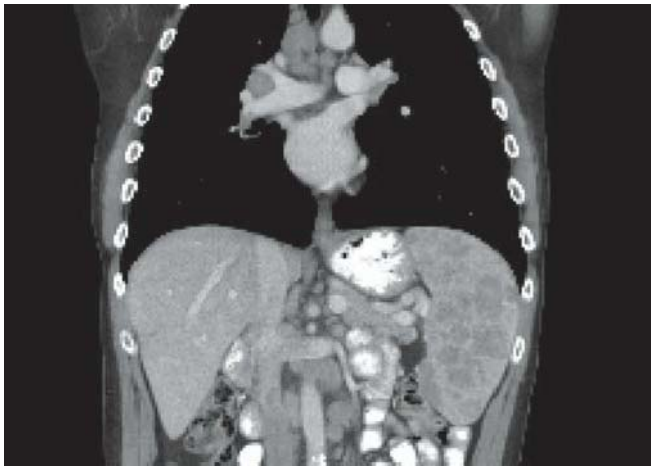

FIGURE 73A

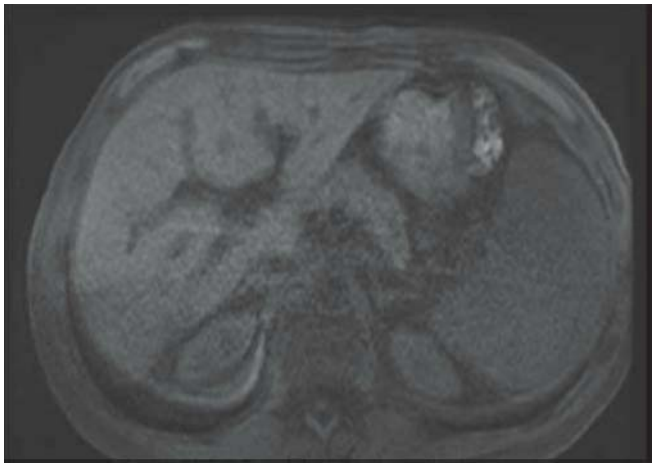

FIGURE 73C

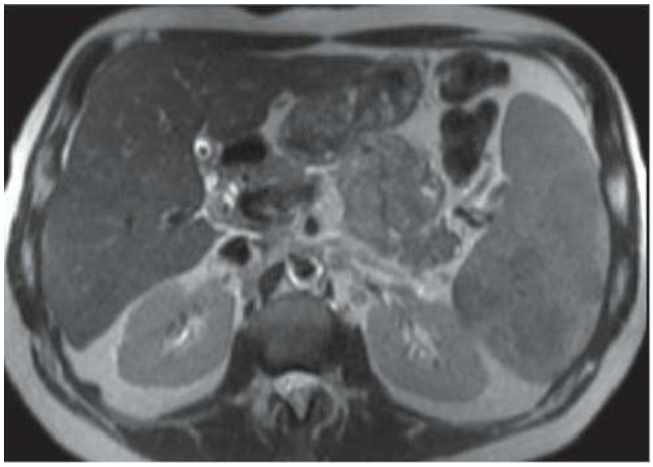

FIGURE 73B

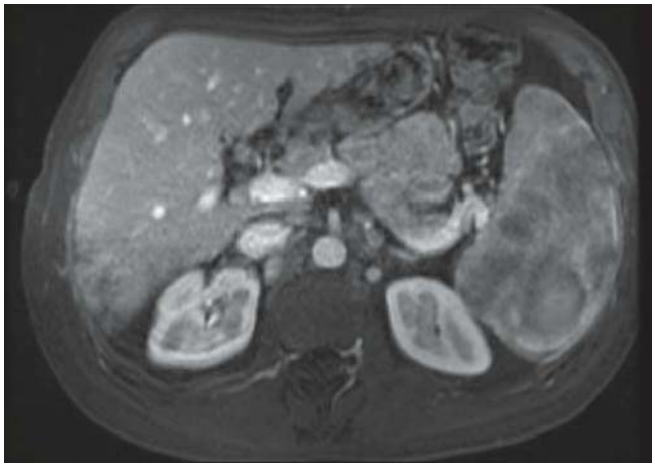

FIGURE 73D

FINDINGS Coronal reformatted CECT image (A) demonstrates multiple centrally enhancing lesions in the spleen. Note the presence of splenomagaly and mediastinal as well as retroperitoneal lymphadenopathy. Axial T2-WI (B) shows the lesions are slightly hypointense. The lesions are isointense to the spleen on the fat-suppressed axial T1-WI (C) and demonstrate central enhancement on the fat-suppressed, gadolinium-enhanced axial T1-WI (D).

DIFFERENTIAL DIAGNOSIS Metastases, abscesses, lymphoma, multiple hemangiomas.

DIAGNOSIS Splenic sarcoidosis.

DISCUSSION Sarcoidosis is a systemic disease of unknown etiology that primarily affects the mediastinal and hilar lymph nodes, lung parenchyma, skin, and eyes. It is characterized by the presence of noncaseating granulomas that can affect almost any organ. Abdominal sarcoidosis is common and splenic involvement is microscopically demonstrated in approximately 24% to 59% of patients, but its clinical significance is uncertain and splenic dysfunction is rare. Mild splenomegaly occurs in 11% to 42% of patients with sarcoidosis. The radiologic features in the abdomen are nonspecific, and most often the diagnosis is made by biopsy of peripheral nodes, liver, or skin. On CT, splenic sarcoidosis is usually not detected or abdominal involvement appears as nonspecific hepatospenomegaly and retroperitoneal lymphadenopathy. Multiple low-density intrasplenic lesions are present in 11% to 33% of cases, ranging in size from 1 to 30 mm. When nodules increase in size, a more coalescent hypodense nodular pattern is seen. Sarcoid nodules are usually dark on T2-WI and demonstrate progressive enhancement on gadolinium-enhanced T1-WI.

CASE 74

CLINICAL HISTORY *45-year-old woman presenting with a questionable liver mass on US performed for right upper quadrant pain.*

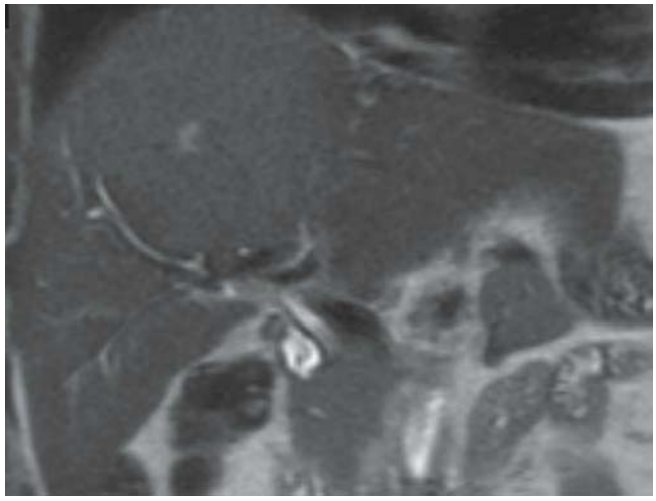

FIGURE 74A

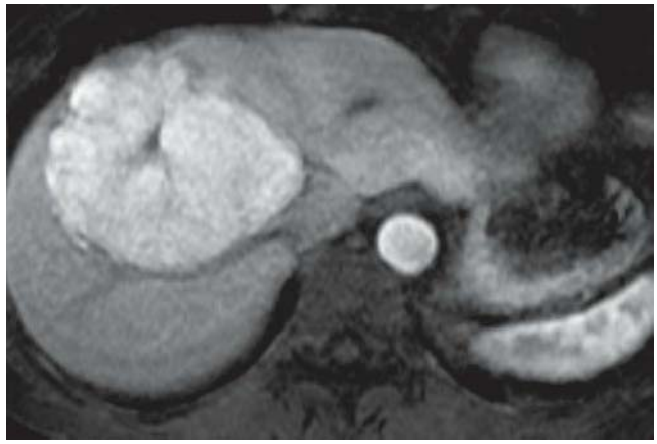

FIGURE 74C

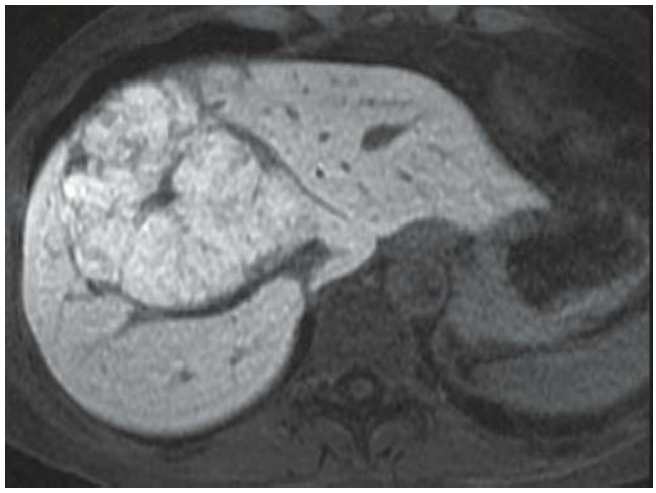

FIGURE 74B

FINDINGS Axial T2-WI (A) and T1-WI (B) demonstrate an isointense to slightly hyperintense lesion with a central scar which is hyperintense on T2-WI. Gadolinium-enhanced, fat-suppressed axial T1-WI in the arterial (C) show early intense homogeneous enhancement.

DIFFERENTIAL DIAGNOSIS Metastasis, hepatocellular adenoma, hepatocellular carcinoma.

DIAGNOSIS Focal nodular hyperplasia.

DISCUSSION Focal nodular hyperplasia (FNH) is a benign tumor like condition in the liver that is composed of abnormally arranged nodules of normal liver separated by fibrous septa. Bile ductules are often present within the fibrous septa or between the hepatocytes. These lesions are unencapsulated and lack the presence of central veins and portal triads. Because of the nature of FNH, one-third of these lesions tend to be isointense and similar in appearance to the normal liver parenchyma on T1-WI and T2-WI, often making it difficult to detect. Approximately two-thirds of FNH are slightly bright on the T2 images, slightly dark on the T1 images, or both. The presence of the central scar makes the diagnosis of FNH most likely. The central scar can often aid in the diagnosis because it will be hypointense on the T1-WI and hyperintense on the T2-WI relative to the liver. In addition, the central scar enhances on the post-gadolinium images. This is in distinction to the central scar seen in fibrolamellar carcinoma, which tends to be hypointense on both the T1- and T2-weighted sequences and enhances late. The increased signal of the central scar in the FNH may be related to the high fluid content of the loose myxomatous fibrous tissue in the central scar. In fibrolamellar hepatocellular carcinoma, however, the central scar is poorly vascularized, and the fibrosis is dense; therefore, its MR characteristics are more typical of those of collagen. The central scar, lack of cirrhosis, and age of the patient makes FNH the best diagnosis.

CASE 75

CLINICAL HISTORY *45-year-old man presenting with epigastric discomfort.*

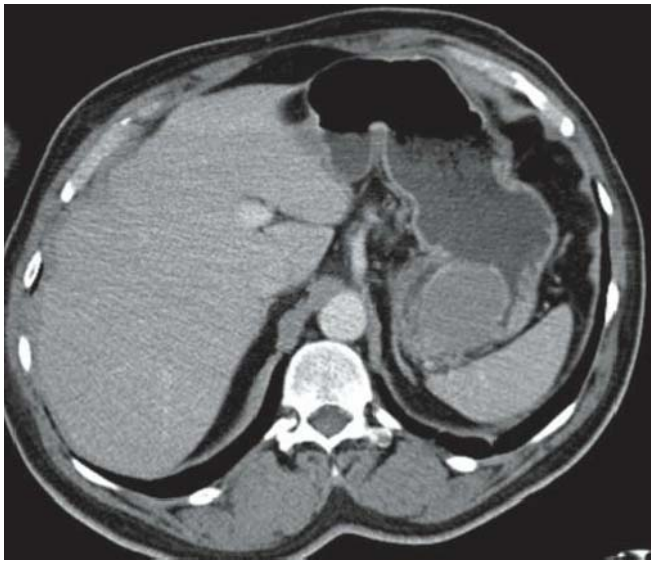

FIGURE 75A

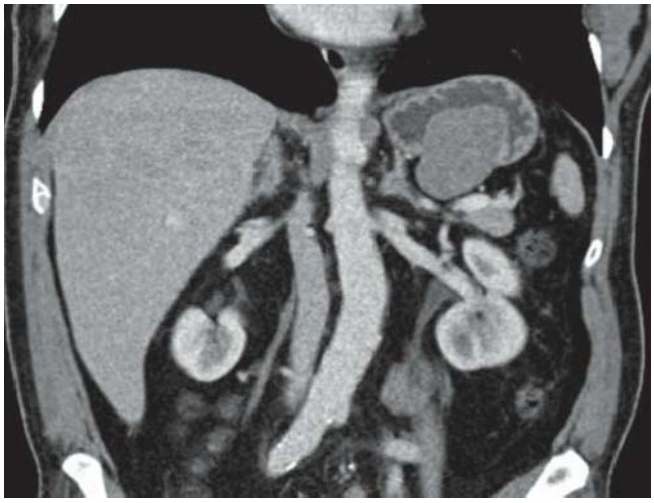

FIGURE 75B

FIGURE 75C

FINDINGS Axial CECT image (A) shows a 4.5-cm, well-defined mass arising from the lesser curvature of the stomach. Coronal (B) and sagittal (C) reformatted images demonstrate the enhancement of the mucosallining of the stomach in the intraluminal aspect of this lesion, confirming its submucosal/intramural location. There is no evidence for perigastric invasion or lymphadenopathy.

DIFFERENTIAL DIAGNOSIS Adenocarcinoma, metastasis, lymphoma.

DIAGNOSIS GI stromal tumor of the stomach.

DISCUSSION GI stromal tumor (GIST) is the most common extra mucosal tumor of the stomach and usually presents as an encapsulated intramural mass. GIST is characterized by immunoreactivity for the receptor c-KIT. At diagnosis, the majority of lesions are benign. Although GIST may arise anywhere in the GI tract, 70% of all GISTs occur in the stomach. Exophytic tumor growth is occasionally observed, resulting in a subserosal exogastric lesion. These lesions may grow to be among the largest tumors of the stomach because of their inclination to remain silent. They also have a limited tendency to cause GI bleeding, which is, in contrast, a common complication of gastric adenocarcinoma. Conventional barium examinations or endoscopy is often nonconclusive in patients with subserosal exogastric GIST because these lesions pass unrecognized due to the normal appearing overlying gastric mucosa. Other intramural gastric lesions include leiomyoma, leiomyoblastoma, lipoma, hemangioma, lymphangioma, schwannoma, and neurofibroma. Because they are composed of smooth muscle cells, GISTs typically show a hypervascular appearance on contrast-enhanced CT and MRI scans.

CASE 76

CLINICAL HISTORY *32-year-old man presenting with acute left flank pain and syncope.*

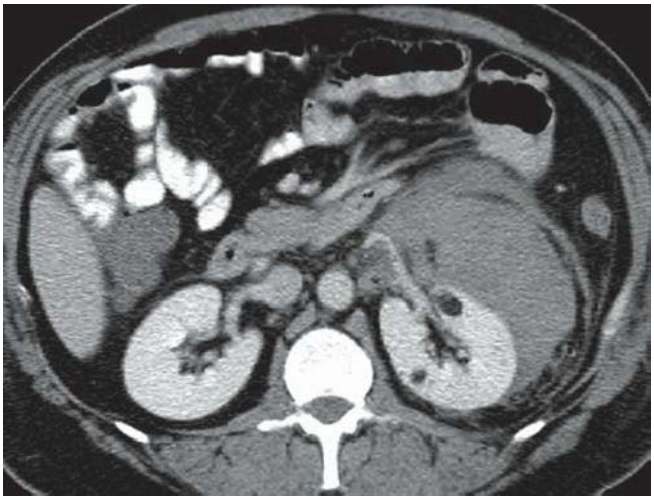

FIGURE 76A

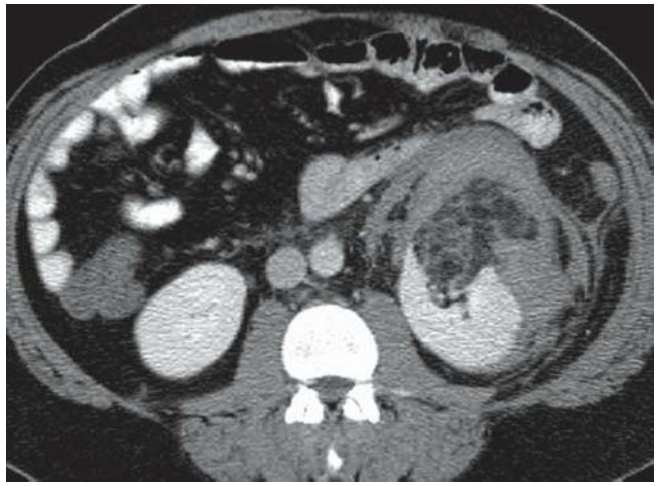

FIGURE 76C

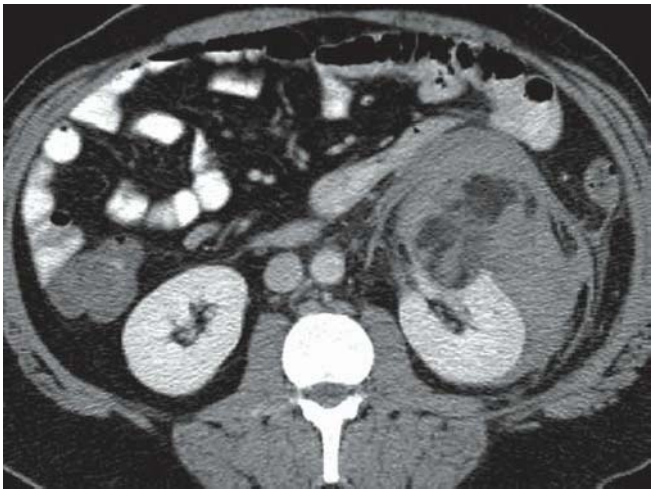

FIGURE 76B

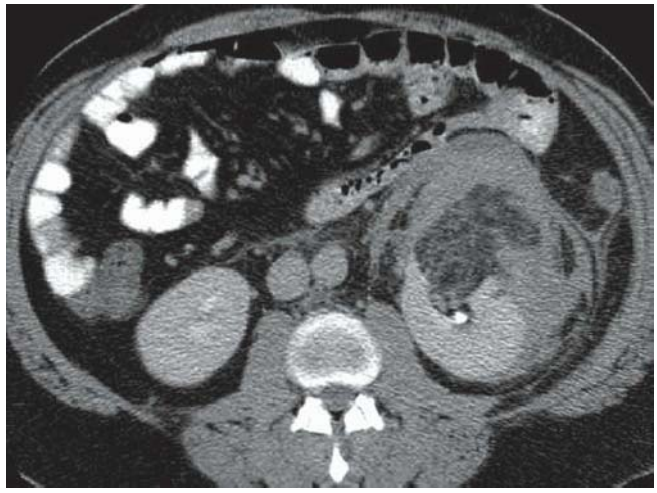

FIGURE 76D

FINDINGS Axial CECT images in the nephrographic phase (A–C) and excretory phase (D) demonstrate several fat-containing lesions in the left kidney, the largest of which measures 6.5 cm × 6.1 cm. Note hyperdense material in the perinephric and anterior pararenal space.

DIFFERENTIAL DIAGNOSIS Retroperitoneal liposarcoma.

DIAGNOSIS Hemorrhage from an angiomyolipoma.

DISCUSSION Angiomyolipoma (AML) is a benign mesenchymal hamartoma of the kidney containing variable amounts of fat, muscle, and blood vessels. Most of these lesions are found sporadically (80%), but there is a high association of AMLs with tuberous sclerosis. When the lesion is sporadic, it is typically found in middle-aged, women. The lesion is usually solitary and found incidentally except when hemorrhage from the lesion occurs, as in this case, producing flank pain. The risk of hemorrhage from an AML is significantly greater when the mass measures 4 cm or more; between 50% and 60% of AMLs above this size bleed spontaneously. CT imaging is usually diagnostic due to the presence of fat within the lesion. The absence of fat, however, does not exclude an AML because variable amounts of each mesenchymal component can be present. If the AML arises from the cortical surface, it can be difficult to distinguish from other retroperitoneal fat-containing tumors, such as liposarcoma. Therefore, it is crucial to find the organ of origin of the fatty mass. In this example, the lesion is shown to arise from the renal parenchyma, confirming the diagnosis of AML.

CASE 77

CLINICAL HISTORY *78-year-old man presenting with rectal bleeding is evaluated with abdominal CECT imaging; the patient was found to have rectal cancer.*

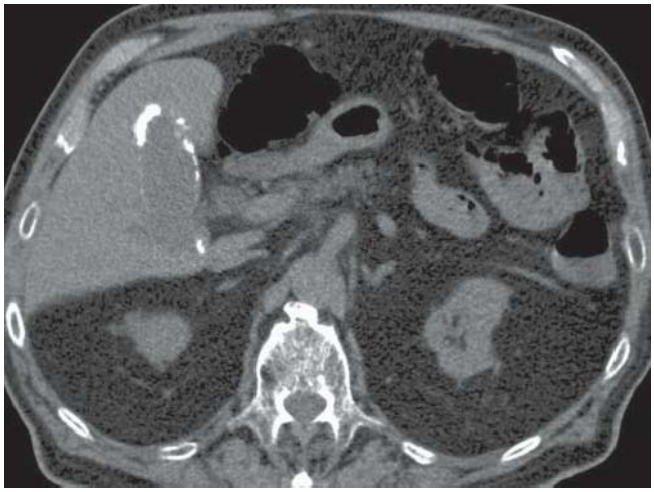

FIGURE 77A

FIGURE 77C

FIGURE 77B

FIGURE 77D

FINDINGS Axial NECT images (A–D) demonstrate extensive calcification within the wall of the gallbladder.

DIFFERENTIAL DIAGNOSIS Echinococcal cyst, calcified hematoma.

DIAGNOSIS Porcelain gallbladder.

DISCUSSION Porcelain gallbladder is due to the extensive deposition of calcium in a chronically inflamed gallbladder wall. Porcelain gallbladder is five times more frequent in women than in men and almost always associated with cholelithiasis. Some patients may present with symptoms including abdominal pain, nausea, vomiting, and fever; others may be asymptomatic. Because of the high incidence of gallbladder carcinoma in patients with porcelain gallbladder (11% to 33%), prophylactic cholecystectomy is advocated for patients even in the absence of clinical symptoms. Calcification of the wall occurs in two different patterns: broad, continuous calcification of the muscularis propria, as seen in this case, or multiple, punctate calcifications scattered throughout the mucosa and submucosa. A reliable diagnosis can be achieved with abdominal CT imaging by showing the characteristic calcification patterns of the gallbladder wall.

CASE 78

CLINICAL HISTORY *36-year-old man presenting with abdominal pain.*

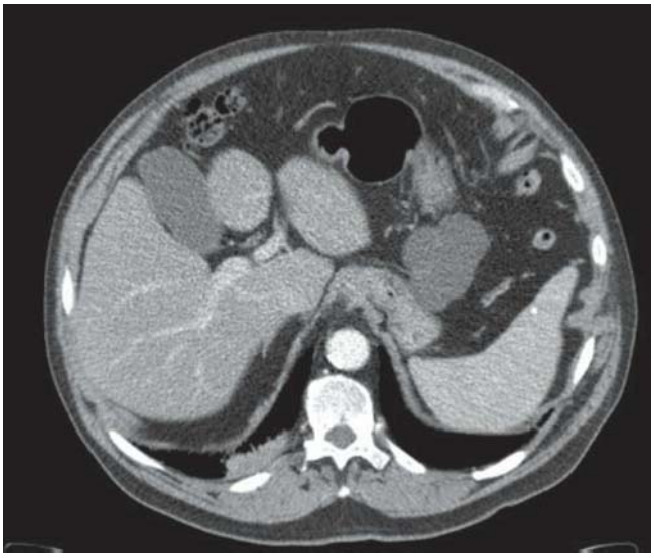

FIGURE 78A

FIGURE 78C

FIGURE 78B

FIGURE 78D

FINDINGS Axial CECT images (A and B) show well-defined 4- to 4.5-cm multiloculated cystic lesion in the pancreatic tail with six cysts. Coronal reformatted CECT images (C and D) demonstrate no significant enhancement of the cystic lesion or septations. No calcification is seen. A right renal calculus is also seen.

DIFFERENTIAL DIAGNOSIS Pancreatic pseudocyst, mucinous cystic tumor.

DIAGNOSIS Macrocystic variant of the serous pancreatic adenoma.

DISCUSSION Serous cystic tumors are composed of epithelial cells that produce serous fluid and show evidence of ductal differentiation. Previously, these tumors were also known as "microcystic adenomas" because they were composed of a large number (>6) of tiny cysts that were typically 2 cm or smaller. Recently, however, a variant of serous cystic tumors of the pancreas lined by epithelial cells indistinguishable from those in microcystic serous adenoma has been reported. This variant is termed "macrocystic serous adenoma of the pancreas" because the cysts are large and there are only a few cysts. Typically, this tumor is uni- or bilocular and contains no mural nodules, papillary projections, or calcifications. It is predominantly seen in women and typically located in the pancreatic head. The distinction between a mucinous cystic tumor and a macrocystic serous pancreatic adenoma cannot be made on the basis of radiologic features alone, and a fine-needle aspiration is typically needed.

CASE 79

CLINICAL HISTORY *50-year-old man presenting with weight loss and abdominal distention.*

FIGURE 79A

FIGURE 79C

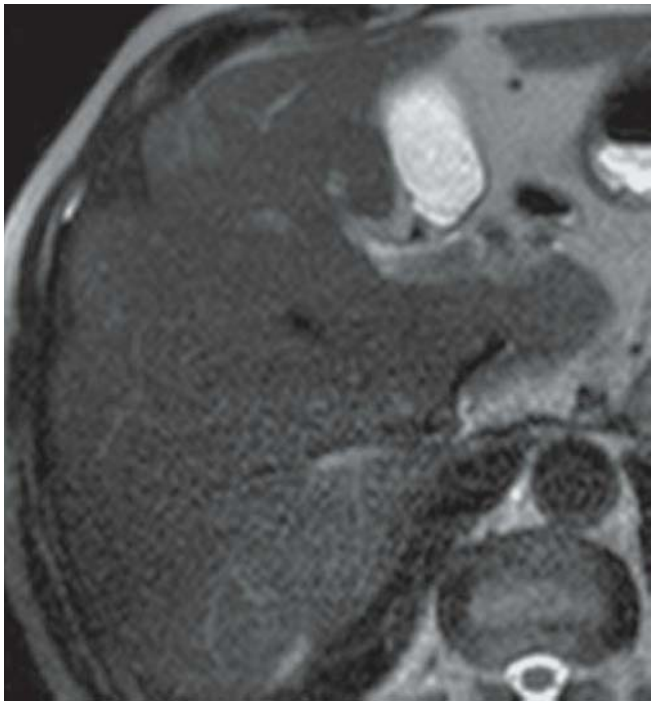

FIGURE 79B

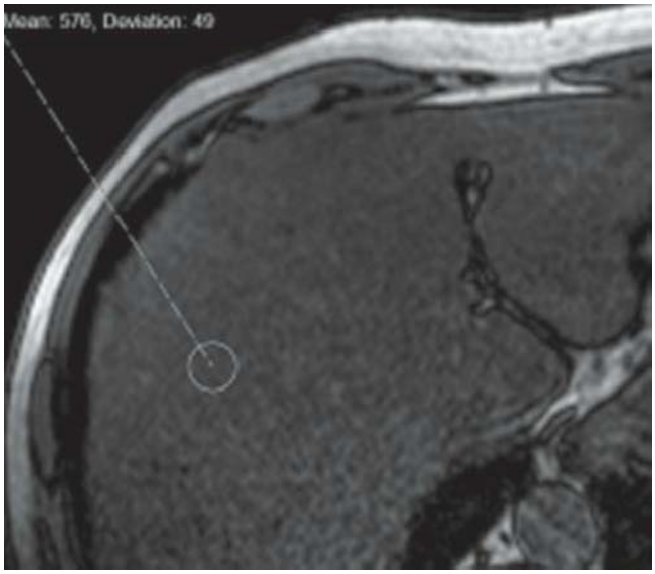

FIGURE 79D

FINDINGS Axial NECT image (A) demonstrates diffusely decreased hepatic attenuation with few focal areas of relatively normal hepatic attenuation. The liver margin is nodular. Axial T2-weighted MRI sequence (B) shows heterogenous signal on T2-weighted sequences. Opposed-phase sequences (C and D) of the same patient demonstrate drop in signal on out-of-phase sequences compatible with steatosis or fatty change.

DIFFERENTIAL DIAGNOSIS Cirrhosis with fatty liver, diffuse infiltrative type of cancer.

DIAGNOSIS Cirrhosis with fatty liver.

DISCUSSION Cirrhosis can produce many findings by CT. These include morphologic changes, such as an enlarged caudate lobe or enlarged left lateral segment, atrophy of the left medial segment and right anterior segments, a nodular contour, fatty change, portal hypertension (with ascites, collaterals, and splenomegaly), increased density of the mesenteric fat due to congestion, and the presence of regenerating nodules and hepatic fibrosis. Fatty liver is a common early finding

of cirrhosis and often precedes other CT findings. As atrophy and fibrosis occur in conjunction with the formation of regenerating nodules, the contour of the liver becomes nodular and retracted. In this example, there is heterogeneous low density to the liver, which could be confused with an uneven fatty change or a diffuse neoplastic process, such as hepatocellular carcinoma. The key to the differentiation is the lack of mass effect by these low areas of attenuation. The vessels are seen to have a normal course through the liver without displacement. MRI, with the use of in- and out-of-phase T1-WI, may bring clarification. Areas that contain fat will show significant drop in signal on the out-of-phase images as in this case.

CASE 80

CLINICAL HISTORY *34-year-old man presenting with left upper quadrant pain.*

FIGURE 80A

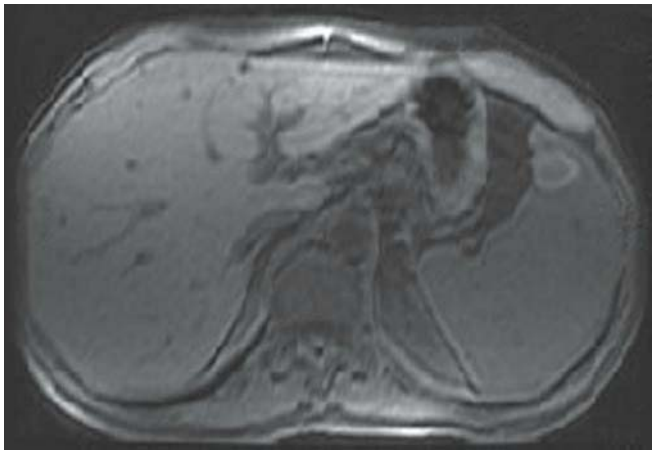

FIGURE 80C

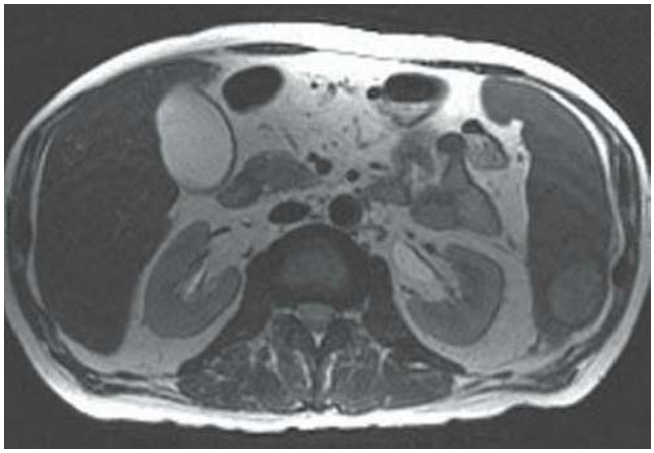

FIGURE 80B

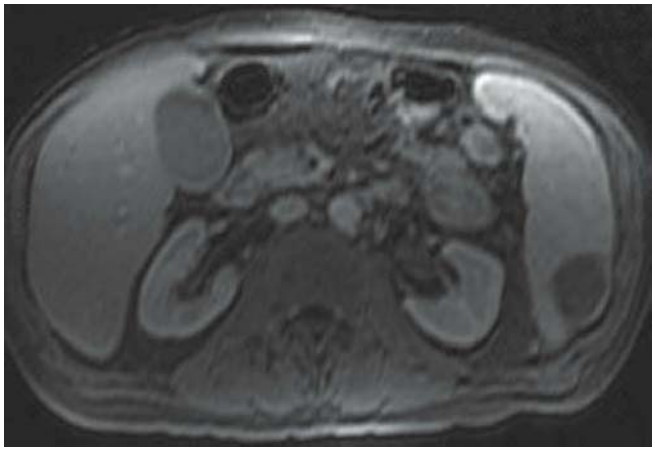

FIGURE 80D

FINDINGS Axial CECT (A) demonstrates two geographic hypo-attenuating areas in the spleen. Axial T2-WI (B) shows an additional round lesion more inferiorly, which has bright signal. On the fat-suppressed axial T1-WI (C), one lesion has a spontaneously bright curvilinear central area. No enhancement is seen on the gadolinium-enhanced, fat-suppressed axial T1-WI (D).

DIFFERENTIAL DIAGNOSIS Splenic laceration, fracture.

DIAGNOSIS Splenic infarcts.

DISCUSSION There are multiple causes for splenic infarcts, including emboli, hematologic diseases, portal hypertension, and iatrogenic causes. In patients younger than 40 years, hemoglobinopathies are the most common cause of splenic infarction. Infarcts can have a variety of CT appearances ranging from the classic peripheral wedge-shaped defect to focal round lesions and ill-defined areas of low attenuation. These lesions are best demonstrated on CECT image. During the acute stage, infarcts are ill-defined and heterogeneously hyperdense due to areas of hemorrhage within them. MRI best shows the internal hemorrhage on the T1-WI, as in this case. As an infarct begins to fibrose, it will appear better demarcated and may cause contraction of the surrounding normal spleen. When serial CT scans demonstrate progressive liquefaction and necrosis with outward extension, developing subcapsular hemorrhage, and free peritoneal hematoma, the possibility of impending rupture or superimposed infection should be considered.

Even though infarcts are typically wedge-shaped, on axial images, they may appear round, as in this case, depending on how the wedge-shaped area is "cut" on the image; this is more commonly seen in infarcts in the superior and inferior aspects of the spleen. Coronal or sagittal reformatted images would show best the true wedge-shaped configuration of the abnormality.

CASE 81

CLINICAL HISTORY *37-year-old woman presenting with known steatohepatitis and alcohol abuse.*

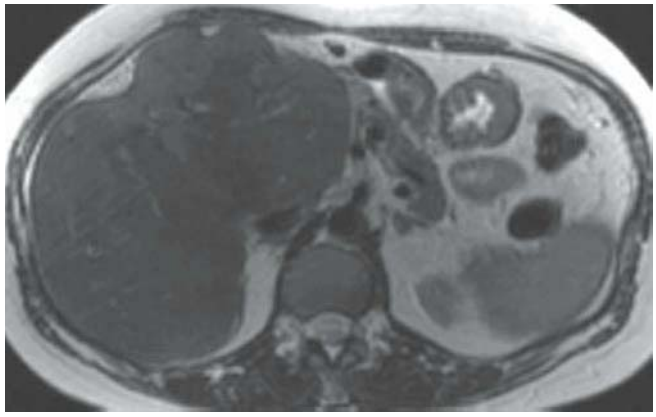

FIGURE 81A

FIGURE 81C

FIGURE 81B

FIGURE 81D

FINDINGS Axial MRI demonstrate marked enlargement of the lateral segment of the left lobe of the liver and concomitant decrease in the size of the right liver lobe. An ill-defined wedge-shaped area within the medial segment of the left liver lobe shows increased signal intensity on the axial T2-WI (A), decreased signal intensity on the fat-suppressed axial T1-WI (B), and delayed enhancement on gadolinium-enhanced, fat-suppressed axial T1-WI (C and D). Hepatic vessels are seen traversing through this region without the evidence of distortion. Also note the capsular retraction adjacent to the abnormal area.

DIFFERENTIAL DIAGNOSIS Hepatocellular carcinoma, intrahepatic cholangiocarcinoma.

DIAGNOSIS Confluent hepatic fibrosis.

DISCUSSION Confluent hepatic fibrosis can present as a masslike area (14%) in patients with underlying cirrhosis, especially primary sclerosing cholangitis. It typically affects the anterior segments of the right lobe and medial segments of the left lobe. Confluent hepatic fibrosis usually has a wedge-shaped appearance, but in some patients, the entire segment might be involved. The typical appearance of confluent hepatic fibrosis is an area of low signal intensity on T1-WI and high signal intensity on T2-WI. It usually demonstrates delayed enhancement on gadolinium-enhanced images. The typical geographic pattern of involvement and retraction of the overlying hepatic capsule can be helpful in diagnosing this condition. Possible explanations for the hyperintense appearance of confluent fibrosis on T2-WI are a relative reduction in the signal of the remaining liver parenchyma due to increased iron deposition, edema due to venous thrombosis, or most likely, inflammatory changes within the fibrosis.

CASE 82

CLINICAL HISTORY *22-year-old man presenting with abdominal pain and tenderness.*

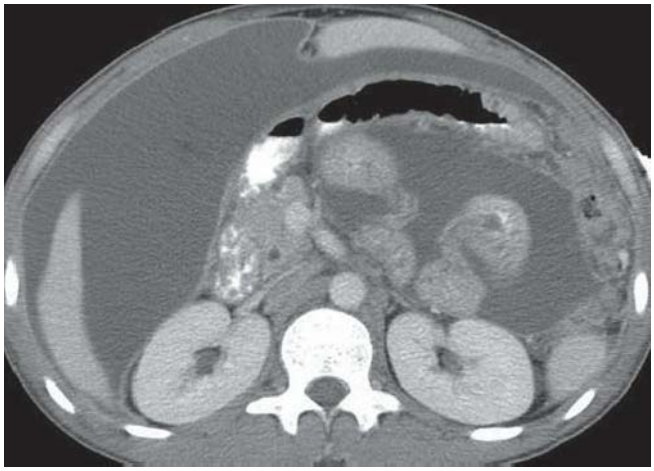

FIGURE 82A

FIGURE 82C

FIGURE 82B

FIGURE 82D

FINDINGS Axial CECT images (A–D) demonstrate high-density ascites as well as a thick enhancing peritoneum. There are also omental and retroperitoneal lymph nodes.

DIFFERENTIAL DIAGNOSIS Peritoneal carcinomatosis, malignant mesothelioma.

DIAGNOSIS Tuberculosis peritonitis and omentitis.

DISCUSSION Although tuberculosis is unusual in Western countries, there has been an increased incidence of tuberculosis due to the large number of chronically immunosuppressed patients due to transplantation, HIV infection, and other causes. Extrapulmonary tuberculosis has proportionally also increased, reaching up to 15% of new cases of tuberculosis documented in the United States. Furthermore, in only 15% of cases of abdominal tuberculosis, there is pulmonary disease. Ascites due to tuberculosis has high attenuation (20 to 45 HU) due to the high protein and cellular contents. CT also demonstrates peritoneal thickening, enhancement, and sometimes nodularity corresponding to the tuberculomas present in it. Omental caking can be seen in up to 82% of patients with abdominal tuberculosis. Peritoneal carcinomatosis is very difficult to distinguish from tuberculous peritonitis except for the fact that, in the latter, there is history of a known malignancy. Peritoneal mesothelioma can also produce some of the findings seen in tuberculous peritonitis, but the peritoneal thickening is much more pronounced, and the ascites is less massive than in tuberculosis.

CASE 83

CLINICAL HISTORY *49-year-old man with chronic affective disorder presenting with lower abdominal pain.*

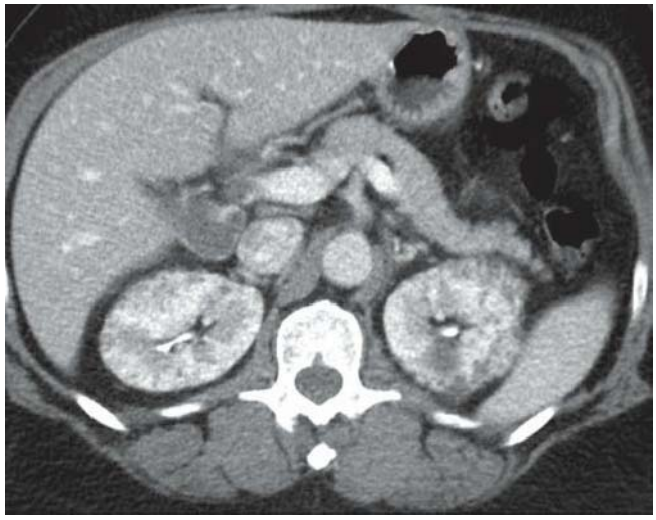

FIGURE 83A

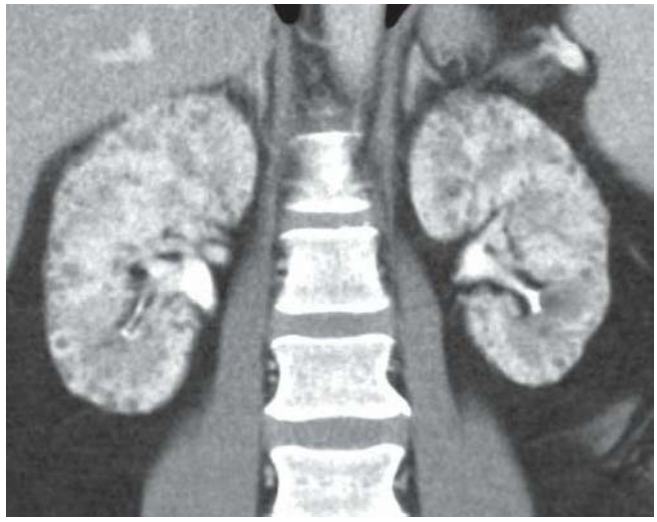

FIGURE 83C

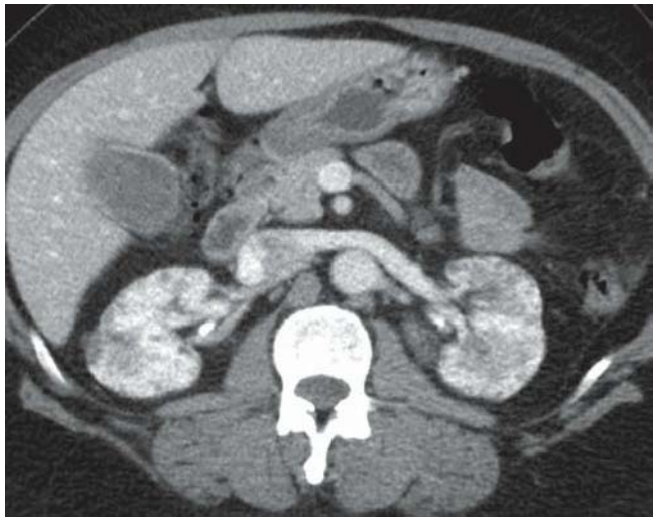

FIGURE 83B

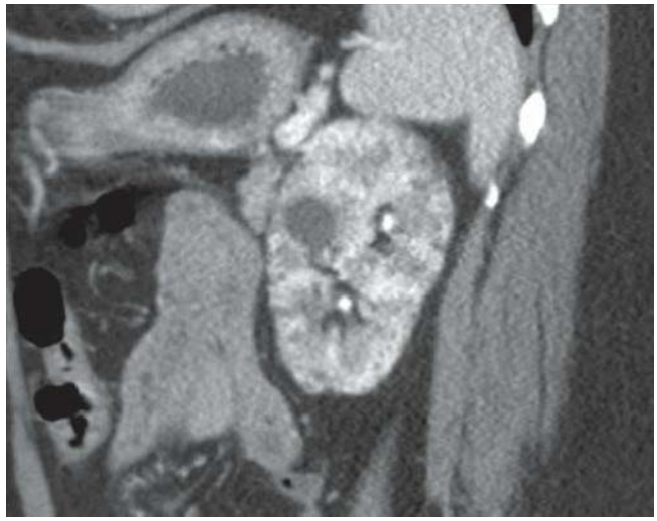

FIGURE 83D

FINDINGS Axial (A and B), coronal reformatted (C), and sagittal reformatted (D) CECT images demonstrate innumerable microcysts in the cortex and medulla of both kidneys.

DIFFERENTIAL DIAGNOSIS Glomerulocystic kidney disease, autosomal recessive polycystic kidney disease, autosomal dominant polycystic kidney disease.

DIAGNOSIS Chronic lithium nephropathy.

DISCUSSION Chronic lithium nephropathy is a progressive condition causing interstitial fibrosis and dilatation of distal tubules with formation of microcysts. These microcysts are identified in 63% of renal biopsy specimens of patients on chronic lithium therapy. The cysts are present in both the cortex and the medulla and measure 1 to 2 mm in size. Progressive decrease in renal function is seen in chronic lithium nephropathy. On the other hand, glomerulocystic kidney disease, occurring in sporadic or familial forms, is characterized by cystic dilatation of Bowman's capsule; the cysts are therefore entirely cortical in distribution, a key distinguishing factor. Patients with autosomal recessive polycystic kidney disease (ARPKD) present in the early life with multiple small renal cysts in massively enlarged kidneys. The juvenile form of ARPKD presents in adolescence with associated findings of portal hypertension. The kidneys of patients with autosomal dominant polycystic kidney disease harbor multiple cysts, but of larger size (several centimeters).

CASE 84

CLINICAL HISTORY *26-year-old woman presenting with an asymptomatic vaginal bulge.*

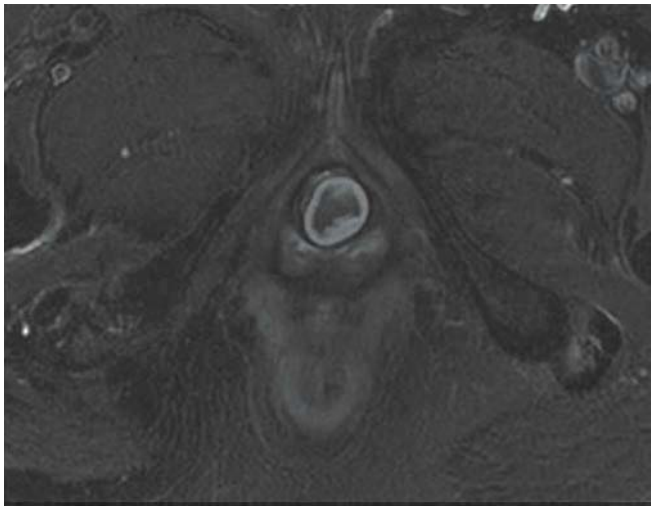

FIGURE 84A

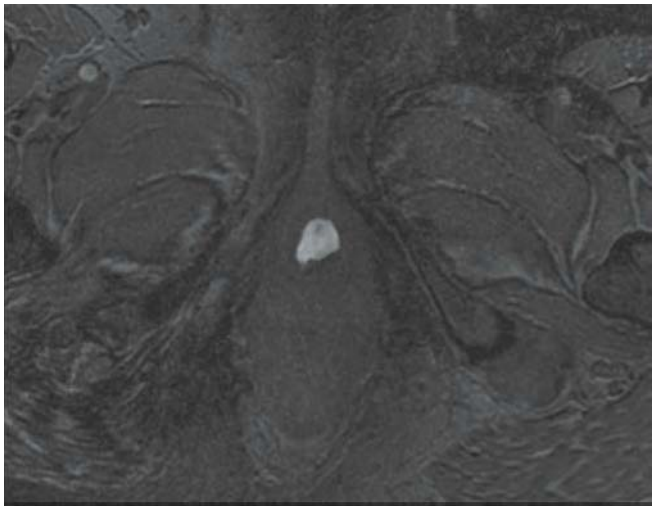

FIGURE 84C

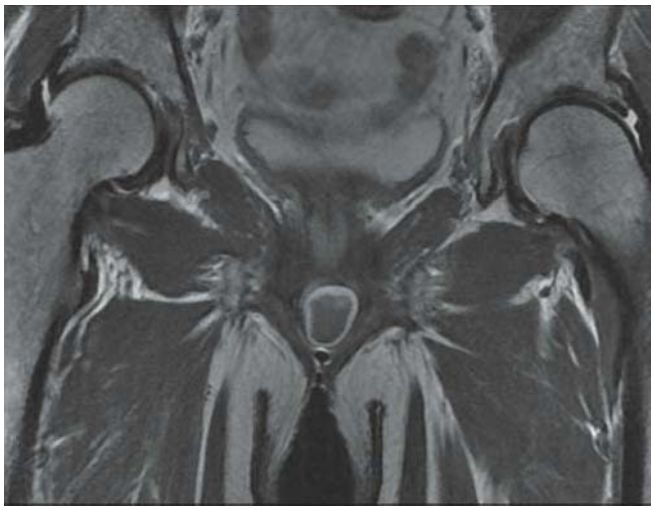

FIGURE 84B

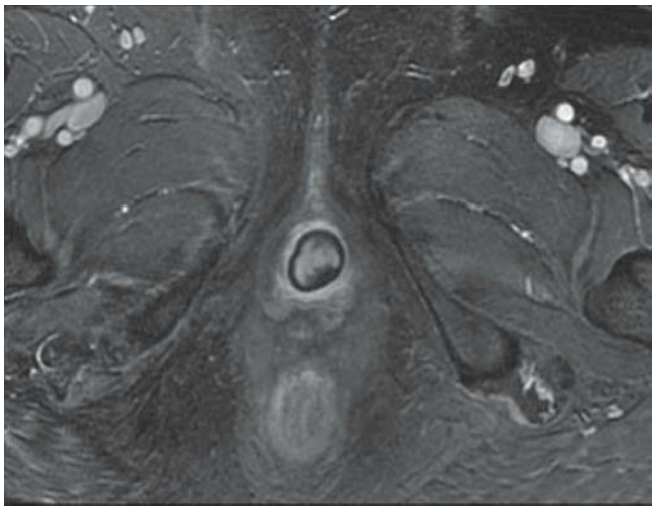

FIGURE 84D

FINDINGS Axial fat-suppressed (A) and coronal (B) T2-WIs show a well-delineated ovoid lesion, located posterior to the urethra, with alternating peripheral hypo- and hyperintense rim. Fat-suppressed axial T1-WI (C) reveals the homogeneous bright content of the mass, suggesting the presence of blood products or protein. Gadolinium-enhanced, fat-suppressed axial T1-WI (D) demonstrates peripheral smooth enhancement.

DIFFERENTIAL DIAGNOSIS Urethral diverticulum, Bartholin gland cyst, Gartner duct cyst.

DIAGNOSIS Skene's gland cyst.

DISCUSSION Skene's glands arise from the lower urethra but drain on the vestibular surface on either side of the urethral meatus. Obstruction and resulting enlargement of a Skene's gland presents as a fluctuant mass that extends inferiorly from the perineum. This case shows a protein/hemorrhage containing (as evidenced by T1 bright and T2 dark signal of the cyst content) periurethral mass with no obvious connection to the urethra. The midline periurethral location, the ovoid shape, and proteineous content are typical features of a Skene's gland cyst. Batholin gland cysts are located laterally at the vaginal meatus. Gartner duct cysts are vaginal cysts arising from the anterolateral wall of the vagina. Urethral diverticula in females arise most commonly from obstructed/infected Skene gland cysts that eventually erupt into the urethra and therefore show a connection on imaging. Moreover, because of their decompression, they typically have a semi-lunar shape and are filled with urine.

CASE 85

CLINICAL HISTORY *45-year-old woman presenting with weight loss.*

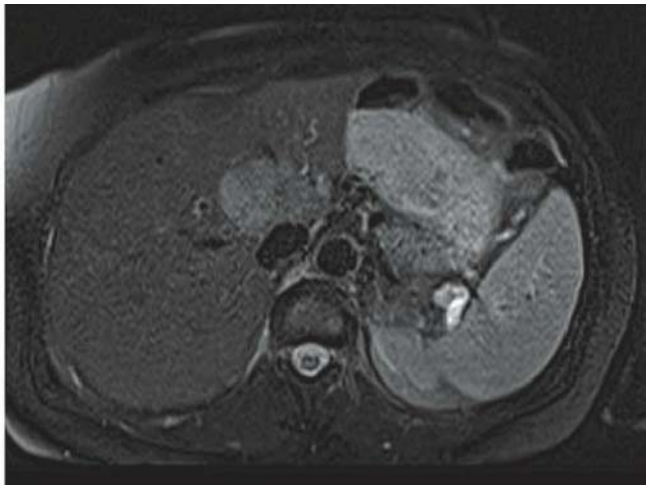

FIGURE 85A

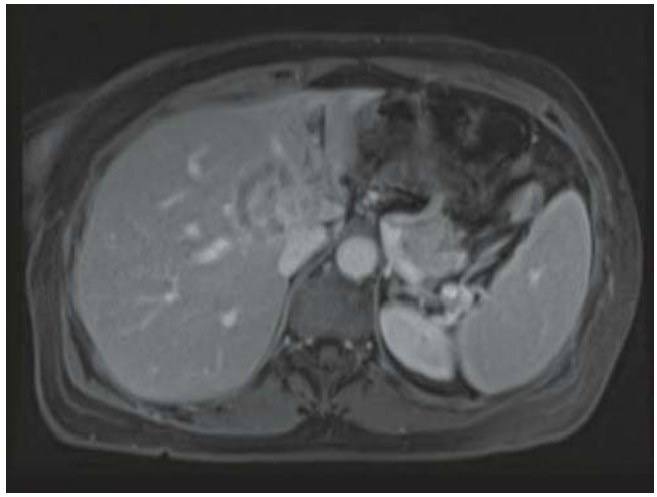

FIGURE 85C

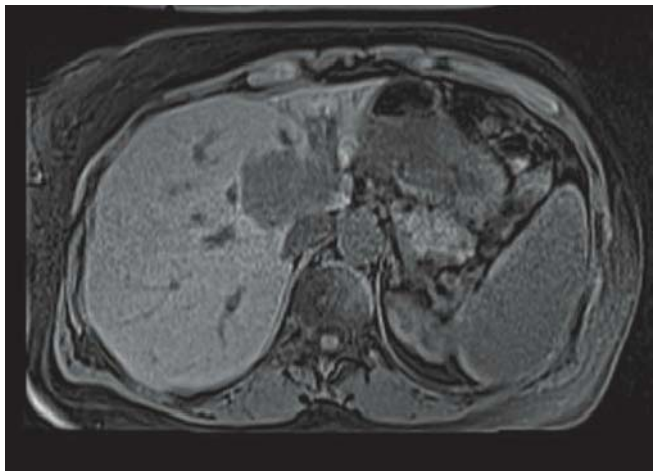

FIGURE 85B

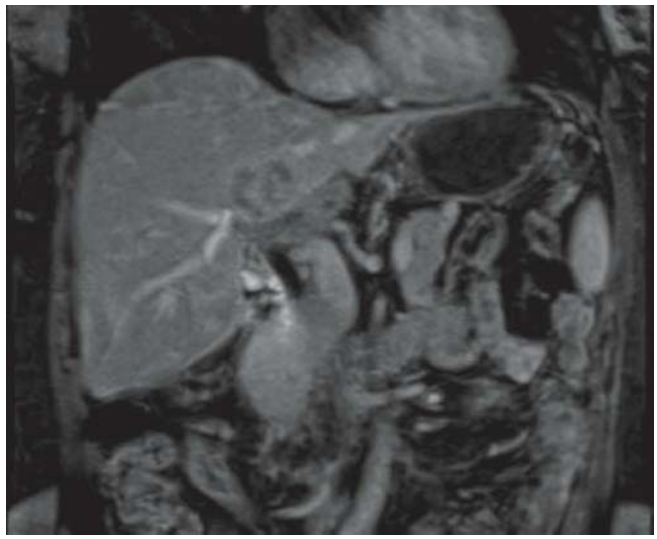

FIGURE 85D

FINDINGS Axial T2-WI (A) shows mildly hyperintense lesion centered within the left lobe surrounding the focally dilated biliary radicals. The left lobe of the liver is markedly atrophic. Pre– (B) and post–gadolinium-enhanced, fat-suppressed axial (C) and coronal (D) T1-WIs obtained in the arterial and delayed phase demonstrate delayed progressive and persistent enhancement of the lesion of the T1 hypointense lesion. There is extension of the tumor into the common hepatic duct.

DIFFERENTIAL DIAGNOSIS Hepatocellular carcinoma, metastasis.

DIAGNOSIS Intrahepatic cholangiocarcinoma.

DISCUSSION Intrahepatic or peripheral cholangiocarcinoma (ICAC), an adenocarcinoma of biliary duct origin, originates in the small intrahepatic ducts; it represents 10% of all cholangiocarcinoma. On MRI, ICAC appears as a large mass of decreased signal intensity on T1-WI and shows mildly increased signal intensity on T2-WI. The pattern of enhancement on gadolinium-enhanced images depends largely on the size of the lesion. Whereas large ICACs (>4 cm) show an early peripheral rimlike enhancement with progressive centripetal fill-in and delayed enhancement of the central area of fibrosis, smaller lesions (2 to 4 cm) may enhance homogeneously. Although a similar pattern of enhancement may also be seen in hemangioma, the degree of enhancement is typically greater in hemangiomas. Other features of ICAC include the presence of satellite nodules, encasement of the portal vein without invasion, capsular retraction, and dilatation of intrahepatic bile ducts distal to the lesion.

CASE 86

CLINICAL HISTORY *64-year-old woman presenting with weight loss.*

FIGURE 86A

FIGURE 86C

FIGURE 86B

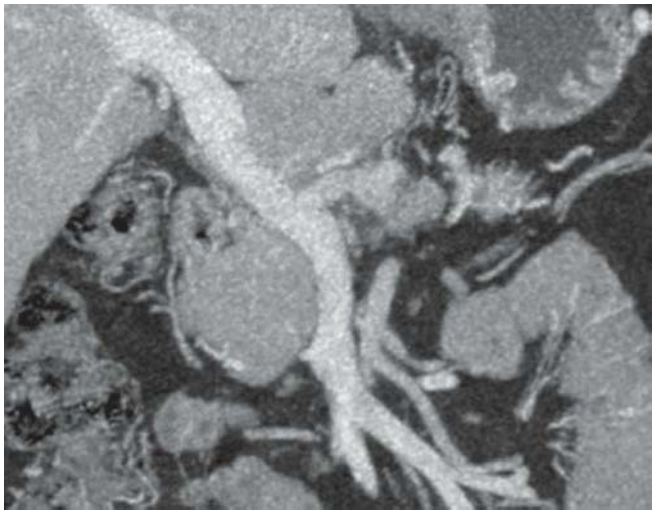

FIGURE 86D

FINDINGS Axial NECT image (A) demonstrates a 5-cm mass in the pancreatic head, with central calcifications. Axial (B), coronal reformatted (C), and curved reformatted (D) CECT images show enhancement of the mass and hypervascular liver lesions. The portal vein is of normal caliber.

DIFFERENTIAL DIAGNOSIS Pancreatic adenocarcinoma, metastasis.

DIAGNOSIS Non-hyperfunctioning endocrine pancreatic tumor.

DISCUSSION Endocrine neoplasms of the pancreas secrete hormones, such as insulin, glucagon, and somatostatin. When the tumor is hyperfunctioning with excessive hormone secretion, these patients usually present early in the course of the disease when the lesion is still small. Except for insulinomas, the majority of these lesions are malignant but tend to be slow growing. Insulinoma is the most common pancreatic endocrine tumor and typically presents in the fourth through sixth decades of life. Insulinomas are small with most being <1.5 cm and solitary (90%). Small calcifications (10%) can be present. Endocrine tumors are most often hypervascular and their metastases to preferentially the liver also demonstrate hypervascularity, as shown in this case. Non-hyperfunctioning endocrine tumors tend to be larger at presentation, are more heterogeneous due to necrosis and hemorrhage, and tend to be more likely malignant. A pancreatic adenocarcinoma of the size of the lesion in this case, located in the pancreatic head, would have narrowed or obstructed the portal vein, which is still widely patent, excluding this diagnosis.

CASE 87

CLINICAL HISTORY *22-year-old pregnant woman presenting with right-sided abdominal pain for 3 days.*

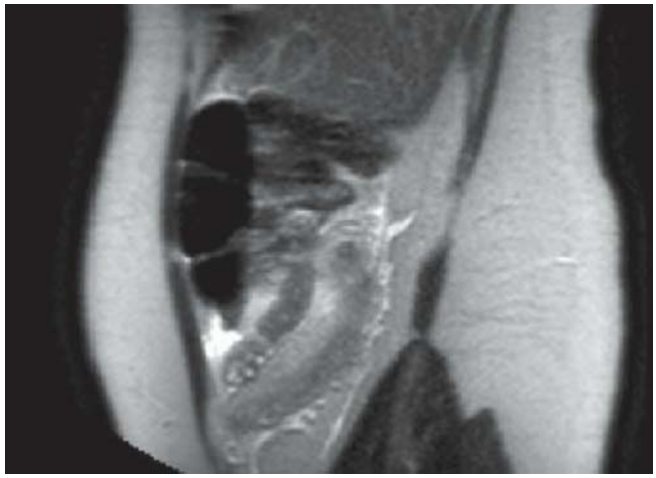

FIGURE 87A

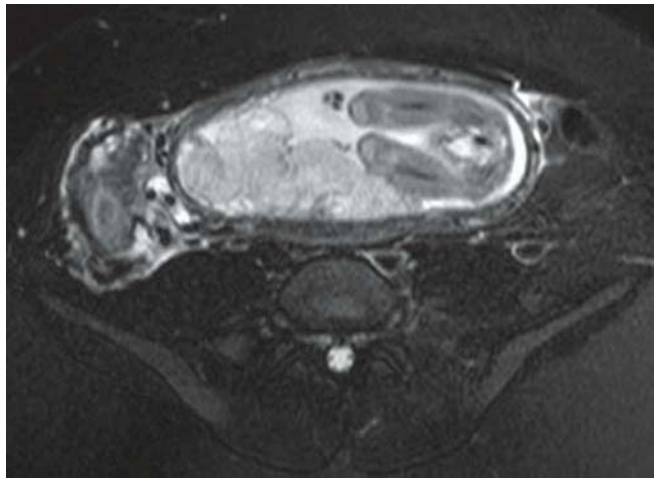

FIGURE 87C

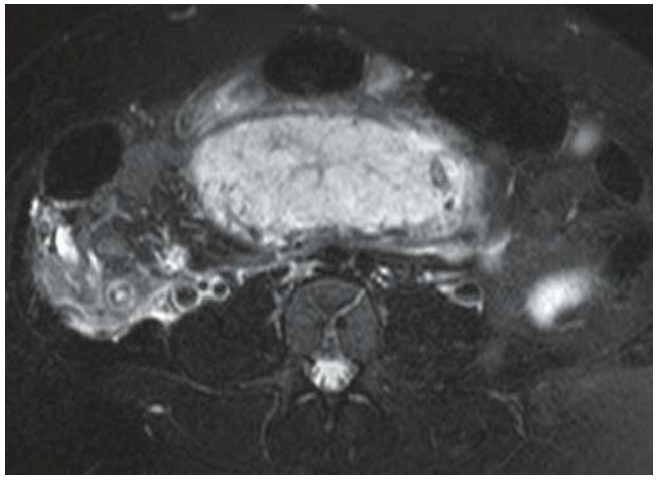

FIGURE 87B

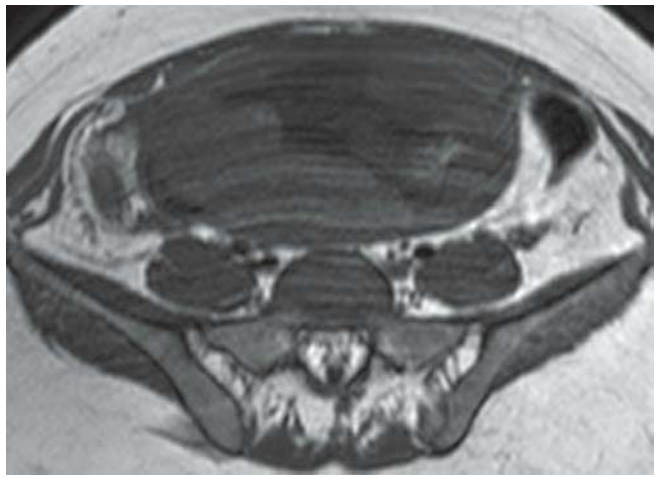

FIGURE 87D

FINDINGS Sagittal T2-WI (A) demonstrates a 1.5 cm in diameter blind-ended tubular structure in the right lower quadrant with surrounding edema. Fat-suppressed axial T2-WIs (B and C) show the wall edema of this structure with a target appearance and the adjacent fat edema. Axial T1-WI (D) also shows the hypointense surrounding fat stranding. Note the gravid uterus.

DIFFERENTIAL DIAGNOSIS None.

DIAGNOSIS Acute appendicitis in pregnancy.

DISCUSSION Acute appendicitis is the most common surgical emergency in pregnant women. The incidence of appendicitis in the pregnant female is similar to the one in the general population (0.05% to 0.07%). The diagnosis is often delayed, and patients present more frequently with perforation (43% versus 4% to 19% in the non-pregnant patients). The white blood count or sedimentation rates are unreliable in pregnancy. The clinical examination is also more difficult as the appendix is often displaced superiorly by the gravid uterus. When appendicitis is suspected in a pregnant woman, ultrasound is usually the first modality of imaging used, with various success rates, not only as it is operator-dependent, but also because the enlarged uterus displaces the bowel loops and pushes all laterally in the abdomen, often obscuring the appendix due to gas. MRI is therefore often used to evaluate the possibility of appendicitis. The inflamed appendix will be enlarged (diameter greater than 6 mm) and will have a target appearance with T2 hyperintense wall and surrounding inflammation in the fat manifested by strands of increased T2 signal. The appendix is sometimes hard to identify on MRI, and therefore, it is easier to first identify the cecum, center the imaging on it, and then try to localize the appendix.

CASE 88

CLINICAL HISTORY *64-year-old man with long-standing right upper quadrant pain presenting with jaundice and recent general deterioration.*

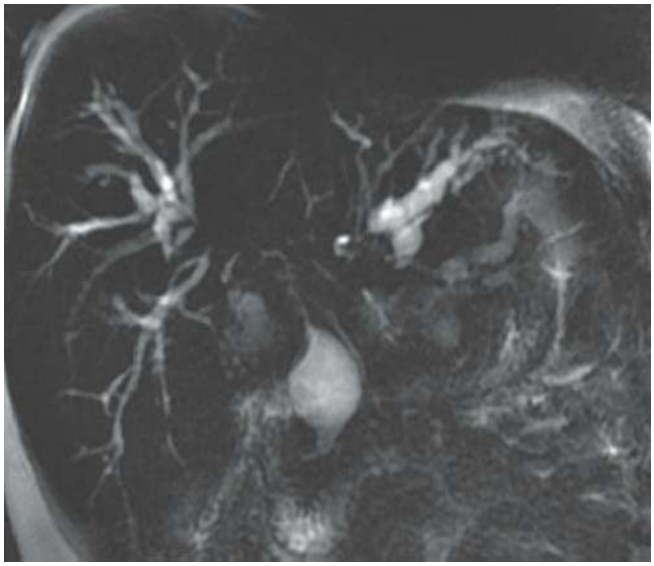

FIGURE 88A

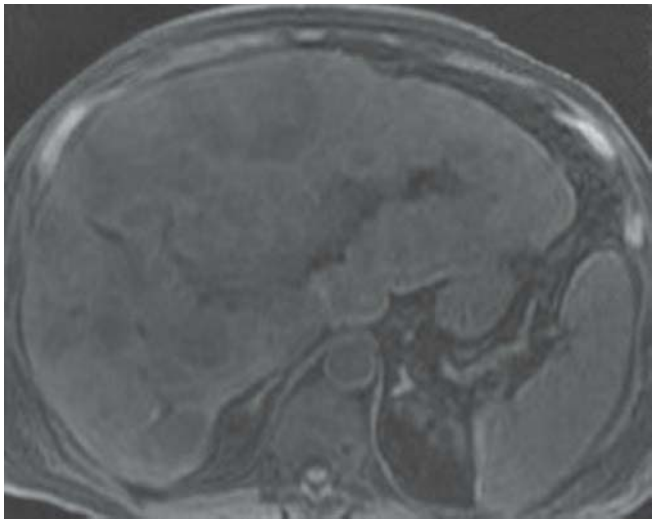

FIGURE 88C

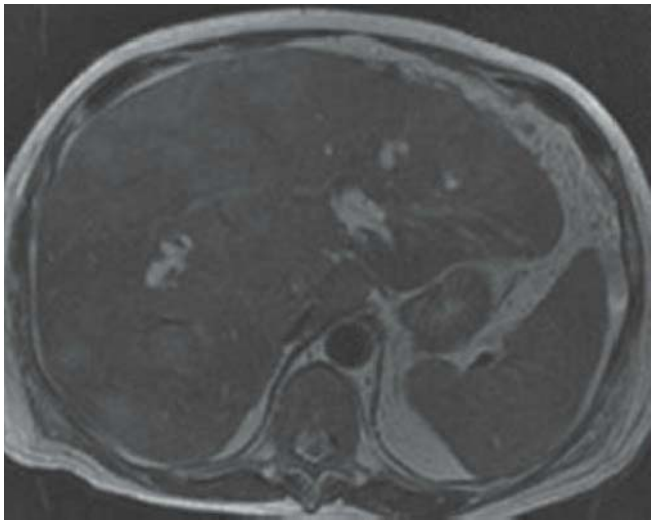

FIGURE 88B

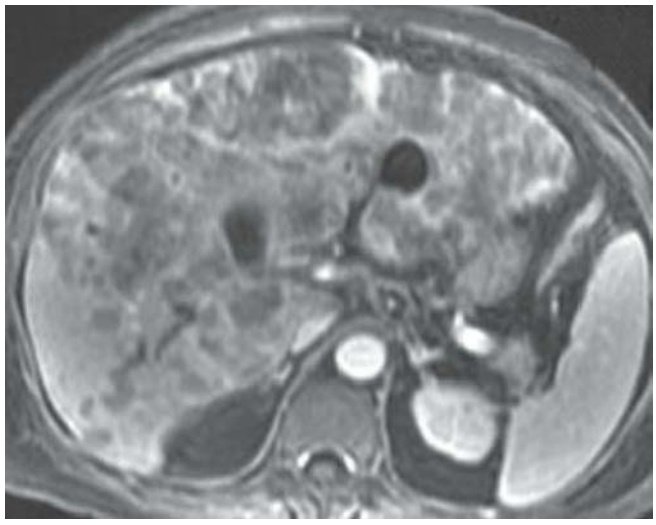

FIGURE 88D

FINDINGS Thick-slab MRCP image (A) demonstrates fusiform dilatation of the inferior common bile duct. Note the nodular indentation of the upper portion of the cyst, with narrowing and obstruction of the upstream extra- and intrahepatic bile ducts. Axial T2-WI (B) shows multiple hyperintense liver lesions that are hypointense on T1-WI (C). They have heterogeneous nodular enhancement on the gadolinium-enhanced, fat-suppressed axial T1-WI (D).

DIFFERENTIAL DIAGNOSIS Metastasis.

DIAGNOSIS Bile duct carcinoma in a type I choledochal cyst.

DISCUSSION Choledochal cyst is a rare congenital malformation with a female-to-male ratio of 3:1. It is much more common in the Orient. Formation of a choledochal cyst is thought to be related to reflux of pancreatic secretions into the bile duct as a consequence of an anomalous junction of the common bile duct and pancreatic duct, the so-called long common channel. The diagnosis is typically made in the childhood due to the presence of one or more symptoms of the classical triad of obstructive jaundice, right upper quadrant pain, and a palpable mass. Todani's classification of choledochal cysts comprises five types of cysts: saccular or fusiform dilatation of the extrahepatic duct (type I), diverticulum of the extrahepatic duct (type II), choledochocele

(type III), multiple cysts or involvement of both the intra- and the extrahepatic ducts (type IV), and intrahepatic bile duct cysts only (type V or Caroli disease). Choledochal cyst not infrequently causes malignant change in the epithelial lining; bile duct carcinoma arising in a choledochal cyst has been reported in up to 15% of cases. On T2-WI or MRCP, the tumor is visualized as solitary or multiple filling defects in the hyperintense choledochal cyst. Gadolinium-enhanced T1-WI in different planes can be used to demonstrate enhancement and extraluminal extension of the tumor. This case shows additional liver metastases from the bile duct carcinoma.

CASE 89

CLINICAL HISTORY *55-year-old man presenting with abdominal pain and vomiting.*

FIGURE 89A

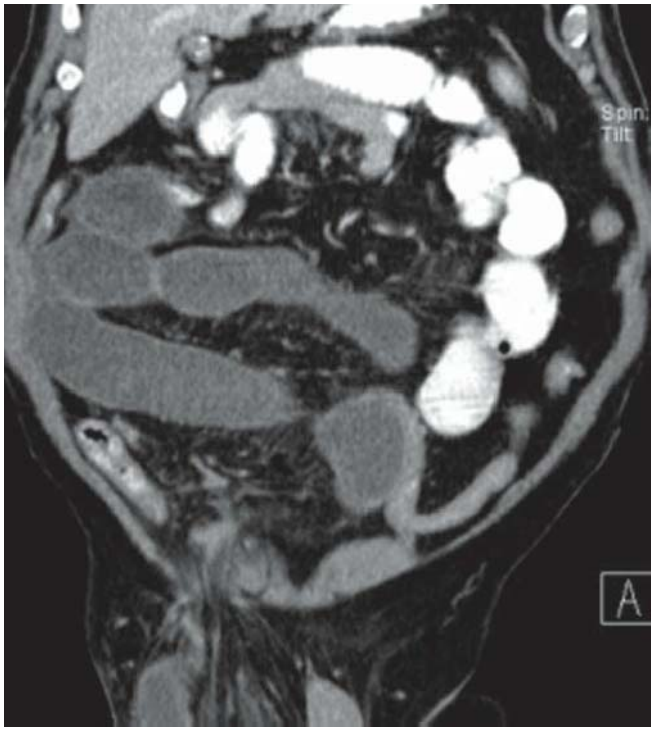

FIGURE 89B

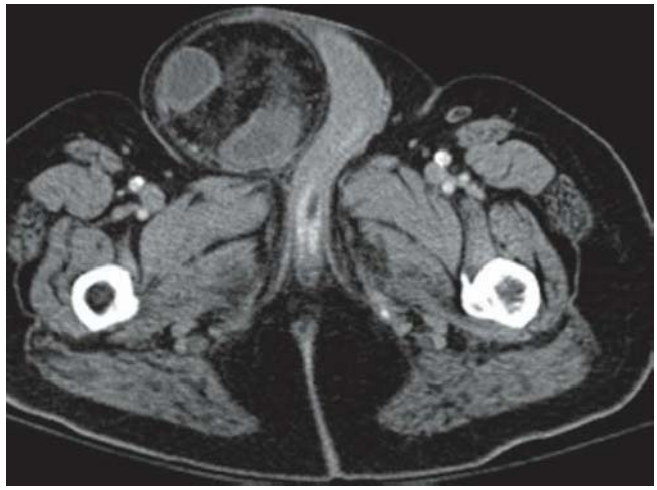

FIGURE 89C

FIGURE 89D

FINDINGS Coronal CECT image (A and B) demonstrates multiple dilated loops of small bowel that can be followed into the left groin, anteromedially to the femoral vessels. Axial images (C and D) demonstrate a right inguinal hernia containing small bowel loops with a transition point with peripheral fat stranding at the neck of the hernia.

DIFFERENTIAL DIAGNOSIS None.

DIAGNOSIS Right inguinal hernia causing small bowel obstruction.

DISCUSSION Inguinal hernias can be either direct or indirect. Indirect hernias are the most common and occur predominantly in males. The peritoneal sac, along with intra-abdominal contents, enters the inguinal canal and exits at the external ring. In males, a hernial sac follows the spermatic

cord and enters into the scrotum. Because of its long course, indirect hernias can become incarcerated, leading to bowel infarction. Direct hernias, on the other hand, are less common and occur when the hernia enters medial to the inferior epigastric vessels. The finding of abdominal contents (e.g., small bowel, sigmoid colon, cecum, and mesenteric fat) in the inguinal canal anteromedially to the femoral vessels, as seen in this case, is diagnostic of an inguinal hernia. In males, this is easily seen as asymmetry in the spermatic cord when compared with the other side. Frequently, hernias are asymptomatic and easily reducible. They can, however, lead to small bowel obstruction due to incarceration, as seen in this case.

CASE 90

CLINICAL HISTORY *59-year-old man with leukemia presenting with fever and abnormal liver function tests.*

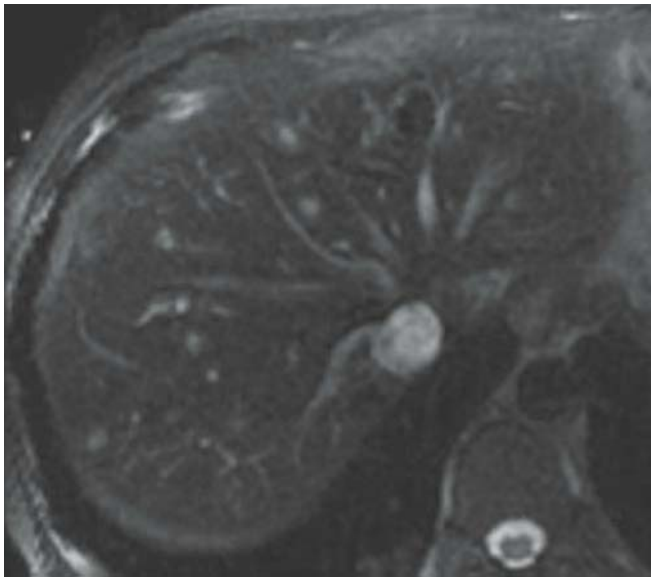

FIGURE 90A

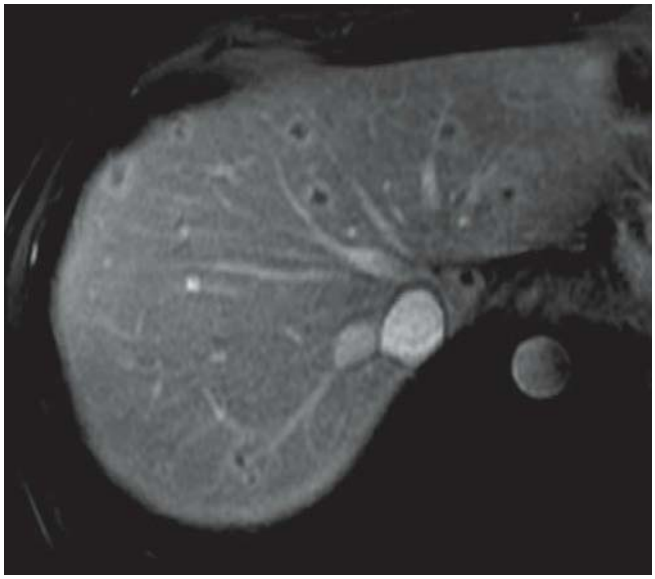

FIGURE 90C

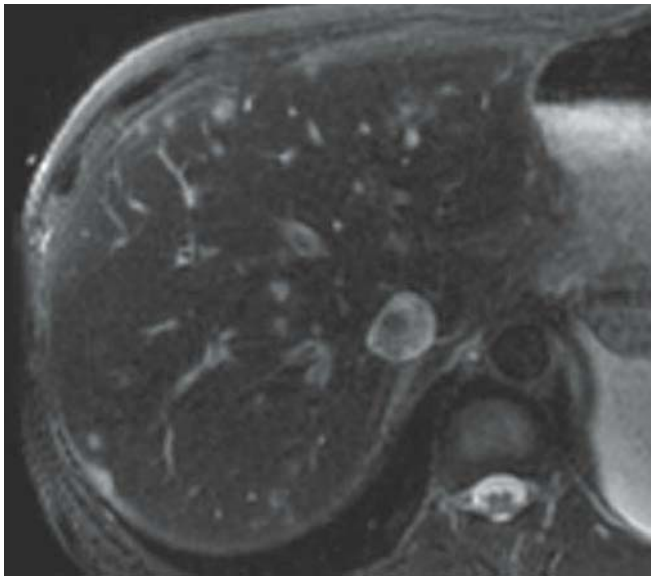

FIGURE 90B

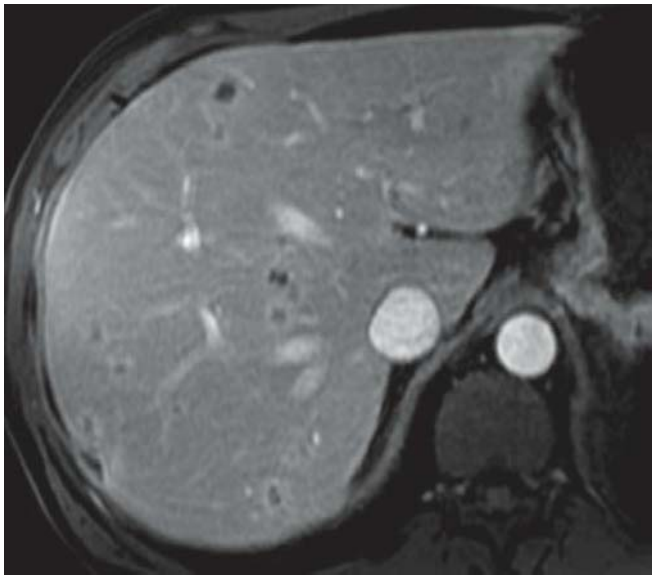

FIGURE 90D

FINDINGS Axial fat-suppressed T2-WIs (A and B) demonstrate multiple hyperintense small lesions within the liver. On the gadolinium-enhanced, fat-suppressed axial T1-WIs (C and D), the lesions show rim enhancement.

DIFFERENTIAL DIAGNOSIS Metastases, leukemia.

DIAGNOSIS Hepatic candidiasis.

DISCUSSION Fungal hepatic abscesses typically occur in immunocompromised patients as opportunistic infections; AIDS, leukemia, lymphoma, and intense chemotherapy are among the predisposing conditions. The hepatic lesions are caused by hematogenous dissemination of the organism that results in small miliary microabscesses scattered throughout the parenchyma. Most hepatic fungal abscesses are caused by *Candida albicans*. Recent studies have shown that MR imaging is superior to CT scanning in depicting hepatic fungal involvement. Hepatic fungal lesions have different appearances depending on their presentations. The untreated abscesses are rounded lesions, less than 1 cm in diameter, that are minimally hypointense on T1-WI, markedly

hyperintense on T2-WI, and have rimlike enhancement on the post-contrast images. In the subacute presentation after treatment, lesions appear mildly to moderately hyperintense on T1-WI and T2-WI and demonstrate enhancement on gadolinium-enhanced images. A dark ring is usually seen around these lesions on all sequences. Completely treated lesions are minimally hypointense on T1-WI, isointense to mildly hyperintense on T2-WI, moderately hypointense on early gadolinium-enhanced images, and minimally hypointense on delayed gadolinium-enhanced images.

CASE 91

CLINICAL HISTORY *63-year-old man presenting with jaundice.*

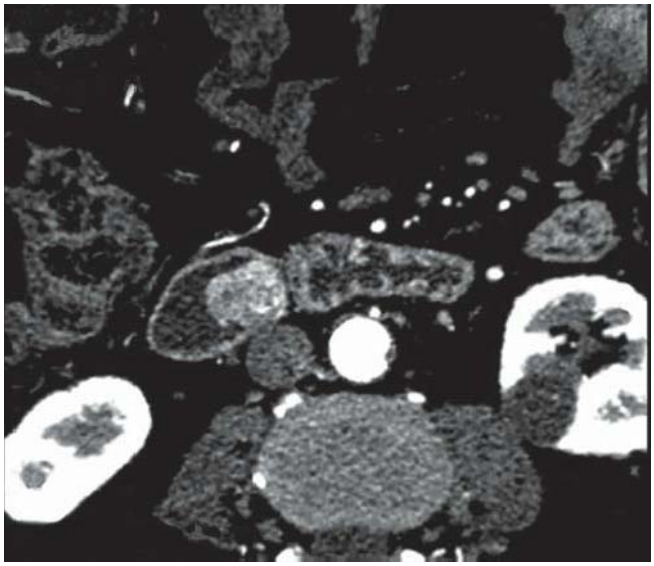

FIGURE 91A

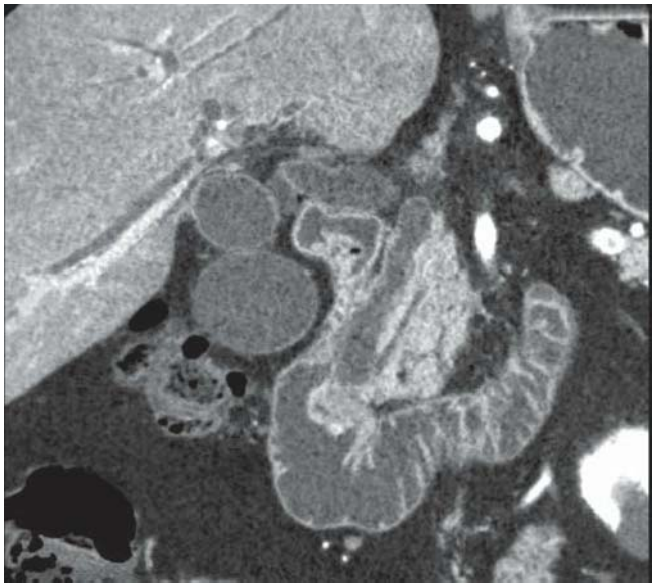

FIGURE 91C

FIGURE 91B

FIGURE 91D

FINDINGS Axial CECT image (A) shows an enhancing mass projecting in the second duodenum medially. Coronal reformatted CECT (B-D) images demonstrate the mass is situated at the ampulla of Vater and causes moderate upstream bile duct dilatation.

DIFFERENTIAL DIAGNOSIS Pancreatic ductal adenocarcinoma, distal cholangiocarcinoma.

DIAGNOSIS Ampullary carcinoma.

DISCUSSION Ampullary malignant tumor, usually a polypoid adenocarcinoma protruding from the papilla, is less common than pancreatic carcinoma and is best identified by endoscopy. Tumors are usually small (50% <3 cm) at presentation, since the lumen of the common bile duct does not permit much encroachment before it becomes obstructed. Cancer of the ampulla generally obstructs both the distal CBD and the pancreatic duct. Shouldering of the obstructed CBD is frequently seen. Pancreatic duct dilatation is mostly absent when the Santorini duct and minor papilla are patent.

On MRCP, ampullary lesions display a true double duct sign with obstruction of the distal CBD and pancreatic duct. In patients with pancreatic ductal adenocarcinoma, MRCP shows the so-called four-segment sign, i.e., an obstructed pancreatic duct and common bile duct with a short normal intrasphincteric segment of normal pancreatic and common bile duct. Enhancement of the mass is invariably present.

Case courtesy of Dr. Alexander Ivanovic, Belgrade, Serbia.

CASE 92

CLINICAL HISTORY *73-year-old woman post allograft bone marrow transplantation for chronic myelogenous leukemia presenting with intractable nausea, vomiting, and diarrhea.*

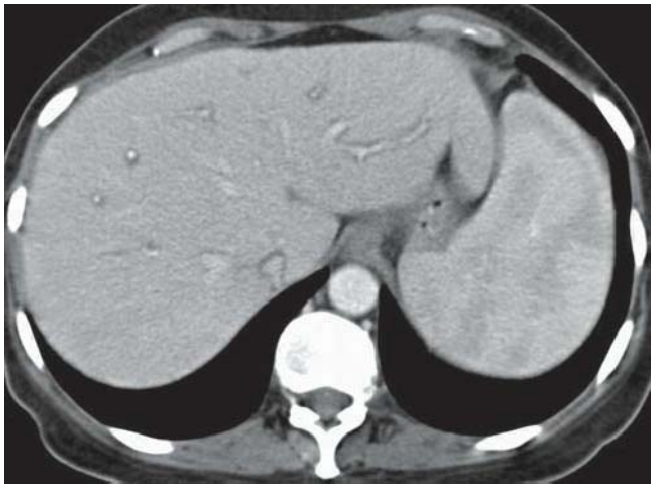

FIGURE 92A

FIGURE 92B

FIGURE 92C

FIGURE 92D

FINDINGS Axial CECT image (A) of the liver shows periportal edema. Axial CECT images (B–D) of the pelvis demonstrate marked thickening and mucosal hyperenhancement of multiple loops of small and large bowel with mesenteric edema and inflammation. A small amount of free fluid is seen in the pelvis.

DIFFERENTIAL DIAGNOSIS Viral enteritis, mesenteric ischemia, radiation enteritis.

DIAGNOSIS Graft-versus-host disease.

DISCUSSION Graft-versus-host disease (GVHD) is due to the presence of immunocompetent cells in the donor marrow that are reacting with cells in the recipient. Acute GVHD can occur up to 100 days after transplantation. It commonly affects the skin, liver, and GI tract. In the GI tract, the small bowel is most commonly involved, but the stomach, duodenum, and colon can also demonstrate changes as well. There is prolonged coating of the small bowel, which can appear as circular collections of barium in cross section or parallel tracks in longitudinal sections. Bowel wall thickening with mural stratification due to mucosal hyperenhancement, mesenteric edema, mesenteric hyperemia, and adenopathy can also be seen. The affected bowel may be normal in caliber or less commonly dilated. This appearance can be indistinguishable from viral enteritis, which can also be a complication of bone marrow transplantation. Mesenteric ischemia would typically involve the proximal portion of the colon. Radiation enteritis would be within the confines of the radiation field. Diagnosis of GVHD is typically made by rectal biopsy.

CASE 93

CLINICAL HISTORY *60-year-old man presenting with cirrhosis.*

FIGURE 93A

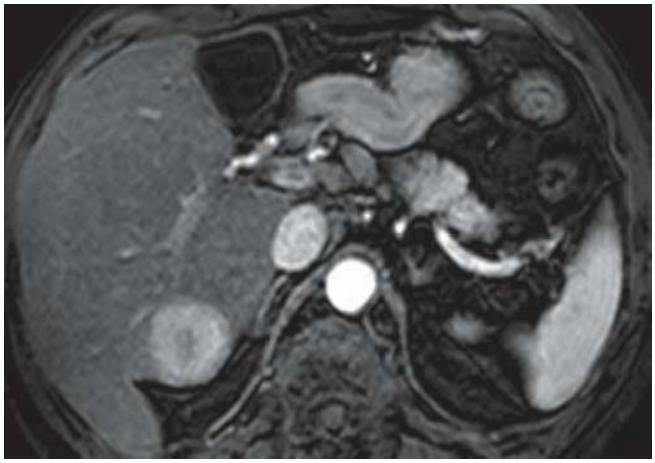

FIGURE 93B

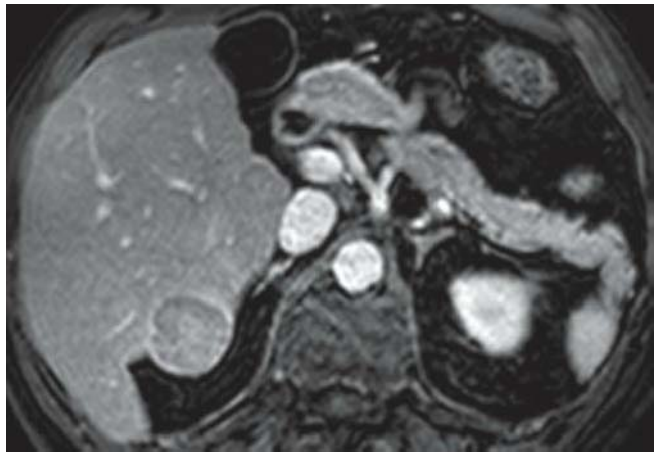

FIGURE 93C

FINDINGS Axial CECT (A) demonstrates an intensely enhancing lesion within the right lobe in cirrhotic liver. Note the presence of a second lesion in segment 4 adjacent to the gallbladder. Gadolinium-enhanced, fat-suppressed axial T1-WI during the arterial phase (B) and portal venous phase (C) show early heterogeneous enhancement and rapid wash out of the right lobe lesion.

DIFFERENTIAL DIAGNOSIS Metastasis.

DIAGNOSIS Hepatocellular carcinoma in a cirrhotic liver.

DISCUSSION There are many different etiologies for hepatocellular carcinoma (HCC), which can be divided into three main categories: chronic hepatitis B, cirrhosis, and carcinogens. Cirrhosis in the United States is most commonly due to alcoholism, and HCCs occur in approximately 3% of these patients. Other causes of cirrhosis that can lead to HCC include hemochromatosis and, less commonly, inborn errors of metabolism such Wilson disease, glycogen storage disease, and alpha-1-antitrypsin deficiency. Carcinogens found to be associated with HCC include aflatoxins produced by the fungus *Aspergillus fumigates*, siderosis from high dietary iron, and Thorotrast. MRI characteristics for HCC vary depending on the amount of fibrosis, fat, necrosis, and hemorrhage present within the lesion. HCC is most commonly hypointense on the T1-WI but can be isointense or hyperintense as well. This is due in part to the amount of fat, hemorrhage, and glycogen present in the tumor, which will have increased signal on the T1-WI. HCC is predominantly hyperintense on the T2-WI and demonstrates early heterogeneous enhancement with gadolinium administration. The rapid washout of contrast during the portal venous phase is crucial for diagnosis of HCC.

CASE 94

CLINICAL HISTORY *62-year-old man presenting with right upper quadrant pain.*

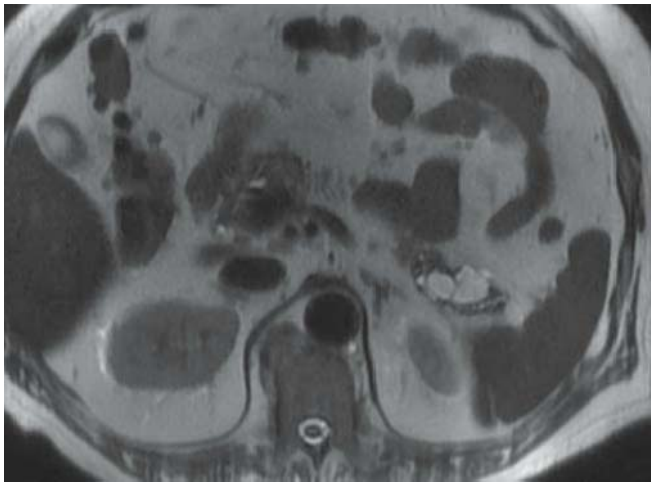

FIGURE 94A

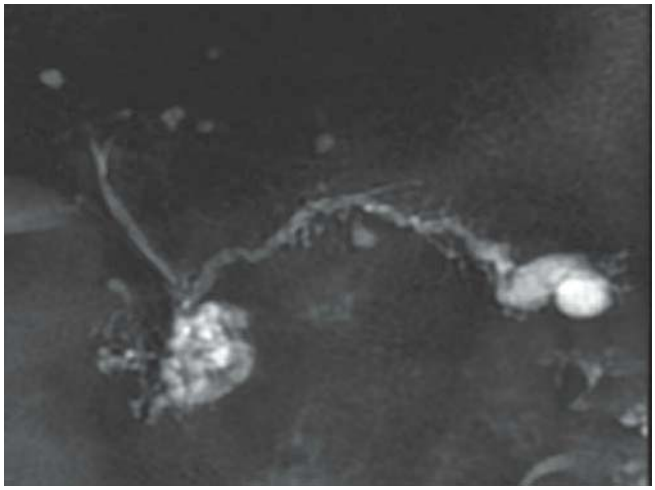

FIGURE 94C

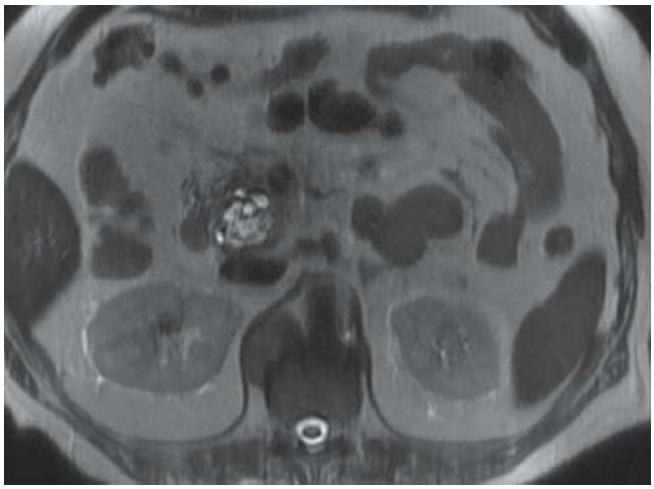

FIGURE 94B

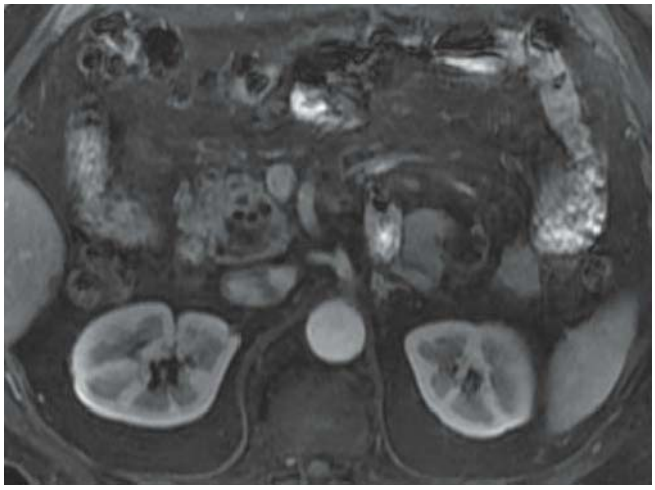

FIGURE 94D

FINDINGS Axial T2-WI (A and B) show clusters of cysts in the pancreatic tail and head. Coronal oblique thick-slab MRCP image (C) displays mild dilatation of the main pancreatic duct in its entirety and of multiple side branches. Gadolinium-enhanced, fat-suppressed axial T1-WI (D) shows neither enhancing nodules within the duct nor papillary protrusions.

DIFFERENTIAL DIAGNOSIS Chronic pancreatitis, ampullary carcinoma, serous microcystic pancreatic adenoma.

DIAGNOSIS Combined-type intraductal papillary mucinous neoplasm (IPMN).

DISCUSSION Intraductal papillary mucinous neoplasm is similar histologically to a mucinous cystic neoplasm, but differs in which it does not contain ovarian stroma and it involves the main pancreatic duct or a side branch of the pancreatic duct or both. IPMN produces mucin that fills the pancreatic duct and causes it to dilate. By ERCP, there are multiple cystic cavities, usually in the uncinate process, which communicate with the main pancreatic duct. There is also a large amount of mucin coming from the ampulla as it is cannulated by the endoscopist. The papilla can be dilated and this has been referred to as the "fish-mouth" papilla. IPMN ranges histologically from benign adenoma to dysplastic lesions, to frankly invasive neoplasms. Adenocarcinoma and rarely colloid carcinoma are the two subtypes recognized among invasive IPMN. Spread of the cancer outside of the pancreas occurs late in the course of the disease so IPMN has a fairly good prognosis after resection. Typically, main duct or combined involvement has a less favorable prognosis than sidebranch involvement only.

CASE 95

CLINICAL HISTORY *79-year-old man who previously had prolonged placement of thoracic venous catheters.*

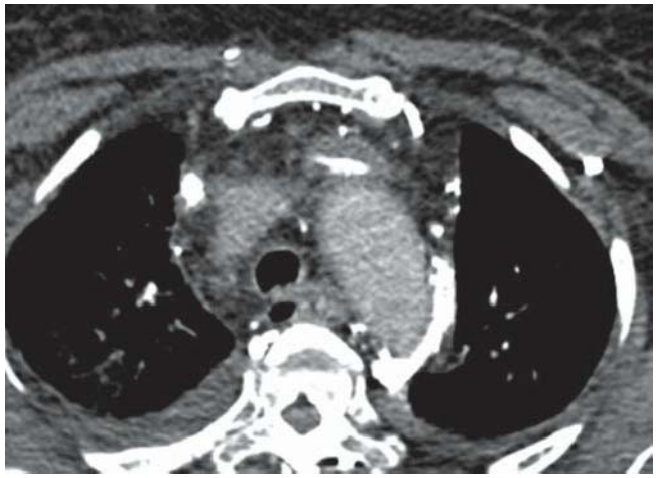

FIGURE 95A

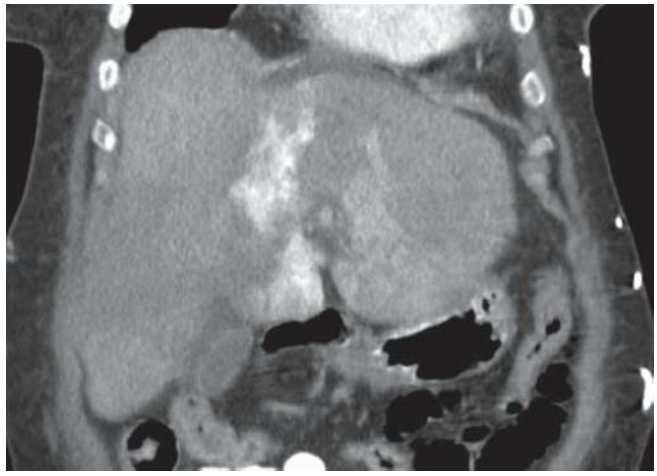

FIGURE 95C

FIGURE 95B

FINDINGS Axial CECT image (A) of the thorax demonstrates multiple mediastinal collateral veins. Axial (B) and coronal reformatted (C) CECT images of the abdomen show dense bright enhancement of the liver centered around the falciform ligament and demonstrate several dilated veins in the anterior abdominal wall.

DIFFERENTIAL DIAGNOSIS Hypervascular metastasis, hepatocellular carcinoma, focal nodular hyperplasia.

DIAGNOSIS SVC thrombosis with "hot quadrate lobe."

DISCUSSION The superior vena cava (SVC) can become obstructed from malignant causes (most commonly lung cancer) or from benign causes (iatrogenic from catheter, fibrosing mediastinitis, vasculitis, and Behçet disease). At the time of an injection of contrast in the upper extremity, in a patient with SVC obstruction, the blood is shunted away through multiple collateral channels that develop or enlarge. One of them is the internal thoracic vein, which then connects with the superior veins of Sappey, representing a third vascular inflow to the liver. This vein drains next to the falciform ligament and enters directly the left lobe of the liver to eventually communicate with small peripheral intrahepatic venules. The dense contrast material from the arm injection causes, through this pathway, a dense blush in the liver parenchyma around the falciform ligament. This phenomenon is referred to as the "hot spot sign" or "hot quadrate lobe." Identification of dilated collateral veins in the setting of a vascular blush around the falciform ligament helps to make the correct diagnosis. The veins of Sappey, as they cause differential perfusion of a portion of the liver, are also responsible for the focal fatty change very often seen on CT in segment IV of the liver.

CASE 96

CLINICAL HISTORY *53-year-old man presenting with hematemesis.*

FIGURE 96A

FIGURE 96B

FIGURE 96C

FIGURE 96D

FINDINGS Axial NECT image (A) shows a soft tissue mass within the first portion of the duodenum causing gastric outlet obstruction. CECT axial image (B) and coronal and sagittal reformatted images (C and D) demonstrate the enhancing tumor arising from the first portion of the duodenum and extending into the gastric outlet. There is invasion of the periduodenal fat and invasion of the pancreatic head.

DIFFERENTIAL DIAGNOSIS Duodenal lymphoma, GI stromal tumor, metastasis.

DIAGNOSIS Duodenal adenocarcinoma.

DISCUSSION Duodenal carcinoma occurs in both sexes worldwide with no predisposing factors in the majority of

cases. There is an increased risk in patients with familial adenomatous polyposis and adenomas of the duodenum. Duodenal carcinoma occurs about 22 years from the diagnosis of familial adenomatous polyposis in about 2% of patients; they constitute over 50% of upper GI cancers occurring in these patients. Carcinomatous changes occur in 30% to 60% of duodenal villous adenomas and much less in tubulovillous and tubular adenomas. These categories of patients should be screened and adequately followed up. The general 5-year survival rate is 17% to 33%, but some centers have achieved 5-year survival rates of 40% to 60% with aggressive management. Small bowel adenocarcinomas frequently appear as solitary proximal small bowel masses and are rarely greater than 8 cm in diameter. Ulceration is seen in a third of adenocarinomas; lymphadenopathy is seen in a half of the tumors. Lymphomas, by contrast, appear as large, annular, aneurysmally ulcerated masses, with big lymphadenopathy. GI stromal tumors are large, locally spreading, bulky, heterogeneous tumors on CT, occasionally with calcifications.

CASE 97

CLINICAL HISTORY *38-year-old woman with abdominal pain.*

FIGURE 97A

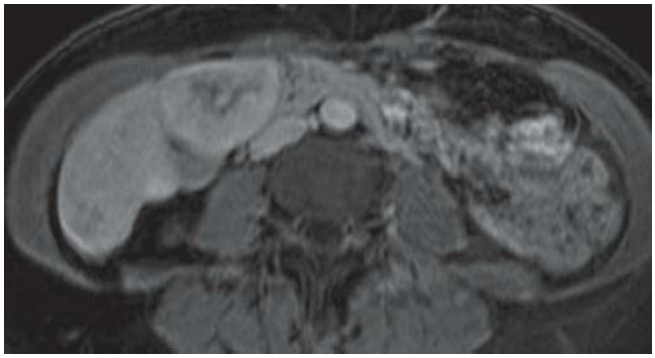

FIGURE 97C

FIGURE 97B

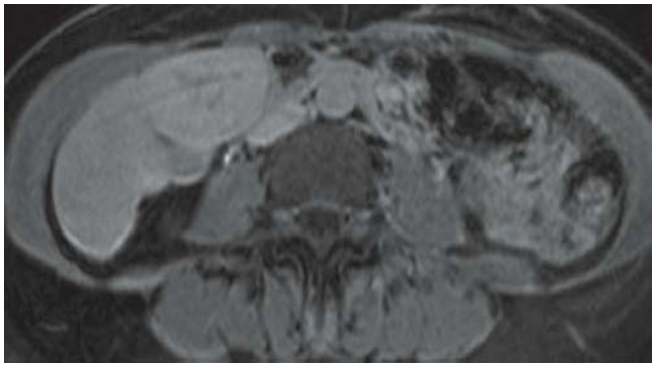

FIGURE 97D

FINDINGS Axial NECT image (A) demonstrates a 7-cm, low-attenuation mass along the inferior margin of segment 4B with a central scar. Axial CECT image (B) reveals this lesion to have heterogeneous enhancement with a central irregular scar without enhancement. Post-gadolinium fat-suppressed arterial (C) and portal venous (D) phase MR images demonstrate the enhancing lesion with a nonenhancing central scar. Note the smooth normal liver margins.

DIFFERENTIAL DIAGNOSIS Hepatic adenoma, focal nodular hyperplasia.

DIAGNOSIS Fibrolamellar hepatocellular carcinoma.

DISCUSSION Fibrolamellar hepatocellular carcinoma (HCC) differs from a typical HCC in that there is no underlying liver disease (cirrhosis), the alpha-fetoprotein level is usually normal, and the age of onset is typically under 40 years of age. Fibrolamellar HCC equally affects males and females. The prognosis for fibrolamellar HCC is better than typical HCC. CT findings include a large heterogeneously enhancing mass with a nonenhancing fibrous central scar, which is well seen in this example. The lesion is typically solitary and can have calcifications centrally within the lesion. A hepatic adenoma could have a similar appearance by CT. However, hepatic adenomas do not usually have a scar, and a history of oral contraceptive use is usually present. Fibrolamellar HCC will often have gallium uptake, which can aid in the diagnostic workup. Heterogeneous enhancement and lack of enhancement of the central scar allow differentiation between fibrolamellar HCC and focal nodular hyperplasia on CECT image.

CASE 98

CLINICAL HISTORY *46-year-old man presenting with left upper quadrant pain.*

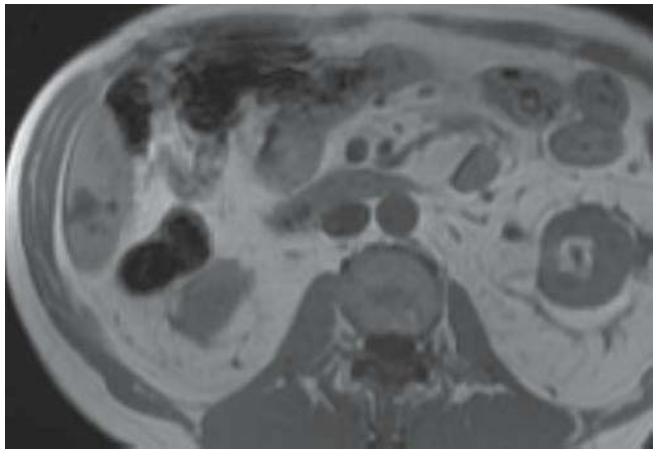

FIGURE 98A

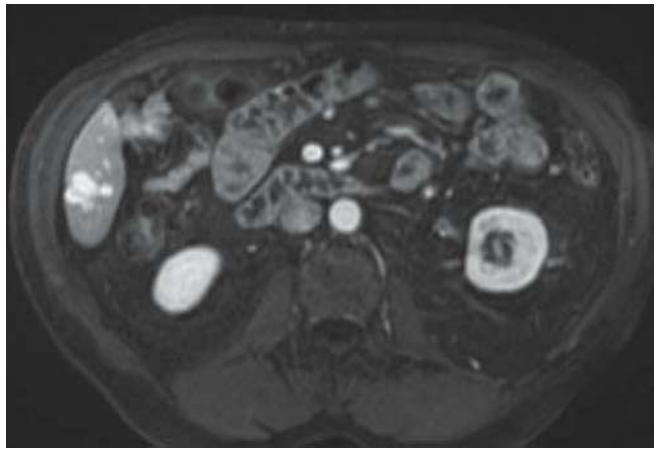

FIGURE 98C

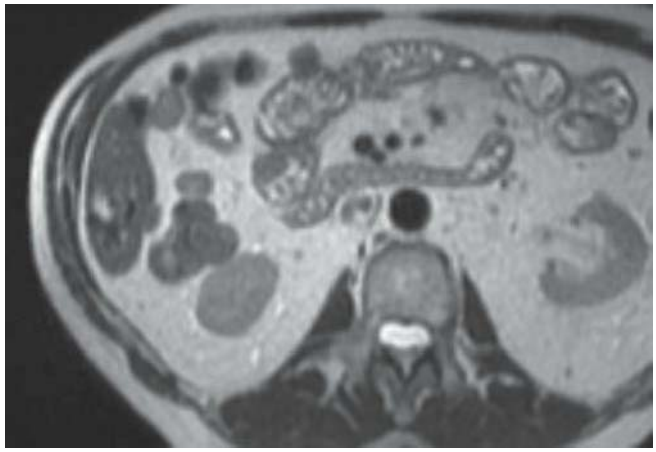

FIGURE 98B

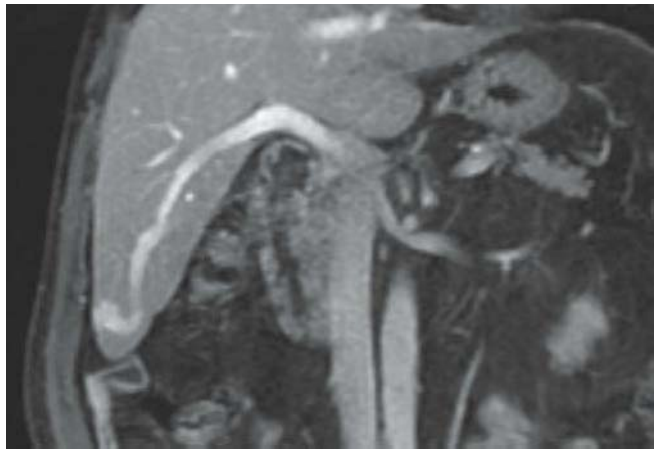

FIGURE 98D

FINDINGS Axial T1-WI (A) demonstrates a hypointense lesion in segment 6 of the liver, which is centrally hyperintense on the axial T2-WI (B). On gadolinium-enhanced, fat-suppressed axial (C) and coronal (D) T1-WIs, the lesion demonstrates enhancement of vascular signal intensity, with a branch of the right portal vein supplying it.

DIFFERENTIAL DIAGNOSIS Hypervascular liver neoplasm, peliosis hepatis.

DIAGNOSIS Intrahepatic portosystemic shunt (hepatic varix).

DISCUSSION Several appearances of intrahepatic portosystemic shunts have been described. The most frequently reported intrahepatic portosystemic shunt is between the right portal vein and the inferior vena cava. This type of portosystemic shunt typically occurs in the clinical setting of portal hypertension. Other appearances of intrahepatic portosystemic shunts include multiple diffuse communications between peripheral portal and hepatic veins, a single communication between a portal vein branch and a hepatic vein in one hepatic segment, and a single communication between a portal vein branch and a hepatic vein through an aneurysm. Both congenital and acquired causes, such as development of intrahepatic portosystemic collaterals vessels in cirrhotic patients and trauma, have been postulated for intrahepatic portosystemic shunts, but their origin is still not fully understood. On gadolinium-enhanced MR images obtained during the portal venous phase, the communication between a portal vein branch and the hepatic vein can be demonstrated. Another imaging finding is an early and asymmetrical enhancement of a hepatic vein in the late arterial phase.

CASE 99

CLINICAL HISTORY *76-year-old woman presenting with an incidental gallbladder nodule identified on US.*

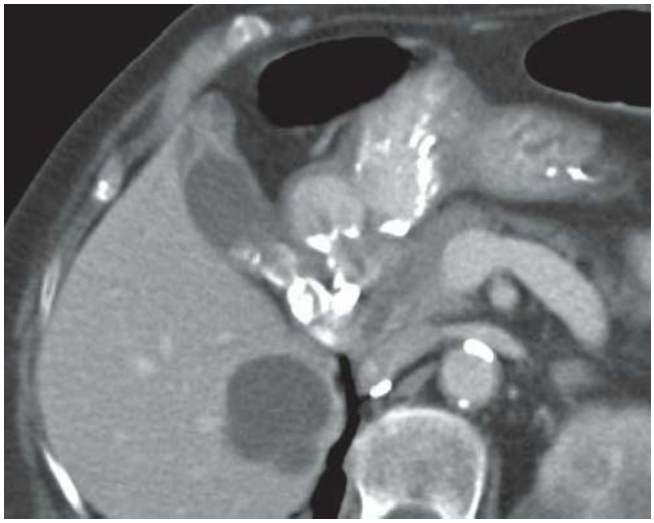

FIGURE 99A

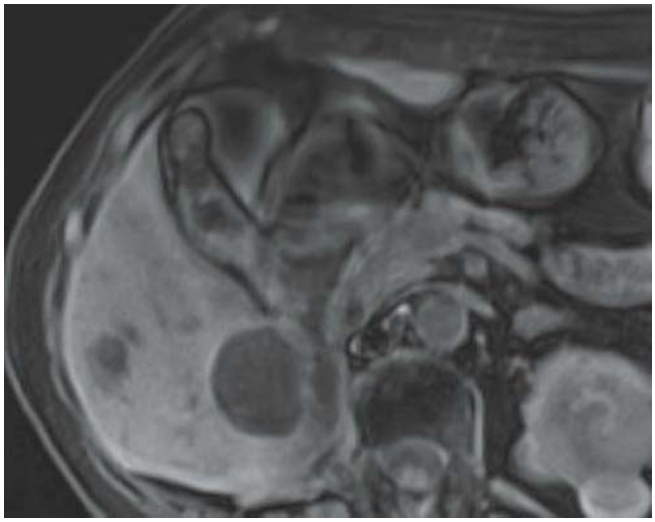

FIGURE 99C

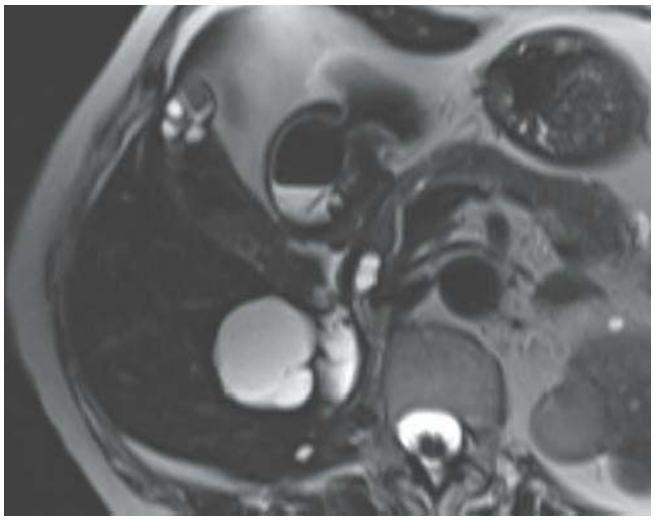

FIGURE 99B

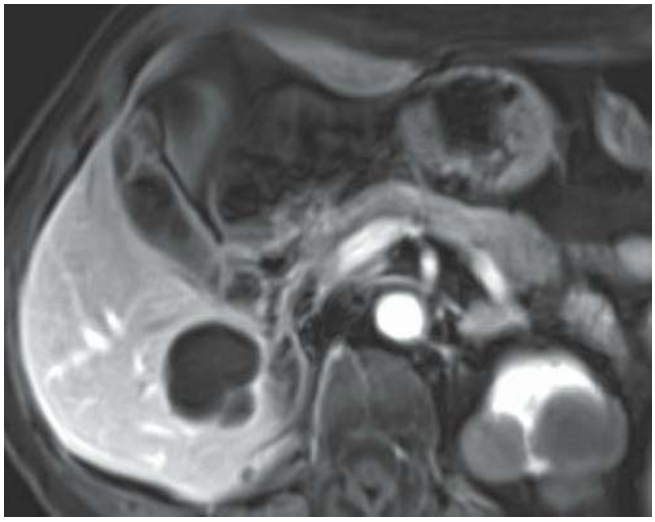

FIGURE 99D

FINDINGS CECT image (A) demonstrates focal nodular thickening of the gallbladder fundus with cystic spaces. Axial T2-WI (B) confirms the fluid signal of the cystic spaces. Fat-suppressed axial T1-WI pre- (C) and post-gadolinium injection (D) show thin non-nodular enhancement between the cystic spaces.

DIFFERENTIAL DIAGNOSIS Gallbladder carcinoma, metastasis, polyp.

DIAGNOSIS Focal gallbladder adenomyomatosis.

DISCUSSION Adenomyomatosis is a benign chronic gallbladder disease, found in up to 5% of cholecystectomy specimens. Most patients are diagnosed in their 50s, but a wide age range has been described, including children. Adenomyomatosis has no malignant potential. It is defined by hypertrophy of the muscularis propria and proliferation of the mucosa. Bile, sludge, or calculi become trapped in intramural diverticulae, called the Rokitansky-Aschoff sinuses. The findings can be diffuse, segmental, or fundal. On imaging, the affected gallbladder portions demonstrate wall thickening. Large enough dilated sinuses can be identified on CT and MRI. The "pearl necklace sign" that can be seen on conventional MRI or MRCP refers to a multitude of dilated fluid-filled Rokitansky-Aschoff sinuses aligned one next to each other, reminiscent of a necklace. If a calculus forms in a dilated sinus, it would appear dark on MRI, unless it contains ionic calcium which would render it bright. As the vast majority of cases of adenomyomatosis are asymptomatic, no treatment is required. The diagnosis then needs to be confidently made on imaging, usually relying on identification of dilated Rokitansky-Aschoff sinuses. Surgery occasionally needs to be performed if it produces rare pain, or if it cannot be distinguished from a malignancy by imaging alone.

CASE 100

CLINICAL HISTORY *45-year-old man with a history of acute myelogenous leukemia evaluated for fever.*

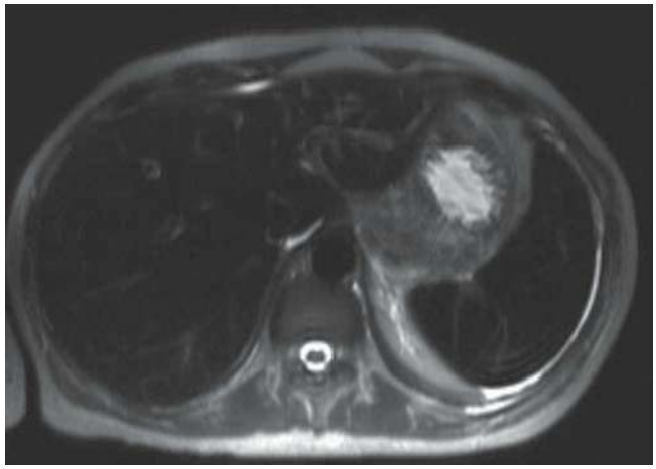

FIGURE 100A

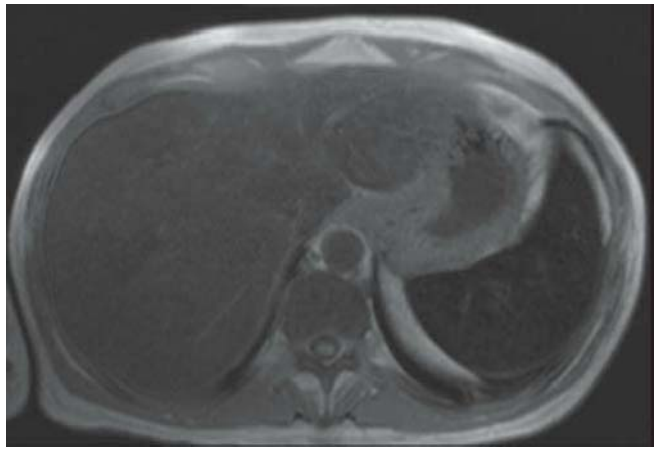

FIGURE 100C

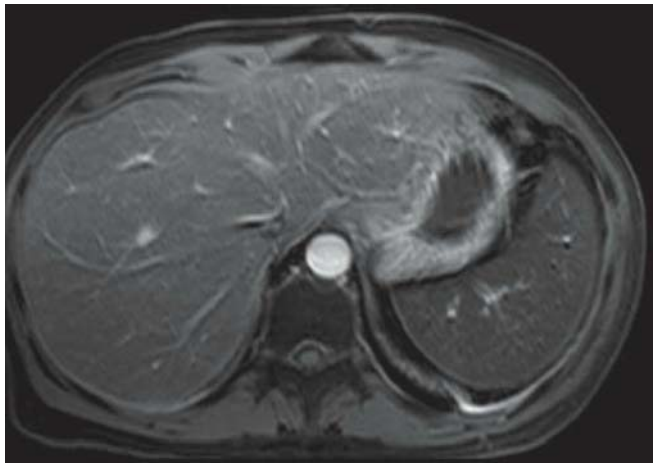

FIGURE 100B

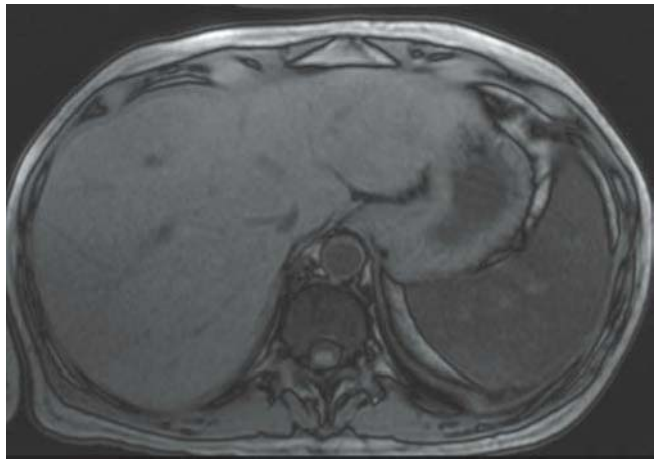

FIGURE 100D

FINDINGS Axial (A) single-shot T2-WI shows decreased signal intensity of both the liver and the spleen. Axial fat-suppressed post-gadolinium T1-WI (B) shows the signal intensity of the spleen, and bone marrow to be lower than spinal muscle. In-phase (C) and out-of-phase sequences (D) of opposed phase imaging reveal marked drop of signal in liver and spleen on in-phase sequences, compatible with hemosiderin deposition.

DIFFERENTIAL DIAGNOSIS Primary hemochromatosis.

DIAGNOSIS Hemosiderosis.

DISCUSSION Iron overload diseases consist of two different groups of disorders depending on the location of iron deposition. Primary hemochromatosis is a common inherited autosomal recessive disorder, consisting of abnormal parenchymal iron deposition, which occurs mainly not only in the hepatocytes but also in the pancreas, heart, and synovium. This parenchymal iron deposition may cause damage and organ dysfunction, such as cirrhosis of the liver and development of hepatocellular carcinoma. Hemosiderosis is the term used for iron deposition in the reticuloendothelial system of the liver, spleen, lymph nodes, and bone marrow; it most commonly develops after multiple blood transfusions (transfusional iron overload) and has little clinical significance. MRI is a sensitive and specific method to detect iron deposition because of the magnetic-susceptibility effect caused by the accumulated iron. This demonstrates a markedly decreased signal intensity (compared with that seen in skeletal muscle) in involved organs on T2-WI, especially on gradient-echo T2*-WI. In hemochromatosis, a low signal intensity on T2-WI and T2*-WI is found in the liver, pancreas, myocardium, and endocrine glands, but the spleen remains normal. In hemosiderosis, spleen, liver, and bone marrow reveal decreased intensity on MRI studies, and the pancreas tends to be spared.

CASE 101

CLINICAL HISTORY *23-year-old man presenting with fatigue and an enlarged spleen on physical exam.*

FIGURE 101A

FIGURE 101B

FIGURE 101C

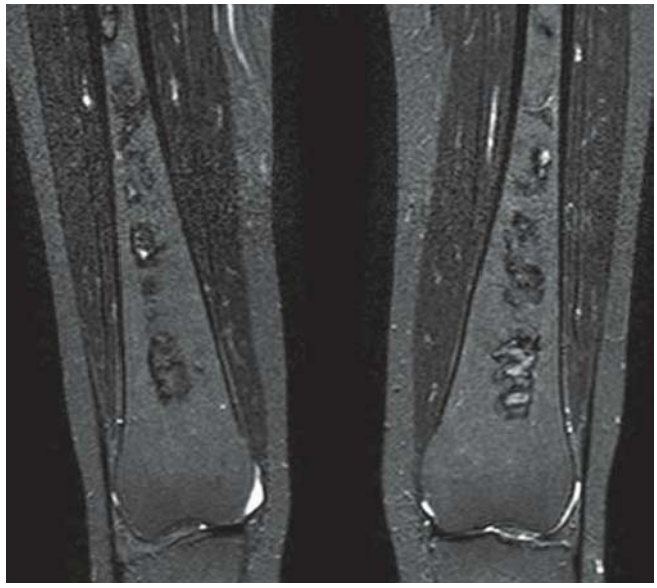

FIGURE 101D

FINDINGS Axial CECT images (A and B) demonstrate a massively enlarged spleen containing innumerable hypodense lesions. Coronal T1-WI of the thighs (C) shows several serpiginous dark lesions, some of which have central marrow signal. On T2-WI (D), some of the lesions have central hyperintensity. Note the distal femoral metaphyseal widening.

DIFFERENTIAL DIAGNOSIS Lymphoma, metastasis.

DIAGNOSIS Gaucher disease.

DISCUSSION Gaucher disease is an autosomal recessive lysosomal disease caused by the lack of the enzyme glucocerebrosidase. This leads to accumulation of glucocerebrosides in the reticuloendothelial system. Signs and symptoms include hypersplenism, pancytopenia, bony pain, and neurological disorders, seen in types 2 (acute infantile neuropathic form) and 3 (chronic neuropathic form) only, such as convulsions, mental retardation, and hypertonia. The most common is type 1, the non-neuropathic form. The accumulation of glucocerebrosides in the spleen results in splenomegaly and the formation of coalescent focal lesions. They are hypodense on CT, isointense on T1-WI, and hypointense on T2-WI. Definitive diagnosis is made with genetic testing, to detect the mutation on chromosome 1. Enzyme replacement therapy is the most commonly used treatment. The presence of bone infarcts and Erlenmeyer flask deformity in this patient helps narrow significantly the differential diagnosis and excludes lymphoma or metastasis. Splenic metastasis would also be unusual in a patient of this age without any known primary tumor.

CASE 102

CLINICAL HISTORY *57-year-old woman complaining of lower abdominal pain.*

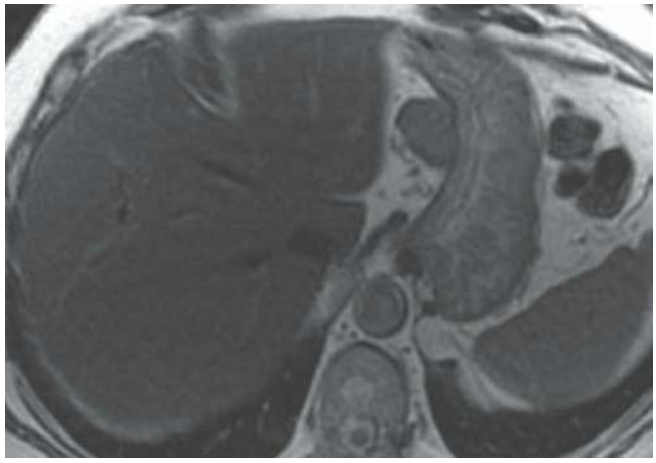

FIGURE 102A

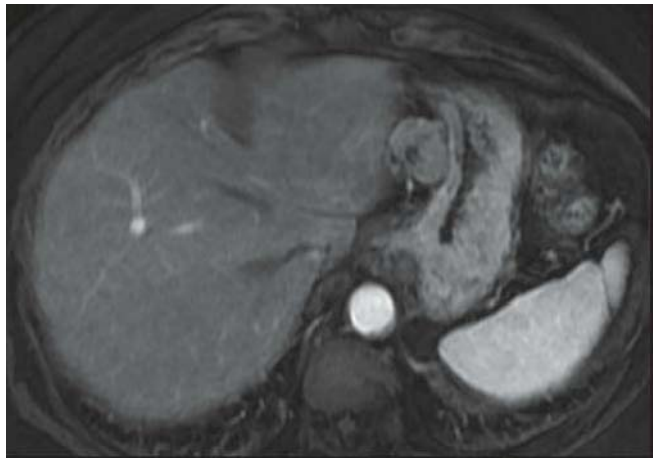

FIGURE 102C

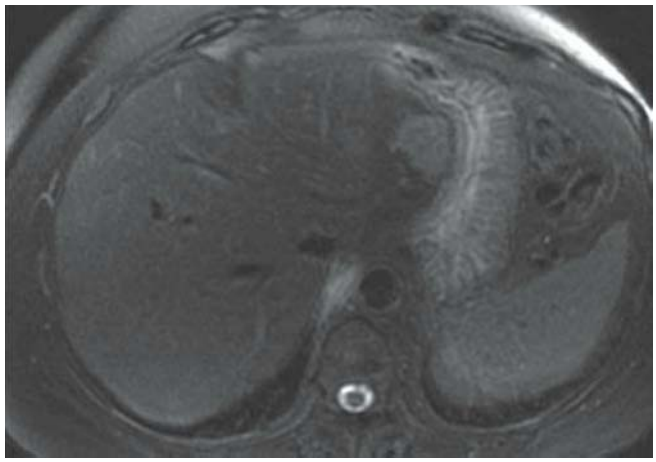

FIGURE 102B

FIGURE 102D

FINDINGS Standard (A) and fat-suppressed (B) axial T2-WI show a 4.2 cm × 2.0 cm mass of intermediate signal intensity along the lesser curvature of the stomach. Axial fat-suppressed gadolinium-enhanced T1-WI in the arterial (C) and portal venous (D) phases show homogeneous enhancement of the lesion except for linear areas of cystic degeneration.

DIFFERENTIAL DIAGNOSIS Metastasis, desmoid (fibromatosis), lymphoma, malignant fibrous histiocytoma (MFH), neurogenic tumor.

DIAGNOSIS Gastrointestinal stromal tumor.

DISCUSSION Gastrointestinal stromal tumor (GIST) is a mesenchymal spindle cell (80%) or epithelioid (20%) neoplasm. GIST is a relatively new entity as in the past most of these tumors were diagnosed pathologically as leiomyomas, leiomyoblastomas, or leiomyosarcomas. The histologic diagnosis is based on a positive C-kit stain. GISTs occur most often in the stomach (60% to 70%), followed by the small bowel, the colon/rectum, and least likely the esophagus (<5%). The majority of GISTs are benign but up to 30% can be malignant. The factors that increase the likelihood of malignancy include an extragastric location, size greater than 5 cm, central necrosis, extension into adjacent organs, and distant metastases (most commonly in the liver and peritoneum). GIST can grow in different patterns. This case exhibits an exoenteric growth pattern with the bulk of the tumor being outside the stomach wall. This is the most common growth pattern (65% of cases) in gastric and small bowel GISTs. Other growth patterns include intramural and intraluminal. Exoenteric GISTs, like this one, are discovered later than the endoenteric ones; the lesion in this case was identified incidentally. They are

not discovered until they attain a large size and present as a palpable mass or bleed into the lumen due to tumoral excavation. Lymphoma may present with a similar appearance, but the lack of adenopathy and the exocentric bowel involvement in this case make lymphoma less likely. Melanoma or breast metastasis may have the same appearance but there is no history for such a primary malignancy. Other sarcomas such as MFH will typically have a faster evolution and be larger with marked central necrosis. Neurogenic tumors can have a similar appearance.

CASE 103

CLINICAL HISTORY *41-year-old woman presenting with nausea and vomiting.*

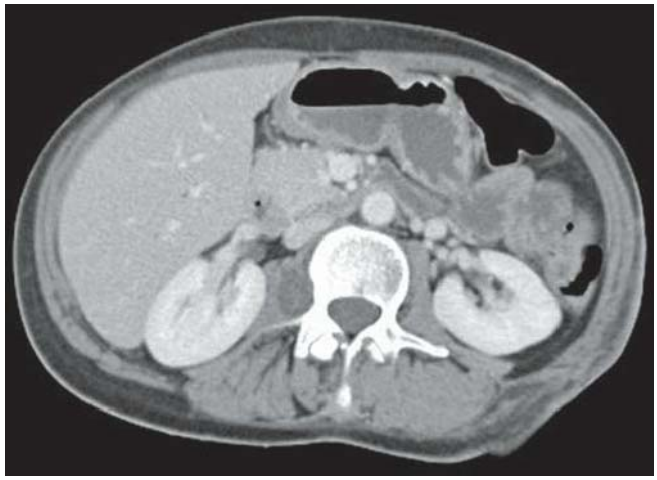

FIGURE 103A

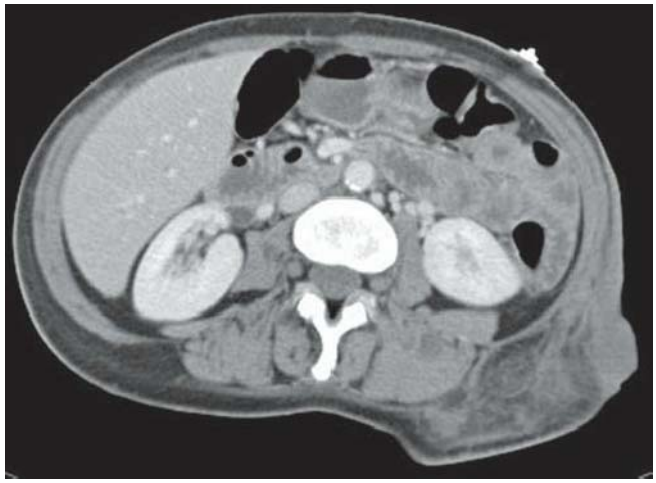

FIGURE 103B

FINDINGS Axial (A–C) and coronal reformatted (D) CECT images demonstrate a large sessile left flank cutaneous mass with underlying subcutaneous fat stranding. Note the other cutaneous nodules, a right paraspinal mass, and genisero-convex scoliosis.

DIFFERENTIAL DIAGNOSIS Metastasis, Kaposi sarcoma.

DIAGNOSIS Neurofibromatosis type 1.

DISCUSSION Neurofibromatosis type 1, also named von Recklinghausen disease, is the most common neurocutaneous syndrome, occurring in 1 of every 3,000 births. It is an autosomal dominant disorder but occurs sporadically in up to 50% of cases due to spontaneous mutation on chromosome 17. The classic tumors occurring outside the central nervous system are neurofibromas, which may be plexiform in nature, as seen in this case in the left flank. In the abdomen,

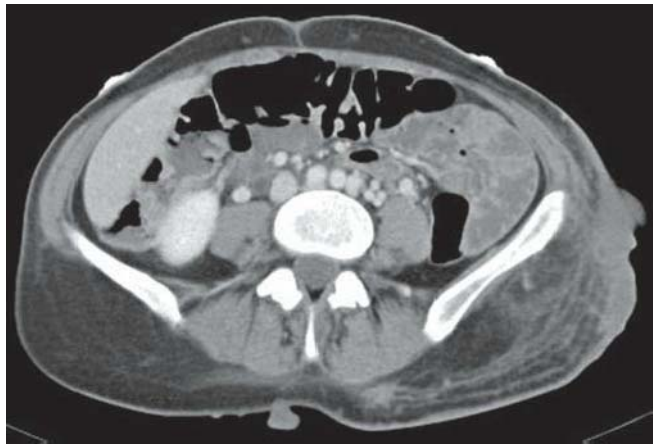

FIGURE 103C

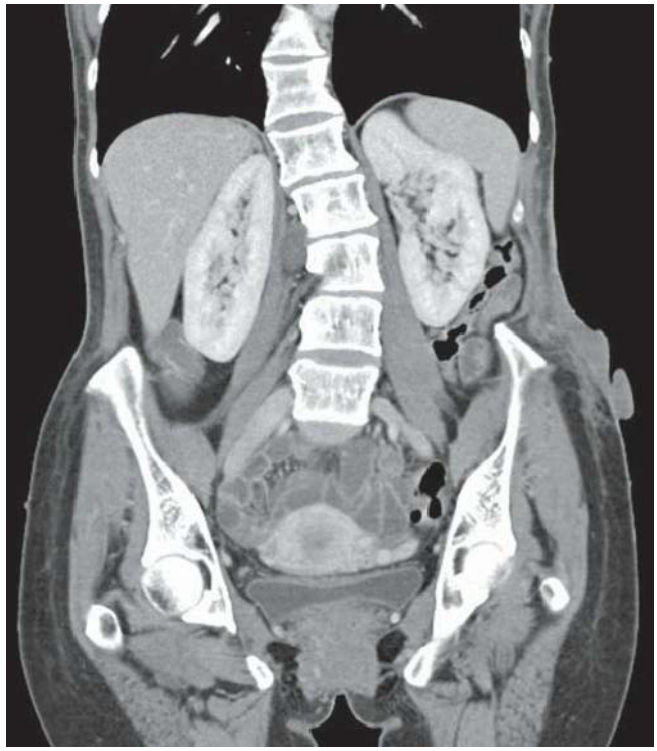

FIGURE 103D

neurofibromas tend to arise in the retroperitoneum, mesentery, and paraspinal regions. Bowel neurofibromas may be seen and occur most frequently in the jejunum. An association with pheochromocytoma, carcinoid, and gastrointestinal tumor, among others, also exists. The urinary tract may also be involved by neurofibromas, the bladder being most commonly affected. As seen in this case, scoliosis and other skeletal deformities are common. The constellation of multiple skin nodules, paraspinal nodule, and scoliosis makes neurofibromatosis type 1 the first diagnostic consideration in this case. In cases of diffuse metastases, a primary tumor is usually known. The absence of immunosuppression and the paraspinal nodule make Kaposi sarcoma unlikely.

CASE 104

CLINICAL HISTORY *56-year-old woman presenting with breast cancer imaged with CT for follow-up.*

FIGURE 104A

FIGURE 104C

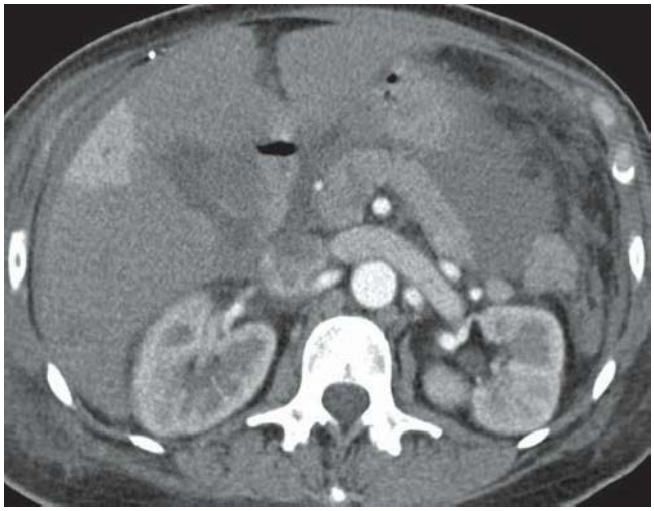

FIGURE 104B

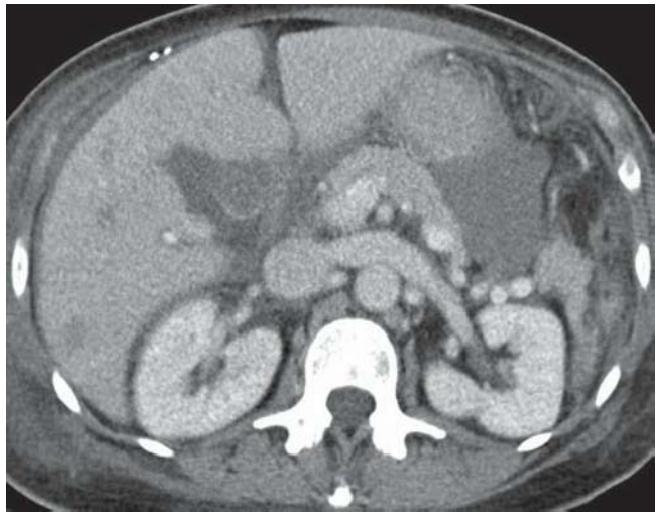

FIGURE 104D

FINDINGS Axial CECT images (A–D) obtained during the arterial phase (A and B) show a heterogeneously enhancing lesion in the right lobe of the liver. Note the triangular area of hyperenhancement peripherally to the tumor; this area has straight, nonspherical boundaries, and a linear nonenhancing structure is seen centrally. On the portal venous phase CECT images (C and D), the triangular area showing arterial enhancement becomes isodense with the rest of the liver parenchyma.

DIFFERENTIAL DIAGNOSIS None.

DIAGNOSIS Transient hepatic attenuation difference (THAD) due to breast cancer metastasis.

DISCUSSION It is well known that malignant liver tumors tend to invade the portal venous system and, to a lesser extent, the hepatic veins. Portal vein thrombosis (PVT) associated with a malignant liver tumor occurs when the tumor extends into the portal vein branches that supply the involved hepatic segments or lobe. PVT is associated with two kinds of hepatic perfusion anomalies. First, a THAD during the late hepatic arterial phase might be present. The reason for this anomaly is thought to be an increase in the attenuation of segments with a dominant arterial flow due to their poor perfusion by the thrombosed portal vein branches. The hyperattenuated areas have straight boundaries, and lack of masslike margins can often be seen during the arterial phase of dynamic contrast-enhanced CT or MRI. Typically, the perfusion anomaly disappears during the portal venous phase. In some cases, depiction of the thrombosed peripheral portal branch is possible in the center of the THAD area. A second type of perfusion anomaly seen with peripheral PVT includes a diminished enhancement of the involved liver segments during the portal venous phase due to locally decreased portal vein perfusion.

CASE 105

CLINICAL HISTORY *19-month-old boy presenting with rising alpha-fetoprotein levels and liver lesion on ultrasound.*

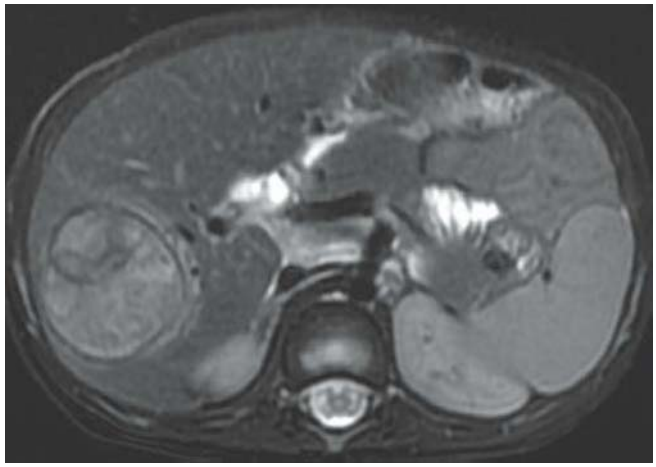

FIGURE 105A

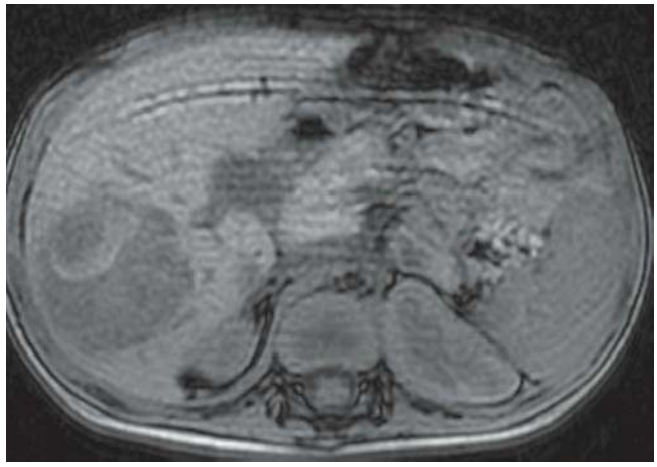

FIGURE 105C

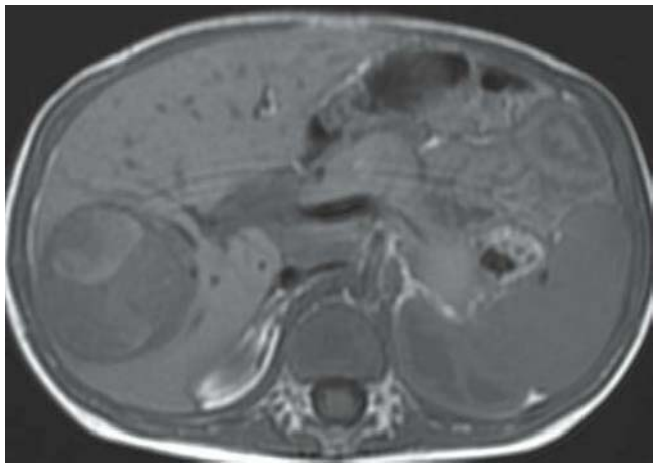

FIGURE 105B

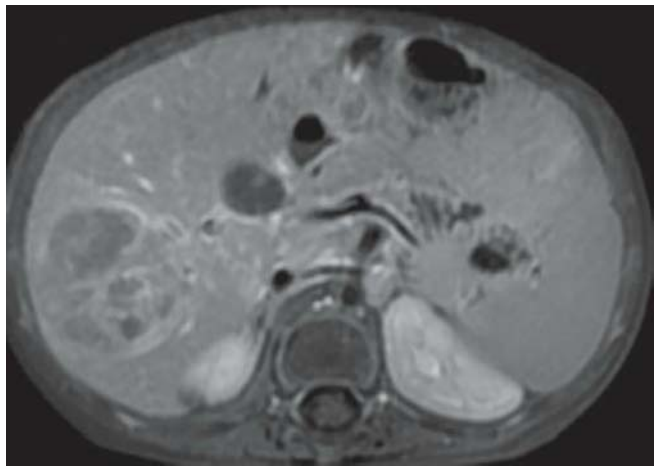

FIGURE 105D

FINDINGS Axial T2-WI (A) demonstrates a 4.5-cm heterogeneous lesion in the liver with a peripheral hypointense capsule. Axial out-of-phase (B) and fat-saturated T1-WI (C) show areas of internal hyperintensity, without internal fat. Post-gadolinium fat-suppressed axial T1-WI (D) shows heterogeneous internal enhancement as well as capsular enhancement.

DIFFERENTIAL DIAGNOSIS Infantile hemangioendothelioma, metastatic neuroblastoma, mesenchymal hamartoma, hepatocellular carcinoma.

DIAGNOSIS Hepatoblastoma.

DISCUSSION Hepatoblastoma is the third most common abdominal malignancy in children following Wilms' tumor and neuroblastoma. They are typically found in children less than 3 years of age with the peak age being less than 18 months. Histologically, hepatoblastomas may be composed of epithelial cells or of mixed cellularity (epithelial and mesenchymal components). Mixed hepatoblastomas frequently have coarse calcifications due to osseous or cartilaginous mesenchymal elements. An elevated AFP almost ensures the diagnosis of hepatoblastoma. On CT, hepatoblastomas are usually low in attenuation in both NECT and CECT. The MRI findings of hepatoblastoma are similar to those seen in a hepatocellular carcinoma. Like hepatocellular carcinoma, hepatoblastomas will be hypointense on T1-WI and hyperintense on the T2-WI. As shown in this case, a capsule can be identified; internal septations can also be seen. Although hemorrhage and necrosis are rare in small hepatoblastomas, they can occasionally occur in very large lesions, as evidenced in this case by the T1 hyperintensity. These areas of hemorrhage and necrosis are not nearly as large as those typically seen in undifferentiated embryonal sarcoma and mesenchymal hamartoma. Both infantile hemangioendothelioma and metastatic neuroblastoma will not produce an elevated alpha-fetoprotein. Metastatic neuroblastomas, like most metastases, tend to be multiple.

Case images courtesy of Dr. Christine Saint-Martin, Montreal Children's Hospital, Montreal, Canada.

CASE 106

CLINICAL HISTORY *34-year-old woman presenting with left flank pain following renal biopsy.*

FIGURE 106A

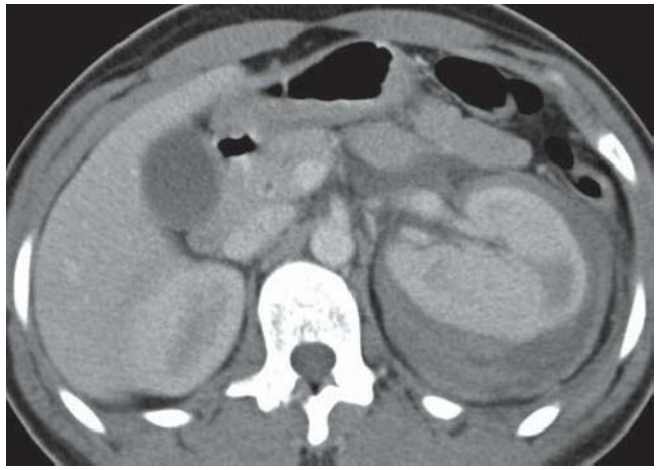

FIGURE 106C

FIGURE 106B

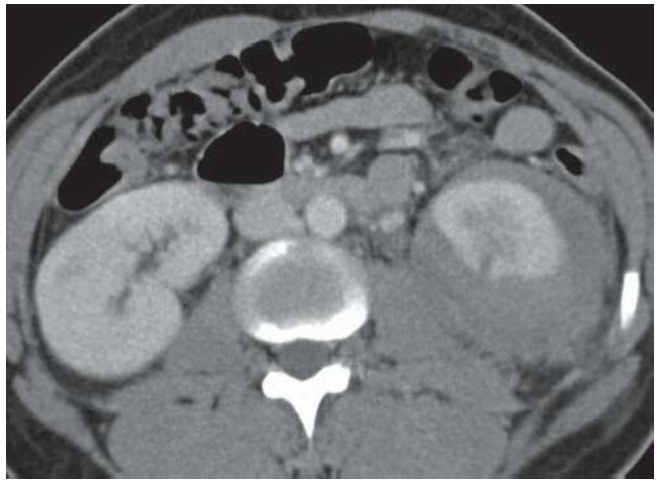

FIGURE 106D

FINDINGS Axial NECT images (A and B) demonstrate high-attenuation material in the left perinephric space, with no detectable enhancement on the axial CECT images (C and D). Note associated fat stranding and linear area of absent enhancement in the left lower renal pole.

DIFFERENTIAL DIAGNOSIS Lymphoma, abscess.

DIAGNOSIS Perirenal hemorrhage.

DISCUSSION Hemorrhage in the perirenal space can be due to blunt or penetrating trauma, anticoagulation therapy, or a hypervascular neoplasm (e.g., angiomyolipoma and renal cell carcinoma). The high-attenuation blood is suggestive of an acute or subacute hemorrhage. If Gerota's fascia has not been disrupted, the hemorrhage will often be contained within the perirenal space. Purulent material from an abscess could also be high in attenuation. Clinical history and the patient's symptoms usually provide enough information to be able to distinguish between the two diagnoses. Lymphoma can often involve the perirenal space but tends to be of soft tissue density, although it can be of high attenuation. In most cases, an underlying neoplasm should be excluded with a follow-up CECT after the hemorrhage has resolved. In this case, the linear area of absent enhancement in the left lower renal pole, which is a clue to the cause of the perirenal hemorrhage, represents blood in the biopsy tract.

CASE 107

CLINICAL HISTORY *55-year-old woman presenting with a history of several years of intermittent epigastric pain and occasional fevers.*

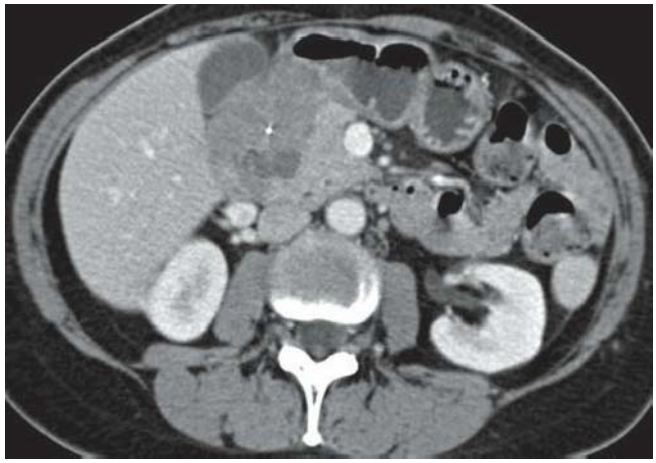

FIGURE 107A

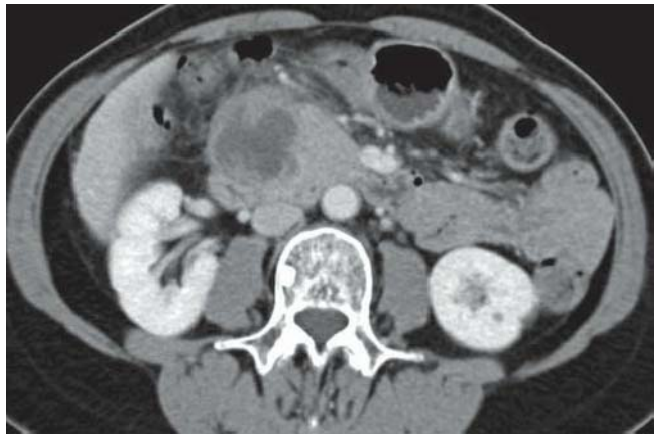

FIGURE 107C

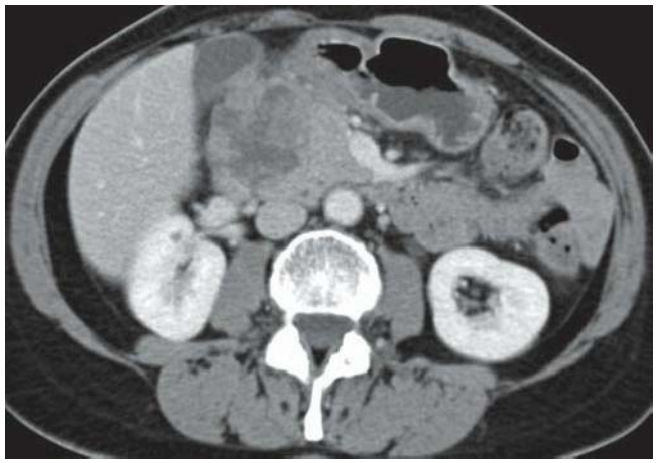

FIGURE 107B

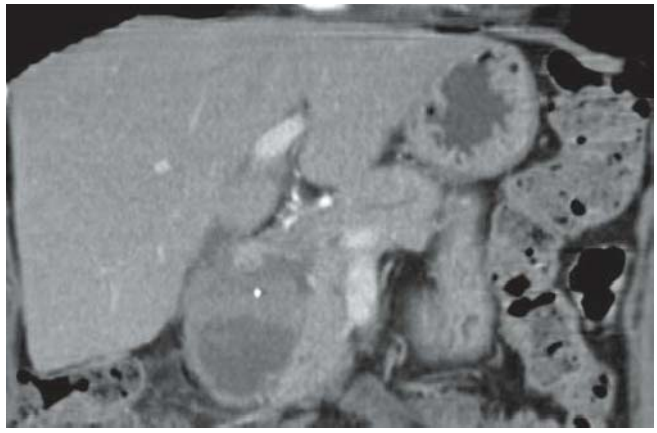

FIGURE 107D

FINDINGS Axial CECT images (A–C) and coronal reformatted image (D) demonstrate a 5-cm mass in the head of the pancreas. The mass is well circumscribed and exophytic in location. There is central necrosis and presence of a punctate calcification. The CBD and pancreatic duct are not dilated.

DIFFERENTIAL DIAGNOSIS Pancreatic ductal adenocarcinoma, endocrine pancreatic tumor, metastasis.

DIAGNOSIS Acinar cell carcinoma.

DISCUSSION Acinar cell carcinoma is a rare malignant neoplasm with poor prognosis due to the frequent presence of liver metastases at the time of diagnosis. Like pancreatic ductal adenocarcinomas, acinar cell carcinomas are seen in elderly patients with a mean age of 65 years. Systemic lipase secretion by acinar cell neoplasms leads to distant fat necrosis in the skin, bone, and joints. The lipase hypersecretion also results in an erythematous rash, lytic bone lesions, and polyarthralgias in these patients. By CT, acinar cell carcinomas tend to be larger than the typical adenocarcinoma, measuring up to 15 cm, and are usually well circumscribed with little desmoplastic reaction. An exophytic location is typical. Because of their larger size, acinar cell neoplasms can have central necrosis, as is seen in this case. Also, calcifications may be present. A nonhyperfunctioning endocrine pancreatic tumor would be a good differential diagnosis for this case because those lesions tend to be large as well, may contain calcifications, and typically are heterogeneous when large.

CASE 108

CLINICAL HISTORY *32-year-old woman presenting with fever and left lower quadrant pain.*

FIGURE 108A

FIGURE 108B

FINDINGS Axial, coronal, and sagittal CECT images (A–C) demonstrate a heterogeneous right adnexal, multiloculated tubular mass with an enhancing thickened wall and surrounding fat stranding. Ultrasound image (D) shows more clearly the tubular configuration of this lesion.

DIFFERENTIAL DIAGNOSIS Dermoid, ovarian cystadenoma, endometriosis, ovarian torsion, ectopic pregnancy.

DIAGNOSIS Tubo-ovarian abscess.

DISCUSSION Tubo-ovarian abscess (TOA) is the most advanced form in the disease continuum of pelvic inflammatory disease (PID). In approximately 1% of women treated for acute salpingitis, the condition progresses to TOA. Patients are usually ill, presenting with pelvic pain, high fever, nausea, and emesis. These systemic symptoms are usually not present in patients with dermoid, ovarian cystadenoma, and endometriosis. However, 15% of patients with TOA are afebrile and have a normal white blood cell count. On clinical and imaging examination, TOA can be difficult to distinguish from ovarian torsion, diverticular or other pelvic abscess, and appendicitis. Most cases of TOA are treated first with intravenous antibiotics. Surgery or percutaneous drainage may be necessary if the patient's symptoms fail to respond clinically within 72 hours after administration of antibiotics or if abscess rupture is suspected. CT scan may demonstrate a tubular or spherical cystic mass. Thick walls and internal septations or gas bubbles may be present. The inflammation causes stranding of the periadnexal fat and thickening of the peritoneum. The latter is typically also absent in patients with dermoid, ovarian cystadenoma, and endometriosis.

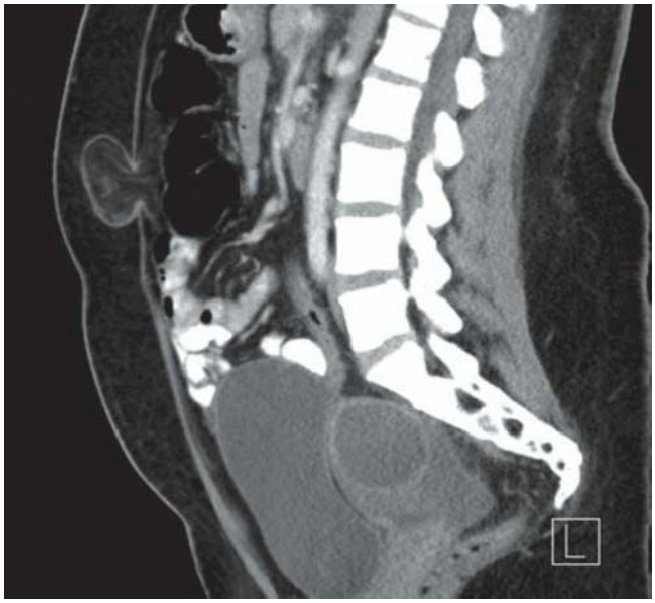

FIGURE 108C

FIGURE 108D

CASE 109

CLINICAL HISTORY *63-year-old man presenting with right flank pain and hematuria.*

FIGURE 109A

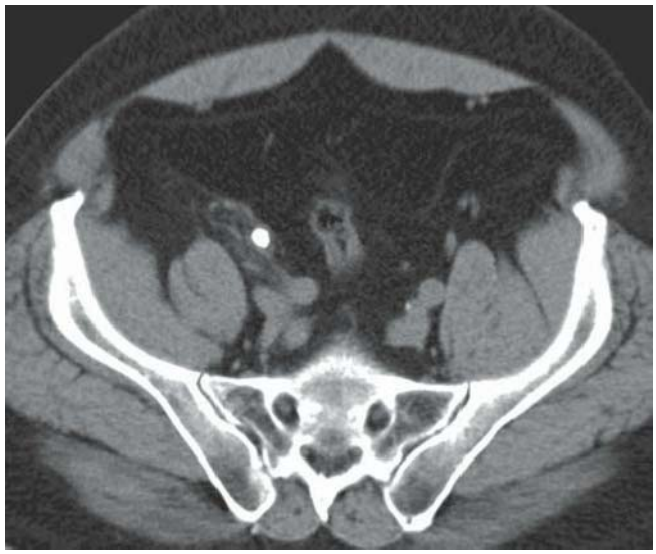

FIGURE 109B

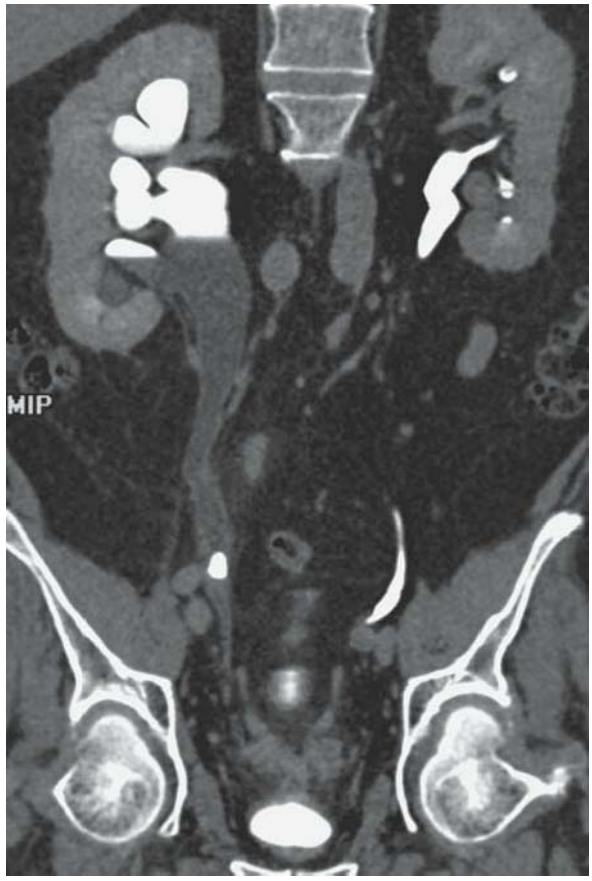

FIGURE 109C

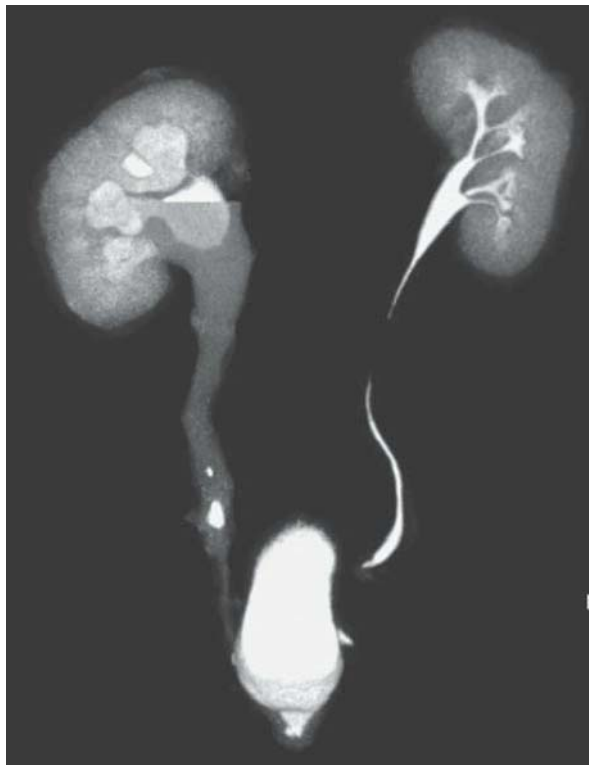

FIGURE 109D

FINDINGS Axial NECT images (A and B) show right hydronephrosis and, adjacent to the iliac vessels, an 8-mm, high-density focus surrounded by a thin rim of soft tissue and fat stranding. Curved maximum-intensity projection (MIP) (C) and three-dimensional, volume-rendered (D) CECT images in the excretory phase confirm the ureteral location of the high-density focus and show delay in contrast excretion by the right kidney.

DIFFERENTIAL DIAGNOSIS None.

DIAGNOSIS Obstructive ureterolithiasis.

DISCUSSION NECT is now the diagnostic test of choice to evaluate obstructive uropathy due to a renal stone. Every renal

calculus is hyperdense on CT, except the rare unmineralized matrix stones and stones caused by indinavir (Crixivan), an HIV medication. On CT, in addition to identification of the stone in the ureter, secondary signs may be present, including hydronephrosis, hydroureter, perinephric and periureteral fat stranding, renal enlargement, and delay in function. In the early hours after passage of a stone in the ureter, when secondary signs have not developed, a helpful sign to ascertain that a high-density focus is in fact in the ureter is the rim sign; a peripheral rim of soft tissue surrounding a calcification indicates that the calcification is intraureteral. The soft tissue represents the inflamed ureteral wall. This sign would not be present if the calcification is a phlebolith, which may be confused for a ureteral calculus. Phleboliths may have a lucent center, which is another differentiating sign from a stone. Also, the "comet tail" sign has been described in association with phleboliths; the comet tail sign is a linear or curvilinear band of soft tissue extending from a calcification.

CASE 110

CLINICAL HISTORY *60-year-old man presenting with abdominal pain.*

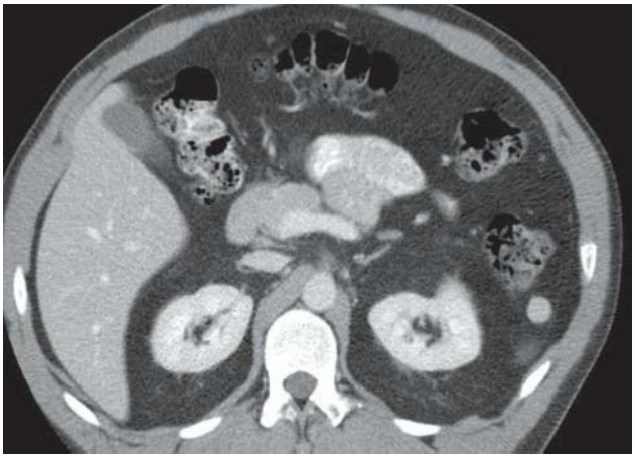

FIGURE 110A

FIGURE 110B

FIGURE 110C

FIGURE 110D

FINDINGS Axial (A and B) CECT images and coronal (C) and sagittal (D) reformatted images demonstrate few nodules adjacent to the spleen. The enhancement of these nodules parallels that of the main spleen.

DIFFERENTIAL DIAGNOSIS Splenosis nodule, lymph node, peritoneal implant.

DIAGNOSIS Accessory spleen.

DISCUSSION Accessory spleens, also known as supernumerary spleens or splenunculi, are congenital foci of normal splenic tissue that are separate from the main body of the spleen. They arise from failure of fusion of the splenic anlage, located in the dorsal mesogastrium, during the fifth week of fetal life. Accessory spleens are relatively common, as they are described in 10% to 30% of cases during autopsy. Although usually asymptomatic and incidentally discovered, they are clinically important in some patients. First, accessory spleen may mimic lymphadenopathy and tumors in other abdominal organs, such as pancreas, adrenal gland, and kidney. Second, they occasionally may become symptomatic due to torsion, spontaneous rupture, hemorrhage, and cyst formation. Third, a surgeon's awareness of their presence may be important when the intention is to remove all functional splenic tissue (e.g., hematologic disorders). The majority of accessory spleens have a characteristic appearance on CT. Typically, they are well-marginated, homogeneously enhancing, round masses that are smaller than 2 cm. Their most frequent location is posteromedial to the spleen. When smaller than 1 cm, they may appear hypodense relative to the spleen.

CASE 111

CLINICAL HISTORY *47-year-old woman presenting with abnormal liver function tests and abdominal pain.*

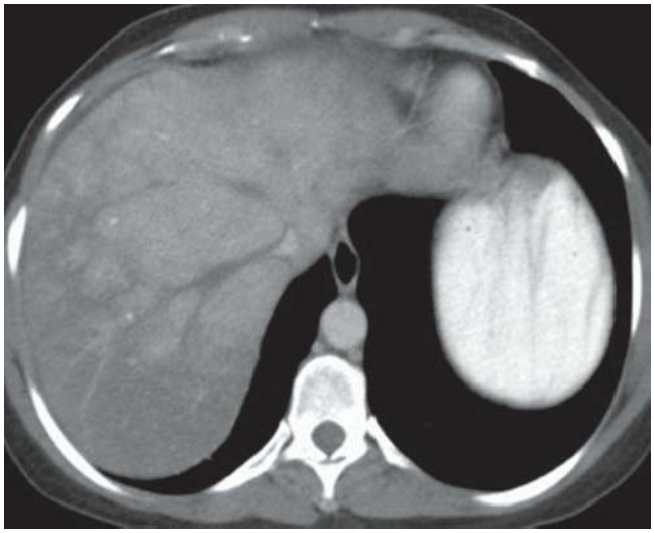

FIGURE 111A

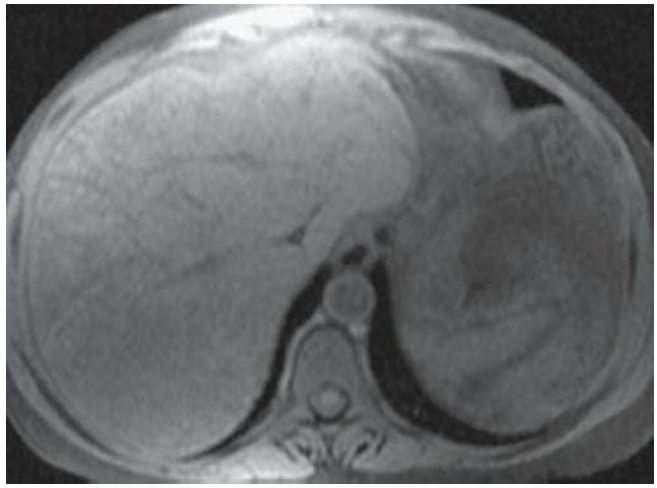

FIGURE 111C

FIGURE 111B

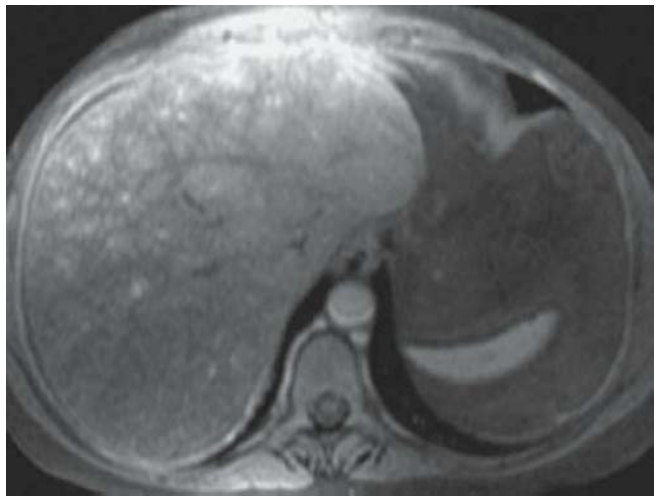

FIGURE 111D

FINDINGS Axial CECT image (A) shows hepatomegaly, ascites, and heterogeneous enhancement of the liver. Note the lack of enhancement of the right and middle hepatic veins. Axial T2-WI (B) and fat-suppressed T1-WI (C) show congestion of the liver, decreased signal intensity on T1-WI, and increased signal intensity on T2-WI. Gadolinium-enhanced, fat-suppressed axial T1-WI (D) confirms the thrombosis of the middle and right hepatic veins.

DIFFERENTIAL DIAGNOSIS Passive hepatic congestion, veno-occlusive disease.

DIAGNOSIS Acute Budd-Chiari syndrome.

DISCUSSION Budd-Chiari syndrome results from the occlusion of the hepatic veins, the inferior vena cava (IVC), or both. Various conditions have been associated with the obstruction of hepatic venous drainage including idiopathic causes, hypercoagulable states from pregnancy, oral contraceptives, polycythemia vera, trauma, tumors involving or obstructing the IVC or hepatic veins, and webs in the IVC. This leads to stasis and increased postsinusoidal pressure in the liver, which decreases portal blood flow. The reduced hepatic venous flow causes ascites, hepatomegaly, collateral vessel formation, and splenomegaly. The poorly enhanced portions of the liver are due to decreased portal flow, venous congestion, and rarely infarcts. MRI is very useful to detect

Budd-Chiari syndrome. The typical findings on CT of mosaiclike enhancement, ascites, and hepatomegaly are readily seen on MR. MR also adds the ability to image in multiple planes, and MR angiography (MRA) can evaluate the hepatic veins and IVC. In this example, there was no evidence of flow in the hepatic veins. Thrombolysis and anticoagulant therapy has limited success in Budd-Chiari syndrome; portosystemic shunting or liver transplantation are therapeutic alternatives.

CASE 112

CLINICAL HISTORY *58-year-old woman with history of abdominal pain presenting with vomiting.*

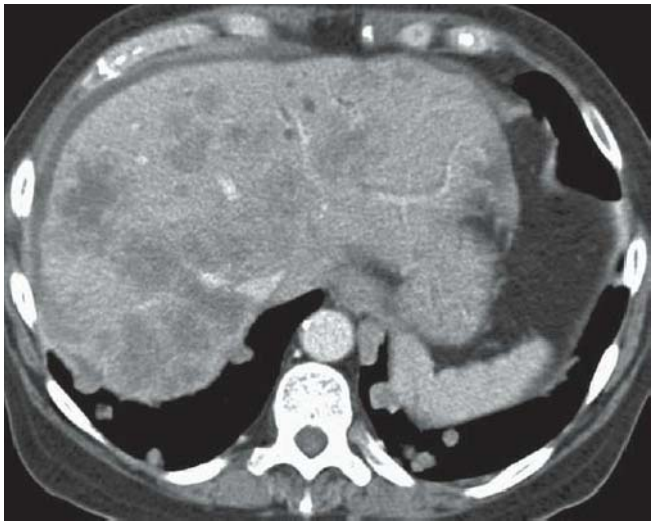

FIGURE 112A

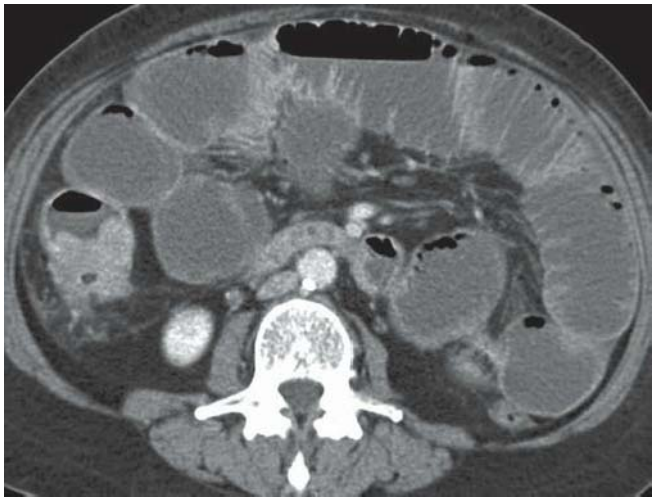

FIGURE 112C

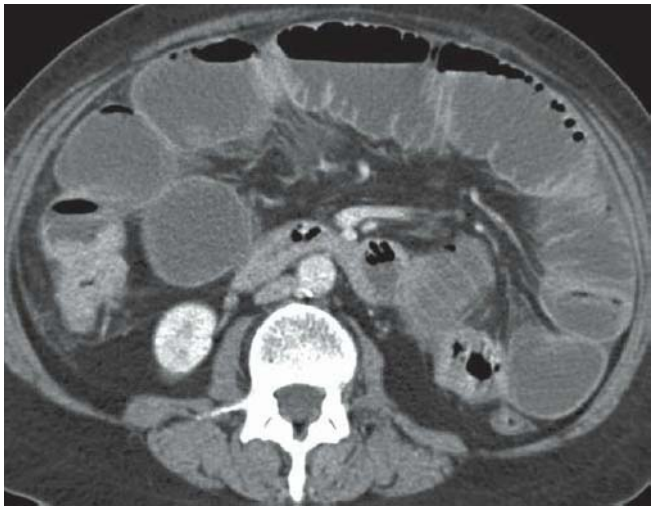

FIGURE 112B

FIGURE 112D

FINDINGS Axial CECT image (A) of the upper abdomen demonstrates numerous pulmonary nodules and low-attenuation masses in the liver. Axial CECT images of mid-abdomen (B–D) reveal a constricting lesion of the ascending colon. Note the lymphadenopathy in the mesocolon and associated bowel obstruction.

DIFFERENTIAL DIAGNOSIS Lymphoma, metastasis.

DIAGNOSIS Metastatic colon cancer.

DISCUSSION Colon cancer is the second most common cancer in men and ranks third in frequency in women living in Western countries. The incidence of colon cancer varies in different parts of the world. In the United States, the incidence is approximately 36 cases per 100,000 people. In many developing countries, the incidence is less than 10 per 100,000 people. Colon carcinoma typically presents on CT as a short segment of luminal irregular wall thickening. Fifty-five percent of colon cancers arise in the rectosigmoid colon; only 15% arise in the ascending colon. Colon cancers arising in the right colon tend to be larger at presentation due to the lack of symptoms. A constricting lesion in the ascending colon and cecum can be due to a variety of etiologies. Tuberculosis (tuberculoma) and amebiasis (ameboma) can have this appearance, and both are more common in the right colon. A stricture from ischemia is also a possibility, although no other signs of ischemia in the remaining bowel are seen, and associated lymphadenopathy, as seen in this case, would be unusual. Although possible, Crohn colitis without terminal ileum involvement is rare. The presence of numerous solid liver lesions, adenopathy in the mesocolon, and an "apple-core" lesion suggests a malignancy. Both lymphoma and adenocarcinoma would be good possibilities in this case.

CASE 113

CLINICAL HISTORY *68-year-old man with a history of renal calculi presents with fevers and left flank pain.*

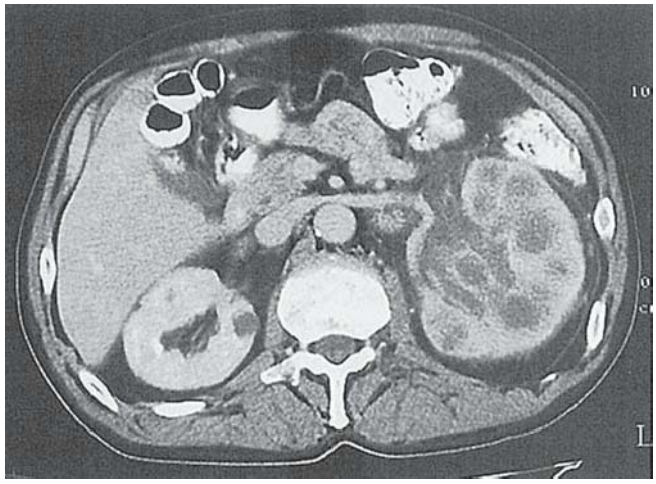

FIGURE 113A

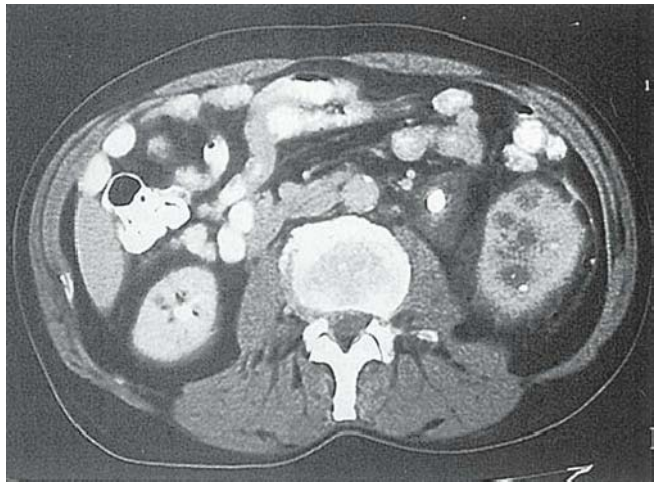

FIGURE 113C

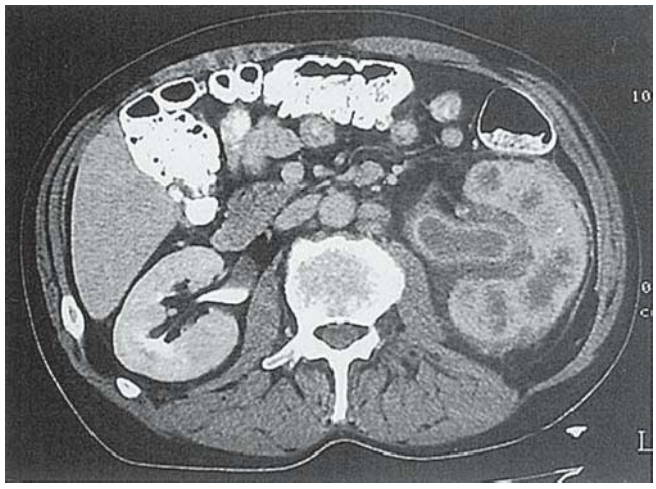

FIGURE 113B

FINDINGS Axial CECT images (A–C) demonstrate an enlarged, poorly perfused left kidney. The renal pelvis and calyces are dilated and irregular in appearance. There is stranding in the renal sinus and perinephric space. Note the multiple low-density lesions in the renal parenchyma. The renal pelvis is dilated due to a proximal ureteral obstructing calculus.

DIFFERENTIAL DIAGNOSIS Transitional cell carcinoma, lymphoma.

DIAGNOSIS Xanthogranulomatous pyelonephritis.

DISCUSSION Xanthogranulomatous pyelonephritis (XGP) is a chronic suppurative granulomatous infection of the kidney secondary to obstruction of the collecting system. As the kidney becomes chronically obstructed, the calyces dilate and fill with purulent material and debris, and the kidney itself enlarges. Typically, there is an obstructing calculus or a staghorn calculus. XGP is much more commonly diffuse (90%) than focal (10%). On CECT image, the affected renal parenchyma is nonfunctioning and diffusely enlarged, with dilated calyces filled with pus. Low-density masses, which may measure fat density, are typically present in the renal parenchyma. An obstructing stone or staghorn calculus is almost always seen, as in this example. Treatment consists of nephrectomy. Simple hydronephrosis would not account for the inflammatory changes around the kidney. An infiltrating malignant process, such as transitional cell carcinoma or lymphoma, can diffusely infiltrate the kidney and globally enlarge it. A dilated collecting system is not commonly seen in these cases unless the tumor involves the ureter.

CASE 114

CLINICAL HISTORY *35-year-old woman referred to CT because of an abnormal abdominal sonogram.*

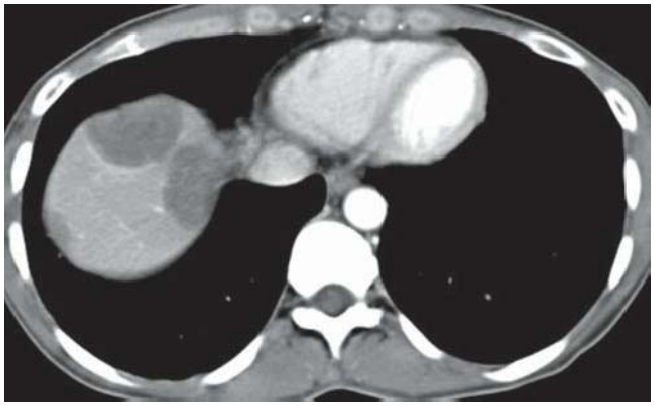

FIGURE 114A

FIGURE 114B

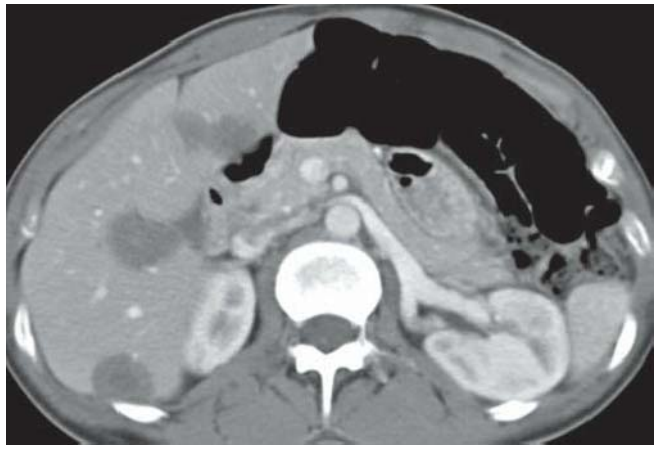

FIGURE 114C

FINDINGS Axial CECT images (A–C) demonstrate multiple hypodense lesions peripherally located in the liver. The lesions have a target appearance and cause capsular retraction.

DIFFERENTIAL DIAGNOSIS Multiple abscesses, lymphoma, multiple metastases.

DIAGNOSIS Epithelial hemangioendothelioma.

DISCUSSION Epithelial hemangioendothelioma (EHE) is a rare malignant hepatic neoplasm of vascular origin. It develops in adults and should not be confused with infantile hemangioendothelioma, which occurs in young children. Some authors consider EHE, an intermediate between hemangioma and angiosarcoma. Like hemangioma, EHE occurs more frequently in women than men. EHE is usually diagnosed incidentally; however, symptoms such as jaundice and liver failure may be present. EHEs appear as multiple nodules that grow, coalesce, and eventually form large confluent masses. Capsular retraction has been reported in 25% to 69% of cases. On NECT images, EHE is of low attenuation, corresponding to the presence of myxoid stroma. Portions of these large, low-attenuation masses may become isodense to the liver parenchyma after administration of contrast material, and therefore, it is often easier to identify the extent of the disease on unenhanced scans. A target sign of concentric zones may be seen on CT or MRI and is due to the presence of a central area of hemorrhage, coagulation necrosis, and calcifications and a peripheral region of cellular proliferation and edema.

CASE 115

CLINICAL HISTORY *19-year-old woman involved in a motor vehicle accident.*

FIGURE 115A

FIGURE 115C

FIGURE 115B

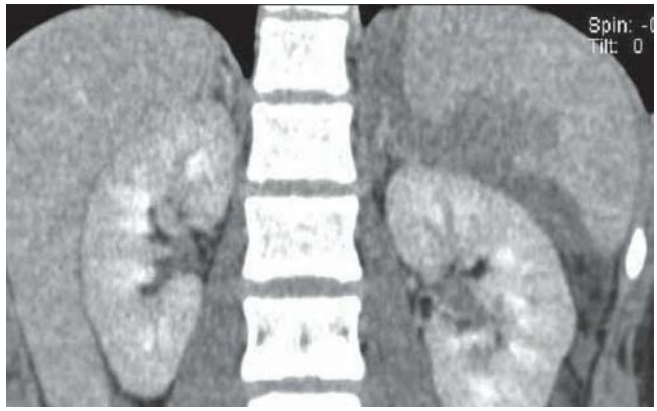

FIGURE 115D

FINDINGS Axial (A–C) and coronal reformatted (D) CECT images demonstrate a stellate area of low attenuation in the medial aspect of the spleen with extension to the splenic hilum. Note the perisplenic high-density fluid (blood).

DIFFERENTIAL DIAGNOSIS None.

DIAGNOSIS Splenic fracture.

DISCUSSION The reported sensitivity of CT scans in the detection of splenic injury varies from 96% to nearly 100%. Injury to the spleen can be demonstrated with CT scan in several ways. There can be an intrasplenic or subcapsular hematoma that typically appears as focal areas of low attenuation on CECT. Areas of high attenuation representing acute to subacute hemorrhage, best appreciated on NECT, can also be present. A laceration can occur, and it will appear as a linear area of low attenuation that does not extend completely across the spleen. This is in contradiction to a fracture that will extend across the spleen, commonly to the splenic hilum. A "shattered" spleen involves multiple areas of fracture and hematoma, which results in a "fragmented" spleen. This case demonstrates a fracture of the spleen that extends completely across the spleen to involve the splenic hilum. In addition, larger focal areas of low attenuation are present, representing intrasplenic hematomas. Luckily for this patient, the hilar vessels were not injured and the hematocrit remained stable, thus requiring only conservative management.

CASE 116

CLINICAL HISTORY *59-year-old woman presenting with pelvic discomfort.*

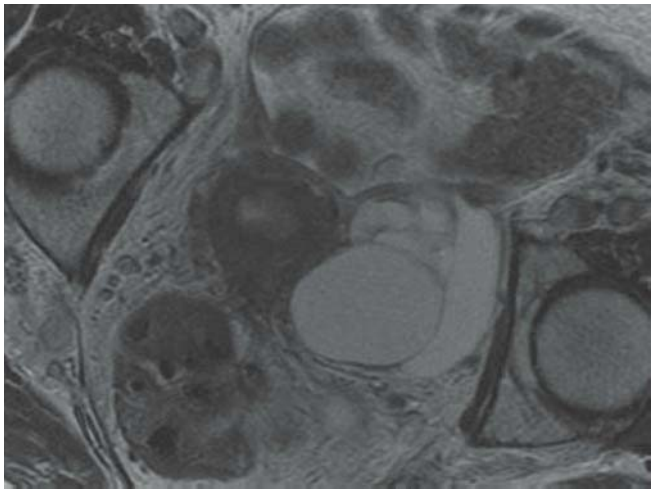

FIGURE 116A

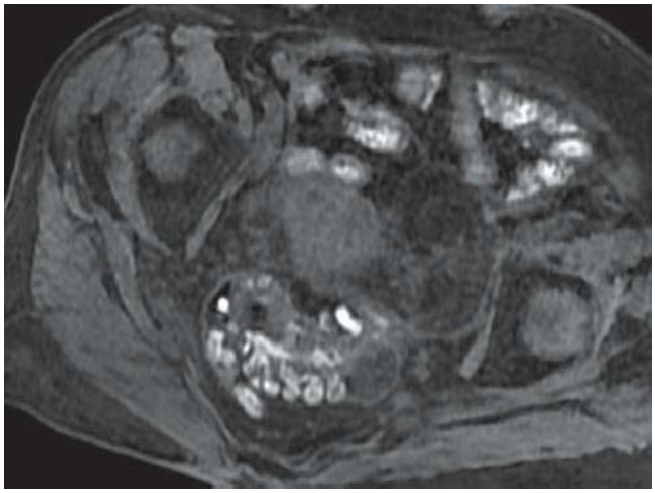

FIGURE 116C

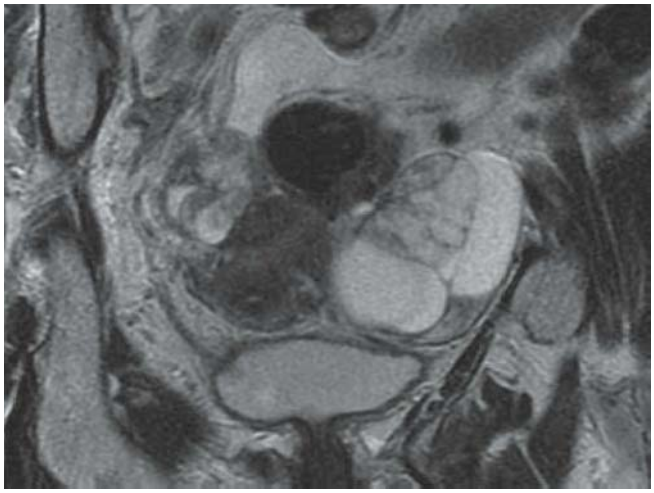

FIGURE 116B

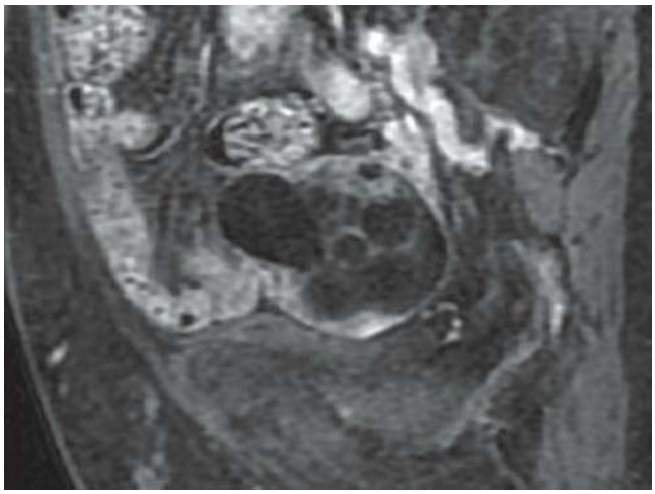

FIGURE 116D

FINDINGS Axial (A) and coronal (B) T2-WIs, unenhanced axial T1-WI (C), and sagittal gadolinium-enhanced, fat-suppressed axial T1-WI (D) show bilateral cystic and solid ovarian masses with enhancement of the solid components.

DIFFERENTIAL DIAGNOSIS Mucinous cystadenocarcinoma, Krukenberg tumor, tubo-ovarian abscess.

DIAGNOSIS Serous cystadenocarcinoma.

DISCUSSION Epithelial ovarian tumors represent 85% of malignant ovarian neoplasms; 50% of them are serous cystadenocarcinomas. Their prevalence peaks in the sixth and seventh decades of life. Risk factors include early menarche, nulliparity, infertility, late menopause, and positive family history for ovarian cancer. In addition to imaging techniques, assessment of serum level of cancer antigen 125 (CA 125) is also of diagnostic use. However, the sensitivity of serum markers is low and depends on the tumor stage (50% in stage I disease). False-positive elevation of CA-125 can occur in endometriosis, uterine leiomyomas, pregnancy, pelvic inflammatory disease, and even in 1% of healthy women. The most important prognostic factors of serous cystadenocarcinoma are tumor grade and residual tumor after initial surgery. Patients with residual disease greater than 2 cm are not considered for further surgery. Staging according to the FIGO guidelines defines as follows: stage I: limited to the ovaries; stage II: involvement of the pelvis; stage III: tumor with intraperitoneal metastasis outside the pelvis and/or positive retroperitoneal nodes; and stage IV: distant metastasis or pleural effusion with positive cytology or hepatic metastasis. Features on imaging suggesting ovarian malignancy are large soft-tissue masses, cyst wall thickness >3 mm, enhancing papillary projections, presence of ascites, peritoneal implants, pelvic wall invasion, and adenopathy.

CASE 117

CLINICAL HISTORY *53-year-old man presenting with severe abdominal pain for 2 days.*

FIGURE 117A

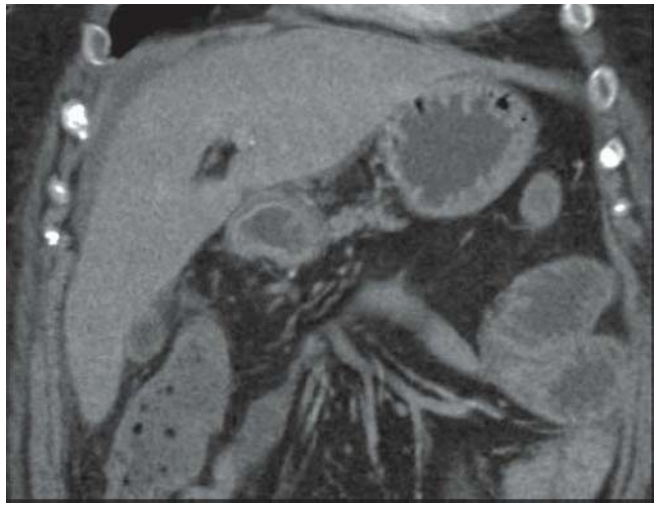

FIGURE 117C

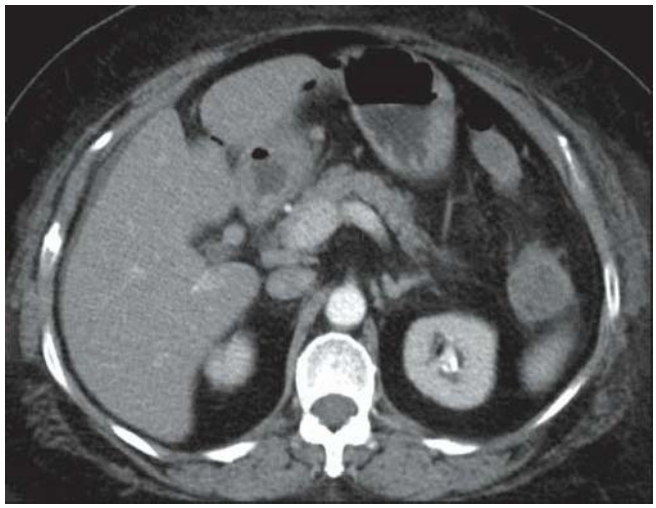

FIGURE 117B

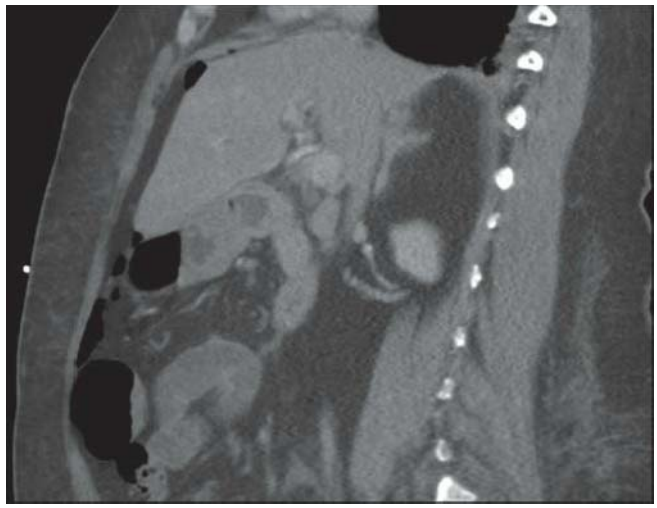

FIGURE 117D

FINDINGS Axial (A and B), coronal reformatted (C), and sagittal reformatted (D) CECT images demonstrate extraluminal free intraperitoneal gas, perihepatic ascites, and edematous wall thickening of the duodenal bulb with mild adjacent fat stranding.

DIFFERENTIAL DIAGNOSIS None.

DIAGNOSIS Perforated duodenal bulb ulcer with pneumoperitoneum.

DISCUSSION Peptic ulcers can occur in the stomach or the duodenum. Duodenal ulcers are two to three times more common than gastric ulcers. Patients typically present with symptoms of epigastric pain often precipitated by food. Almost all duodenal ulcers are benign, whereas a percentage of gastric ulcers can be malignant (ulcerated gastric adenocarcinomas). The majority of duodenal ulcers are located on the anterior wall of the duodenal bulb, which has an intraperitoneal location. Complications of peptic ulcer disease include gastrointestinal hemorrhage, perforation, obstruction, and fistula formation. Because of the mixed peritoneal–retroperitoneal location of the duodenum, perforations may manifest as spillage of intraluminal content and gas in the peritoneum in cases of perforation of the duodenal bulb, as seen in this case, or in the retroperitoneum if the perforation arises from the second or third portion of the duodenum. The differential diagnosis of pneumoperitoneum includes bowel perforation secondary to blunt or penetrating trauma, perforation of an ulcer, diverticulum, or neoplasm, iatrogenic bowel injury, and surgery.

CASE 118

CLINICAL HISTORY *53-year-old woman presenting with gross hematuria.*

FIGURE 118A

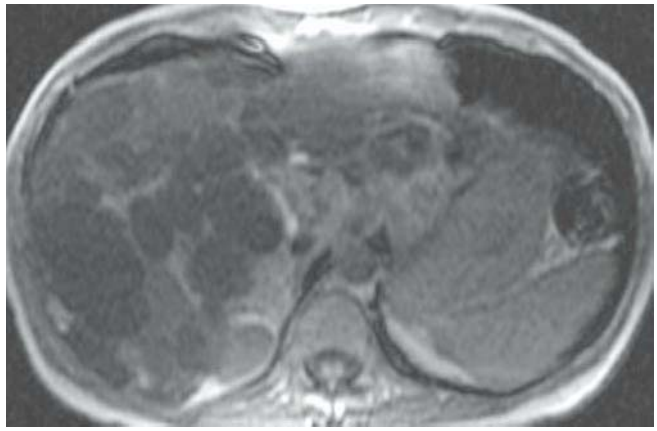

FIGURE 118C

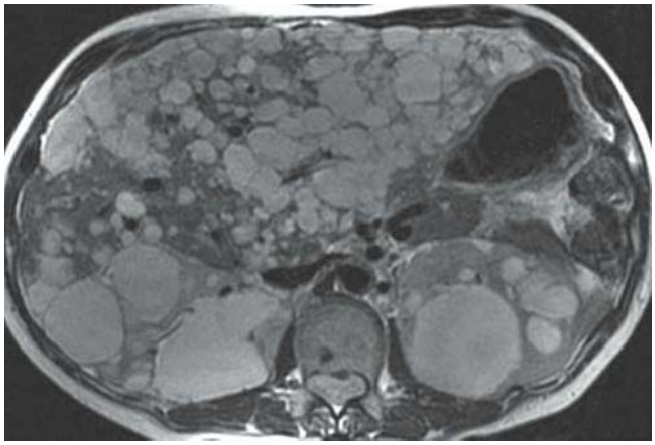

FIGURE 118B

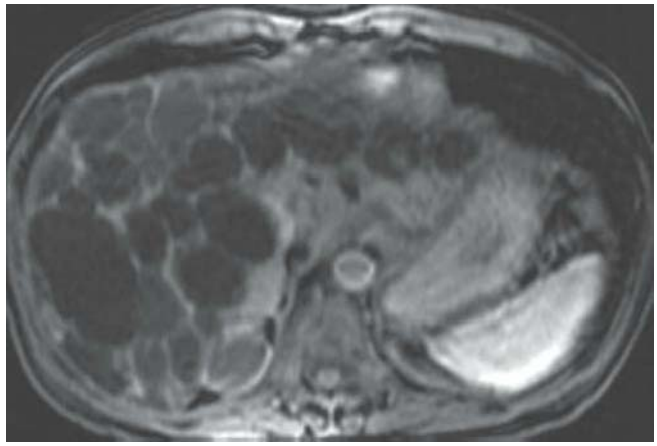

FIGURE 118D

FINDINGS Axial CECT image (A) shows multiple cysts of varying size, replacing the liver parenchyma and both kidneys. Axial T2-WI (B) and T1-WI (C) confirm the cystic nature of the lesions. The signal intensity of the lesions varies on T1-WI, representing various degrees of protein content. Gadolinium-enhanced, fat-suppressed axial T1-WI (D) shows the lack of enhancement of the cystic lesions.

DIFFERENTIAL DIAGNOSIS Caroli disease, multiple hepatic abscesses, cystic metastases.

DIAGNOSIS Autosomal dominant polycystic disease.

DISCUSSION Autosomal dominant polycystic liver disease is often found in association with renal polycystic disease and is thought to result from progressive dilation of abnormal ducts as part of a ductal plate malformation at the level of the small intrahepatic bile ducts. These small bile ducts do not have continuity with the remaining biliary tree, which explains the noncommunicating nature of the cysts in polycystic liver disease. Patients are usually asymptomatic, and liver dysfunction occurs only sporadically. On unenhanced CT scans, polycystic liver disease typically appears as multiple homogeneous and hypodense cystic lesions; cysts do not show wall or content enhancement on contrast-enhanced images. At MRI, hepatic cysts in polycystic liver disease typically demonstrate very low signal intensity on T1-WI and homogeneous high signal intensity on T2-WI. The signal intensity of the lesions can vary on T1-WI, representing various degrees of protein content. Cysts do not enhance after administration of intravenous gadolinium. Although the diagnosis of polycystic liver disease is easily made with both CT and MRI, MRI is more sensitive for the detection of complicated cysts.

CASE 119

CLINICAL HISTORY *71-year-old man presenting with deep right upper quadrant pain.*

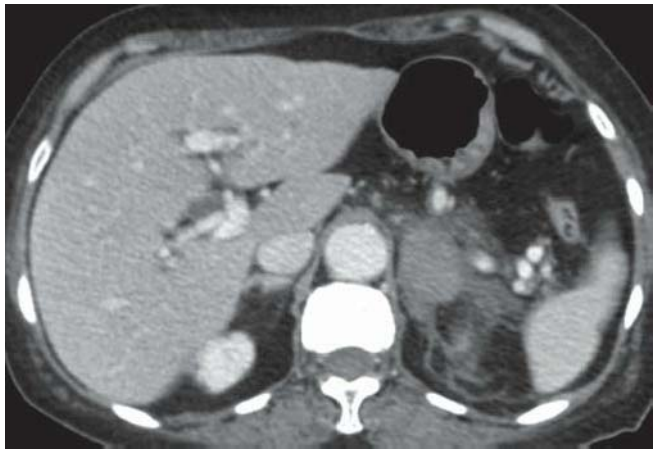

FIGURE 119A

FIGURE 119C

FIGURE 119B

FIGURE 119D

FINDINGS Axial (A and B) and coronal reformatted (C) CECT images demonstrate a 4.0 cm × 3.4 cm hyperdense left gland nodule. Marked peri-adrenal fat stranding is present. Note the fluid/fluid level on the sagittal reformatted CECT image (D).

DIFFERENTIAL DIAGNOSIS Metastasis.

DIAGNOSIS Acute adrenal hemorrhage.

DISCUSSION Adrenal hematomas may be traumatic or non-traumatic (due to anticoagulation, stress related to surgery, sepsis, hypotension, or rarely idiopathic) in etiology. Traumatic hemorrhage occurs more commonly on the right side (90%) due to compression of the right adrenal gland between the spine and the liver. Sudden increase in intra-abdominal pressure at the time of the trauma and resultant transmission of that pressure to the adrenal gland also plays a role in the development of adrenal hematomas. On CT, the acute or subacute hematoma is initially hyperdense, with a density ranging from 50 to 90 Hounsfield units. Adrenal hemorrhage has a round or oval configuration in up to 83% of cases, but may obliterate the gland in 9% or cause diffuse uniform enlargement in 9%. Gradually, the density of the blood decreases and the hematoma regresses. On occasion, residual pathologic changes persist in the form of an adrenal pseudocyst. In the present case, keys to the diagnosis are the presence of the significant amount of surrounding fat stranding which is almost invariably present in cases of hemorrhage, and the fluid–fluid level identified on the sagittal image.

CASE 120

CLINICAL HISTORY *62-year-old woman with a history of aortic surgery presenting with hematemesis.*

FIGURE 120A

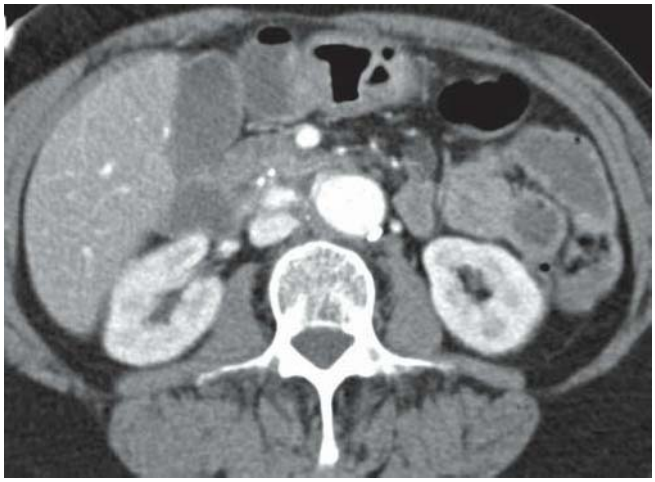

FIGURE 120C

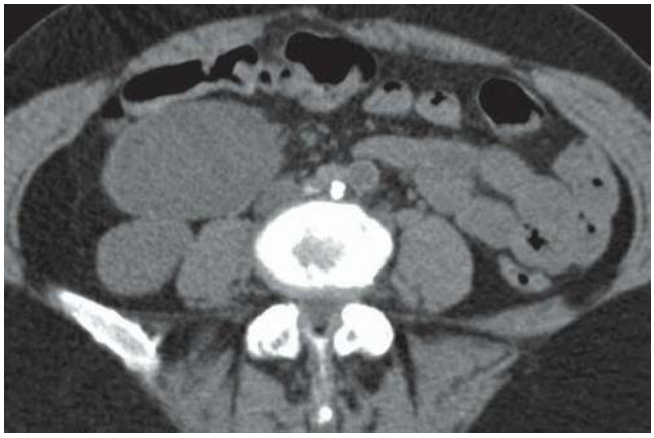

FIGURE 120B

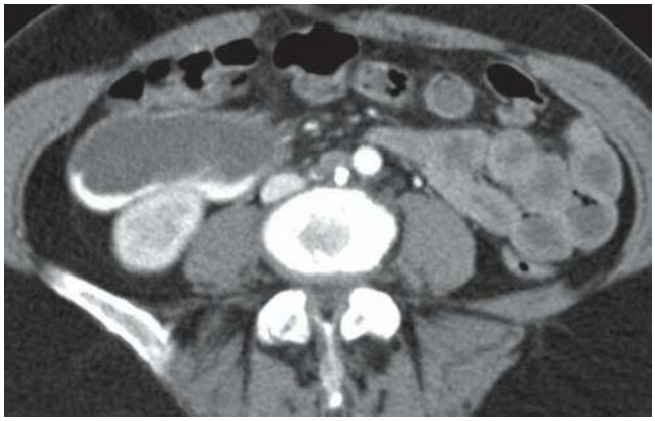

FIGURE 120D

FINDINGS Axial NECT images (A and B) show a status post-aortic aneurysm repair, a dilated third portion of the duodenum, and soft-tissue density stranding between the duodenum and aorta. Following intravenous administration of iodinated contrast, axial CECT images (C and D) show extravasation of contrast into the duodenum.

DIFFERENTIAL DIAGNOSIS None.

DIAGNOSIS Aortoduodenal fistula.

DISCUSSION The aorta lies in proximity with the GI tract for much of its thoracic and abdominal course. Aortoenteric fistulas, therefore, can potentially involve the gut anywhere from the esophagus to the colon. The majority of cases occur in the presence of aortic aneurysm disease, either as a primary event or as a secondary complication following surgical repair. The duodenum participates in the majority of aortoenteric fistulas, owing to the proximity between its third portion and the abdominal aorta. Primary aortoduodenal fistula is a rare life-threatening cause of GI bleeding that results most commonly from an atherosclerotic aortic aneurysm. Unusual causes of a primary fistula include aortitis, radiation therapy, malignancy, and peptic ulcer disease. Most patients have GI bleeding, but the classic triad of abdominal pain, GI bleeding, and pulsatile mass is present in fewer than 25% of cases. A "herald bleed" frequently precedes lethal exsanguination, and patient survival hinges on prompt diagnosis and emergent therapeutic laparotomy. Unfortunately, a correct preoperative diagnosis is determined in only a minority of cases, underscoring the importance of heightened clinical suspicion. CT provides rapid and effective evaluation in hemodynamically stable patients suspected of having an aortoenteric fistula. CT findings, such as perianeurysmal hematoma, pseudoaneurysm, contrast agent extravasation, periaortic or intraluminal gas, and focal duodenal wall thickening, are highly suggestive of a fistula in the appropriate clinical setting.

CASE 121

CLINICAL HISTORY *72-year-old woman with recent duodenal surgery presenting with abdominal distention.*

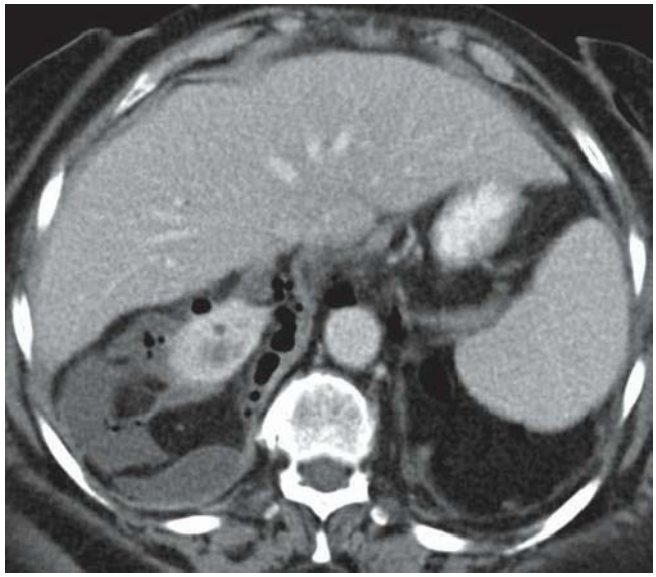

FIGURE 121A

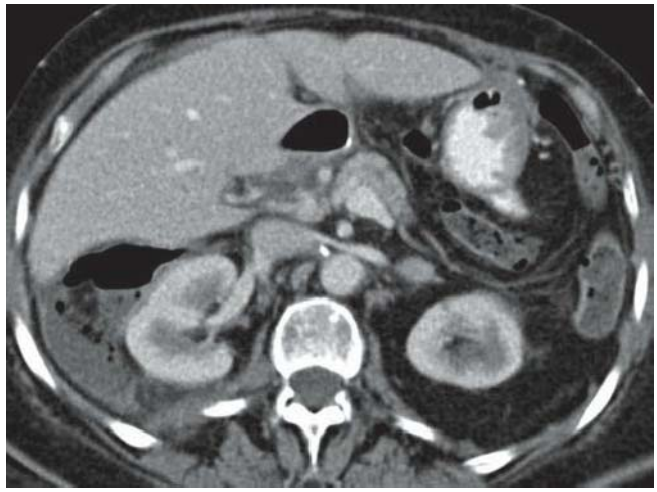

FIGURE 121C

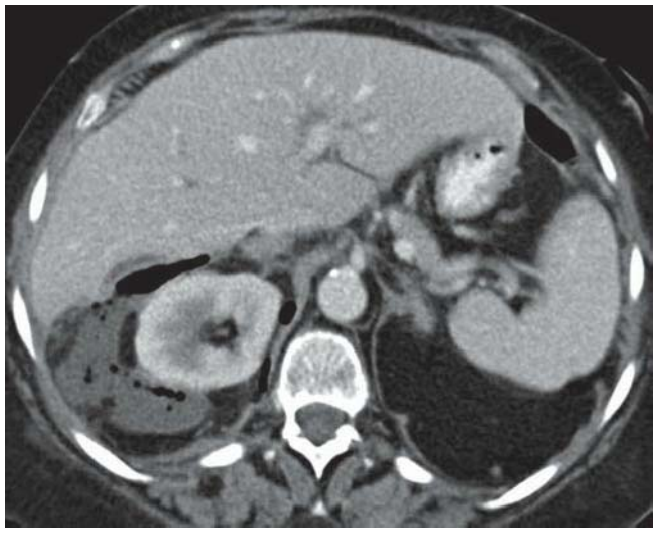

FIGURE 121B

FIGURE 121D

FINDINGS Axial CECT images (A–D) in the corticomedullary phase demonstrate several collections with air–fluid levels, gas bubbles, and fat stranding in the right perinephric and pararenal space.

DIFFERENTIAL DIAGNOSIS Trauma, instrumentation.

DIAGNOSIS Perirenal abscess.

DISCUSSION Air in the perirenal space originates either from gas-forming organisms or is introduced into the perirenal space from either penetrating trauma (e.g., stab wound and gunshot) or instrumentation (e.g., biopsy and surgery). Air from the latter two causes does not necessarily imply infection. A perirenal abscess, however, requires antibiotics and drainage either percutaneously or surgically. Given the history of recent surgery in this case, the abscesses were a surgical complication. Pyelonephritis with extension through the renal capsule, forming a perirenal abscess, is a common cause of perirenal abscess. Acute obstruction with a ruptured fornix can also lead to a perirenal abscess, but in this case, there is no evidence of renal calculi or collecting system obstruction to suggest this diagnosis. The lack of air in the renal parenchyma excludes emphysematous pyelonephritis.

CASE 122

CLINICAL HISTORY *75-year-old woman presenting with a history of metastatic colon cancer and remote history of motor vehicle accident 20 years ago.*

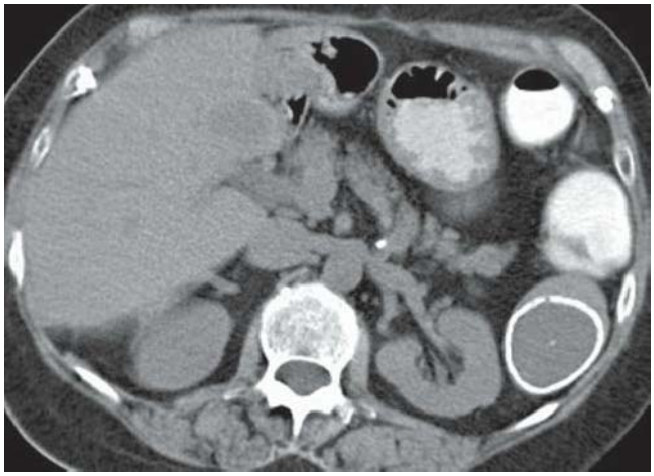

FIGURE 122A

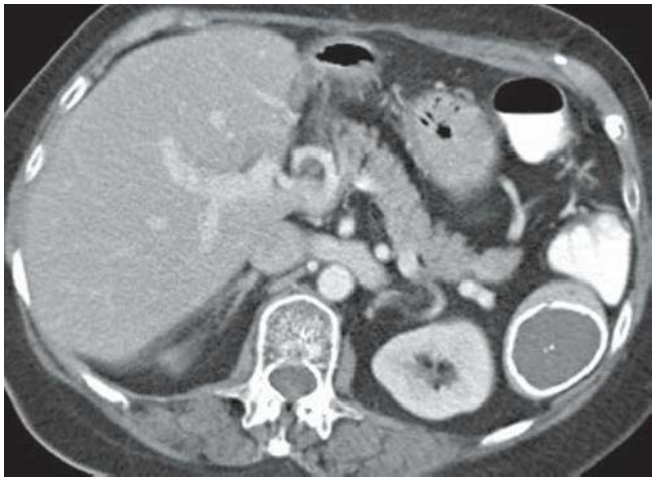

FIGURE 122C

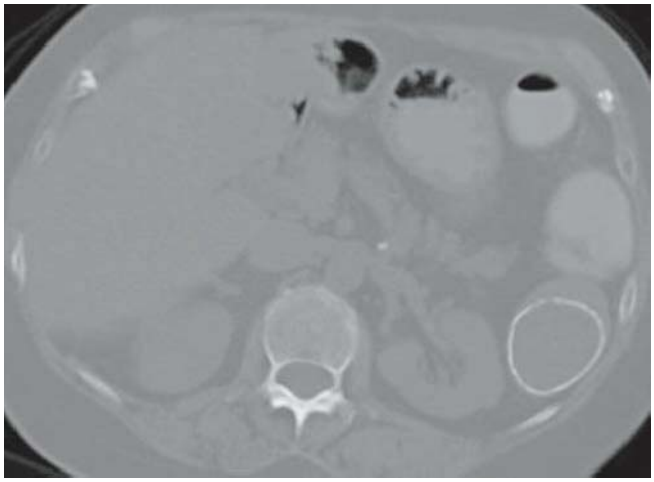

FIGURE 122B

FIGURE 122D

FINDINGS Axial NECT images in soft tissue (A) and bone window (B) show a rim-calcified cystic splenic lesion in the lower pole measuring 4.3 cm × 3.7 cm. Axial (C) and coronal (D) CECT images confirm the lack of enhancement of the lesion and location within the spleen.

DIFFERENTIAL DIAGNOSIS Epidermoid cyst, postinfectious cyst, hydatid cyst, infarct, pancreatic pseudocyst.

DIAGNOSIS Posttraumatic cyst.

DISCUSSION Cysts in the spleen can be divided into true cysts (primary or epidermoid) and false cysts (secondary or posttraumatic). Posttraumatic cysts account for 80% of all splenic cysts. True cysts possess an epithelial lining, are usually unilocular, and are detected most often in childhood and adolescents. Secondary cysts do not possess an epithelial lining but have a fibrous capsule. They are a result of prior infections, infarctions, or hematoma within the spleen. False cysts are usually smaller than true cysts and may contain internal debris. False cysts tend to be subcapsular in location and can calcify in the periphery in up to 50% of the cases. Other lesions that can present with eggshell calcifications include epidermoid cysts, hydatid cysts, and pancreatic pseudocysts. Clinical history is helpful in these situations to help narrow the differential diagnosis. The remote history of trauma and lack of clinical symptoms are suggestive of the diagnosis of posttraumatic (false) cyst.

CASE 123

CLINICAL HISTORY *59-year-old man with previous Billroth II surgery presenting with acute left upper quadrant pain.*

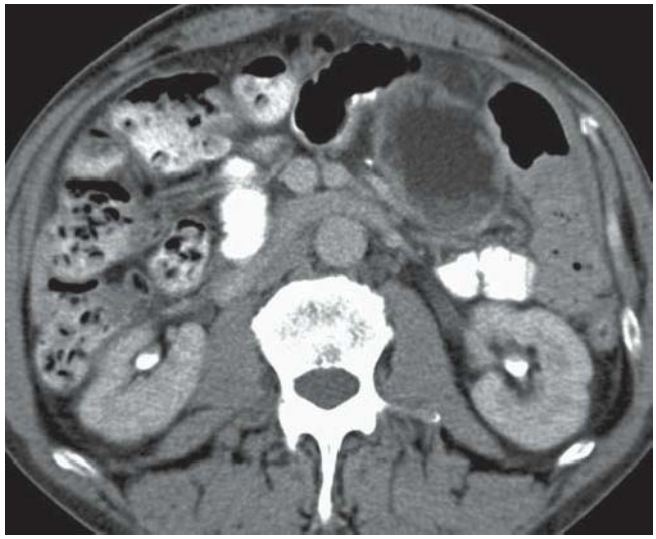

FIGURE 123A

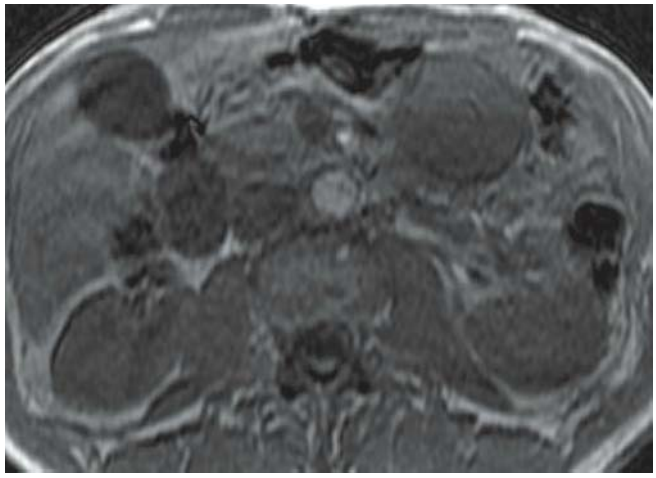

FIGURE 123B

FIGURE 123C

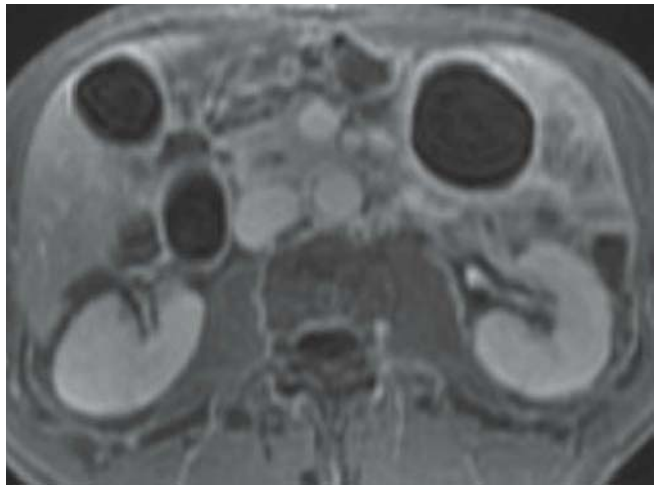

FIGURE 123D

FINDINGS Axial CECT image (A) shows a 6.4 cm × 4.5 cm, fat-containing mesenteric mass with dependent debris surrounded by a nodular rim of soft-tissue density. MRI shows a fat–fluid level within the mass with nondependent bright fluid on the in-phase axial T1-WI (B) that suppresses on the out-of-phase axial T1-WI (C). Gadolinium-enhanced, fat-suppressed axial T1-WI (D) shows a rim-enhancing unilocular cyst.

DIFFERENTIAL DIAGNOSIS Liposarcoma, lipoma, teratoma, lymphangioma, duplication cyst, abscess, pancreatic pseudocyst.

DIAGNOSIS Chylous cyst (nonpancreatic pseudocyst).

DISCUSSION A chylous cyst is a rare type of mesenteric cyst, classified as a nonpancreatic pseudocyst. It contains chyle in various quantities, which accounts for the fat attenuation identified on CT. A fat–fluid level, the less dense fat being nondependent, is thought to be almost diagnostic of lesions containing chyle. On MRI, the liquid composed of microscopic fat would appear bright on T1-WI, and the intensity of that liquid would suppress on the out-of-phase T1-WI. The dependent debris identified on CT and the thick walls in this case are likely related to internal hemorrhage because multiple abnormal blood vessels were identified around the cyst at pathology. A lymphangioma or a teratoma would be the best differential diagnosis in this case. Lymphangiomas may contain chyle and thus have negative attenuation values, but they are often multilocular. Teratomas may have an identical appearance to chylous cysts. Identification of calcifications or of a hairball is helpful to allow the diagnosis of a teratoma. Liposarcomas and lipomas are solid fat-containing lesions and would not have a fat–fluid level. This is the same for duplication cysts, abscesses, and pancreatic pseudocysts that are also thick-walled cysts in a mesenteric location and typically do not contain fat.

CASE 124

CLINICAL HISTORY *23-year-old woman presenting with acute right upper quadrant pain.*

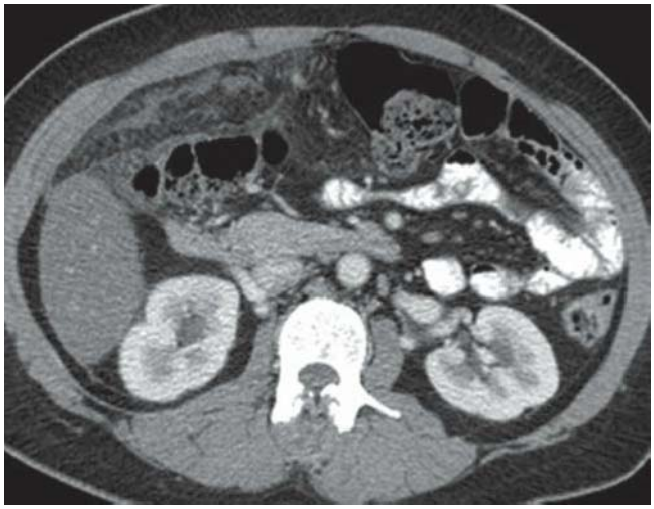

FIGURE 124A

FIGURE 124B

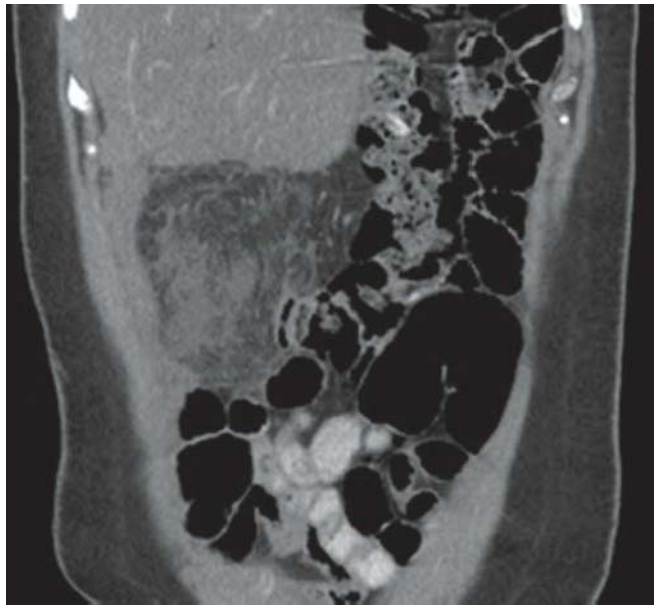

FIGURE 124C

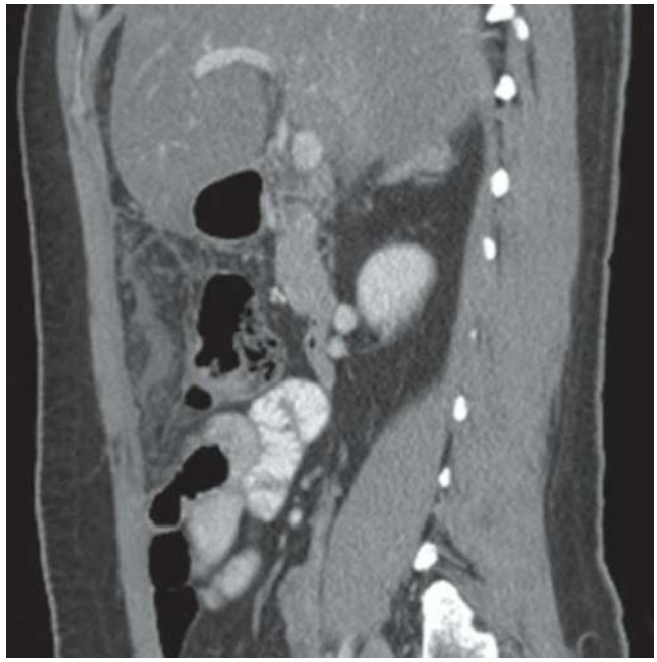

FIGURE 124D

FINDINGS Axial (A and B), coronal reformatted (C), and sagittal reformatted (D) CECT images demonstrate fat stranding and focal fluid anterior to the proximal transverse colon associated with peritoneal thickening anteriorly. Adjacent bowel loops have normal wall thickness.

DIFFERENTIAL DIAGNOSIS Epiploic appendagitis, lymphoma, tuberculosis, liposarcoma, metastasis.

DIAGNOSIS Omental infarct.

DISCUSSION Omental infarct is seen more frequently in females and obesity, as seen in this case, appears to be a predisposing factor. Patients typically present with acute lower quadrant pain. The infarct may be due to torsion of the omentum, adhesions, precarious blood supply, or prior surgery. On CT, focal infiltration of the affected omentum by soft-tissue stranding is seen, but a more masslike lesion mimicking a fat-containing neoplasm, such as liposarcoma, may be encountered. Clinically, an omental infarct may mimic acute appendicitis, epiploic appendagitis, or diverticulitis. Making the diagnosis by imaging is important as the treatment for this condition is symptomatic relief without surgical intervention. Spontaneous and complete resolution of the symptoms is typically observed within 2 weeks. Epiploic appendagitis is a smaller fatty lesion on the anti-mesenteric

side of the colon surrounded by a hyperdense rim and may have a central dot representing a thrombosed vessel. Omental lymphoma is exceedingly rare without any other involved region. Tuberculous peritonitis does not usually present acutely but could have the same CT appearance. Omental metastases are uncommon in younger adults and a primary tumor is usually known at the time of diagnosis. Liposarcomas almost invariably develop in the retroperitoneum.

CASE 125

CLINICAL HISTORY *18-year-old woman presenting with painless left labial swelling.*

FIGURE 125A

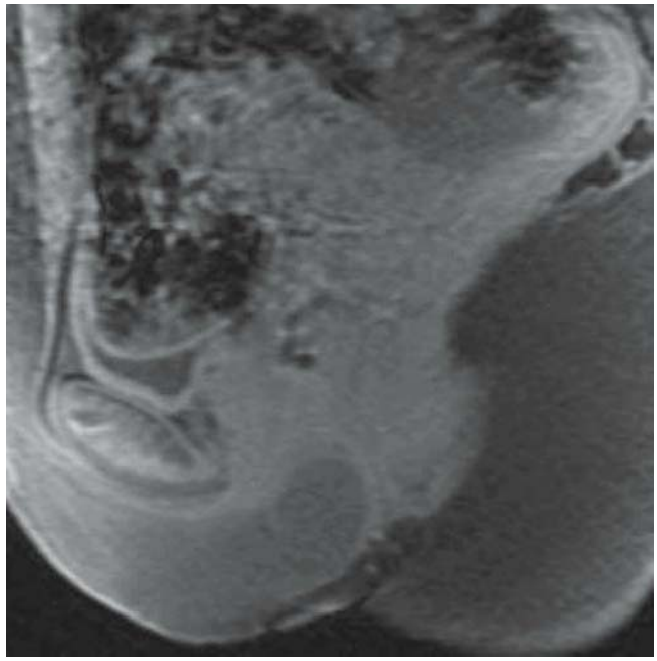

FIGURE 125C

FIGURE 125B

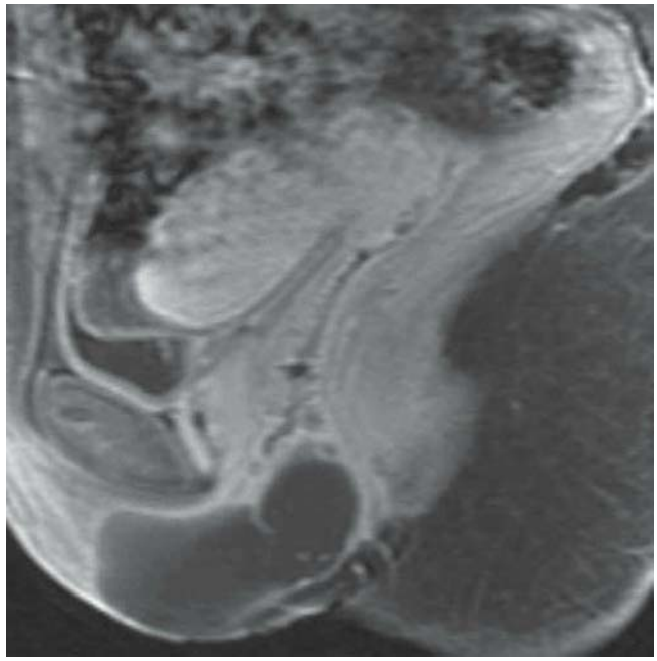

FIGURE 125D

FINDINGS Axial (A) and sagittal (B) T2-WIs and unenhanced (C) and gadolinium-enhanced (D) fat-suppressed sagittal T1-WIs demonstrate a comma-shaped cystic mass measuring 6.3 cm × 5.0 cm in the left labia, with a thin enhancing wall and a single septation.

DIFFERENTIAL DIAGNOSIS Bartholin gland cyst, inguinal hernia, epidermal inclusion cyst, mucous cyst of the vestibule, Skene gland cyst.

DIAGNOSIS Cyst of the canal of Nuck.

DISCUSSION The processus vaginalis peritonei, through which the testes descend in males, is a tubular fold of peritoneum. In females, it invaginates along the round ligament in the inguinal canal. Normally, it is completely closed in the first year of life. When it remains patent in females, it is called the canal of Nuck. It establishes a communication between the peritoneal cavity and the inguinal canal. The degree and level of closure defines the type of inguinal hernia or hydrocele that results. Partial proximal closure with a patent distal portion makes the lesion a cyst of the canal of Nuck, as seen in this case. Inguinal hernias are associated in one-third of the patients. Based on the lack of omental or intestinal contents within the cystic mass, the differentiation can be made. A cyst of the canal of Nuck is soft and compressible on clinical examination. On imaging, a typical comma-shaped cystic lesion with a thin enhancing wall in the major labia or mons pubis is classic for such pathology.

CASE 126

CLINICAL HISTORY *73-year-old man presenting with a complaint of having a "rounder face" and found to have hyperglycemia.*

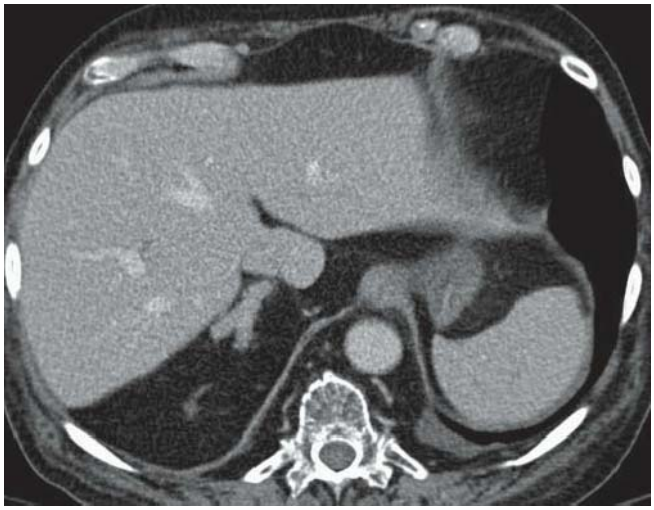

FIGURE 126A

FIGURE 126C

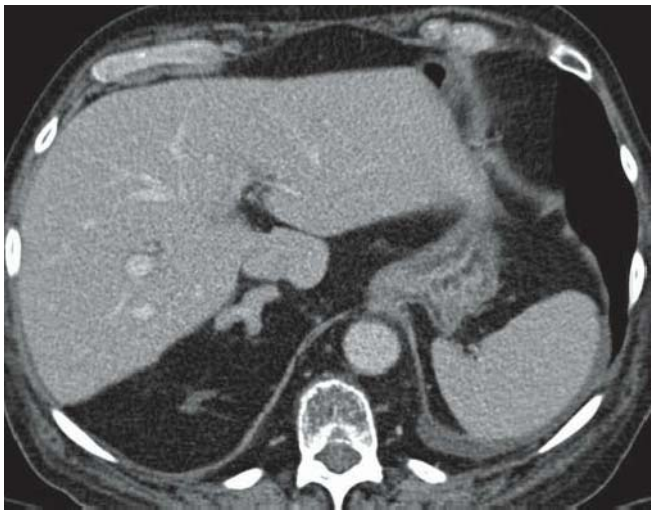

FIGURE 126B

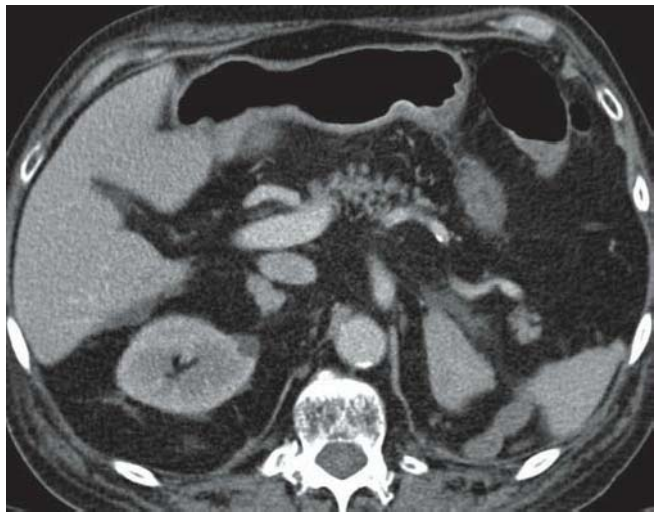

FIGURE 126D

FINDINGS Axial CECT images (A–D) demonstrate smooth enlargement of both adrenal glands, with the left gland being greater than the right.

DIFFERENTIAL DIAGNOSIS Conn syndrome, hemorrhage, stress-induced adrenal hyperplasia, normal adrenal aging.

DIAGNOSIS Cushing syndrome due to adrenal hyperplasia.

DISCUSSION Cushing syndrome is caused by excess glucocorticoid production, either endogenous or exogenous. Seventy percent of cases are caused by overproduction of adrenocorticotropic hormone (ACTH) by a pituitary adenoma (Cushing disease) or ACTH-producing tumors (such as bronchial carcinoid and small-cell lung cancer). Benign functioning adenoma (20%) and adrenocortical carcinoma (10%) cause the remainder of cases. The enlarged limbs of the adrenal glands, due to overstimulation by ACTH, may be smooth or can become nodular. Conn syndrome, due to excess mineralocorticoid production, is caused by an adrenal adenoma in 70% of cases. However, some cases may be produced by adrenal hyperplasia. Other causes of adrenal hyperplasia may be stress related due to physiologic release of ACTH or related to the normal aging process of the adrenal glands. Adrenal hemorrhage can be bilateral, but usually causes a masslike lesion in the adrenal gland with surrounding fat stranding; both features were absent in the present case.

CASE 127

CLINICAL HISTORY *30-year-old woman being evaluated for renal transplantation.*

FIGURE 127A

FIGURE 127B

FIGURE 127C

FIGURE 127D

FINDINGS Axial NECT image (A) shows a left iliac fossa kidney. Axial CECT images (B and C) and coronal MIP image (D) obtained 2 years later demonstrate a 6.0 cm × 4.7 cm × 4.1 cm ovoid mass in the left lower quadrant with peripherally located coarse calcifications and central areas of fat attenuation. Note the absence of native kidneys in the upper abdomen.

DIFFERENTIAL DIAGNOSIS Sarcoma, pelvic kidney.

DIAGNOSIS Chronic renal transplantation rejection.

DISCUSSION Renal transplantation is the treatment of choice for patients with end-stage renal failure because survival is much longer than with peritoneal dialysis or hemodialysis. Transplanted kidneys are usually placed extraperitoneally in the right iliac fossa. Despite more effective immunosuppression, chronic rejection is the most common cause of late graft loss. It develops months to years

after transplantation surgery. In the early stage of chronic rejection, the graft is enlarged and has increased cortical thickness. Later, cortical thinning, mild hydronephrosis, atrophy, and cortical nephrocalcinosis develop. In this case, knowledge of the history of previous renal transplantation and identification of the absence of the native kidneys are keys to establish the correct diagnosis. Otherwise, the renal graft may be mistaken for a soft-tissue sarcoma, and the patient may be referred for a biopsy. The lateral orientation of the renal sinus in this case makes a congenitally ectopic kidney less likely. In the early embryology, the renal sinus faces anteriorly and progressively rotates medially as the kidney ascends; it almost never faces laterally when the kidney remains in the pelvis.

CASE 128

CLINICAL HISTORY *21-year-old woman with chronic left upper abdominal pain.*

FIGURE 128A

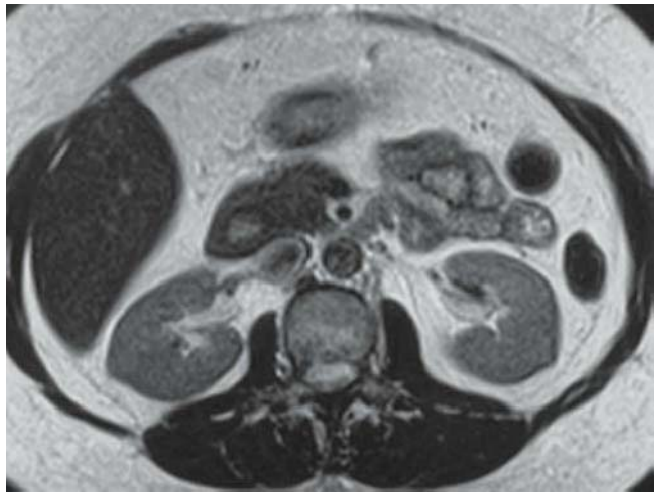

FIGURE 128C

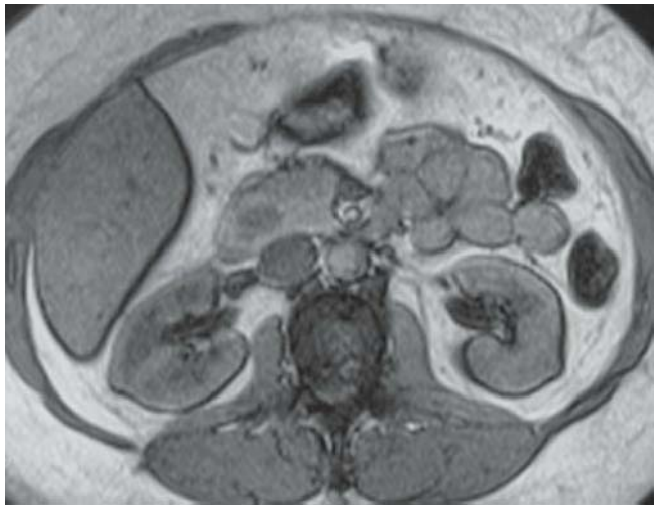

FIGURE 128B

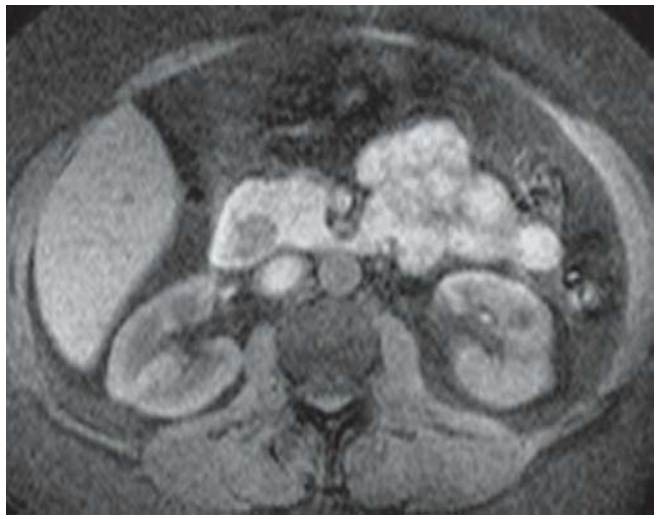

FIGURE 128D

FINDINGS Axial CECT image (A) shows a round low-density lesion within the pancreatic head. The duodenum is not visualized. Axial T1-WI (B), T2-WI (C), and fat-saturated T1-WI show that the tissue surrounding the cystic lesion follows the signal intensity of normal pancreatic parenchyma.

DIFFERENTIAL DIAGNOSIS Cystic pancreatic neoplasm, pseudocyst.

DIAGNOSIS Annular pancreas.

DISCUSSION Annular pancreas is a rare congenital anomaly in which incomplete rotation of the ventral anlage leads to a segment of the pancreas encircling the second part of the duodenum. The incidence of annular pancreas is 1 in 2,000, occurring as either an isolated finding or in association with other congenital abnormalities. In approximately half of symptomatic cases, annular pancreas will present in the neonate with gastrointestinal obstruction or bile duct obstruction possibly associated with pancreatitis. In the adult, it may manifest with symptoms of peptic ulcer disease, duodenal obstruction, or pancreatitis. In general, annular pancreas obstructs the duodenum in 10% of cases. There are two types of annular pancreas: extramural and intramural. In the extramural type, the ventral pancreatic duct runs around the duodenum to join the main pancreatic duct. In the intramural type, the pancreatic tissue is intermingled with muscle fibers in the duodenal wall, and small ducts drain directly into the duodenum. Annular pancreas can be diagnosed on the basis of CT and MR findings that reveal pancreatic tissue and an annular duct encircling the descending duodenum.

CASE 129

CLINICAL HISTORY *47-year-old man presenting with left flank pain.*

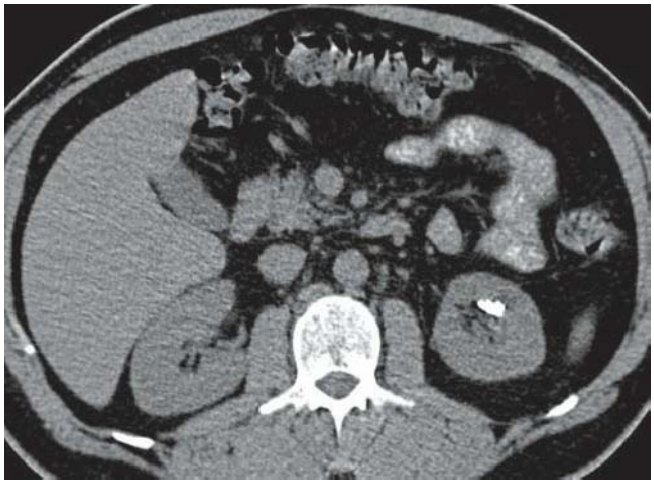

FIGURE 129A

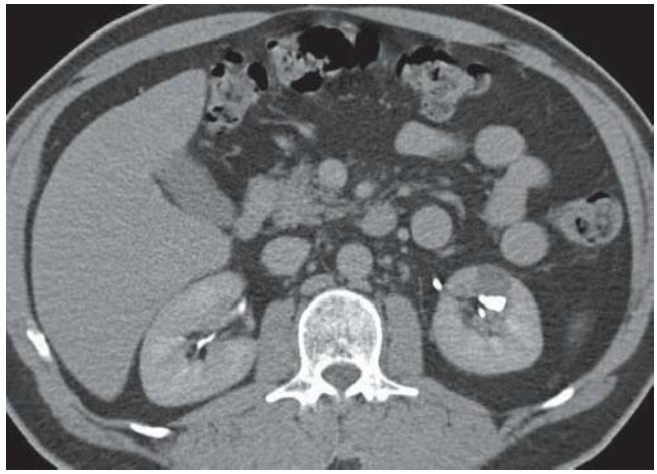

FIGURE 129C

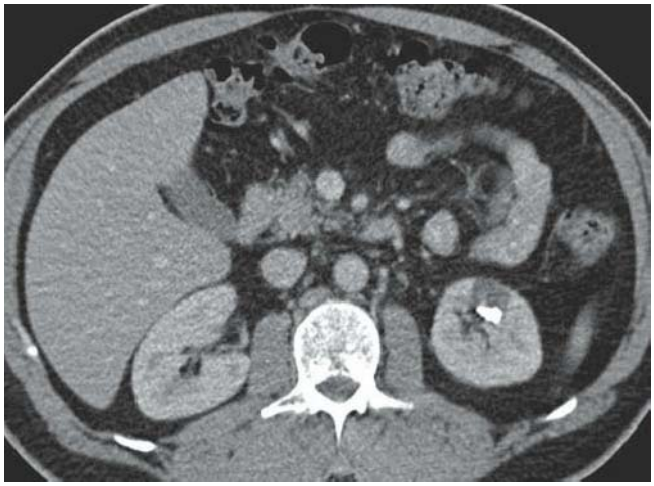

FIGURE 129B

FIGURE 129D

FINDINGS Axial NECT image (A) and CECT images in the nephrographic (B) and excretory (C) phases demonstrate a 1.9 cm × 2.1 cm cystic lesion in the left upper pole renal parenchyma. Dependent stones are present within the lesion. Axial CECT image in the excretory phase (D), which was obtained with the patient in the prone position, shows filling of the cystic lesion by excreted contrast. The stones fall dependently.

DIFFERENTIAL DIAGNOSIS Renal cyst, cystic renal cell carcinoma.

DIAGNOSIS Calyceal diverticulum.

DISCUSSION Calyceal diverticulum is a urine-filled cystic lesion within the renal parenchyma. It is most often congenital, but a lesion of similar appearance may occur after infection when a communication between the pyelocalyceal system and an abscess cavity persists or because of focal calyceal dilatation due to scarring. Two types of diverticula have been described; type I, which is the most common one, communicates with a minor calyx, whereas type II communicates directly with the renal pelvis or a major calyx. Up to 39% of diverticula contain layering stones or milk of calcium secondary to urine stasis because of a narrow diverticular neck. By CECT, the diverticular lumen gradually fills with excreted contrast, with the density within the lumen increasing with time; this should not be misinterpreted as enhancement of a solid lesion. As in this case, positional changes of the patient may be necessary to demonstrate a communication between the diverticulum and the collecting system. Because no solid enhancing component was present in this lesion, a renal cell carcinoma was excluded. Both renal cell carcinomas and renal cysts do not communicate with the pyelocalyceal system.

CASE 130

CLINICAL HISTORY *34-year-old woman presenting with left lower quadrant pain.*

FIGURE 130A

FIGURE 130C

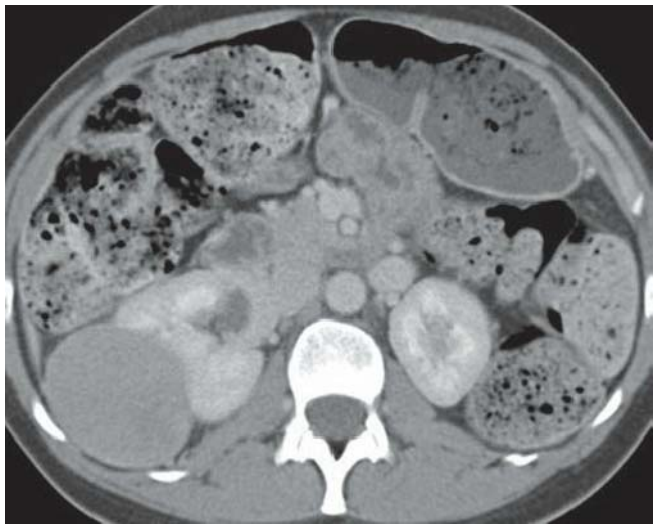

FIGURE 130B

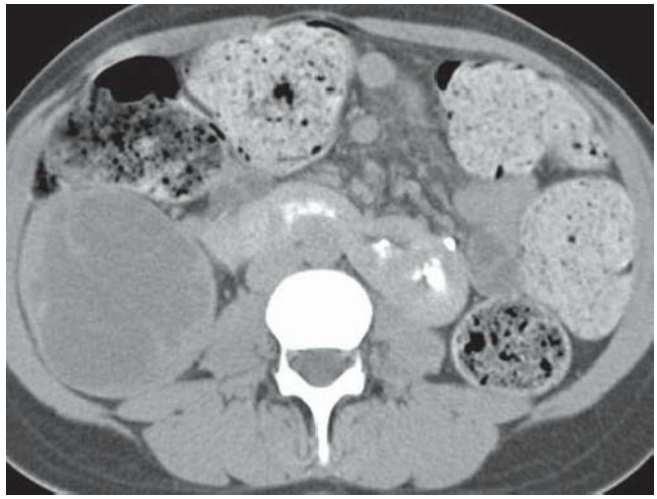

FIGURE 130D

FINDINGS Coronal reformatted CECT image in the corticomedullary phase (A) and axial CECT images in the nephrographic (B and C) and excretory (D) phases demonstrate a 12 cm × 5.7 cm × 6.2 cm, bilobed, exophytic right renal mass. The cranial solid component shows enhancement, and the caudal component is cystic with thick enhancing wall and septations. Note the fusion of the lower renal poles at the midline.

DIFFERENTIAL DIAGNOSIS Renal cell carcinoma, lymphoma, metastasis, oncocytoma.

DIAGNOSIS Primary renal carcinoid in a horseshoe kidney.

DISCUSSION During normal embryology, the kidneys develop anterior to the sacrum and then progressively ascend to reach their adult position. If the metanephric buds fuse early during development, usually at the lower poles, a horseshoe kidney will form, and the ascent will be blocked by the root of the inferior mesenteric artery. Horseshoe kidneys occur 1 to 4 times per every 1,000 births and are associated with vesicoureteral reflux and ureteropelvic junction obstruction. Primary carcinoid tumors of the kidney are extremely rare neoplasms; only approximately 30 cases have been reported in the English literature. They occur between 60 and 85 times more commonly in horseshoe kidneys than in normal kidneys. They occur in patients in the second to seventh decades of life. Renal carcinoids may be solid or cystic in appearance. An interestingly described appearance is that of a bilobed mass, with one component being solid and the other one cystic, as seen in this case. Preoperative diagnosis is usually not made because most solid renal masses are presumed to be renal cell carcinomas until proven otherwise. Metastasis would be unlikely in the absence of a known primary tumor. Renal lymphoma presents as a mass of homogeneous soft tissue density. Oncocytomas, when large, may have a classic appearance of a homogeneous mass, occasionally with a central stellate scar.

CASE 131

CLINICAL HISTORY *47-year-old woman who underwent treatment for a renal mass.*

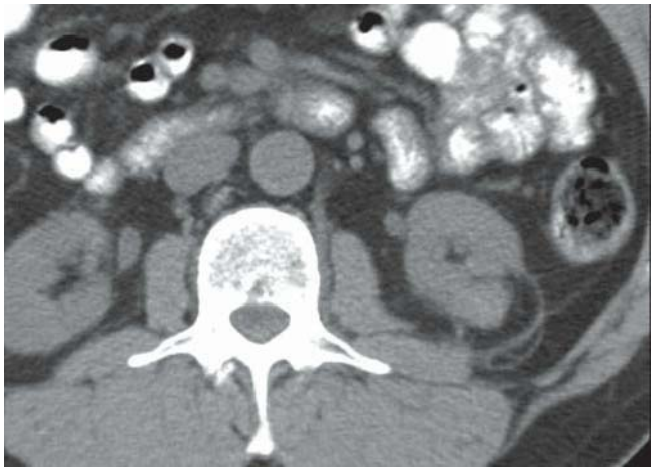

FIGURE 131A

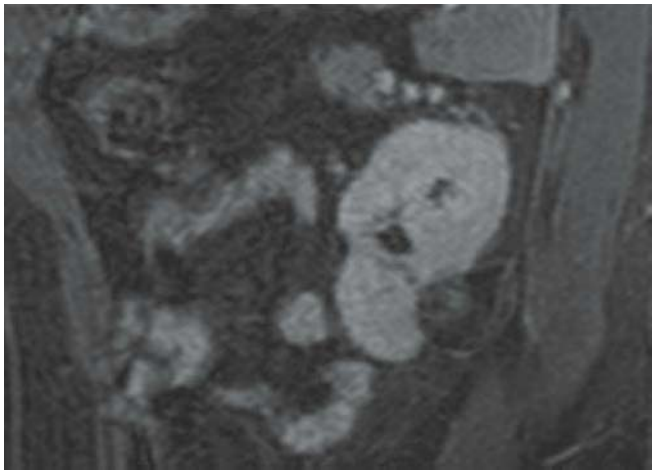

FIGURE 131C

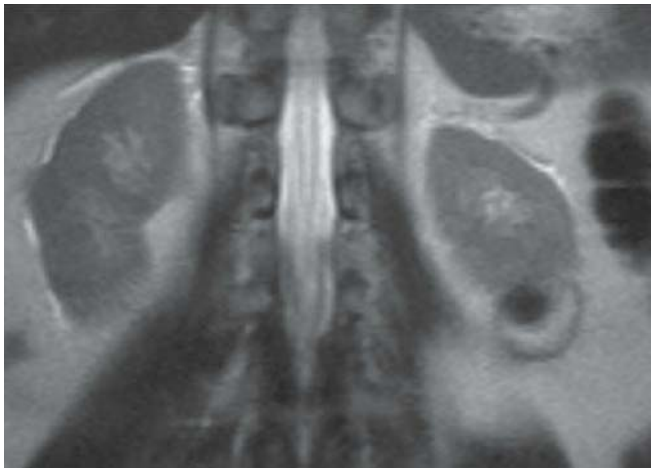

FIGURE 131B

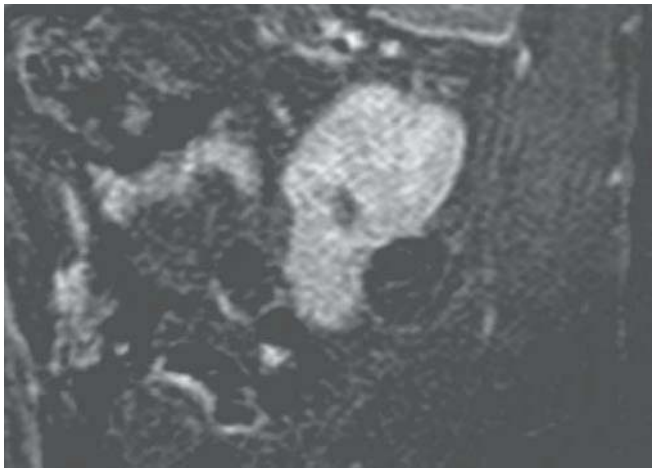

FIGURE 131D

FINDINGS Axial NECT image (A) shows a 2-cm hyperdense renal lesion in the lower pole of the left kidney. The lesion is hypointense on the coronal T2-WI (B). On the gadolinium-enhanced, fat-suppressed sagittal T1-WI (C), internal hyperintensity is present, but the area is almost entirely hypointense on the subtraction sagittal post-contrast image (D). Perinephric fat surrounding the mass is seen, bordered by a thin non-enhancing rim.

DIFFERENTIAL DIAGNOSIS Angiomyolipoma.

DIAGNOSIS Cryoablated renal cell carcinoma.

DISCUSSION Numerous small solid renal masses are now discovered incidentally. This has led to advances in minimally invasive treatment techniques. Thermal ablation of small renal tumors can be performed using either radiofrequency ablation or cryoablation. This renal mass was biopsied prior to cryoablation and was proven to be a renal cell carcinoma. Follow-up imaging studies are performed to document regression of the tumor and also absence of residual or recurrent enhancement in the lesion. Portions of the renal parenchyma are usually included in the ablation zone to ensure the tumor has been entirely covered. The ablation zone also usually extends, as in this case, into the perinephric fat. The border of the ablation zone is delimited by a thin non-enhancing rim seen in the perinephric fat, as seen on the post-treatment images. Knowledge of the prior cryoablation of a renal cancer is critical to avoid interpreting the rim in the perinephric fat as the border of a fat-containing lesion, and therefore, wrongfully diagnose an angiomyolipoma. Subtraction post-gadolinium images are very helpful in assessing any nodular internal enhancement suspicious for residual or recurrent tumor, as spontaneous hyperintensity may be present in the ablation zone due to coagulation necrosis.

CASE 132

CLINICAL HISTORY *31-year-old man presenting with acute epigastric pain.*

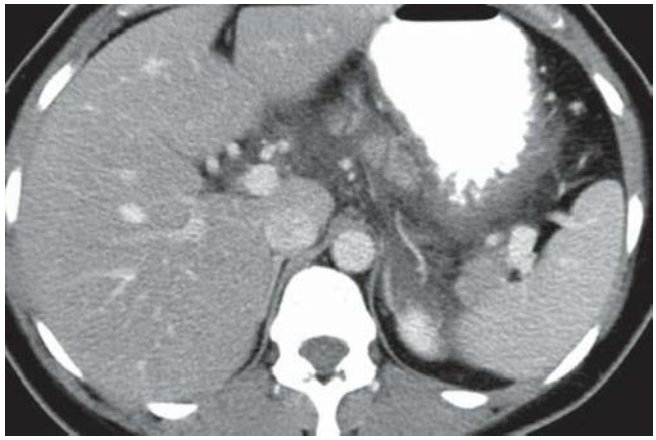

FIGURE 132A

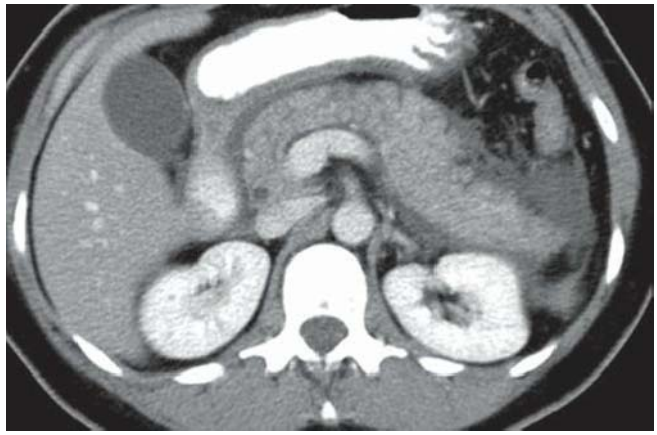

FIGURE 132C

FIGURE 132B

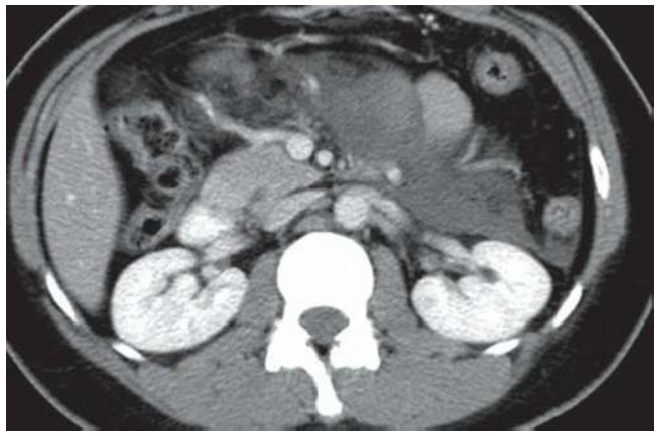

FIGURE 132D

FINDINGS Axial CECT images (A–D) demonstrate extensive peripancreatic inflammation and fluid tracing to the left anterior pararenal space. The fluid extends down into the transverse mesocolon and mesenteric root. Note that the pancreas appears edematous but there are no areas of pancreatic necrosis.

DIFFERENTIAL DIAGNOSIS None.

DIAGNOSIS Acute interstitial pancreatitis.

DISCUSSION This case demonstrates the extra-peritoneal spaces. The pancreas is located within the anterior pararenal space just anterior to Gerota fascia, which separates it from the perirenal space that contains the kidney. Fluid and inflammation from pancreatitis will pool within the anterior pararenal space and frequently spare the kidney and the perirenal space, as is seen in this case. Fluid can also accumulate in the posterior pararenal space, which is not contiguous with the anterior pararenal space at this level. Fat and the lateroconal fascia separate them from each other. The three spaces, anterior and posterior pararenal spaces and perirenal space, communicate in the infrarenal space. This anatomy is important to understand because it helps define the source of an abnormality in the retroperitoneum.

CASE 133

CLINICAL HISTORY *53-year-old man presenting with epigastric malaise.*

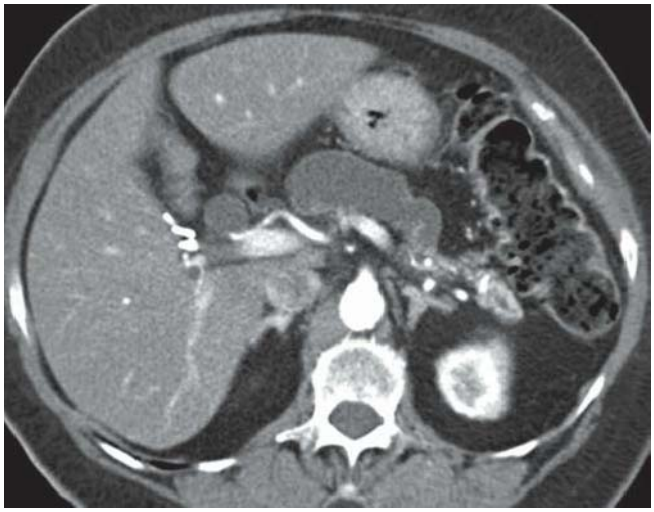

FIGURE 133A

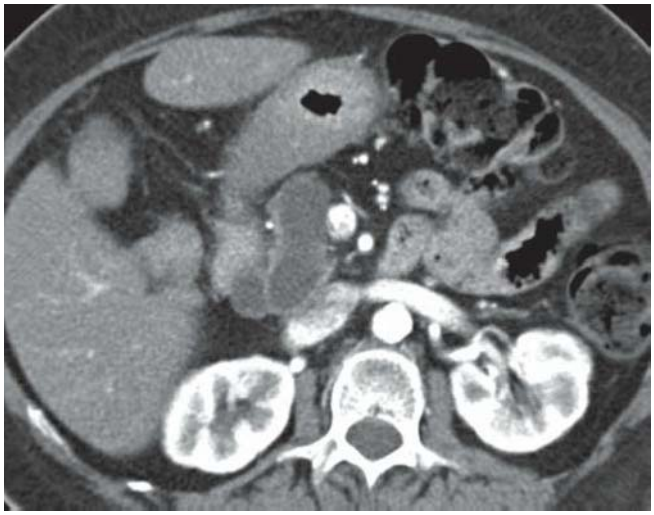

FIGURE 133B

FIGURE 133C

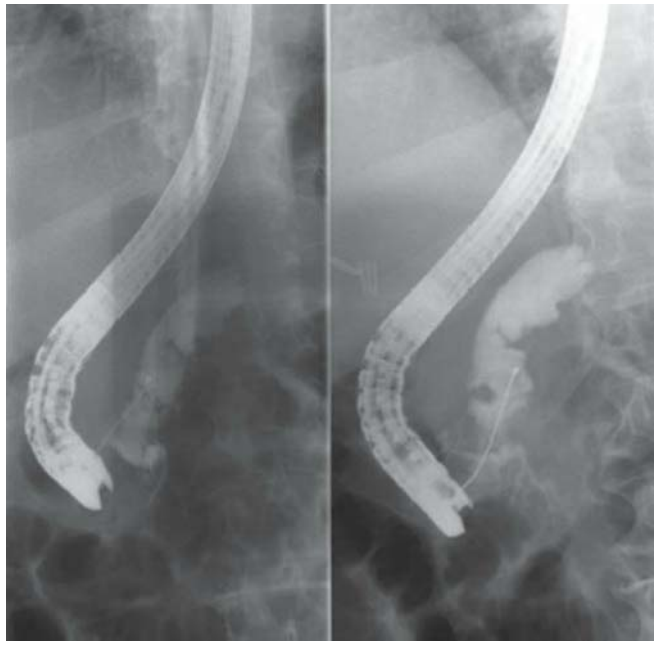

FIGURE 133D

FINDINGS Axial CECT (A and B) and curved reformatted (C) images demonstrate a dilated pancreatic duct extending to the papilla. Note the severe atrophy of the pancreatic parenchyma. No obstructing pancreatic mass is identified. ERCP image (D) confirms the dilatation of the pancreatic duct, and shows wall irregularity and nodularity.

DIFFERENTIAL DIAGNOSIS Chronic pancreatitis, ampullary carcinoma.

DIAGNOSIS Main-duct intraductal papillary mucinous neoplasm (IPMN).

DISCUSSION Intraductal papillary mucinous neoplasm (IPMN) is a mucin-producing neoplasm that can involve the main duct, a side branch, or both. Side-branch IPMN is characterized by grapelike cystic dilatation of a side branch of the pancreatic duct predominantly affecting the uncinate process. An identifiable associated soft tissue mass is rarely seen by CT as side-branch IPMN tend to be more likely benign. In patients with main or combined duct IPMN, often the only finding is dilatation of the pancreatic duct and small cysts that communicate with the main duct. Presence of papillary projections, soft tissue masses, ductal dilatation

more than 1 cm, bulging papilla, and calcifications have all been associated with an increased risk of malignancy. In this patient, without a history of alcohol ingestion and episodes of recurrent pancreatitis, chronic pancreatitis would be unlikely. Nevertheless, patients with main-duct IPMN develop chronic obstructive pancreatitis, with calcification formation in the tail, as seen in this case. An ampullary carcinoma can cause dilatation of the pancreatic duct but it is usually associated with dilatation of the common bile duct as well.

CASE 134

CLINICAL HISTORY *74-year-old woman with a history of chronic myelogenous leukemia presenting with septic shock.*

FIGURE 134A

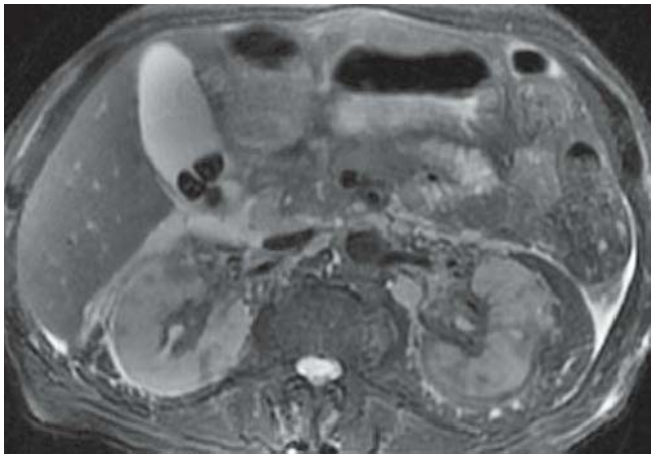

FIGURE 134B

FIGURE 134C

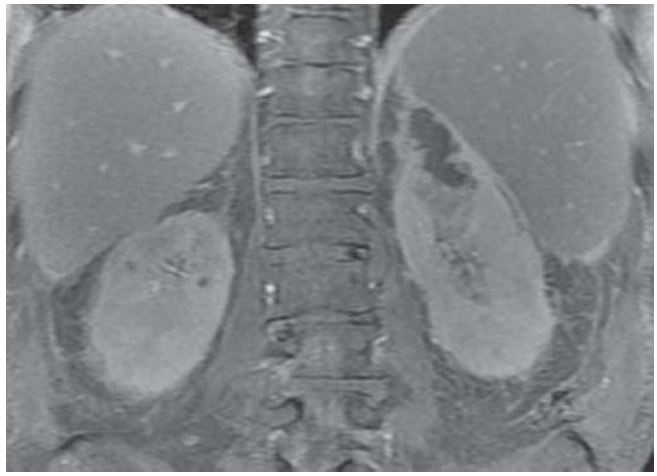

FIGURE 134D

FINDINGS Coronal T2-WI (A) demonstrates a 2.8 cm × 4.8 cm × 3.4 cm, exophytic, left upper pole, hyperintense, thick-walled lesion. Fat-suppressed axial T2-WI (B) shows wedge-shaped areas of decreased signal intensity. Gadolinium-enhanced, fat-suppressed axial (C) and coronal (D) T1-WIs show enhancement of the irregular wall of the left upper pole cystic lesion and wedge-shaped areas of decreased enhancement of the renal parenchyma. Note left interpolar renal scarring, cholelithiasis, and para-aortic lymph node.

DIFFERENTIAL DIAGNOSIS Renal cell carcinoma, necrotic metastasis, leukemic infiltration.

DIAGNOSIS Renal abscess complicating pyelonephritis.

DISCUSSION Renal abscesses are commonly the result of obstruction from calculi, tumors, or strictures, resulting in an ascending infection. Hematogenous spread can also occur from infection of the skin or endocarditis, as seen in intravenous drug abusers, which result in microabscesses that can coalesce and form a large abscess. The most common infecting organisms are *Escherichia coli* and *Proteus mirabilis*. Renal abscesses can be single or multiple. Multiple abscesses are more commonly due to hematogenous spread. By CT or MRI, the lesion is typically of fluid attenuation (10 to 20 HU) or signal intensity with a thick wall that can demonstrate enhancement. There can be spread of inflammation outside the kidney, with thickening of Gerota fascia. The presence of air within the fluid is pathognomonic of a renal abscess. The wedge-shaped areas present in the kidneys, as seen in this case, suggest pyelonephritis, although renal leukemic infiltration may present similarly. A simple cyst would not have a thick wall or fluid of high attenuation. The appearance of this lesion is indistinguishable from a cystic renal cell carcinoma, although a neoplasm was excluded by observing resolution on subsequent imaging. Clinical symptoms can usually help differentiate the two entities, as in this case.

Case images courtesy of Dr. Caroline Reinhold, McGill University Health Center, Montreal, Canada.

CASE 135

CLINICAL HISTORY *43-year-old woman treated for metastatic breast cancer.*

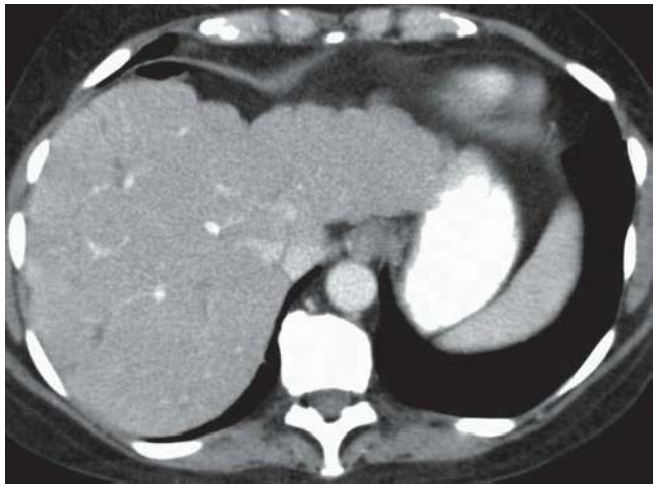

FIGURE 135A

FIGURE 135C

FIGURE 135B

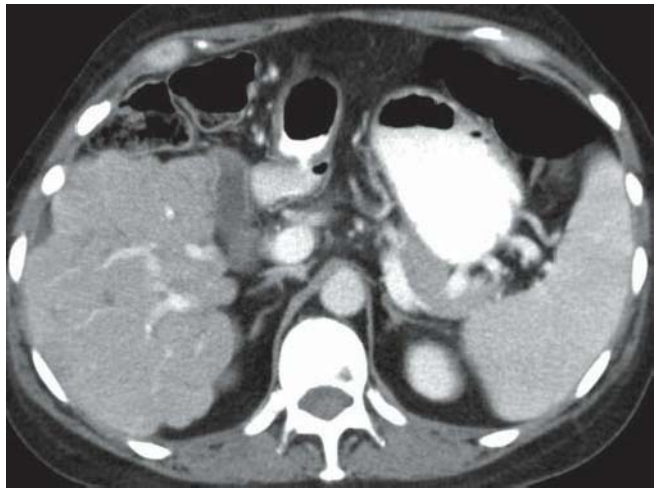

FIGURE 135D

FINDINGS Axial CECT images demonstrate several small low-density lesions in the liver and a nodular contour of the liver due to hepatic capsular retraction.

DIFFERENTIAL DIAGNOSIS Cirrhosis.

DIAGNOSIS Pseudocirrhosis in metastatic breast cancer.

DISCUSSION In patients with hepatic metastases from breast cancer, hepatic capsular retraction occurs adjacent to subcapsular hepatic metastases and is typically seen after treatment with chemotherapy. Although this appearance mimics cirrhosis, most of these patients do not experience the sequelae of portal hypertension, such as variceal bleeding, ascites, and cytopenia. In fact, the pathogenesis of this pseudocirrhotic appearance is not clearly understood; it may result from hepatic infiltration by the metastatic tumor and/or hepatotoxic effects of chemotherapy. Since cirrhosis and pseudocirrhosis due to diffuse metastatic disease of the liver require different clinical management strategies, it is crucial to correlate imaging findings with clinical history to reach an accurate diagnosis.

CASE 136

CLINICAL HISTORY *34-year-old woman presenting with left flank pain.*

FIGURE 136A

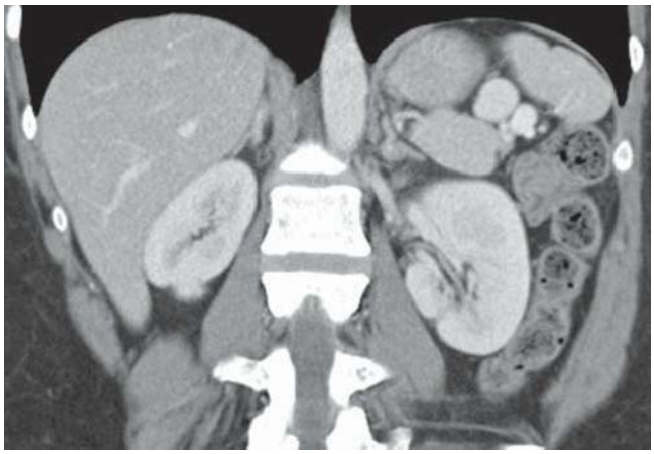

FIGURE 136B

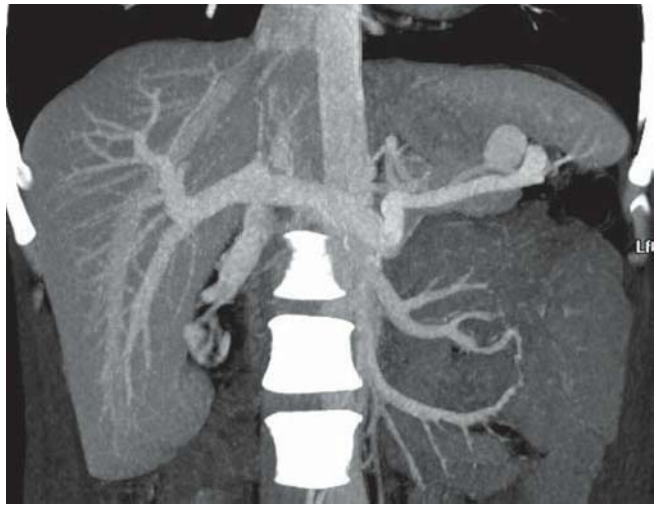

FIGURE 136C

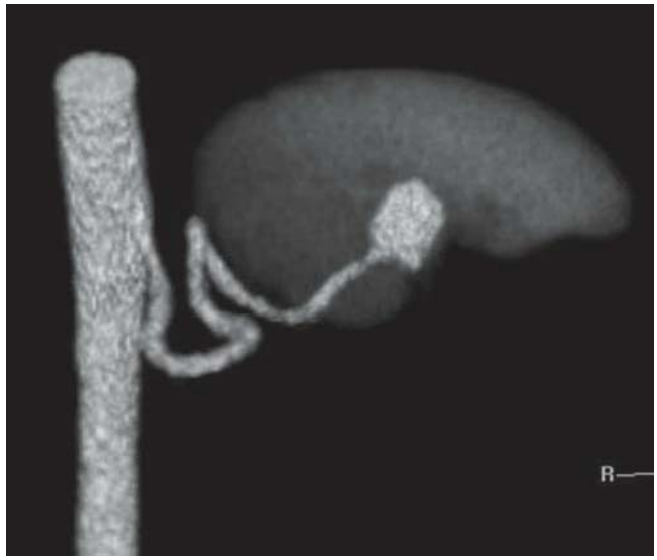

FIGURE 136D

FINDINGS Axial (A) and coronal (B) CECT images show an enhancing nodule, isodense to the aorta, in the splenic hilum. Coronal maximum-intensity projection (C) and three-dimensional, volume-rendered (D) images show that the nodule connects to the splenic artery.

DIFFERENTIAL DIAGNOSIS None.

DIAGNOSIS Splenic artery aneurysm.

DISCUSSION Splenic artery aneurysm is the most common abdominal visceral artery aneurysm, representing approximately 60% of visceral arterial aneurysms. Various causes and predisposing conditions may lead to splenic artery aneurysm, including portal hypertension, pregnancy and history of multiparity, pancreatitis, arteriosclerotic disease, penetrating gastric ulcer, trauma, and vasculitis. Splenic aneurysms are most often saccular, and over 75% occur at the distal third of the splenic artery. They are multiple in 20% of cases and range in size from less than 1 to 3 cm. Splenic artery aneurysms are usually diagnosed by the presence of ring calcification in the left upper quadrant on plain film, CT, or US. On NECT, splenic aneurysm appears as a well-defined, low-density mass with or without calcifications; after intravenous contrast medium administration, marked and early arterial enhancement within the residual patent lumen may be demonstrated. On MRI, splenic aneurysm may demonstrate a well-defined ring of low signal intensity at the periphery, corresponding to the aneurysm wall, whereas the signal intensity within the aneurysm depends on the presence and the velocity of flowing blood and the presence and age of the thrombus. Fast-flowing blood within the patent lumen usually produces a signal void, which persists on all spin-echo sequences.

CASE 137

CLINICAL HISTORY *19-year-old man presenting with intermittent abdominal pain.*

FIGURE 137A

FIGURE 137C

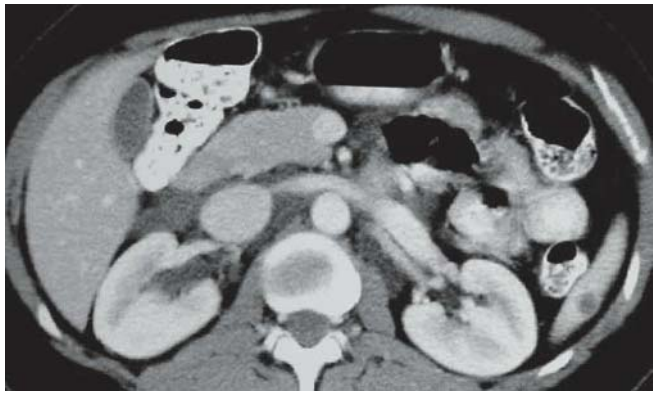

FIGURE 137B

FINDINGS Axial CECT images demonstrate an infiltrating retroperitoneal cystic lesion surrounding multiple vascular structures. Note small cystic lesion in the spleen.

DIFFERENTIAL DIAGNOSIS Cystic mesothelioma, pseudocyst, hematoma.

DIAGNOSIS Lymphangioma.

DISCUSSION Lymphangiomas are congenital benign neoplasms. They occur because of failure of several lymphatic channels to establish normal communication with the rest of the lymphatics. Lymphangiomas are more common in males than in females. The vast majority occur in the head and neck region; they occur rarely in the retroperitoneum. At imaging, they are multilocular cystic lesions with thin walls. They may cross between one retroperitoneal space to another, which is a characteristic finding. Other multilocular retroperitoneal cystic lesions include cystic mesotheliomas, pseudocysts, and hematomas. Cystic mesotheliomas are rare benign mesothelial tumors more commonly seen in females and more commonly occurring along peritoneal surfaces than in the retroperitoneum. Pseudocysts, which may be pancreatic or nonpancreatic, may be multilocular, but a clinical history of recent acute pancreatitis or infection is often present. A retroperitoneal hematoma starts liquefying soon after its development and may give rise to multifocal or multilocular cystic-appearing lesions.

CASE 138

CLINICAL HISTORY *3-month-old boy presenting with incidental liver lesions discovered on US done for pyelonephritis.*

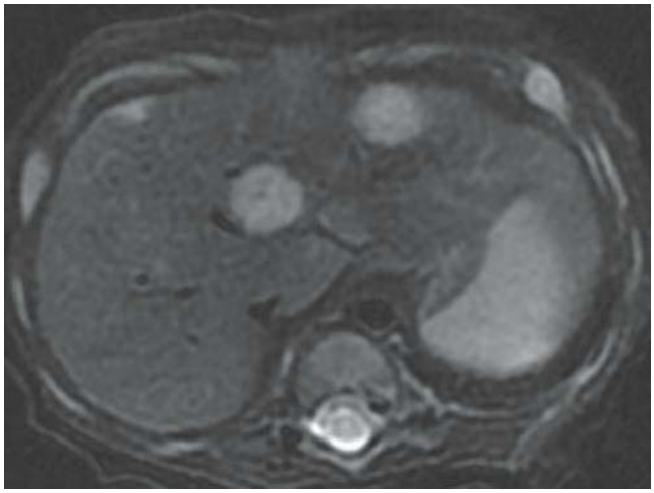

FIGURE 138A

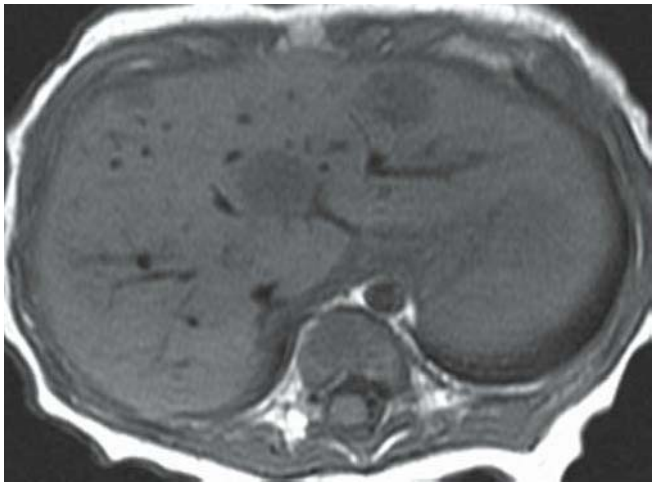

FIGURE 138C

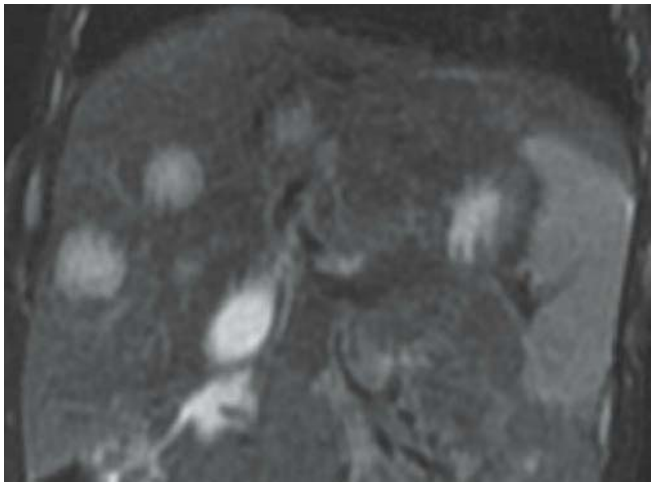

FIGURE 138B

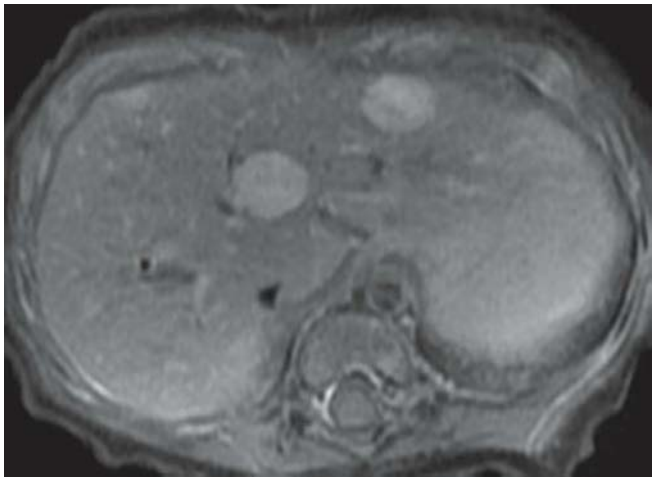

FIGURE 138D

FINDINGS Axial (A) and coronal (B) fat-suppressed T2-WIs show numerous well-defined homogeneous hyperintense lesions scattered throughout the liver. Axial pre-contrast (C) and fat-suppressed, gadolinium-enhanced T1-WIs (D) demonstrate homogeneous low signal and enhancement of the lesions on the portal venous phase, respectively.

DIFFERENTIAL DIAGNOSIS Hepatoblastoma, metastases, mesenchymal hamartoma.

DIAGNOSIS Infantile hemangioendotheliomas.

DISCUSSION Infantile hemangioendotheliomas are vascular tumors derived from endothelial cells. They are considered benign but can occasionally show aggressive features and distant metastasis. They become clinically evident when large due to platelet sequestration, congestive heart failure, and Kasabach-Merrit syndrome. Most occur in children younger than 6 months of age (90% less than 1 year); they tend to spontaneously regress after 18 months. Some have been reported to persist into adulthood. The lesions can range in size from a few millimeters up to 10 to 15 cm in size and are usually multiple. Calcifications, when they occur, tend to be fine and granular rather than coarse. Infantile hemangioendotheliomas tend to be intensely bright on T2-WI like hemangiomas. However, they can also be heterogeneous on both T1-WI and T2-WI due to the areas of hemorrhage, necrosis, and scarring. Their enhancement pattern is similar to that of cavernous hemangiomas. Mesenchymal hamartomas are typically not multiple, are diagnosed in older children, and rarely have a large solid component. The multiple lesions and absence of elevated alpha-fetoprotein make infantile hemangioendotheliomas the best diagnosis.

Case images courtesy of Dr. Christine Saint-Martin, Montreal Children's Hospital, Montreal, Canada.

CASE 139

CLINICAL HISTORY *66-year-old man with a history of longstanding Crohn disease presenting with abdominal pain.*

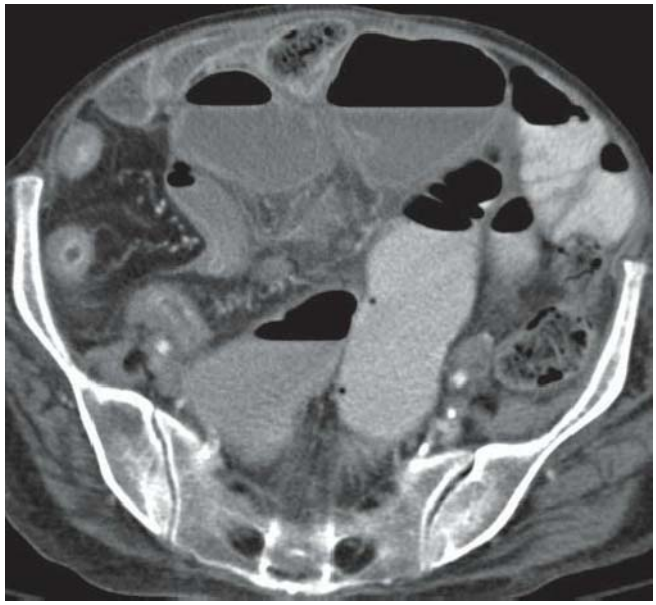

FIGURE 139A

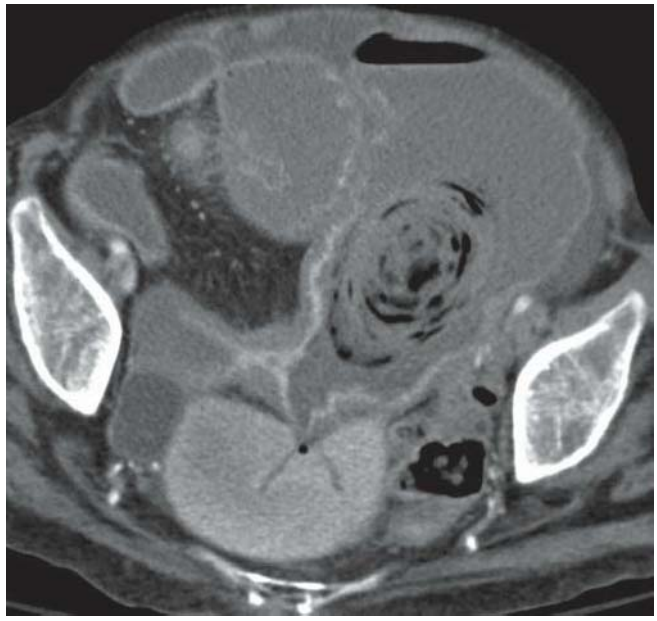

FIGURE 139C

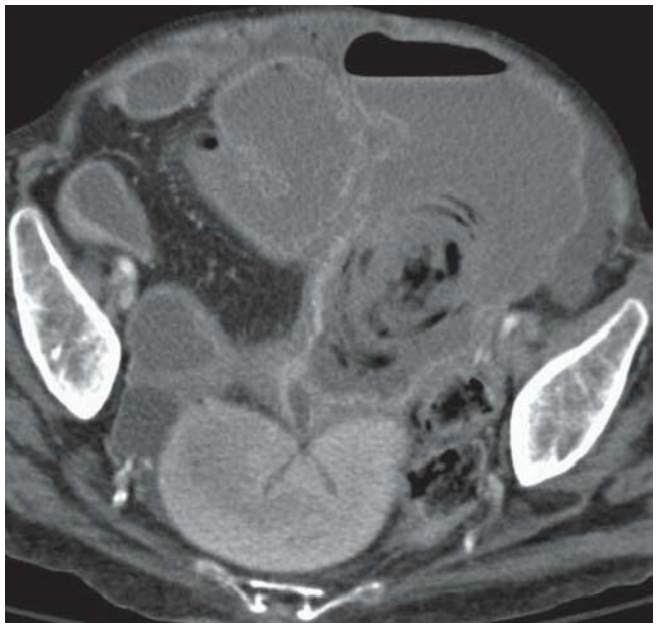

FIGURE 139B

FIGURE 139D

FINDINGS Axial CT images (A-D) obtained after oral administration of a neutral contrast agent show an alternating pattern of dilated and strictured small bowel segments. Sharply delineated areas of mucosal hyperenhancement are present. Also note the intraluminal mass in the mid-abdomen; the mass consists of concentric rings, of which some contain air. A small amount of ascites is seen.

DIFFERENTIAL DIAGNOSIS Radiation enteritis.

DIAGNOSIS Small bowel Crohn disease (acute or chronic) with bezoar formation.

DISCUSSION Crohn disease is an inflammatory condition of the bowel that affects approximately half a million patients in North America. Symptomatic patients with Crohn disease may be affected by active inflammatory disease or inactive chronic disease (e.g., fibrous stricture). CT findings of mural stratification, mucosal and mural hyperenhancement,

edema in the perienteric mesenteric fat, and engorged ileal vasa recta correlate with active inflammation. Submucosal fat deposition and mural thickening without enhancement or mural stratification typically correlate with fibrotic or quiescent disease. The sensitivity of CT for Crohn disease is estimated to be 71%, with lower detection of early mucosal disease. A bezoar is a ball of swallowed foreign material (usually hair or fiber) that collects in the intestines, especially the stomach. When a bezoar is composed of hair, it is referred to as a hairball or trichobezoar. When a bezoar is composed of vegetable materials, it is referred to as a phytobezoar or food ball. When a bezoar is composed of hair and food, it is referred to as a trichophytobezoar or hairy food ball.

CASE 140

CLINICAL HISTORY *77-year-old woman evaluated for systemic arteritis.*

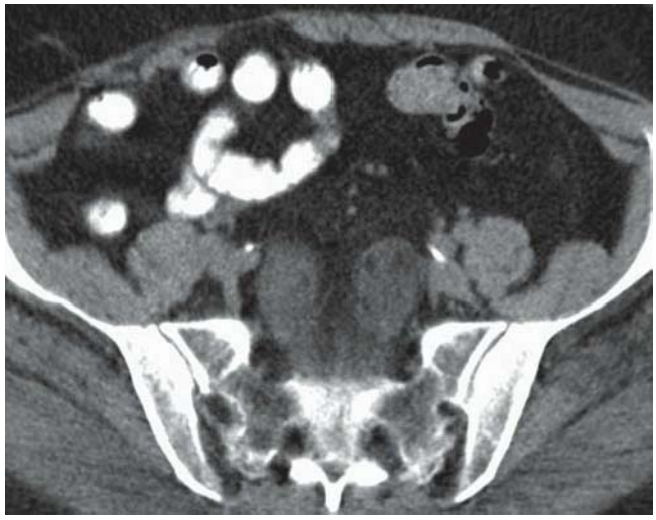

FIGURE 140A

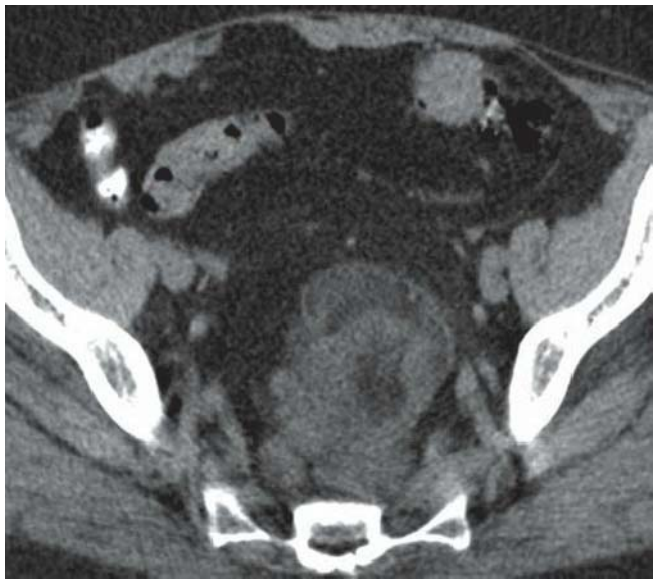

FIGURE 140B

FIGURE 140C

FIGURE 140D

FINDINGS Axial NECT images (A–D) demonstrate a large midline presacral mass containing fat and soft tissue density.

DIFFERENTIAL DIAGNOSIS Liposarcoma, teratoma, myelolipoma.

DIAGNOSIS Retroperitoneal extramedullary hematopoiesis.

DISCUSSION Extramedullary hematopoiesis (EMH) is a compensatory response for inadequate hematopoiesis by the bone marrow. It can be observed in congenital hemoglobinopathies or acquired marrow disorders, such as leukemia, lymphoma, carcinoma, and myelofibrosis; it is rarely idiopathic. EMH can develop in any tissue of mesenchymal origin. It most commonly occurs in the liver, spleen, and lymph nodes. Small EMH nodules can be encountered in the kidney or fat; larger masses occasionally occur in the pelvis or retroperitoneum. On CT, a solid, hyperdense, round, or lobulated, soft tissue mass is classically identified. Varying amounts of fat may also be present in the mass, and this may reflect fatty transformation due to disappearance of the factor promoting the EMH. Without a history of chronic anemia or bone marrow disease, it is difficult to differentiate EMH from a neoplasm, especially from liposarcoma or teratoma, when macroscopic fat is identified. The correct diagnosis can be made by image-guided percutaneous biopsy, as was performed in this case, or nuclear medicine sulfur colloid scan.

CASE 141

CLINICAL HISTORY *72-year-old man presenting with coronary artery disease.*

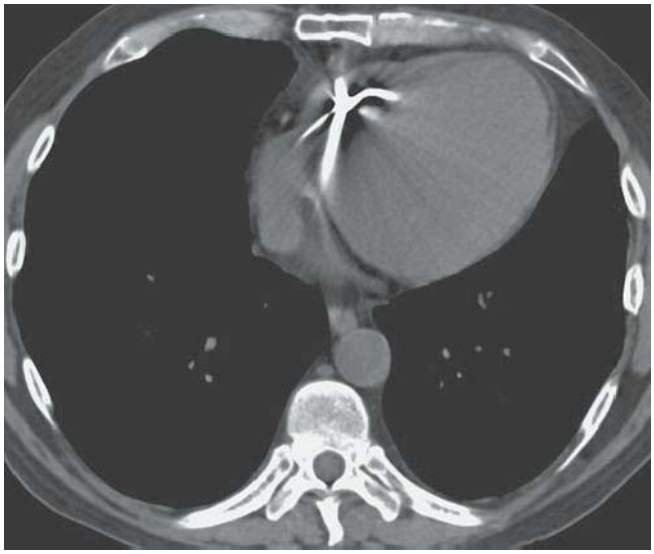

FIGURE 141A

FIGURE 141C

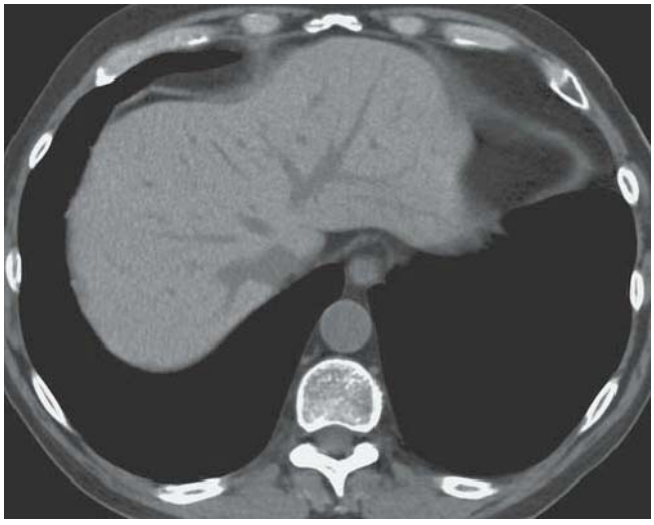

FIGURE 141B

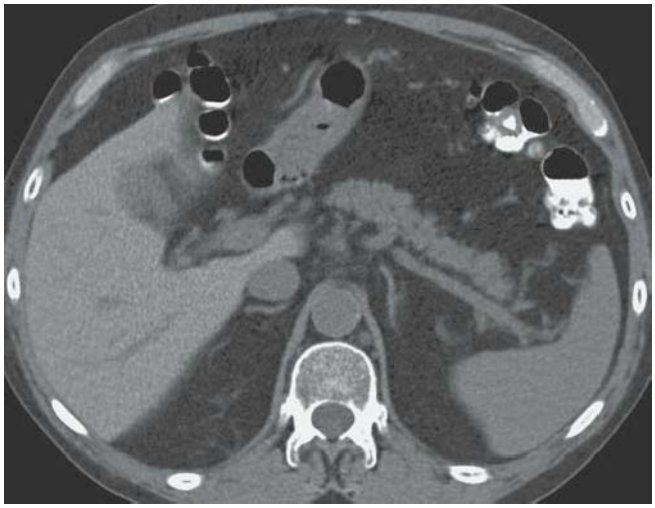

FIGURE 141D

FINDINGS Thoracic axial NECT image (A) demonstrates a cardiac pacemaker lead. On hepatic axial NECT images (B–D), the density of the liver is homogeneously increased.

DIFFERENTIAL DIAGNOSIS Primary hemochromatosis, Wilson disease, Thorotrast, methotrexate, gold.

DIAGNOSIS Hyperdense liver due to amiodarone.

DISCUSSION The normal liver attenuation on NECT is very similar to spleen, typically less than 10 HU more. Homogeneous increased density of the liver may be due to a variety of different causes, including drug toxicity, primary hemochromatosis, hemosiderosis, and cirrhosis. Pharmaceuticals that may cause an increase in liver density on CT include Thorotrast, thallium, gold, methotrexate, and amiodarone. Amiodarone is an antiarrhythmic drug with an iodine content of approximately 40%. During long-term therapy, both the drug and its major metabolite, desethylamiodarone, are deposited in the liver. The accumulation of iodine within the liver causes a homogeneous increased density of the organ on NECT images. Increased liver density may occur with therapeutic levels of the drug and does not necessarily correlate with amiodarone toxicity.

CASE 142

CLINICAL HISTORY *49-year-old woman presenting with diarrhea and a painless perianal mass.*

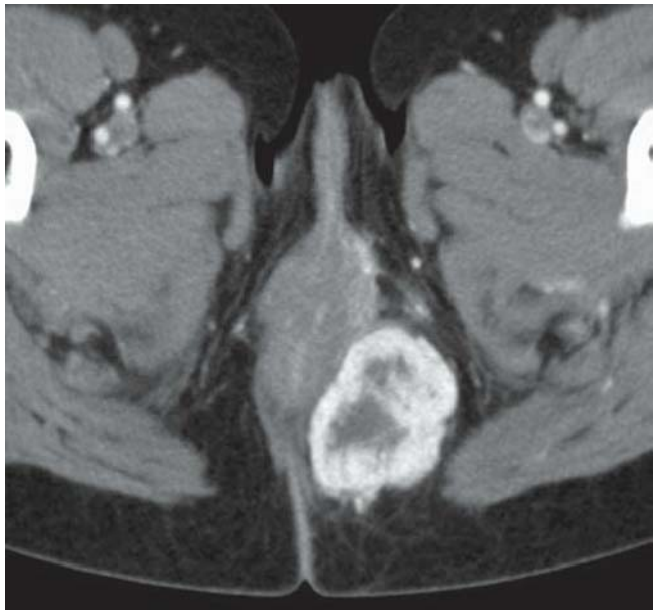

FIGURE 142A

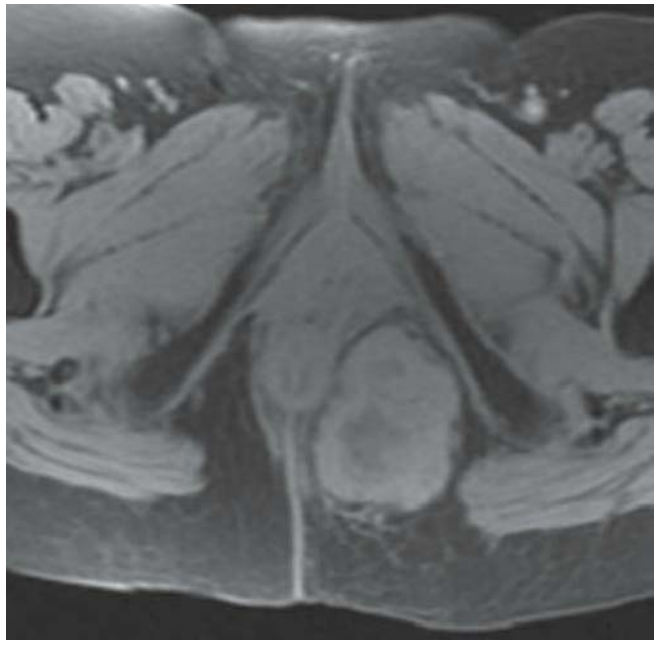

FIGURE 142C

FIGURE 142B

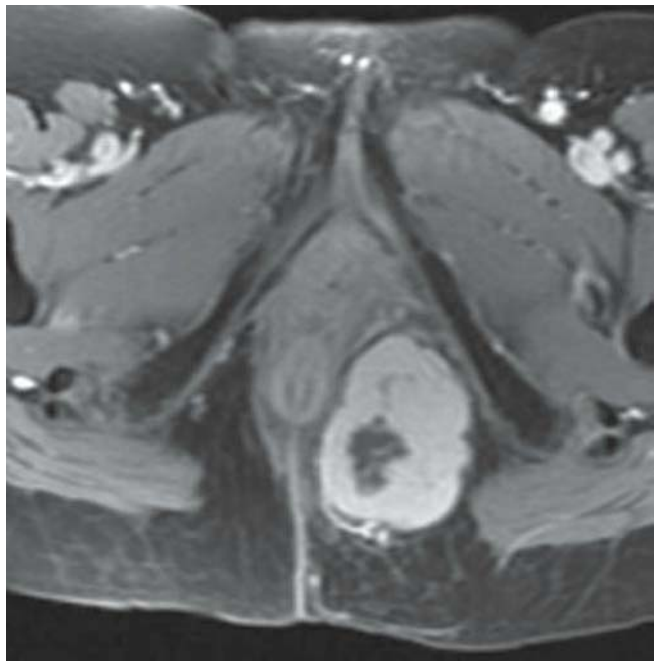

FIGURE 142D

FINDINGS Axial CECT image (A), coronal T2-WI (B), and unenhanced (C) and gadolinium-enhanced axial (D) fat-suppressed T1-WI demonstrate a heterogeneous hypervascular mass in the left ischioanal fossa, abutting and displacing the anal canal.

DIFFERENTIAL DIAGNOSIS Malignant fibrous histiocytoma, leiomyosarcoma, rhabdomyosarcoma, fibrous pseudotumor, hemangiopericytoma, aggressive fibromatosis, infectious/inflammatory process.

DIAGNOSIS Malignant solitary fibrous tumor.

DISCUSSION Soft tissue masses are difficult to classify on MRI. In 30% of cases, signal intensity characteristics represent important clues to the histologic origin of the tumor

(lipomas: homogeneous fat content; hemangiomas: central dot sign representing vessels, T2 hyperintensity). In addition, many malignant soft tissue tumors appear misleadingly benign; a well-defined lesion with an apparent capsule is not a reliable feature of a benign process. The most important role of imaging is to determine the exact localization, the size, and the extent of the lesion to guide further therapy. Furthermore, more than 50% of malignant soft tissue tumors recur locally. Local recurrences usually appear as hyperintense masses on T2-WI, and they typically enhance rapidly; fibrosis has a lower T2 signal and enhances in a more delayed fashion.

CASE 143

CLINICAL HISTORY *58-year-old woman presenting with history of breast cancer, screening for metastasis.*

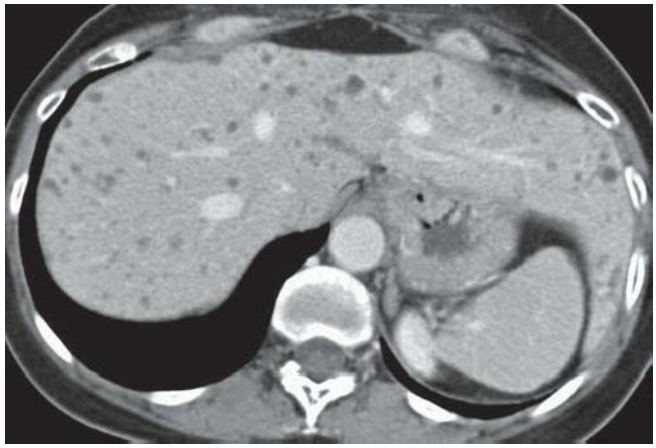

FIGURE 143A

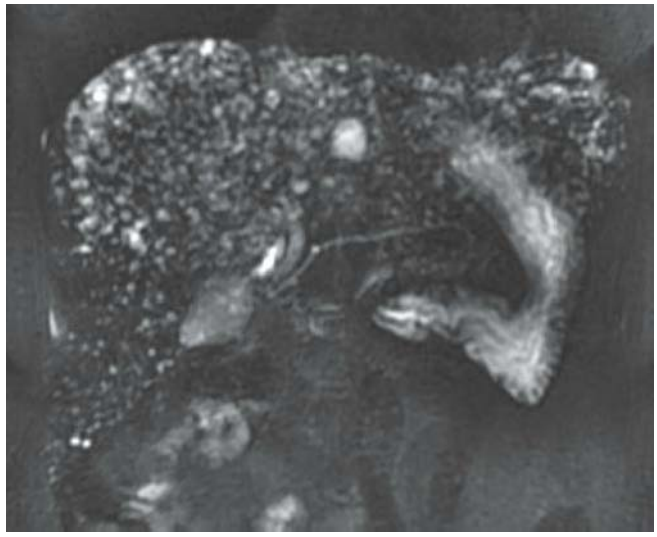

FIGURE 143C

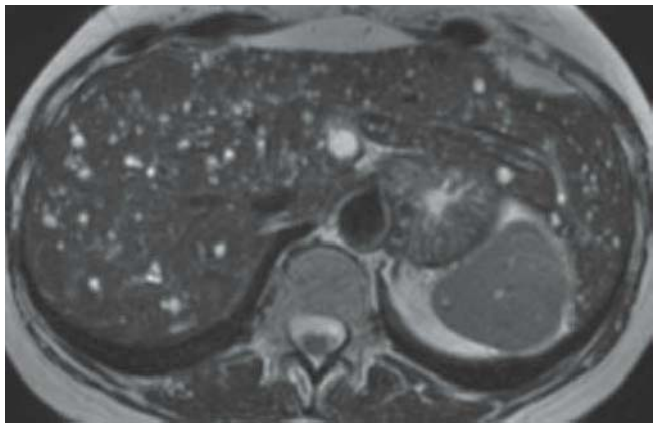

FIGURE 143B

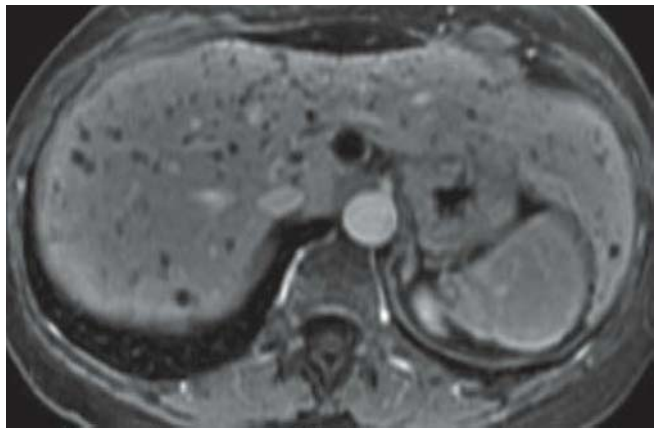

FIGURE 143D

FINDINGS Axial CECT image (A) demonstrates multiple, small, nonenhancing, low-density lesions throughout the liver. Axial T2-WI (B) and thick-slab coronal-oblique MRCP image (C) show the lesions to be markedly hyperintense. No enhancement is seen on the gadolinium-enhanced, fat-suppressed axial T1-WI (D).

DIFFERENTIAL DIAGNOSIS Metastases, infection (fungal), multiple bile duct cysts.

DIAGNOSIS Bile duct hamartomas.

DISCUSSION Bile duct hamartomas (von Meyenburg complexes) are dilated clusters of biliary ducts that are lined by a single layer of cuboidal epithelium within a fibrous stroma. These clusters are filled with proteinaceous material and biliary fluid. They can be single or multiple in their presentation. They are part of the spectrum of fibropolycystic hepatorenal diseases and are, therefore, sometimes associated with polycystic liver disease, polycystic kidney disease, congenital hepatic fibrosis, and Caroli disease. As is seen in this case, the lesions are usually small (<1 to 1.5 cm) and have low attenuation. Typically, they are adjacent to the portal area or subcapsular in location. Because of their fluid content, they are markedly hyperintense on T2-WI. They are typically more irregular in shape than bile duct cysts. Unlike Caroli disease, the cysts do not communicate with the biliary tree. Because they can be multiple, they can be confused with metastatic disease or disseminated infections; however, the latter typically demonstrate peripheral enhancement on postcontrast CT and MRI.

CASE 144

CLINICAL HISTORY *26-year-old woman presenting with hypoglycemia.*

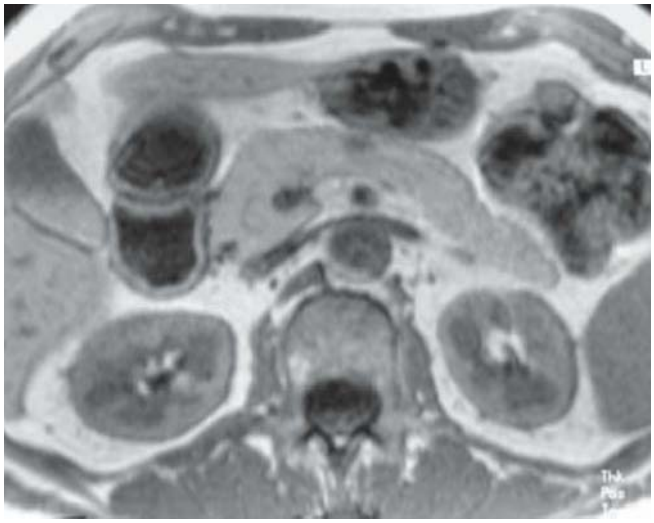

FIGURE 144A

FIGURE 144C

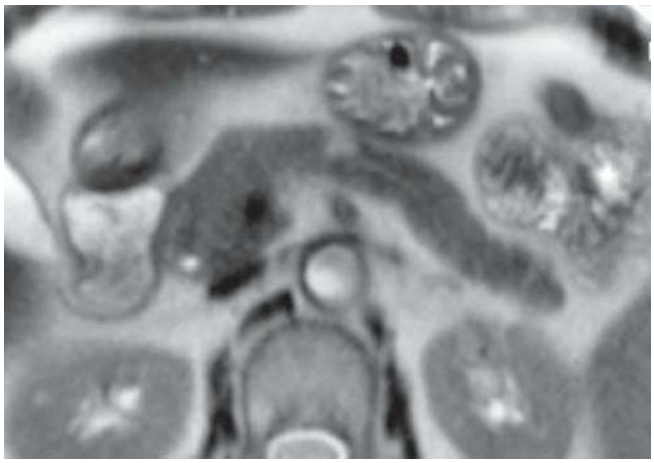

FIGURE 144B

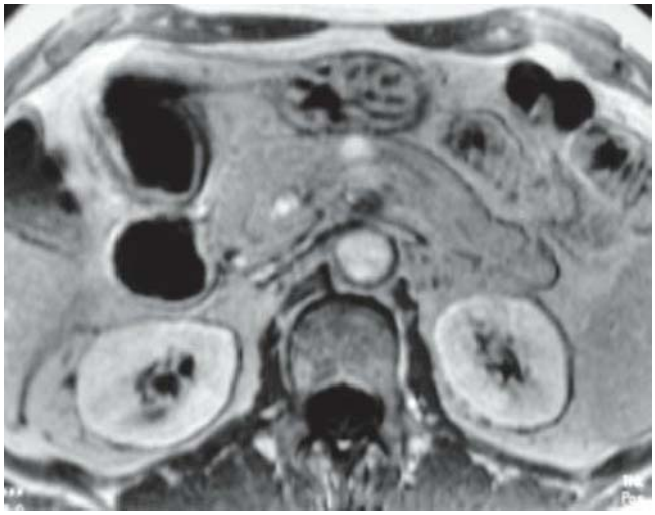

FIGURE 144D

FINDINGS Axial T1-WI (A) and T2-WI (B) demonstrate a small lesion in the pancreatic body that is hypointense and markedly hyperintense, respectively. Projective coronal oblique thick-slab MRCP image (C) shows the lesion as hyperintense, and no obvious connection with the pancreatic duct is identified. Axial gadolinium-enhanced T1-WI (D) shows marked homogeneous enhancement of the lesion.

DIFFERENTIAL DIAGNOSIS Solid and papillary epithelial tumor.

DIAGNOSIS Insulinoma.

DISCUSSION Insulinoma is the most common endocrine tumor of the pancreas (~60%), but only 5% to 10% are malignant. The Whipple triad (starvation attack, hypoglycemia after a fasting period, and relief by intravenous dextrose) is typically associated with the clinical onset of an insulinoma. At the time of diagnosis, 50% of the tumors are smaller than 1.5 cm. Malignant insulinomas present with a larger diameter (mean diameter, 6.2 cm). In only 5% to 10% of cases, multiple insulinomas are found, and there is a slightly higher incidence for the body and tail. On multiphasic CECT, insulinomas present as hypervascularized lesions that are best seen in the early phases of pancreatic enhancement. The most striking evidence for malignancy is evidence of metastatic disease of the liver or local lymph nodes. On MRI, insulinomas appear as lesions with low signal intensity on T1-WI and as lesions with high signal intensity on T2-WI. Fat-suppression sequences are useful in emphasizing the signal intensity differences between tumor and normal pancreatic tissue. The use of intravenous gadolinium chelates is helpful in the detection of endocrine tumors because these tumors are hypervascularized.

CASE 145

CLINICAL HISTORY *44-year-old man with a history of pneumonia that did not respond to typical antibiotics now presents with abdominal pain and diarrhea.*

FIGURE 145A

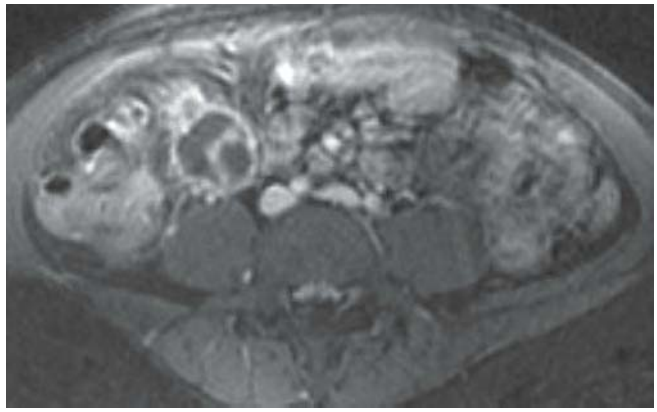

FIGURE 145C

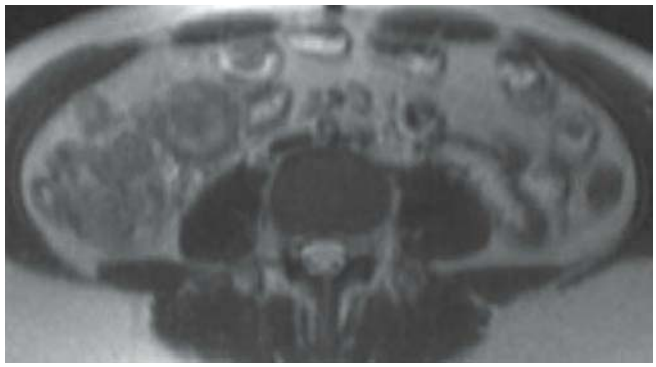

FIGURE 145B

FINDINGS Axial CECT image (A) shows asymmetrical thickening of the cecal wall and pericolonic lymphadenopathy. Axial T2-WI (B) shows the intermediate signal of the wall thickening and a large sentinel lymph node. Gadolinium-enhanced, fat-suppressed axial T1-WI (C) shows enhancement of the cecal wall and necrosis of the sentinel lymph node.

DIFFERENTIAL DIAGNOSIS Crohn colitis, lymphoma, amebiasis, *Yersinia* infection, ischemic colitis.

DIAGNOSIS Tuberculosis of the cecum.

DISCUSSION Intestinal tuberculosis is thought to be due to hematogenous spread, swallowing of infected sputum, or infected cow's milk. Typically, GI tract tuberculosis is associated with pulmonary tuberculosis, and an abnormal radiograph or positive sputum stain and cultures can suggest diagnosis. However, positive chest film findings are present in only 50% of cases of GI tract tuberculosis. The findings of tuberculosis are similar to those seen in Crohn disease, and tuberculosis should be considered when Crohn disease is a potential diagnosis. Early in the disease, there is thickening and nodularity of the mucosa, which involves the cecum more than the terminal ileum. Ulcers form, which usually heal by fibrosis, eventually causing strictures. The cecum can become rigid from the inflammation and scarring and appear cone shaped. This can simulate a carcinoma. Several pathologic processes involve both the terminal ileum and the cecum. Crohn colitis is the most common, but other entities, such as *Yersinia* colitis, amebiasis, and ischemia, can have this appearance as well. The segmental involvement of the cecum and the coexistence of a necrotic lymph node in a patient with antibiotic-resistant pneumonia make tuberculosis the best diagnosis in this case.

Case images courtesy of Dr. Adelard De Backer, St-Lucas Ziekenhuis, Ghent, Belgium.

CASE 146

CLINICAL HISTORY *43-year-old woman presenting with rectal bleeding and anemia.*

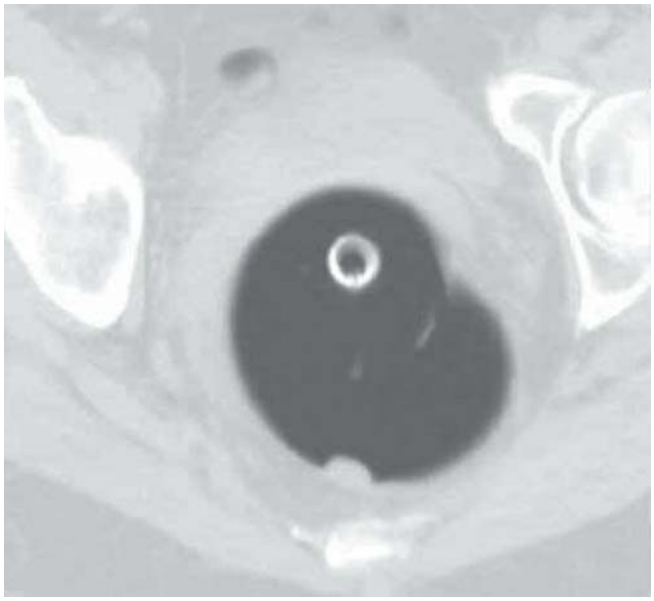

FIGURE 146A

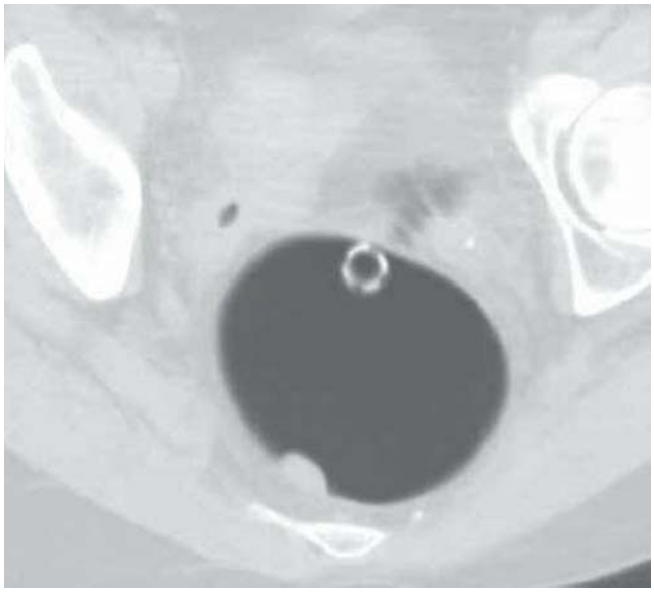

FIGURE 146B

FIGURE 146C

FIGURE 146D

FINDINGS Axial NECT images obtained with the patient in supine position (A) and prone position (B) and displayed in lung windows show a 1.6-cm polypoid lesion arising from the posterior rectal wall. Axial NECT image displayed in soft tissue windows (C) shows that the mass is homogeneous. A three-dimensional, volume-rendered endoluminal image (D) confirms its polypoid appearance.

DIFFERENTIAL DIAGNOSIS Adherent stool, colon cancer.

DIAGNOSIS Colonic adenomatous polyp.

DISCUSSION On CT-colonography, colorectal polyps appear as round, oval, or lobulated intraluminal projections and are homogeneous in attenuation and enhance after contrast administration. Villous tumors often appear heterogeneous and can mimic stool. The majority of colonic adenomas that will develop into cancer are polypoid or villous in shape. A small proportion of adenomas is "flat" or

depressed and has been shown to be difficult to identify on CT-colonography. Positive predictive characteristics of adenoma with increased propensity to develop into cancer are its size and the total number of adenomas. Polyps greater than 10 mm in diameter and more than three polyps, regardless of size, have been reported as risk factors for transformation into colorectal cancer through the "adenoma-carcinoma sequence." Retained stool often has a heterogeneous aspect due to incorporated air or high-density food particles. Lack of wall attachment, enhancement, and changing location on prone/supine images favors fecal origin. An entity to keep in mind when observing mobile filling defects is pedunculated polyps with a long stalk. The morphology of the polyp with head and stalk is helpful in differentiating these lesions from mobile fecal material. Fecal material can be round, oval, or lobulated but often presents angled borders and irregular geometric morphology. Fecal tagging also helps to differentiate immobile retained stool from real lesions.

CASE 147

CLINICAL HISTORY *48-year-old woman presenting with left upper quadrant pain.*

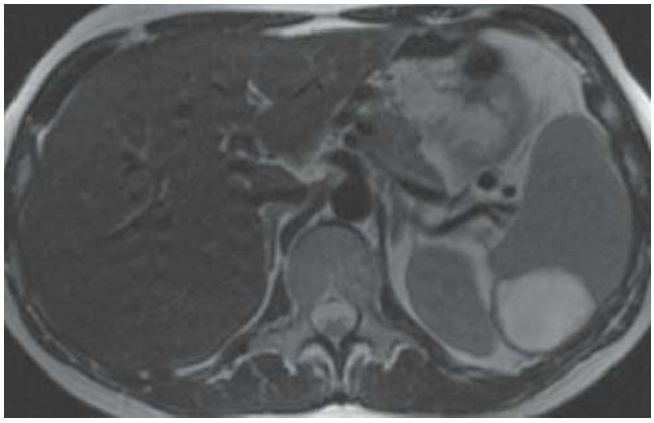

FIGURE 147A

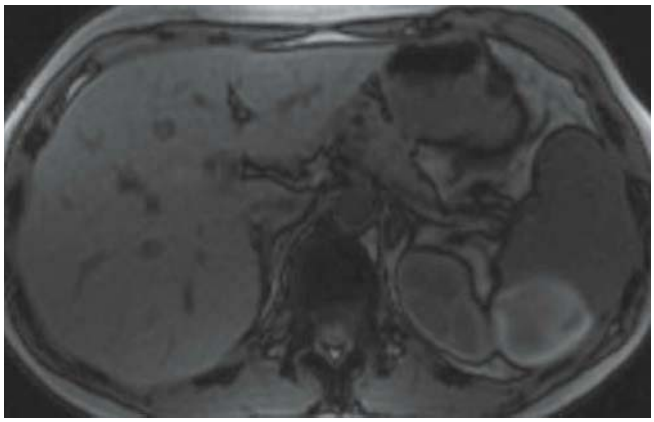

FIGURE 147B

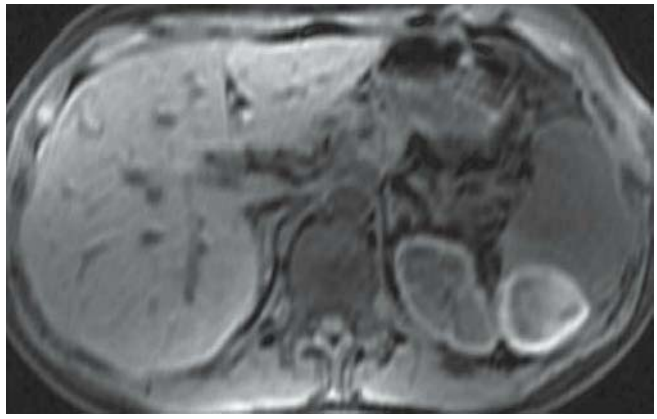

FIGURE 147C

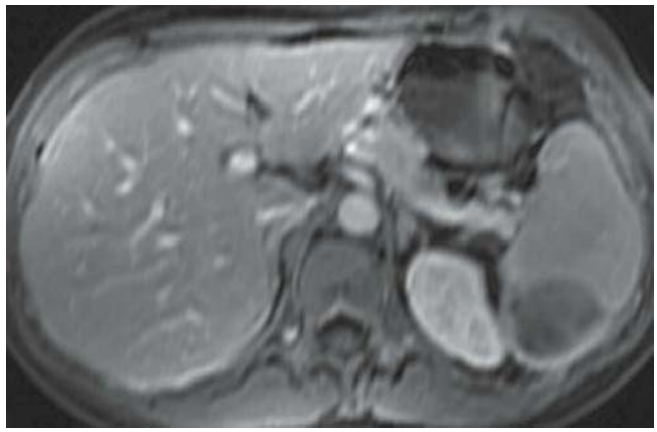

FIGURE 147D

FINDINGS Axial T2-WI (A), out-of-phase T1-WI (B), and unenhanced (C) and gadolinium-enhanced (D), fat-suppressed axial T1-WI demonstrate a 6-cm subcapsular splenic nonenhancing lesion, which displaces the spleen anteriorly. The lesion is high in signal on T1-WI due to the paramagnetic effect of methemoglobin.

DIFFERENTIAL DIAGNOSIS Pyogenic abscess, hydatid cyst.

DIAGNOSIS Subcapsular splenic hematoma.

DISCUSSION CT has definitely become the imaging modality of choice in the evaluation of patients with suspected splenic trauma. Splenic injuries can be classified on CT scans as subcapsular or intraparenchymal hematomas, lacerations, fractures, or vascular pedicles injuries. Intrasplenic hematomas typically appear as hypodense areas within the spleen after the administration of contrast medium, but in some cases, they may be nearly isodense. Subcapsular hematomas usually appear as crescentic or round fluid collection along the lateral aspect of the spleen, which may be difficult to distinguish from perisplenic fluid. MRI is seldom employed in the acute setting of splenic trauma, although it has high sensitivity for the detection of blood and blood breakdown products. The signal intensity of hematomas depends on the age of the extravascular blood. During the first 48 hours following extravasation, blood undergoes transformation into deoxyhemoglobin and other paramagnetic products. Deoxyhemoglobin within red blood cells may be identified on T2-WI within a few hours after trauma. Subacute hematomas are of high signal on T1-WI because of the paramagnetic effect of the extracellular methemoglobin, which shortens the T1 relaxation time.

CASE 148

CLINICAL HISTORY *35-year-old woman post-gastric bypass surgery.*

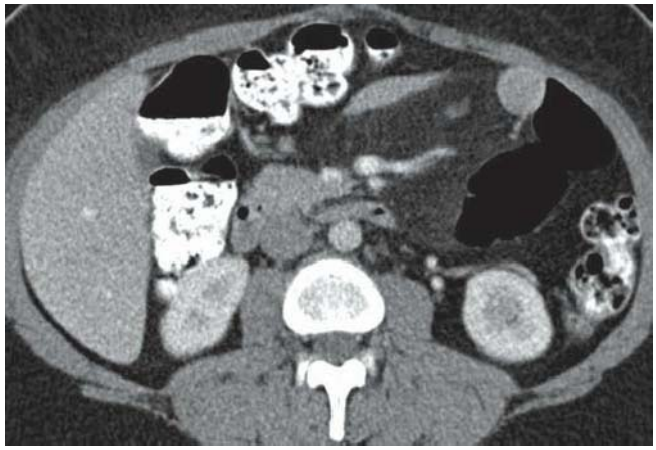

FIGURE 148A

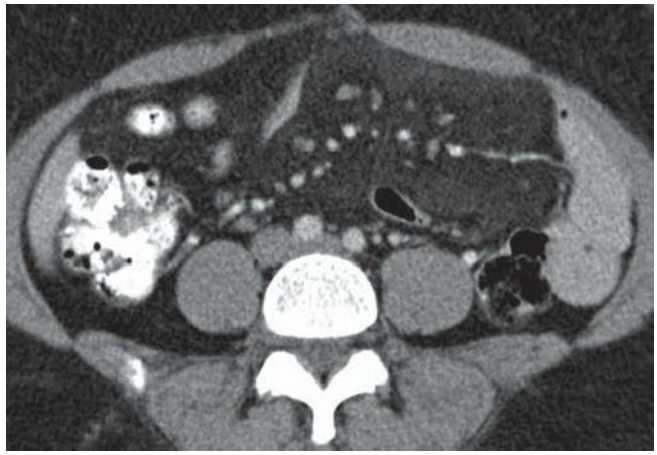

FIGURE 148C

FIGURE 148B

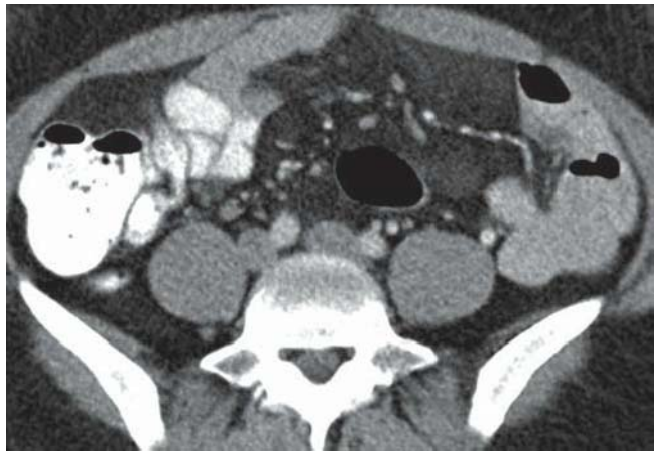

FIGURE 148D

FINDINGS Axial CT images (A-D) demonstrate a large mass, with a density slightly higher than the retroperitoneal fat and causing mass effect on adjacent bowel loops. A hypodense fatty halo surrounds the multiple small mesenteric nodules. The mesenteric veins are engorged.

DIFFERENTIAL DIAGNOSIS Lymphoma, lipoma, liposarcoma, peritoneal carcinomatosis.

DIAGNOSIS Sclerosing mesenteritis (mesenteric panniculitis).

DISCUSSION Sclerosing mesenteritis is a disorder of unknown etiology that results in chronic inflammation and eventually fibrosis. When the predominant process is inflammatory, it is subcategorized as mesenteric panniculitis. It is associated with other autoimmune processes such as retroperitoneal fibrosis, sclerosing cholangitis, Riedel thyroiditis, and orbital pseudotumor. An association with malignancies, such as lymphoma, melanoma, breast, lung, and colon cancer, has been described in up to 69% of patients. CT features are discrete fat stranding in the mesenteric fat, which may have a masslike appearance; a left-sided orientation; scattered, less than 5-mm, soft tissue nodules; a hypodense fatty halo (called "fat ring sign") surrounding the nodules and vessels; and a hyperattenuating stripe surrounding the mass. The constellation of these features is quite unique to mesenteric panniculitis and, when present, allows a more confident diagnosis. These imaging characteristics would not be present in lymphoma, lipoma, liposarcoma, or peritoneal carcinomatosis. Lymphoma may be the hardest to differentiate from mesenteric panniculitis, but the fat ring sign, not seen in cases of lymphoma, would be a key distinguishing feature.

CASE 149

CLINICAL HISTORY *31-year-old woman presenting with chronic pelvic pain.*

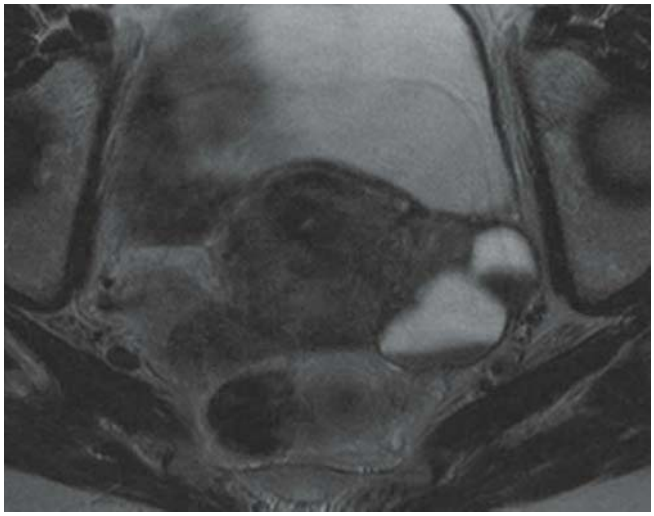

FIGURE 149A

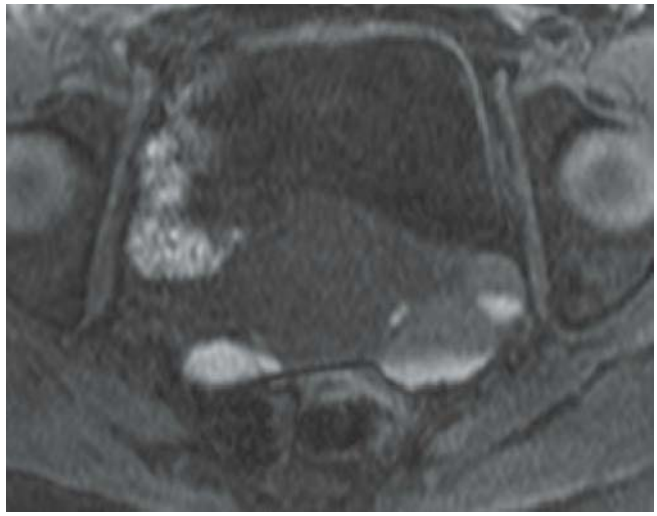

FIGURE 149C

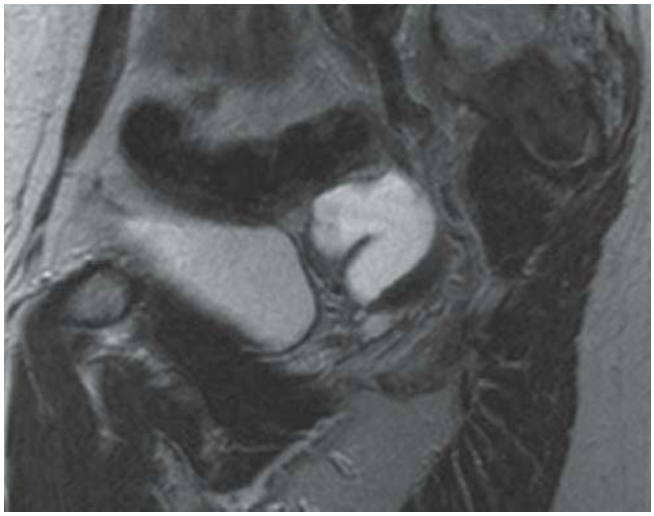

FIGURE 149B

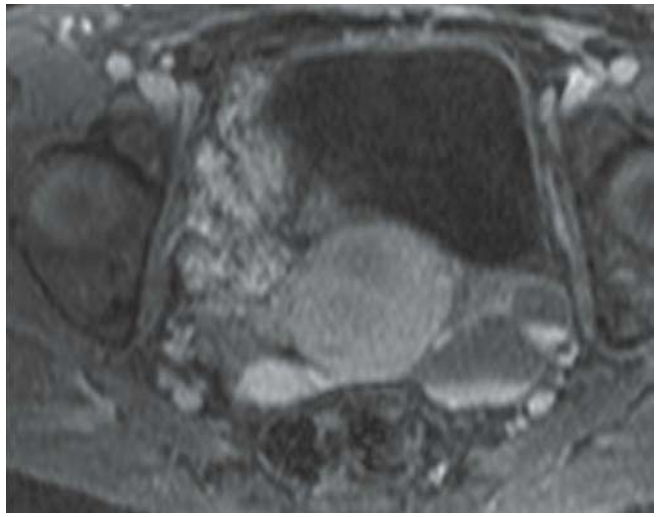

FIGURE 149D

FINDINGS Axial (A) and sagittal (B) T2-WIs demonstrate a left adnexal tubular lesion with hyperintense–hypointense fluid–fluid level. The dependent signal is hyperintense on the fat-suppressed axial T1-WI (C). Only thin peripheral enhancement of the wall is present on the gadolinium-enhanced, fat-suppressed axial T1-WI (D). Note the right adnexal T2 hypointense, T1 hyperintense nonenhancing cystic lesion.

DIFFERENTIAL DIAGNOSIS Hydro/pyosalpinx, ovarian (functional) cyst, serous ovarian cystadenoma, pelvic hematoma/lymphocele.

DIAGNOSIS Endometriosis (adnexal endometrioma and hematosalpinx).

DISCUSSION Hydrosalpinx is defined by a dilated fluid-filled fallopian tube due to tubal occlusion, which can be caused by peritubal inflammation, endometriosis, or salpingitis. On imaging, they typically appear as fluid-filled tubular adnexal structures, folded upon them to form a C or S shape. The key feature to differentiate a dilated fallopian tube from other adnexal structures is the presence of incomplete septations (plicae). They result from the effacement of the mucosa and submucosa from dilatation of the tube or blunting of

the mucosal folds. They may become flattened or absent in severe cases of tubal dilatation. In one plane, these folds may appear nodular, but as a ridge in an orthogonal plane. The wall shows enhancement on gadolinium-enhanced T1-WI. In cases of hematosalpinx, typically due to endometriosis, the tube becomes filled with blood products. The signal intensity of the tubal fluid is then similar to an endometrioma (high on T1-WI and low on T2-WI). In this case, the presence of blood-containing right adnexal cysts and left hematosalpinx makes endometriosis the best diagnosis. In acute salpingitis, wall thickening with a double-layered appearance of the tubal wall may be present.

CASE 150

CLINICAL HISTORY *36-year-old woman being evaluated for infertility.*

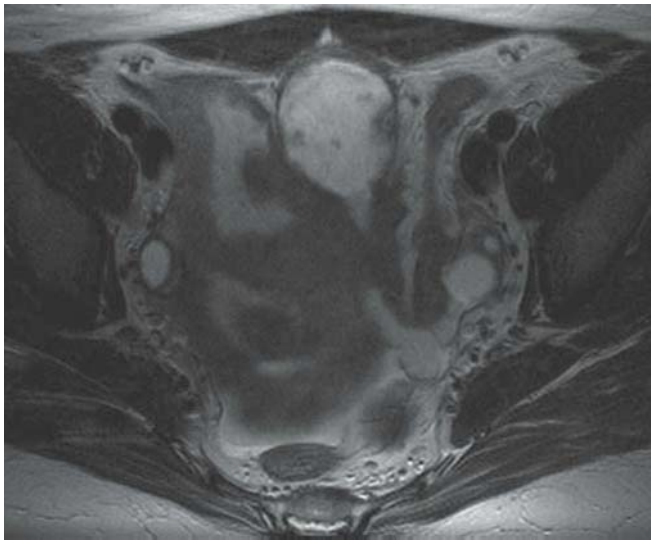

FIGURE 150A

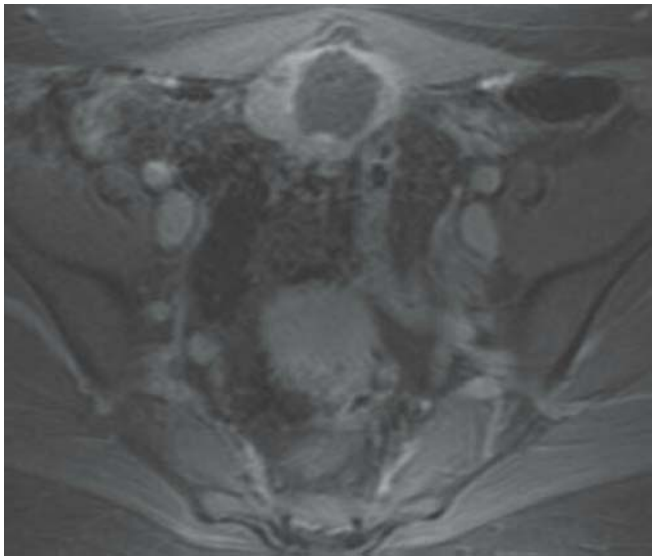

FIGURE 150C

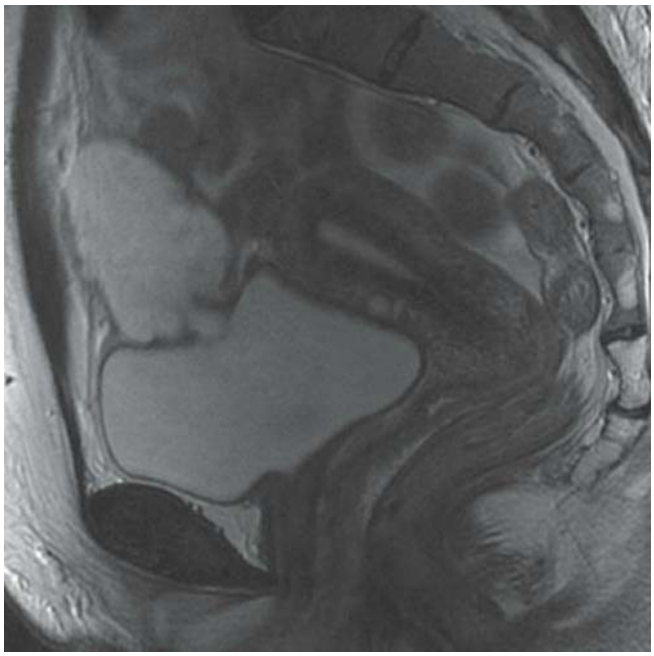

FIGURE 150B

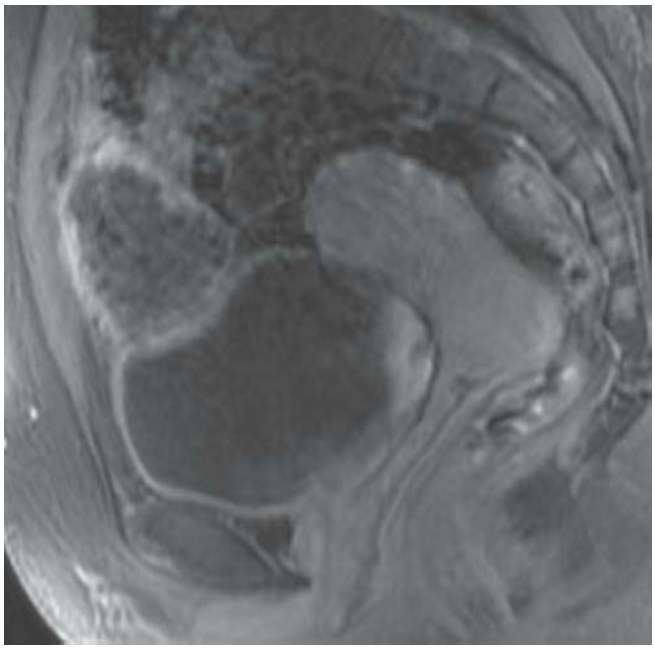

FIGURE 150D

FINDINGS Axial (A) and coronal (B) T2-WIs demonstrate a 5.4 cm × 3.7 cm × 2.3 cm cystic lesion with nodular wall located superiorly to the bladder dome at the midline level. Gadolinium-enhanced, fat-suppressed axial (C) and sagittal (D) T1-WIs show enhancement of the nodular wall. Note the absence of communication of the lesion with the bladder lumen.

DIFFERENTIAL DIAGNOSIS Abscess, urachal cyst, transitional cell carcinoma in a bladder diverticulum.

DIAGNOSIS Urachal carcinoma.

DISCUSSION The urachus is a vestigial remnant of the cloaca and allantoid. It extends over the midline from the umbilicus to the anterior superior surface of the bladder. The transitional epithelium of the urachus can undergo metaplasia and dysplasia and even become malignant and convert to a mucin-producing adenocarcinoma. This accounts for almost 70% of the malignancies in the urachus. They are commonly cystic with septations. Because of the mucin produced, these

urachal adenocarcinomas often have stippled or granular calcifications, which are best assessed by CT. The presence of a cystic mass at the superior anterior surface of the bladder at the midline level is highly suggestive of a urachal mucinous adenocarcinoma. Other malignancies of the urachus include sarcomas, transitional cell carcinoma, and squamous cell carcinoma; these malignancies are less commonly seen but can arise either from the urachus or the bladder. Urachal abscess may be indistinguishable from a urachal mucinous adenocarcinoma by imaging, and only the clinical history may help to differentiate the two. A communication with the bladder lumen was not present in this case, which excludes a bladder or urachal diverticulum. An uncomplicated urachal cyst should have smooth walls.

LIVER AND BILIARY SYSTEM

HEPATIC NEOPLASMS

- Albrecht T, Hohmann J, Oldenburg A, et al. Detection and characterisation of liver metastases. *Eur Radiol.* 2004;8:P25–P33.
- Boechat MI, Kangarloo H, Ortega J, et al. Primary liver tumors in children: comparison of CT and MR imaging. *Radiology* 1988;169:727–732.
- Bogner B, Hegedus G. Ciliated hepatic foregut cyst. *Pathol Oncol Res.* 2002;8:278–279.
- Brancatelli G, Federle MP, Grazioli L, et al. Focal nodular hyperplasia: CT findings with emphasis on multiphasic helical CT in 78 patients. *Radiology* 2001;219:61–68.
- Brancatelli G, Federle MP, Vilgrain V, et al. Fibropolycystic liver disease: CT and MR imaging findings. *Radiographics* 2005;25:659–670.
- Choi BI, Lee JM, Han JK. Imaging of intrahepatic and hilar cholangiocarcinoma. *Abdom Imaging.* 2004;29:548–557.
- Choi H, Loyer EM, DuBrow RA, et al. Radiofrequency ablation of liver tumors: assessment of therapeutic response and complications. *Radiographics* 2001;21:S41–S54.
- Coumbaras M, Wendum D, Monnier-Cholley L, et al. CT and MR imaging features of pathologically proven atypical giant hemangiomas of the liver. *Am J Roentgenol.* 2002;179:1457–1463.
- Dachman AH, Lichtenstein JE, Friedman AC, et al. Infantile hemangioendothelioma of the liver: a radiologic-pathologic-clinical correlation. *Am J Roentgenol.* 1983;140:1091–1096.
- Danet IM, Semelka RC, Braga L, et al. Giant hemangioma of the liver: MR imaging characteristics in 24 patients. *Magn Reson Imaging.* 2003;21:95–101.
- Diaz-Ruiz MJ, Falco J, Martin J, et al. Hepatocellular carcinoma presenting as portal thrombosis with intrabiliary growth: US and MR findings. *Abdom Imaging.* 2000;25:263–265.
- Fang SH, Dong DJ, Zhang SZ. Imaging features of ciliated hepatic foregut cyst. *World J Gastroenterol.* 2005;11:4287–4289.
- Fennessy FM, Mortele KJ, Kluckert T, et al. Hepatic capsular retraction in metastatic carcinoma of the breast occurring with increase or decrease in size of subjacent metastasis. *Am J Roentgenol.* 2004;182:651–655.
- Freeny PC, Baron RL, Teefey SA. Hepatocellular carcinoma: reduced frequency of typical findings with dynamic contrast enhanced CT in a non-Asian population. *Radiology* 1992;182:143–148.
- Furui S, Yuji I, Yamauchi T. Hepatic epithelioid hemangioendothelioma: report of five cases. *Radiology* 1989;171:63–68.
- Gallego C, Velasco M, Marcuello P, et al. Congenital and acquired anomalies of the portal venous system. *Radiographics* 2002;22:141–159.
- Gibbs JF, Litwin AM, Kahlenberg MS. Contemporary management of benign liver tumors. *Surg Clin North Am.* 2004;84:463–480.
- Hussain SM, Terkivatan T, Zondervan PE, et al. Focal nodular hyperplasia: findings at state-of-the-art MR imaging, US, CT, and pathologic analysis. *Radiographics* 2004;24:3–17.
- Ito K, Higuchi M, Kada T, et al. CT of acquired abnormalities of the portal venous system. *Radiographics* 1997;17:897–917.
- Kadoya M, Matsui O, Nakanuma Y, et al. Ciliated hepatic foregut cyst: radiologic features. *Radiology* 1990;175:475–477.
- Kanematsu M, Kondo H, Goshima S, et al. Imaging liver metastases: review and update. *Eur J Radiol.* 2006;58:217–228.
- Kanematsu M, Semelka RC, Leonardou P, et al. Hepatocellular carcinoma of diffuse type: MR imaging findings and clinical manifestations. *J Magn Reson Imaging.* 2003;18:189–195.
- Khan SA, Thomas HC, Davidson BR, et al. Cholangiocarcinoma. *Lancet* 2005;366:1303–1314.
- Kim MJ, Kim KW, Kim HC, et al. Unusual malignant tumors of the gallbladder. *AJR Am Roentgenol* 2006;187:473–480.
- Koyama T, Fletcher JG, Johnson CD, et al. Primary hepatic angiosarcoma: findings at CT and MR imaging. *Radiology* 2002;222:667–673.
- Levy AD. Malignant liver tumors. *Clin Liver Dis.* 2002; 6:147–164.
- Lewin M, Mourra N, Honigman I, Flejou JF, et al. Assessment of MRI and MRCP in diagnosis of biliary cystadenoma and cystadenocarcinoma. *Eur Radiol.* 2006;16:407–413.
- Limanond P, Zimmerman P, Raman SS, et al. Interpretation of CT and MRI after radiofrequency ablation of hepatic malignancies. *Am J Roentgenol.* 2003;181:1635–1640.
- Lu DS, Yu NC, Raman SS, et al. Radiofrequency ablation of hepatocellular carcinoma: treatment success as defined by histologic examination of the explanted liver. *Radiology* 2005;234:954–960.
- Lyburn ID, Torreggiani WC, Harris AC, et al. Hepatic epithelioid hemangioendothelioma: sonographic, CT, and MR imaging appearances. *Am J Roentgenol.* 2003;180:1359–1364.
- Maetani Y, Itoh K, Watanabe C, et al. MR imaging of intrahepatic cholangiocarcinoma with pathologic correlation. *Am J Roentgenol.* 2001;176:1499–1507.
- Marti-Bonmati L, Lonjedo E, Mathieu D, et al. Tumoural portal vein thrombosis. Enhancement with MnDPDP. *Acta Radiol.* 1997;38:655–659.
- Martin J, Sentis M, Zidan A, et al. Fatty metamorphosis of hepatocellular carcinoma: detection with chemical shift gradient-echo MR imaging. *Radiology* 1995;195:125–130.
- Mathieu D, Grenier P, Larde D, et al. Portal vein involvement in hepatocellular carcinoma: dynamic CT features. *Radiology* 1984;152:127–132.
- Mathieu D, Vasile N, Grenier P. Portal thrombosis: dynamic CT features and course. *Radiology* 1985;154:737–741.
- Matsui O, Masumi K, Tomiaki K. Benign and malignant nodules in cirrhotic livers: distinction based on blood supply. *Radiology* 1991;178:493–497.
- Matsushita M, Shimizu S, Nagasawa M, et al. Epithelioid hemangioendothelioma of the liver: imaging diagnosis of a rare hepatic tumor. *Dig Surg.* 2005;22:416–418.
- Mermuys K, Vanhoenacker PK, Roskams T, et al. Epithelioid hemangioendothelioma of the liver: radiologic-pathologic correlation. *Abdom Imaging.* 2004;29:221–223.
- Miller WJ, Dodd GD 3rd, Federle MP, et al. Epithelioid hemangioendothelioma of the liver: imaging findings with pathologic correlation. *Am J Roentgenol.* 1992;159:53–57.
- Mortele B, Mortele KJ, Seynaeve P, et al. Hepatic bile duct hamartomas (von Meyenburg complexes): MR and MR cholangiography imaging Findings. *J Comput Assist Tomogr.* 2002;26:438–443.

- Mortele KJ, De Keukeleire K, Praet M, et al. Malignant focal hepatic lesions complicating underlying liver disease: dual-phase contrast-enhanced spiral CT sensitivity and specificity in OLT patients. *Eur Radiol.* 2001;1:1631–1638.
- Mortele KJ, Mergo PJ, Urrutia M, et al. Dynamic gadolinium-enhanced MRI findings in infantile hepatic hemangioendothelioma. *J Comput Assist Tomogr.* 1998;22:714–717.
- Mortele KJ, Praet M, Van Vlierberghe H, et al. Focal nodular hyperplasia of the liver: assessment with plain and dynamic-enhanced MRI. *Abdom Imaging.* 2002;27:700–707.
- Mortele KJ, Praet M, Van Vlierberghe H, et al. CT and MR imaging findings in focal nodular hyperplasia of the liver: radiologic-pathologic correlation. *Am J Roentgenol.* 2000;175: 687–692.
- Mortele KJ, Ros PR. Benign liver neoplasms. *Clin Liver Dis.* 2002;6:119–145.
- Mortele KJ, Ros PR. Cystic focal liver lesions in the adult: differential CT and MR imaging features. *Radiographics* 2001;21:895–910.
- Mortele KJ, Stubbe J, Praet M, et al. Intratumoral steatosis in focal nodular hyperplasia coinciding with diffuse hepatic steatosis: CT and MRI findings with histologic correlation. *Abdom Imaging.* 2000;25:179–181.
- Mortele KJ, Vanzieleghem B, Mortele B, et al. Gadolinium-enhanced MR imaging of infantile hemangioendothelioma: atypical features. *Eur Radiol.* 2002;12:862–865.
- Murakami T, Chikazumi K, Taro M, et al. Regenerating nodules in hepatic cirrhosis: MR findings with pathologic correlation. *Am J Roentgenol.* 1990;155:1227–1231.
- Murphy BJ, Casillas J, Ros PR, et al. The CT appearance of cystic masses of the liver. *Radiographics* 1989;9:307–322.
- Nascimento AB, Mitchell DG, Rubin R, et al. Diffuse desmoplastic breast carcinoma metastases to the liver simulating cirrhosis at MR imaging: report of two cases. *Radiology* 2001;221:117–121.
- Outwater E, Tomaszewski J, Daly J, et al. Hepatic colorectal metastases: correlation of MR imaging and pathologic appearance. *Radiology* 1991;180:327–332.
- Peterson MS, Baron RL, Rankin SC. Hepatic angiosarcoma: findings on multiphasic contrast-enhanced helical CT do not mimic hepatic hemangioma. *Am J Roentgenol.* 2000;175:165–170.
- Powers C, Ros PR, Stoupis C, et al. Primary liver neoplasms: MR imaging with pathologic correlation. *Radiographics* 1994;14:459–482.
- Prasad SR, Wang H, Rosas H, et al. Fat-containing lesions of the liver: radiologic-pathologic correlation. *Radiographics* 2005;25:321–331.
- Quinn SF, Benjamin GG. Hepatic cavernous hemangiomas: simple diagnostic sign with dynamic bolus CT. *Radiology* 1992;182:545–548.
- Radin DR, Craig JR, Colletti PM, et al. Hepatic epithelioid hemangioendothelioma. *Radiology* 1988;169:145–148.
- Ros PR, Buck JL, Goodman ZD, et al. Intrahepatic cholangiocarcinoma: radiologic-pathologic correlation. *Radiology* 1988;167:689–693.
- Ros PR, Zachary DG, Ishak KG, et al. Mesenchymal hamartoma of the liver: radiologic-pathologic correlation. *Radiology* 1986;158:619–624.
- Sanders LM, Botet JF, Straus DJ, et al. CT of primary lymphoma of the liver. *Am J Roentgenol.* 1989;152:973–976.
- Sans N, Fajadet P, Galy-Fourcade D, et al. Is capsular retraction a specific CT sign of malignant liver tumor? *Eur Radiol.* 1999;9:1543–1545.
- Shamsi K, Deckers F, De Schepper A. Unusual cystic liver lesions: a pictorial essay. *Eur J Radiol.* 1993;16:79–84.
- Soyer P, Bluemke DA, Vissuzaine C, et al. CT of hepatic tumors: prevalence and specificity of retraction of the adjacent liver capsule. *Am J Roentgenol.* 1994;162:1119–1122.
- Stocker JT, Ishak KG. Undifferentiated (embryonal) sarcoma of the liver. *Cancer* 1978;42:336–348.
- Sugawara Y, Yamamoto J, Yamasaki S, et al. Cystic liver metastases from colorectal cancer. *J Surg Oncol.* 2000; 74:148–152.
- Takayasu K, Hiroyoshi F, Wakao Y, et al. CT diagnosis of early hepatocellular carcinoma: sensitivity, findings, and CT-pathologic correlation. *Am J Roentgenol.* 1995;164:885–890.
- Valls C, Iannacconne R, Alba E, et al. Fat in the liver: diagnosis and characterization. *Eur Radiol.* 2006;14:1–17.
- Valls C, Rene M, Gil M, et al. Giant cavernous hemangioma of the liver: atypical CT and MR findings. *Eur Radiol.* 1996; 6:448–450.
- Vilgrain V, Boulos L, Vullierme MP, et al. Imaging of atypical hemangiomas of the liver with pathologic correlation. *Radiographics* 2000;20:379–397.
- Vogt DP, Henderson JM, Chmielewski E. Cystadenoma and cystadenocarcinoma of the liver: a single center experience. *J Am Coll Surg.* 2005;200:727–733.
- Wong LK, Link DP, Frey CF, et al. Fibrolamellar hepatocarcinoma: radiology, management, and pathology. *Am J Roentgenol.* 1982;139:172–175.
- Wu T, Boitnott J. Dysplastic nodules: a new term for premalignant hepatic nodular lesions. *Radiology* 1996; 201:21–22.
- Yoshikawa J, Matsui O, Takashima T, et al. Fatty metamorphosis in hepatocellular carcinoma: radiologic features in 10 cases. *Am J Roentgenol.* 1988;15:717–720.

DIFFUSE LIVER DISEASES

- Adler D, Glazer G, Silver T. Computed tomography of liver infarction. *Am J Roentgenol.* 1984;142:315–318.
- Akhan O, Akpinar E, Oto A, et al. Unusual imaging findings in Wilson's disease. *Eur Radiol.* 2002;12(suppl 3):S66–S69.
- Basaran C, Karcaaltincaba M, Akata D, et al. Fat-containing lesions of the liver: cross-sectional imaging findings with emphasis on MRI. *Am J Roentgenol.* 2005;184:1103–1110.
- Benya EC, Sivit CJ, Quinones RR. Abdominal complications after bone marrow transplantation in children: sonographic and CT findings. *Am J Roentgenol.* 1993;161:1023–1027.
- Coy DL, Ormazabal A, Godwin JD, et al. Imaging evaluation of pulmonary and abdominal complications following hematopoietic stem cell transplantation. *Radiographics* 2005; 25:305–317.
- Elsayes KM, Narra VR, Yin Y, et al. Focal hepatic lesions: diagnostic value of enhancement pattern approach with contrast-enhanced 3D gradient-echo MR imaging. *Radiographics* 2005;25:1299–1320.
- Farman J, Ramirez G, Brunetti J, et al. Abdominal manifestations of sarcoidosis. CT appearances. *Clin Imaging.* 1995;19:30–33.
- Fennessy FM, Mortele KJ, Kluckert T, et al. Hepatic capsular retraction in metastatic carcinoma of the breast occurring with increase or decrease in size of subjacent metastasis. *Am J Roentgenol.* 2004;182:651–655.
- Goldman IS, Winkler ML, Raper SE, et al. Increased hepatic density and phospholipidosis due to amiodarone. *Am J Roentgenol.* 1985;144:541–546.

- Harrison SA, Torgerson S, Hayashi PH. The natural history of nonalcoholic fatty liver disease: a clinical histopathological study. *Am J Gastroenterol.* 2003;98:2042–2047.
- Hommeyer SC, Teefey SA, Jacobson AF, et al. Veno-occlusive disease of the liver: prospective study of US evaluation. *Radiology* 1992;184:683–686.
- Hood MN, Ho VB, Smirniotopoulos JG, et al. Chemical shift: the artifact and clinical tool revisited. *Radiographics* 1999;19:357–371.
- Jung G, Brill N, Poll LW, et al. MRI of hepatic sarcoidosis: large confluent lesions mimicking malignancy. *Am J Roentgenol.* 2004;183:171–173.
- Kalantari BN, Mortele KJ, Cantisani V, et al. CT features with pathologic correlation of acute gastrointestinal graft-versus-host disease after bone marrow transplantation in adults. *Am J Roentgenol.* 2003;181:1621–1625.
- Kawamoto S, Soyer PA, Fishman EK, et al. Nonneoplastic liver disease: evaluation with CT and MR imaging. *Radiographics* 1998;18:827–848.
- Kemper J, Jung G, Poll LW, et al. CT and MRI findings of multifocal hepatic steatosis mimicking malignancy. *Abdom Imaging.* 2002;27:708–710.
- Koslin DB, Stanley RJ, Shin MS, et al. Hepatic perivascular lymphedema: CT appearance. *Am J Roentgenol.* 1988; 150:111–113.
- Koyama T, Ueda H, Togashi K, et al. Radiologic manifestations of sarcoidosis in various organs. *Radiographics* 2004;24:87–104.
- Larson RE, Semelka RC. Magnetic resonance imaging of the liver. *Top Magn Reson Imaging.* 1995;7:71–81.
- Martin DR. Magnetic resonance imaging of diffuse liver diseases. *Top Magn Reson Imaging.* 2002;13:151–163.
- Mathieu D, Vasile N, Menu Y, et al. Budd-Chiari syndrome: dynamic CT. *Radiology* 1987;165:409–413.
- Mortele KJ, Ros PR. Imaging of diffuse liver disease. *Semin Liver Dis.* 2001;21:195–212.
- Mortele KJ, Ros PR. MR imaging in chronic hepatitis and cirrhosis. *Semin Ultrasound CT MR.* 2002;23:79–100.
- Mortele KJ, Van Vlierberghe H, Wiesner W, et al. Hepatic veno-occlusive disease: MRI findings. *Abdom Imaging.* 2002;27:523–526.
- Ohtomo K, Baron RL, Dodd GD 3rd, et al. Confluent hepatic fibrosis in advanced cirrhosis: appearance at CT. *Radiology* 1993;188:31–35.
- Ohtomo K, Baron RL, Dodd GD 3rd, et al. Confluent hepatic fibrosis in advanced cirrhosis: evaluation with MR imaging. *Radiology* 1993;189:871–874.
- Oliva MR, Mortele KJ, Segatto E, et al. Computed tomography features of nonalcoholic steatohepatitis with histopathologic correlation. *J Comput Assist Tomogr.* 2006;30:37–43.
- Patrick D, White FE, Adams PC. Long-term amiodarone therapy: a cause of increased hepatic attenuation on CT. *Br J Radiol.* 1984;57:573–576.
- Prasad SR, Wang H, Rosas H, et al. Fat-containing lesions of the liver: radiologic-pathologic correlation. *Radiographics* 2005;25:321–331.
- Saadeh S, Younossi ZM, Remer EM, et al. The utility of radiological imaging in nonalcoholic fatty liver disease. *Gastroenterology* 2002;123:745–750.
- Siegelman E, Mitchell D, Rubin R, et al. Parenchymal versus reticuloendothelial iron overload in the liver: distinction with MR imaging. *Radiology* 1991;179:361–366.
- Siegelman ES. MR imaging of diffuse liver disease. Hepatic fat and iron. *Magn Reson Imaging Clin North Am.* 1997; 5:347–365.
- Stark D, Hahn P, Trey C, et al. MRI of the Budd-Chiari syndrome. *Am J Roentgenol.* 1986;146:1141–1148.
- Tom WW, Yeh BM, Cheng JC, et al. Hepatic pseudotumor due to nodular fatty sparing: the diagnostic role of opposed-phase MRI. *Am J Roentgenol.* 2004;183:721–724.
- Valls C, Iannacconne R, Alba E, et al. Fat in the liver: diagnosis and characterization. *Eur Radiol.* 2006;14:1–17.
- Van den Bosch MA, Van Hoe L. MR imaging findings in two patients with hepatic veno-occlusive disease following bone marrow transplantation. *Eur Radiol.* 2000;10:1290–1293.
- Vitellas KM, Tzalonikou MT, Bennett WF, et al. Cirrhosis: spectrum of findings on unenhanced and dynamic gadolinium-enhanced MR imaging. *Abdom Imaging.* 2001;26:601–615.
- Vogelzang R, Anschuetz S, Gore R. Budd-Chiari syndrome: CT observations. *Radiology* 1987;163:329–333.
- Yang DM, Kim HS, Cho SW, et al. Pictorial review: various causes of hepatic capsular retraction: CT and MR findings. *Br J Radiol.* 2002;75:994–1002.

BILIARY DISEASE

- Atri M, Bonifacio A, Ryan M, et al. Dropped gallstones post laparoscopic cholecystectomy mimicking peritoneal seeding: CT and ultrasound features. *J Comput Assist Tomogr.* 2002;26:1000–1005.
- Bennett GL, Balthazar EJ. Ultrasound and CT evaluation of emergent gallbladder pathology. *Radiol Clin N Am.* 2003; 41:1203–1216.
- Boscak AR, Al-Hawary M, Ramsburgh SR. Best cases from the AFIP. Adenomyomatosis of the gallbladder. *Radiographics* 2006;26:941–946.
- Chan F, Man S, Leong LL, et al. Evaluation of recurrent pyogenic cholangitis with CT: analysis of 50 patients. *Radiology* 1989;170:165–169.
- Fidler J, Paulson EK, Layfield L. CT evaluation of acute cholecystitis: findings and usefulness in diagnosis. *Am J Roentgenol.* 1996;166:1085–1088.
- Gore RM, Yaghmai V, Newmark GM, et al. Imaging benign and malignant disease of the gallbladder. *Radiol Clin North Am.* 2002;40:1307–1323.
- Grand D, Horton KM, Fishman EK. CT of the gallbladder: spectrum of disease. *Am J Roentgenol.* 2004;183:163–170.
- Ishak KG, Willis GW, Cummins SD, et al. Biliary cystadenoma and cystadenocarcinoma. *Cancer* 1977;38:322–338.
- Ito K, Mitchell DG, Outwater EK, et al. Primary sclerosing cholangitis: MR imaging features. *Am J Roentgenol.* 1999;172:1527–1533.
- Kim YJ, Kim MJ, Kim KW, et al. Preoperative evaluation of common bile duct stones in patients with gallstone disease. *Am J Roentgenol.* 2005;184:1854–1859.
- Kondo S, Isayama H, Akahane M, et al. Detection of common bile duct stones: comparison between endoscopic ultrasonography, magnetic resonance cholangiography, and helical-computed-tomographic cholangiography. *Eur J Radiol.* 2005;54:271–275.
- Korobkin M, Stephens DH, Lee JKT, et al. Biliary cystadenoma and cystadenocarcinoma: CT and sonographic findings. *Am J Roentgenol.* 1989;153:507–511.
- Maldjian C, Stancato-Pasik A, Shapiro RS. Abscess formation as a late complication of dropped gallstones. *Abdom Imaging.* 1995;20:217–218.
- Mortele KJ, Wiesner W, Cantisani V, et al. Usual and unusual causes of extrahepatic cholestasis: assessment with magnetic resonance cholangiography and fast MRI. *Abdom Imaging.* 2004;29:87–99.

- Mortele KJ, Ji H, Ros PR. CT and magnetic resonance imaging in pancreatic and biliary tract malignancies. *Gastrointest Endosc.* 2002;56(suppl 6):S206–S212.
- Rubens DJ. Hepatobiliary imaging and its pitfalls. *Radiol Clin North Am.* 2004;42:257–278.
- Sakamoto I, Iwanaga S, Nagaoki K, et al. Intrahepatic biloma formation (bile duct necrosis) after transcatheter arterial chemoembolization. *Am J Roentgenol.* 2003;181:79–87.
- Shanmugam V, Beattie GC, Yule SR, et al. Is magnetic resonance cholangiopancreatography the new gold standard in biliary imaging? *Br J Radiol.* 2005;78:888–893.
- Sood B, Jain M, Khandelwal N, et al. MRI of perforated gallbladder. *Australas Radiol.* 2002;46:438–440.
- Stefanidis D, Sirinek KR, Bingener J. Gallbladder perforation: risk factors and outcome. *J Surg Res.* 2006;131:204–208.
- Thurley PD, Dhingsa R. Laparoscopic cholecystectomy: postoperative imaging. *Am J Roentgenol.* 2008;191:794–801.
- Tsai HM, Lin XZ, Chen CY, et al. MRI of gallstones with different compositions. *Am J Roentgenol.* 2004;182:1513–1519.
- Tseng JH, Pan KT, Hung CF, et al. Choledochal cyst with malignancy: magnetic resonance imaging and magnetic resonance cholangiopancreatographic features in two cases. *Abdom Imaging.* 2003;28:838–841.
- Tumer AR, Yuksek YN, Yasti AC, et al. Dropped gallstones during laparoscopic cholecystectomy: the consequences. *World J Surg.* 2005;29:437–440.
- Vitellas KM, Keogan MT, Freed KS, et al. Radiologic manifestations of sclerosing cholangitis with emphasis on MR cholangiopancreatography. *Radiographics* 2000;20:959–975.
- Weiner SN, Koenigsberg M, Morehouse H, et al. Sonography and computed tomography in the diagnosis of carcinoma of the gallbladder. *Am J Roentgenol.* 1984;142:735–739.
- Yoshikane H, Hashimoto S, Hidano H, et al. Multiple early bile duct carcinoma associated with congenital choledochal cyst. *J Gastroenterol.* 1998;33:454–457.
- Yu JS, Kim KW, Park MS, et al. Bile duct injuries leading to portal vein obliteration after transcatheter arterial chemoembolization in the liver: CT findings and initial observations. *Radiology* 2001;221:429–436.
- Zissin R, Osadchy A, Shapiro-Feinberg M, et al. CT of a thickened-wall gall bladder. *Br J Radiol.* 2003;76:137–143.

INFECTION

- Acunas B, Izzet R, Levent C, et al. Purely cystic hydatid disease of the liver: treatment with percutaneous aspiration and injection of hypertonic saline. *Radiology* 1992;182:541–543.
- Balci NC, Semelka RC, Noone TC, et al. Pyogenic hepatic abscesses: MRI findings on T1- and T2-weighted and serial gadolinium-enhanced gradient-echo images. *J Magn Reson Imaging.* 1999;9:285–290.
- Balci NC, Sirvanci M. MR imaging of infective liver lesions. *Magn Reson Imaging Clin N Am.* 2002;10:121–135.
- Beggs I. The radiology of hydatid disease. *Am J Roentgenol.* 1985;145:639–648.
- Choliz J, Olaverri FJ, Casas T, et al. Computed tomography in hepatic echinococcosis. *Am J Roentgenol.* 1982;139:699–702.
- Elizondo G, Weissleder R, Stark D, et al. Amebic liver abscess: diagnosis and treatment evaluation with MR imaging. *Radiology* 1987;165:795–800.
- Francis I, Glazer G, Amendola A, et al. Hepatic abscesses in the immunocompromised patient role of CT in detection, diagnosis, management, and follow-up. *Gastrointest Radiol.* 1986;11: 257–262.
- Mathieu D, Vasile N, Pierre-Louis F, et al. Dynamic CT features of hepatic abscesses. *Radiology* 1985;154:749–752.
- Mendez R, Schiebler M, Outwater E, et al. Hepatic abscesses: MR imaging findings. *Radiology* 1994;190:431–436.
- Mortele KJ, Segatto E, Ros PR. The infected liver: radiologic-pathologic correlation. *Radiographics* 2004;24:937–955.
- Oto A, Akhan O, Ozmen M. Focal inflammatory diseases of the liver. *Eur J Radiol.* 1999;32:61–75.
- Ralls P, Barnes P, Johnson M, et al. Medical treatment of hepatic amebic abscess: rare need for percutaneous drainage. *Radiology* 1987;165:805–807.
- Ralls P, Henley D, Colletti P, et al. Amebic liver abscess: MR imaging. *Radiology* 1987;165:801–804.
- Shirkhoda A. CT findings in hepatosplenic and renal candidiasis. *J Comput Assist Tomogr.* 1987;11:795–798.

MISCELLANEOUS

- Bluemke DA, Fishman EK, Kuhlman JE, et al. Complications of radiation therapy: CT evaluation. *Radiographics* 1991; 11:581–600.
- Casillas VJ, Amendola MA, Gascue A, et al. Imaging of nontraumatic hemorrhagic hepatic lesions. *Radiographics* 2000; 20:367–378.
- Dickson AM. The focal hepatic hot spot sign. *Radiology* 2005;237:647–648.
- Finley DS, Hinojosa MW, Paya M, et al. Hepatic artery pseudoaneurysm: a report of seven cases and a review of the literature. *Surg Today.* 2005;35:543–547.
- Florio F, Nardella M, Balzano S, et al. Congenital intrahepatic portosystemic shunt. *Cardiovasc Intervent Radiol.* 1998;21: 421–424.
- Gallego C, Velasco M, Marcuello P, et al. Congenital and acquired anomalies of the portal venous system. *Radiographics* 2002;22:141–159.
- Ito K, Higuchi M, Kada T, et al. CT of acquired abnormalities of the portal venous system. *Radiographics* 1997;17:897–917.
- Kawamoto S, Soyer PA, Fishman EK, et al. Nonneoplastic liver disease: evaluation with CT and MR imaging. *Radiographics* 1998;18:827–848.
- Kim HJ, Kim KW, Kim AY, et al. Hepatic artery pseudoaneurysms in adult living-donor liver transplantation: efficacy of CT and Doppler sonography. *Am J Roentgenol.* 2005;184:1549–1555.
- Lee KH, Han JK, Jeong JY, et al. Hepatic attenuation differences associated with obstruction of the portal or hepatic veins in patients with hepatic abscess. *Am J Roentgenol.* 2005;185: 1015–1023.
- Lipson JA, Qayyum A, Avrin DE, et al. CT and MRI of hepatic contour abnormalities. *Am J Roentgenol.* 2005;184:75–81.
- Parvey HR, Raval B, Sandler CM. Portal vein thrombosis: imaging findings. *Am J Roentgenol.* 1994;162:77–81.
- Romano L, Giovine S, Guidi G, et al. Hepatic trauma: CT findings and considerations based on our experience in emergency diagnostic imaging. *Eur J Radiol.* 2004;50:59–66.
- Shanmuganathan K. Multi-detector row CT imaging of blunt abdominal trauma. *Semin Ultrasound CT MR.* 2004;25:180–204.
- Sheth S, Ebert MD, Fishman EK. Superior vena cava obstruction evaluation with MDCT. *Am J Roentgenol* 2010;194:336–346.
- Tublin ME, Dodd GD 3rd, Baron RL. Benign and malignant portal vein thrombosis: differentiation by CT characteristics. *Am J Roentgenol.* 1997;168:719–723.
- Yoon W, Jeong YY, Kim JK, et al. CT in blunt liver trauma. *Radiographics* 2005;25:87–104.

PANCREAS

INFLAMMATION

- Aksik MG, Sandrasegaran K, Aisen AA, Maglinte DDT, Sherman S, Lehman GA. Dynamic secretin-enhanced MR cholangiopancreatography. *Radiographics* 2006;26:665–677.
- Amano Y, Oishi T, Takahashi M. Nonenhanced magnetic resonance imaging of mild acute pancreatitis. *Abdom Imaging.* 2001;26:59–63.
- Balthazar E, Ranson BM, Naidich D, et al. Acute pancreatitis: prognostic value of CT. *Radiology* 1985;156:767–772.
- Balthazar E, Robinson D, Megibow A, et al. Acute pancreatitis: value of CT in establishing prognosis. *Radiology* 1990;174: 331–336.
- Balthazar EJ. CT diagnosis and staging of acute pancreatitis. *Radiol Clin North Am.* 1989;27:19–37.
- De Backer AI, Mortele KJ, Ros PR, et al. Chronic pancreatitis: diagnostic role of computed tomography and magnetic resonance imaging. *JBR-BTR.* 2002;85:304–310.
- Elmas N. The role of diagnostic radiology in pancreatitis. *Eur J Radiol.* 2001;38:120–132.
- Freeny PC. Classification of pancreatitis. *Radiol Clin North Am.* 1989;27:1–3.
- Johnson PT, Outwater EK. Pancreatic carcinoma versus chronic pancreatitis: dynamic MR imaging. *Radiology* 1999;212: 213–218.
- Lecesne R, Laurent F, Drouillard J, et al. Chronic pancreatitis. In: Baert AL, Delorme G, Van Hoe L, eds. *Radiology of the Pancreas*. 2nd ed. Heidelberg: Springer-Verlag; 1999:145–180.
- Lecesne R, Taourel P, Bret PM, et al. Acute pancreatitis: interobserver agreement and correlation of CT and MR cholangiopancreatography with outcome. *Radiology* 1999; 211:727–735.
- Matos C, Metens T, Deviere J, et al. Pancreatic duct: Morphologic and functional evaluation with dynamic MR pancreatography after secretin stimulation. *Radiology* 1997;203:435–441.
- Mortele KJ, Banks PA, Silverman SG. State-of-the-art imaging of acute pancreatitis. *JBR-BTR.* 2003;86:193–208.
- Mortele KJ, Mergo PJ, Taylor HM, et al. Peripancreatic vascular abnormalities complicating acute pancreatitis: Contrast-enhanced helical CT findings. *Eur J Radiol.* 2004;52:67–72.
- Mortele KJ, Mergo PJ, Taylor HM, et al. Renal and perirenal space involvement in acute pancreatitis: state-of-the-art spiral CT findings. *Abdom Imaging.* 2000;25:272–278.
- Mortele KJ, Wiesner W, Cantisani V, et al. Usual and unusual causes of extrahepatic cholestasis: assessment with magnetic resonance cholangiography and fast MRI. *Abdom Imaging.* 2004;29:87–99.
- Mortele KJ, Wiesner W, Intriere L, et al. A modified CT severity index for evaluating acute pancreatitis: improved correlation with patient outcome. *Am J Roentgenol.* 2004;183:1261–1265.
- Robinson PJA, Sheridan MB. Pancreatitis: computed tomography and magnetic resonance imaging. *Eur Radiol.* 2000;10:401–408.
- Russell RT, Sharp KW. Mucinous cystadenoma of the pancreas associated with acute pancreatitis and concurrent pancreatic pseudocyst. *Am Surg*. 2005;71:292–297.
- Sahani DV, Kalva SP, Farrell J, et al. Autoimmune pancreatitis: imaging features. *Radiology* 2004:233:345–352.
- Sica GT, Braver J, Cooney MJ, et al. Comparison of endoscopic retrograde cholangiopancreatography with MR cholangiopancreatography in patients with pancreatitis. *Radiology* 1999;210:605–610.
- Ward J, Chalmers AG, Guthrie AJ, et al. T2-weighted and dynamic enhanced MRI in acute pancreatitis: comparison with contrast-enhanced CT. *Clin Radiol.* 1997;52:109–114.

NEOPLASMS

- Baek SY, Sheafor DH, Keogan MT, et al. Two-dimensional multiplanar and three-dimensional volume-rendered vascular CT in pancreatic carcinoma: interobserver agreement and comparison with standard helical techniques. *Am J Roentgenol.* 2001;176:1467–1473.
- Boland GW, O'Malley ME, Saez M, et al. Pancreatic-phase versus portal vein-phase helical CT of the pancreas: optimal temporal window for evaluation of pancreatic adenocarcinoma. *Am J Roentgenol.* 1999;172:605–608.
- Buetow PC, Parrino TV, Buck JL, et al. Islet cell tumors of the pancreas: pathologic-imaging correlation among size, necrosis and cysts, calcification, malignant behavior and functional status. *Am J Roentgenol.* 1995;165:1175–1179.
- Cantisani V, Mortele KJ, Levy A, et al. MR imaging features of solid-pseudopapillary tumor of the pancreas in adult and pediatric patients. *Am J Roentgenol.* 2003;181:395–401.
- Choi BI, Chung MJ, Han JK, et al. Detection of pancreatic adenocarcinoma: Relative value of arterial and late phases of spiral CT. *Abdom Imaging.* 1997;22:199–203.
- Choi BI, Kim KW, Han MC, et al. Solid and papillary epithelial neoplasms of the pancreas: CT findings. *Radiology* 1988;166:413–416.
- Chung MJ, Choi BI, Han JK, et al. Functioning islet cell tumor of the pancreas: localization with dynamic spiral CT. *Acta Radiol.* 1997;38:135–138.
- Compagno J, Oertel JE. Mucinous cystic neoplasms of the pancreas with overt and latent malignancy (cystadenocarcinoma and cystadenoma). *Am Soc Clin Pathol.* 1978;69:573–580.
- Diehl SJ, Lehmann KJ, Sadick M, et al. Pancreatic cancer: value of dual-phase helical CT in assessing resectability. *Radiology* 1998;206:373–378.
- Ellsmere J, Mortele KJ, Sahani D, et al. Does multidetector-row CT eliminate the role of diagnostic laparoscopy in assessing the resectability of pancreatic head adenocarcinoma? *Surg Endosc.* 2005;19:369–373.
- Erturk SM, Mortele KJ, Oliva MR, et al. State-of-the-art computed tomographic and magnetic resonance imaging of the gastrointestinal system. *Gastrointest Endosc Clin N Am.* 2005;15:581–614.
- Fishman EK, Horton KM, Urban BA. Multidetector CT angiography in the evaluation of pancreatic carcinoma: preliminary observation. *J Comput Assist Tomogr.* 2000; 24:849–853.
- Freeny PC, Mark, WM, Ryan JA, et al. Pancreatic ductal adenocarcinoma: diagnosis and staging with dynamic CT. *Radiology* 1988;166:125–133.
- Friedman AC, Lichtenstein JE, Dachman AH. Cystic neoplasms of the pancreas. *Radiology* 1983;149:45–50.
- Friesen SR. Tumors of the endocrine pancreas. *N Engl J Med.* 1982;306:580–590.
- Frucht H, Doppman JL, Norton JA, et al. Gastrinomas: comparison of MR imaging with CT, angiography, and US. *Radiology* 1989;171:713–717.
- Gabata T, Matsui O, Kadoya M, et at. Small pancreatic adenocarcinoma: efficacy of MR imaging with fat-suppression and gadolinium enhancement. *Radiology* 1994;193:683–688.
- Graf O, Boland GW, Warshaw AL, et al. Arterial versus portal venous helical CT for revealing pancreatic adenocarcinoma:

conspicuity of tumor and critical vascular anatomy. *Am J Roentgenol.* 169:119–123.
- Ichikawa T, Haradome H, Hachiya J, et al. Pancreatic ductal adenocarcinoma: Preoperative assessment with helical CT versus dynamic MR imaging. *Radiology* 1997;202: 655–662.
- Itai Y, Ohhashi K, Furui S, et al. Microcystic adenoma of the pancreas: spectrum of computed tomographic findings. *J Comput Assist Tomogr.* 1988;12:797–803.
- Johnson CD, Stephens DH, Charboneau JW, et al. Cystic pancreatic tumors: CT and sonographic assessment. *Am J Roentgenol.* 1988;151:1133–1138.
- Kanematsu M, Shiratori Y, Hoshi H, et al. Pancreas and peripancreatic vessels: effect of imaging delay on gadolinium enhancement at dynamic gradient-recalled-echo MR imaging. *Radiology* 2000;215:95–102.
- Keogan MT, McDermott VG, Paulson EK, et al. Pancreatic malignancy: effect of dual-phase helical CT in tumor detection and vascular opacification. *Radiology* 1997;205:513–518.
- Khurana B, Mortele KJ, Glickman JN, et al. Macrocystic serous adenoma of the pancreas: radiologic-pathologic correlation. *Am J Roentgenol.* 2003;181:119–123.
- Kim T, Murakami T, Takamura M, et al. Pancreatic mass due to chronic pancreatitis: Correlation of CT and MR imaging features with pathologic findings. *Am J Roentgenol.* 2001; 177:367–371.
- Kraus BB, Ros PR. Insulinoma: diagnosis with suppressed MR imaging. *Am J Roentgenol.* 1994;162:69–70.
- McNulty N, Francis IR, Platt JF, et al. Multi-detector row helical CT of the pancreas: effect of contrast-enhanced multiphasic imaging on enhancement of the pancreas, peripancreatic vasculature, and pancreatic adenocarcinoma. *Radiology* 2001; 220:97–102.
- Mortele KJ, Ji H, Ros PR. CT and magnetic resonance imaging in pancreatic and biliary tract malignancies. *Gastrointest Endosc.* 2002;56(suppl 6):S206–S212.
- Mortele KJ, Mortele B, Silverman SG. CT features of the accessory (supernumerary) spleen. *Am J Roentgenol.* 2004; 183:1653–1657.
- Mortele KJ, Wiesner W, Cantisani V, et al. Usual and unusual causes of extrahepatic cholestasis: assessment with magnetic resonance cholangiography and fast MRI. *Abdom Imaging.* 2004;29:87–99.
- Nishiharu T, Yamashota Y, Abe Y, et al. Local extension of pancreatic carcinoma: Assessment with thin-section helical CT versus breath-hold fast MR imaging: ROC analysis. *Radiology* 1999;212:445–452.
- Peters HE, Vitellas KM. Magnetic resonance cholangiopancreatography (MRCP) of intraductal papillary-mucinous neoplasm (IPMN) of the pancreas: case report. *Magn Reson Imaging.* 2001;19:1139–1143.
- Procacci C, Carbognin G, Accordini S, et al. Nonfunctioning endocrine tumors of the pancreas: possibilities of spiral CT characterization. *Eur Radiol.* 2001;11:1626–1630.
- Radin DR, Colletti PM, Forrester DM. Pancreatic acinar cell carcinoma with subcutaneous and intraosseous fat necrosis. *Radiology* 1986;158:67–68.
- Raptopoulos V, Steer ML, Sheiman RG, et al. The use of helical CT and CT angiography to predict vascular involvement from pancreatic cancer: correlation with findings at surgery. *Am J Roentgenol.* 1997;168:971–977.
- Ros PR, Hamrick-Turner JE, Chiechi MV, et al. Cystic masses of the pancreas. *Radiographics* 1992;12:673–686.
- Rosebrook JL, Glickman JN, Mortele KJ. Pancreatoblastoma in an adult woman: sonography, CT, and dynamic gadolinium-enhanced MRI features. *Am J Roentgenol.* 2005;184;S78–S81.
- Scott J, Martin I, Redhead D, et al. Mucinous cystic neoplasms of the pancreas: imaging features and diagnostic difficulties. *Clin Radiol* 2000;55:187–192.
- Semelka RC, Kroeker MA, Shoenut JP, et al. Pancreatic disease: prospective comparison of CT, ERCP and 1.5 Tesla MR imaging with dynamic gadolinium enhancement and fat suppression. *Radiology* 1991;181:785–791.
- Sugiyama M, Atomi Y, Hachiya J. Intraductal papillary tumors of the pancreas: Evaluation with magnetic resonance cholangiopancreatography. *Am J Gastroenterol.* 1998;93:156–159.
- Tabuchi T, Itoh K, Ohshio G, et al. Tumor staging of pancreatic adenocarcinoma using early and late-phase helical CT. *Am J Roentgenol.* 1999;173:375–380.
- Taouli B, Vilgrain V, Vullierme MP, et al. Intraductal papillary mucinous tumors of the pancreas: Helical CT with histopathologic correlation. *Radiology* 2000;217:757–764.
- Tatli S, Mortele KJ, Levy AD, et al. CT and MR imaging features of pure acinar cell carcinoma of the pancreas in adults. *Am J Roentgenol.* 2005;184:511–519.
- Teefey SA, Stephens DH, Sheedy PF, et al. CT appearance of primary pancreatic lymphoma. *Gastrointest Radiol.* 1986;11:41–43.
- Yamashita Y, Ito K, Noda Y, et al. A case of mucinous cystadenoma of the pancreas resected after a 10-year follow-up. *Nihon Shokakibyo Gakkai Zasshi*. 2011;108(7):1280–1287. Japanese. PubMed PMID: 21737981.

DEVELOPMENTAL ANOMALIES

- Agha FP, Williams KD. Pancreas divisum: incidence, detection and clinical significance. *Am J Gastroenterol.* 1987;82:315–320.
- Bret PM, Reinhold C, Taourel P, et al. Pancreas divisum: evaluation with MR cholangiopancreatography. *Radiology* 1996;199:99–103.
- Guclu M, Serin E, Ulucan S. Agenesis of the dorsal pancreas in a patient with recurrent acute pancreatitis: case report and review. *Gastrointest Endosc.* 2004;60:472–475.
- Hough DM, Stephens DH, Johnson CD, et al. Pancreatic lesions in von Hippel-Lindau disease: prevalence, clinical significance, and CT findings. *Am J Roentgenol.* 1994;162:1091–1094.
- Inoue Y, Nakamura H. Aplasia or hypoplasia of the pancreatic uncinate process: comparison in patients with and patients without intestinal nonrotation. *Radiology* 1997;205:531–533.
- Jimenez JC, Emil S, Podnos Y, et al. Annular pancreas in children: a recent decade's experience. *J Ped Surg.* 2004;39:1654–1657.
- Kamisawa T, Yuyang T, Egawa N, et al. A new embryologic hypothesis of annular pancreas. *Hepatogastroenterology* 2001; 48:277–278.
- Klein SD, Affronti JP. Pancreas divisum, an evidence-based review: part I, pathophysiology. *Gastrointest Endosc.* 2004; 60:419–425.
- Leyendecker JR, Elsayes KM, Gratz BI, et al. MR cholangiopancreatography: spectrum of pancreatic duct abnormalities. *Am J Roentgenol.* 2002;179:1465–1471.
- Manfredi R, Costamagna G, Brizi MG, et al. Pancreas divisum and "santorinicele": diagnosis with dynamic MR cholangiopancreatography with secretin stimulation. *Radiology* 2000;217:403–408.
- Mortele KJ, Wiesner W, Silverman SG, et al. Asymptomatic non-specific serum hyperamylasemia and hyperlipasemia: spectrum of MRCP findings and clinical implications. *Abdom Imaging.* 2004;29:109–114.

- Nijs E, Callahan MJ, Taylor GA. Disorders of the pediatric pancreas: imaging features. *Pediatr Radiol.* 2005;35:358–373.
- Schulte SJ. Embryology, normal variation, and congenital anomalies of the pancreas. In: *Margulis' and Burhenne's Alimentary Tract Radiology*. 5th ed. St Louis, MO: Mosby; 1994:1039–1051.
- Soto JA, Lucey BC, Stuhlfaut JW. Pancreas divisum: depiction with multi-detector row CT. *Radiology* 2005;235:503–508.

GASTROINTESTINAL TRACT

NEOPLASMS

- Balthazar EJ, Megibow AJ, Hulnick D, et al. Carcinoma of the colon: detection and preoperative staging by CT. *Am J Roentgenol*. 1988;150:301–306.
- Bleday R, Telford JJ, Mortele KJ. Evaluation and staging of rectal cancer. *Sem Colon Rectal Surg*. 2002;13:139–143.
- Borhani AA, Hosseinzadeh K, Almusa O, Furlan A, Nalesnik M. Imaging of posttransplantation lymphoproliferative disorder after solid organ transplantation. *Radiographics* 2009; 29:981–1002.
- Buck JL, Sobin LH. Carcinoids of the gastrointestinal tract. *Radiographics* 1990;10:1081–1095.
- de Lange EE, Fechner RE, Edge SB, et al. Preoperative staging of rectal carcinoma with MR imaging: surgical and histopathologic correlation. *Radiology* 1990;176:623–628.
- Fiscback W, Kestel W, Kirchner T, et al. Malignant lymphomas of the upper gastrointestinal tract. *Cancer* 1992;70:1075–1080.
- Freeny PC, Marks, WM, Ryan JA, et al. Colorectal carcinoma evaluation with CT: preoperative staging and detection of postoperative recurrence. *Radiology* 1986;158:347–353.
- Gould M, Johnson RJ. Computed tomography of abdominal carcinoid tumor. *Br J Radiol*. 1986;59:881–885.
- Hong X, Choi H, Loyer EM, et al. Gastrointestinal stromal tumor: role of CT in diagnosis and in response evaluation and surveillance after treatment with imatinib. *Radiographics* 2006;26:481–495.
- Megibow AJ, Balthazar EJ, Naidich DP, et al. Computed tomography of gastrointestinal lymphoma. *Am J Roentgenol*. 1983;141:541–547.
- Picus D, Glazer HS, Levitt RG, et al. Computed tomography of abdominal carcinoid tumors. *Am J Roentgenol*. 1984; 143:581–584.
- Tatli S, Mortele KJ, Breen EL, et al. Local staging of rectal cancer using pelvic phased-array and endorectal coil. *J Magn Reson Imaging*. 2006;23:535–540.
- Weingrad DN, Decosse JJ, Sherlock P, et al. Primary gastrointestinal lymphoma: a 30-year review. *Cancer* 1982;49:1258–1265.
- Williams SM, Berk RN, Harned RK. Radiologic features of multinodular lymphoma of the colon. *Am J Roentgenol*. 1984;143:87–91.

INFLAMMATION

- Balthazar EJ, Megibow AJ, Hulnick D, et al. CT of appendicitis. *Am J Roentgenol*. 1986;147:705–710.
- Balthazar EJ, Megibow AJ, Schinella RA, et al. Limitations in the CT diagnosis of acute diverticulitis: comparison of CT, contrast enema, and pathologic findings of 16 patients. *Am J Roentgenol*. 1990;154:281–285.
- Balthazar EJ, Yen BC, Gordon RB. Ischemic colitis: CT evaluation of 54 cases. *Radiology* 1999;211:381–388.
- Bartlett JG. *Clostridium difficile*: clinical considerations. *Rev Infect Dis*. 1990;12:S243–S251.
- Bartram CI. Radiology in the current assessment of ulcerative colitis. *Gastrointest Radiol*. 1997;1:383–392.
- Berkmen YM, Rabinowitz J. Gastrointestinal manifestations of the strongyloidiasis. Am J *Roentgenol Radium Ther Nucl Med*. 1972;115:306–311.
- Cardoso JM, Kimura K, Stoopen M, et al. Radiology of invasive amebiasis of the colon. *Am J Roentgenol*. 1977;128:935–941.
- Del Frate C, Mortele KJ, Tuncali K, et al. Myometrial abscess caused by diverticulitis. *J Women's Imaging*. 2003;5:187–191.
- Eyvazzadeh AD, Pedrosa I, Rofsky NM, Siewert B, Farrar N, Abbott J, Levine D. MRI of right-sided abdominal pain in pregnancy. *Am J Roentgenol* 2004;183:907–914.
- Fishman EK, Kavuru BS, Jones B, et al. Pseudomembranous colitis: CT evaluation of 26 cases. *Radiology* 1991;180:57–60.
- Fultz PJ, Skucas J, Weiss SL. CT in upper gastrointestinal tract perforations secondary to peptic ulcer disease. *Gastrointest Radiol*. 1992;17:5–8.
- Gore RM, Marn CS, Kirby DF, et al. CT findings in ulcerative, granulomatous, and indeterminate colitis. *Am J Roentgenol*. 1984;143:279–284.
- Horton KM, Corl FM, Fishman EK. CT evaluation of the colon: Inflammatory disease. *Radiographics* 2000;20:399–418.
- Hulnick DH, Megibow AJ, Balthazar EJ, et al. Computed tomography in the evaluation of diverticulitis. *Radiology* 1984;152:491–495.
- Jang HJ, Lim HK, Park CK, et al. Segmental wall thickening in the colonic loop distal to colonic carcinoma at CT: importance and histopathological correlation. *Radiology* 2000;216:712–717.
- Liberman JM, Haaga JR. Computed tomography of diverticulitis. *J Comput Assist Tomogr*. 1983;7:431–433.
- Louisy CL, Barton CJ. The radiological diagnosis of *Strongyloides stercoralis* enteritis. *Radiology* 1971;98:535–541.
- Merine D, Fishman EK, Jones B. Pseudomembranous colitis: CT evaluation. *J Comput Assist Tomogr*. 1987;6:1017–1020.
- Philpotts LE, Heiken JP, Westcott MA, et al. Colitis: use of CT findings in differential diagnosis. *Radiology* 1994;190:445–449.
- Ros PR, Buetow PC, Pantograg-Brown L. Pseudomembranous colitis. *Radiology* 1996;198:1–9.
- Segatto E, Mortele KJ, Hoon J, et al. Acute small bowel ischemia: CT imaging findings. *Semin Ultrasound CT MRI*. 2003;24:364–376.
- Trinh T, Jones B, Fishman EK. Amyloidosis of the colon presenting as ischemic colitis: a case report and review of the literature. *Gastrointest Radiol*. 1991;16:133–136.
- Wiesner W, Mortele KJ, Glickman JN, et al. Cecal gangrene: a rare cause of right-sided inferior abdominal quadrant pain, fever, and leukocytosis. *Emergency Radiol*. 2002;9:292–295.
- Wiesner W, Mortele KJ, Barthi K, et al. CT findings in isolated ischemic proctosigmoiditis. *Eur Radiol*. 2002;12:1762–1767.
- Wiesner W, Mortele KJ, Glickman JN, et al. Normal colonic wall thickness and its relation to colonic distension: how thick may a normal colonic wall appear at CT? *J Comput Assist Tomogr*. 2002;26:102–106.
- Wiesner W, Mortele KJ, Glickman JN, et al. Pneumatosis intestinalis and portomesenteric venous gas in intestinal ischemia: correlation of CT findings with severity of ischemia and clinical outcome. *Am J Roentgenol*. 2001;177:1319–1323.
- Wiesner W, Mortele KJ, Glickman JN, et al. Portal venous gas unrelated to bowel ischemia. *Eur Radiol*. 2002;12:1432–1437.
- Wold PB, Fletcher JG, Johnson CD, et al. Assessment of small bowel Crohn disease: noninvasive perioral CT enterography compared with other imaging methods and endoscopy—feasibility study. *Radiology* 2003;229:275–281.

- Wolfe MM, Jenson RT. Zollinger-Ellison syndrome. *N Engl J Med*. 1987;317:1200–1209.

MISCELLANEOUS

- Ballantyne GH, Brandner MD, Beart RW, et al. Volvulus of the colon. *Ann Surg*. 1985;202:83–92.
- Boudiaf M, Soyer P, Terem C, et al. CT evaluation of small bowel obstruction. *Radiographics* 2001;21:613–624.
- Bova JC, Friedman AC, Weser E, et al. Adaptation of the ileum in nontropical sprue: reversal of the jejunoileal fold pattern. *Am J Roentgenol*. 1985;144:299–302.
- Cantisani V, Mortele KJ, Viscomi SG, et al. Rectal inflammation as first manifestation of graft-versus-host disease: radiologic-pathologic findings. *Eur Radiol*. 2003;13:75–78.
- Cundiff GW, Fenner D. Evaluation and treatment of women with rectocele: focus on associated defecatory and sexual dysfunction. *Obstet Gynecol*. 2004;104:1403–1421.
- De Backer AI, Van Overbeke LN, Mortele KJ, et al. Inflammatory pseudopolyposis in a patient with toxic megacolon due to pseudomembranous colitis. *JBR-BTR*. 2001;84:201.
- Doubleday LC, Bernardino ME. CT findings in the perirectal area following radiation therapy. *J Comp Assist Tomogr*. 1980;4:634–638.
- Fishman EK, Zinreich ES, Jones B, et al. Computed tomographic diagnosis of radiation ileitis. *Gastrointest Radiol*. 1984;9:149–152.
- Fisk JD, Shulman HM, Greening RR, et al. Gastrointestinal radiographic features of human graft-vs-host disease. *Am J Roentgenol*. 1981;136:329–336.
- Gardner EJ, Burt RW, Freston JW. Gastrointestinal polyposis: syndromes and genetic mechanisms. *West J Med*. 1980; 132:488–499.
- Gayer G, Barsuk D, Hertz M, et al. CT diagnosis of afferent loop syndrome. *Clin Radiol*. 2002;57:835–839.
- Hill LD. Incarcerated paraesophageal hernia. *Am J Surg*. 1973;126:286–291.
- Hillyard RW, El-Mandi M, Schellhammer PF. Intestinal strictures complicating preoperative radiation therapy followed by radical cystectomy. *J Urol*. 1986;136:98–101.
- Horton KM, Fishman EK. Current role of CT in imaging the stomach. *Radiographics* 2003;23:75–87.
- Iko BO, Teal JS, Siram SM, et al. Computed tomography of adult colonic intussusception: clinical and experimental studies. *Am J Roentgenol*. 1984;143:769–772.
- Jones B, Kramer SS, Saral R, et al. Gastrointestinal inflammation after bone marrow transplantation: graft-versus-host disease or opportunistic infection? *Am J Roentgenol*. 1988;150:277–281.
- Kalantari BN, Mortele KJ, Cantisani V, et al. CT features with pathologic correlation of acute gastrointestinal graft-versus-host disease after bone marrow transplantation in adults. *Am J Roentgenol*. 2003;181:1621–1625.
- Kurz R, Steinhilper U, Buck J, Laqua D, Heinkelein J. Ileocoecal intussusception of the terminal ileum caused by a carcinoid tumor. *Z Gastroenterol*. 2003;41(7):659–662.
- Leyendecker JR, Bloomfeld RS, DiSantis DJ, Waters GS, Mott R, Bechtold RE. MR enterography in the management of patients with Crohn disease. *Radiographics* 2009;29:1827–1846.
- Long FR, Kramer SS, Markowitz RI. Intestinal malrotation in children: tutorial on radiographic diagnosis in difficult cases. *Radiology* 1996;198:775–780.
- Loren I, Lasson A, Anders A, et al. Gallstone ileus demonstrated by CT. *J Comp Assist Tomogr*. 1994;18:262–265.
- Martin LC, Merkle EM, Thompson WM. Review of internal hernias: radiographic and clinical findings *Am J Roentgenol*. 2006;186:703–717.
- Moore CJ, Corl FM, Fishman EK. CT of cecal volvulus: unraveling the image. *Am J Roentgenol* 2001;177:95–98.
- Mori H, Hayashi K, Futagawa S. Vascular compromise in chronic volvulus with midgut malrotation. *Pediatr Radiol*. 1987;17:277–281.
- Mortele KJ, Govaere F, Vogelaerts D, et al. Giant Meckel diverticulum containing enteroliths: CT imaging findings. *Eur Radiol*. 2002;2:82–84.
- Odulate AS, Mortele KJ. The eligible patient: indications and contraindications. In: Lefere P, Gryspeerdt S, eds. *Virtual Colonoscopy*. Berlin: Springer-Verlag; 2006:13–22.
- Olmsted WW, Cooper PH, Madewell JE. Involvement of the gastric antrum in Menetrier's disease. *Am J Roentgenol*. 1976;126:524–529.
- Patak MA, Mortele KJ, Ros PR. Multidetector row CT of the small bowel. *Radiol Clin North Am*. 2005;43:1063–1077.
- Pickhardt PJ, Bhalia S, Balfe DM. Acquired gastrointestinal fistulas: classification, etiologies, and imaging evaluation. *Radiology* 2002;224:9–23.
- Reese DF, Hodgson JR, Dockerty MB. Giant hypertrophy of the gastric mucosa (Menetrier's disease): a correlation of the roentgenographic pathologic, and clinical findings. *Am J Roentgenol*. 1962;88:619–626.
- Rociu E, Stoker J, Zwamborn AW, et al. Endoanal MR imaging of the anal sphincter in fecal incontinence. *Radiographics* 1999;19:171–177.
- Rosen A, Korobkin M, Silverman PM, et al. Mesenteric vein thrombosis: CT identification. *Am J Roentgenol*. 1984;143:83–86.
- Rosenberg HK, Seola FT, Koch P, et al. Radiographic features of gastrointestinal graft-vs-host disease. *Radiology* 1981; 138:371–374.
- Searcy RM, Malagelada JR. Menetrier's disease and idiopathic hypertrophic gastropathy. *Ann Intern Med*. 1984;100:555–570.
- Siskind BN, Burrell MI, Pun H, et al. CT demonstration of gastrointestinal involvement in Henoch-Schonlein syndrome. *Abdom Imaging*. 1985;10:352–354.
- Skaane P, Schindler G. Computed tomography of adult ileocolic intussusception. *Gastrointest Radiol*. 1985;10:355–357.
- Styles RA, Larsen CR. CT appearance of adult intussusception. *J Comp Assist Tomogr*. 1983;7:331–333.
- Swift SE, Spencer JA. Gallstone ileus: CT findings. *Clin Radiol*. 1998;53:451–456.
- Trier JS. Celiac sprue. *N Engl J Med*. 1991;325:1709–1719.
- Vandaele P, Oliva MR, Barish MA, et al. CT colonography: the essentials. *Appl Radiol*. 2006;35:8–17.
- Zerin JM, DiPietro MA. Mesenteric vascular anatomy at CT: normal and abnormal appearances. *Radiology* 1991;179:739–742.

SPLEEN

NEOPLASMS

- Barrier A, Lacaine F, Callard P, et al. Lymphangiomatosis of the spleen and 2 accessory spleens. *Surgery* 2002;131:114–116.
- Bezzi M, Spinelli A, Pierleoni M, et al. Cystic lymphangioma of the spleen: US-CT-MRI correlation. *Eur Radiol*. 2001;11:1187–1190.
- Dachman AH, Buck JL, Krishnan J, et al. Primary non-Hodgkin's splenic lymphoma. *Clin Radiol*. 1998;53:137–142.
- Dachman AH, Ros PR, Olmsted WW, et al. Nonparasitic splenic cysts: a report of 52 cases with radiologic-pathologic correlation. *Am J Roentgenol*. 1986;147:537–542.

- Fernandez-Canton G, Capelastegui A, Merino A, et al. A typical MRI presentation of a small splenic hamartoma. *Eur Radiol*. 1999;9:883–885.
- Ferrozzi F, Bova D, Draghi F, et al. CT findings in primary vascular tumors of the spleen. *Am J Roentgenol*. 1996;166:1097–1101.
- Fishman EK, Kuhlman JE, Jones RJ. CT of lymphoma: spectrum of disease. *Radiographics* 1991;11:647–669.
- Ha HK, Kim HH, Kim BK, et al. Primary angiosarcoma of the spleen: CT and MR imaging. *Acta Radiol*. 1994;35:455–458.
- Hahn PF, Weissleder R, Stark DD, et al. MR imaging of focal splenic tumors. *Am J Roentgenol*. 1988;150:823–827.
- Karakas HM, Demir M, Ozyilmaz F, et al. Primary angiosarcoma of the spleen: in vivo and in vitro MRI findings. *Clin Imaging*. 2001;25:192–196.
- Mortele KJ, Mergo PJ, Kunnen M, et al. Tumoral pathology of the spleen. In: De Shepper AM, Vanhoenacker F, eds. *Medical Imaging of the Spleen*. 1st ed. Berlin: Springer; 2000:101–122.
- Rabushka LS, Kawashima A, Fishman EK. Imaging of the spleen: CT with supplemental MR examination. *Radiographics* 1994;14:307–332.
- Ramani M, Reinhold C, Semelka RC, et al. Splenic hemangiomas and hamartomas: MR imaging characteristics of 28 lesions. *Radiology* 1997;202:166–172.
- Rao BK, AuBuchon J, Lieberman LM, et al. Cystic lymphangiomatosis of the spleen: a radiologic-pathologic correlation. *Radiology* 1981;141:781–782.
- Ros PR, Moser RP, Dachman AH, et al. Hemangioma of the spleen: radiologic-pathologic correlation in ten cases. *Radiology* 1987;162:73–77.
- Rose SC, Kumpe DA, Manco-Johnson ML. Radiographic appearance of diffuse splenic hemangiomatosis. *Gastrointest Radiol*. 1986;11:342–345.
- Shirkoda A, Freeman J, Armin AR, et al. Imaging features of splenic epidermoid cysts with pathologic correlation. *Abdom Imaging*. 1995;20:449–451.
- Strijk SP, Wagener DJT, Bogman MJJT, et al. The spleen in Hodgkin disease: diagnostic value of CT. *Radiology* 1985;154:753–757.
- Thacker C, Korn R, Millstine J, Harvin H, Van Lier Ribbink JA, Gotway MB. Sclerosing angiomatoid nodular transformation of the spleen: CT, MRI, PET, and ^{99m}Tc-sulfur colloid SPECT CT findings with gross and histopathological correlation. *Abdom Imaging*. 2010;35:683–689.
- Urrutia M, Mergo, PJ, Ros PR, et al. Cystic masses of the spleen: radiologic-pathologic correlation. *Radiographics* 1996; 16:107–129.

INFECTION

- Callen PW, Filly RA, Marcus FS. Ultrasonography and computed tomography in the evaluation of hepatic microabscesses in the immunosuppressed patient. *Radiology* 1980;136:433–434.
- Chew FS, Smith PL, Barboriak D. Candidal splenic abscesses. *Am J Roentgenol*. 1981;156:474.
- Drevelengas A. The spleen in infectious disorders. In: De Shepper AM, Vanhoenacker F, eds. *Medical Imaging of the Spleen*. 1st ed. Berlin: Springer; 2000:67–80.
- Franquet T, Montes M, Lecumbern FJ, et al. Hydatid disease of the spleen: imaging findings in nine patients. *Am J Roentgenol*. 1990;154:525–528.
- Pierkarski J, Federle MP, Moss AA, et al. Computed tomography of the spleen. *Radiology* 1980;135:683–689.
- Shirkhoda A. CT findings in hepatosplenic and renal candidiasis. *J Comput Assist Tomogr*. 1987;11:795–798.
- Vardhanabhuti V, Venkatanarasimha N, Bhatnagar G, Maviki M, Iyengar S, Adams WM, Suresh P. Extra-pulmonary manifestations of sarcoidosis. *Clin Radiol*. 2012 Mar;67(3): 263–276. doi: 10.1016/j.crad.2011.04.018. Epub 2011, Nov 16.

TRAUMA

- Do HM, Cronan JJ. CT appearance of splenic injuries managed nonoperatively. *Am J Roentgenol*. 1991;157:757–760.
- Emery KH. Splenic emergencies. *Radiol Clin North Am*. 1997;35:831–843.
- Gavant ML, Schurr M, Flick PA, et al. Predicting clinical outcome of nonsurgical management of blunt splenic injury; using CT to reveal abnormalities of splenic vasculature. *Am J Roentgenol*. 1997;168:207–212.
- Jeffrey RB, Laing FC, Federle MP, et al. Computed tomography of splenic trauma. *Radiology* 1981;141:729–732.
- Malangoni MA, Cue JI, Fallat ME, et al. Evaluation of splenic injury by computed tomography and its impact on treatment. *Ann Surg*. 1990;211:592–599.
- Mirvis SE, Whitley NO, Gens DR. Blunt splenic trauma in adults: CT-based classification and correlation with prognosis and treatment. *Radiology* 1981;171:33–39.
- Naylor R, Coln D, Shires GT. Morbidity and mortality from injuries to the spleen. *J Trauma*. 1974;14:773–778.
- Umlas SL, Cronan JJ. Splenic trauma: can CT grading systems enable prediction of successful nonsurgical treatment? *Radiology* 1991;178:481–487.
- Wolfman NT, Bechtold RE, Scharling ES, et al. Blunt upper abdominal trauma: evaluation by CT. *Am J Roentgenol*. 1992;158:492–501.

MISCELLANEOUS

- Allen KB, Gay BB, Skandalakis JE. Wandering spleen: anatomic and radiologic considerations. *South Med J*. 1992;85:976–984.
- Balcar I, Seltzer SE, Davis S, et al. CT patterns of splenic infarction: a clinical and experimental study. *Radiology* 1984;151:723–729.
- Darling JD, Flickinger FW. Splenosis mimicking neoplasm in the perirenal space: CT characteristics. *J Comput Assist Tomogr*. 1990;14:839–841.
- Elsayes KM, Narra VM, Mukundan G, Lewis JS, Menias CO, Heiken JP. MR imaging of the spleen: spectrum of abnormalities. *Radiographics* 2005;25:967–982.
- Folz SJ, Johnson CD, Swensen SJ. Abdominal manifestations of sarcoidosis in CT studies. *J Comput Assist Tomogr*. 1995;19:573–579.
- Freeman JL, Jafri SZH, Roberts JL, et al. CT of congenital and acquired abnormalities of the spleen. *Radiographics* 1993;13:597–610.
- Gentry LR, Brown JM, Lindgren RD. Splenosis: CT demonstration of heterotopic autotransplantation of splenic tissue. *J Comput Assist Tomogr*. 1982;6:1184–1187.
- Gorden DH, Burell MI, Levin DC, et al. Wandering spleen—the radiological and clinical spectrum. *Radiology* 1977;125:39–46.
- Hoeffel C, Bokemeyer C, Hoeffel JC, et al. CT hepatic and splenic appearances with sarcoidosis. *Eur J Radiol*. 1996; 23:94–96.
- Ito K, Mitchell DG, Honjo K, et al. MR imaging of acquired abnormalities of the spleen. *Am J Roentgenol*. 1997;168:697–702.
- Jaroch MT, Broughan TA, Hermann RE. The natural history of splenic infarction. *Surgery* 1986;100:743–749.

- Kessler A, Mitchell DG, Israel HL, et al. Hepatic and splenic sarcoidosis: ultrasound and MR imaging. *Abdom Imaging*. 1993;18:159–163.
- Magid D, Fishman EK, Charache S, et al. Abdominal pain in sickle cell disease: the role of CT. *Radiology* 1987;163: 325–328.
- Magid D, Fishman EK, Seigelman SS. Computed tomography of the spleen and liver in sickle cell disease. *Am J Roentgenol*. 1984;143:245–249.
- Mortele KJ, Mortele B, Silverman SG. CT features of the accessory spleen. *Am J Roentgenol*. 2004;183: 1653–1657.
- Mortele KJ, Praet M, Van Vlierberghe H, et al. Splenic and perisplenic involvement in acute pancreatitis: determination of prevalence and morphological helical CT features. *J Comput Assist Tomogr*. 2001;25:50–54.
- Shiels WE, Johnson JF, Stephenson SR, et al. Chronic torsion of the wandering spleen. *Pediatr Radiol*. 1989;19:465–467.
- Tawfik AM, Batouty NM, Zaky MM, Eladalany MA, Elmokadem AH. Polysplenia syndrome: a review of the relationship with viscero-atrial situs and the spectrum of extra-cardiac anomalies. *Surg Radiol Anat*. 2013 Mar 19.
- Torres GM, Terry NL, Mergo PJ, et al. MR imaging of the spleen. *Magn Reson Imaging Clin North Am*. 1995;3:39–50.
- Tsuda K, Nakamura H, Murakami T, et al. Peliosis of the spleen with intraperitoneal hemorrhage. *Abdom Imaging*. 1993; 18:283–285.

MESENTERY, OMENTUM, AND PERITONEUM

- Akhan O, Pringot J. Imaging of abdominal tuberculosis. *Eur Radiol*. 2002;12:312–323.
- Bowen B, Ros PR, McCarthy MJ, et al. Gastrointestinal teratomas: CT and US appearance with pathologic correlation. *Radiology* 1987;162:431–433.
- Bui-Mansfield LT, Kim-Ahn G, O'Bryant LK. Multicystic mesothelioma of the peritoneum. *Am J Roentgenol*. 2002;178:402.
- Busch JM, Kruskal JB, Wu B. Best cases from the AFIP: malignant peritoneal mesothelioma. *Radiographics* 2002;22:1511–1515.
- Coley BD, Shiels II WE, Elton S, et al. Sonographically guided aspiration of cerebrospinal fluid pseudocysts in children and adolescents. *Am J Roentgenol*. 2004;183:1507–1510.
- Crim JR, Seeger LL, Yao L, et al. Diagnosis of soft-tissue masses with MR imaging: can benign masses be differentiated from malignant ones? *Radiology* 1992;185:581–586.
- Daskalogiannaki M, Voloudaki A, Prassopoulos P, et al. CT evaluation of mesenteric panniculitis: prevalence and associated diseases. *Am J Roentgenol*. 2000;174:427–431.
- Debatin JF, Spritzer CE, Dunnick R. Castleman disease of the adrenal gland: MRI imaging features. *Am J Roentgenol*. 1991;157:781–783.
- Dowe MF, Shanmuganathan K, Mirvis SE, et al. CT findings of mesenteric injury after blunt trauma: implications for surgical intervention. *Am J Roentgenol*. 1997;168:425–428.
- Faria SC, Iyer RB, Rashid A, et al. Desmoid tumor of the small bowel and the mesentery. *Am J Roentgenol*. 2004;183:118.
- Fisher MF, Fletcher BD, Dahms BB, et al. Abdominal lipoblastomatosis: radiographic, echographic, and computed tomographic findings. *Radiology* 1981;138:593–596.
- Fishman EK, Kuhlman JE, Schuchter LM, et al. CT of malignant melanoma in the chest, abdomen, and musculoskeletal system. *Radiographics* 1990;10:603–620.
- Fleck RM, Schade RR, Kowal CD, et al. Testicular choriocarcinoma with metastasis to gastric mucosa. *Gastrointest Endosc*. 1984;30:188–189.
- Fujita N, Noda Y, Kobayashi G, et al. Chylous cyst of the mesentery: US and CT diagnosis. *Abdom Imaging*. 1995;20:259–261.
- Garcia P, Garcia-Giannoli H, Meyran S, et al. Primary dissecting aneurysm of the hepatic artery: sonographic, CT and angiographic findings. *Am J Roentgenol*. 1996;166:1316–1318.
- Ha HK, Jung JI, Lee MS, et al. CT differentiation of tuberculous peritonitis and peritoneal carcinomatosis. *Am J Roentgenol*. 1996;167:743–748.
- Hamed RK, Buck JL, Olmsted WW, et al. Extracolonic manifestations of the familial adenomatous polyposis syndromes. *Am J Roentgenol*. 1991;156:481–485.
- Horton KM, Kamel I, Hofman L, et al. Carcinoid tumors of the small bowel: a multitechnique imaging approach. *Am J Roentgenol*. 2004;182:559–567.
- Horton KM, Lawler LP, Fishman EK. CT findings in sclerosing mesenteritis (panniculitis): spectrum of disease. *Radiographics* 2003;23:1561–1567.
- Hui GC, Amaral J, Stephens D, et al. Gas distribution in intraabdominal and pelvic abscesses on CT is associated with drainability. *Am J Roentgenol*. 2005;184:915–919.
- Huppert BJ, Farrell MA. Case 60: cavitating mesenteric lymph node syndrome. *Radiology* 2003;228:180–184.
- Koh DM, Langroudi B, Padley SPG. Abdominal CT in patients with AIDS. *Imaging* 2002;14:24–34.
- Korobkin M, Silverman PM, Quint LE, et al. CT of the extraperitoneal space: normal anatomy and fluid collections. *Am J Roentgenol*. 1992;159:933–941.
- Levy AD, Cantisani V, Miettinen M. Abdominal lymphangiomas: imaging features with pathologic correlation. *Am J Roentgenol*. 2004;182:1485–1491.
- Levy AD, Remotti HE, Thompson WM, et al. Gastrointestinal stromal tumors: radiologic features with pathologic correlation. *Radiographics* 2003;23:283–304.
- Lubner M, Menias C, Rucker C, et al. Blood in the belly: CT findings of hemoperitoneum. *Radiographics* 2007;27:109–125.
- McDermott VG, Low VH, Keogan MT, et al. Malignant melanoma metastatic to the gastrointestinal tract. *Am J Roentgenol*. 1996;166:809–813.
- McLeod AJ, Zornoza J, Shirkhoda A. Leiomyosarcoma: computed tomographic findings. *Radiology* 1984;152:133–136.
- Meador TL, McLarney JK. CT features of Castleman disease of the abdomen and pelvis. *Am J Roentgenol*. 2000;175:115–118.
- Miller FH, Keppke AL, Dalal K, et al. MRI of pancreatitis and its complications: part 1, acute pancreatitis. *Am J Roentgenol*. 2004;183:1637–1644.
- Miyake T, Hoshino S, Yoshida Y, et al. Multiple ectopic hepatocellular carcinomas arising in the abdominal cavity. *Case Rep Gastroenterol*. 2012;6(3):629–634.
- Murphey MD, Carroll JF, Flemming DJ, et al. From the archives of the AFIP: benign musculoskeletal lipomatous lesions. *Radiographics* 2004;24:1433–1466.
- Pannu HK, Bristow RE, Montz FJ, et al. Multidetector CT of peritoneal carcinomatosis from ovarian cancer. *Radiographics* 2003;23:687–701.
- Pereira JM, Madureira AJ, Vieira A, et al. Abdominal tuberculosis: imaging features. *Eur J Radiol*. 2005;55:173–180.
- Pereira JM, Sirlin CB, Pinto PS, et al. CT and MR imaging of extrahepatic fatty masses of the abdomen and pelvis: techniques,

diagnosis, differential diagnosis, and pitfalls. *Radiographics* 2005;25:69–85.
- Pernas JC, Catala J. Case 72: pseudocyst around ventriculoperitoneal shunt. *Radiology* 2004;232:239–243.
- Pickhardt PJ, Bhalla S. Primary neoplasms of peritoneal and subperitoneal origin: CT findings. *Radiographics* 2005;25:983–995.
- Ros PR, Yuschok TJ, Buck JL, et al. Peritoneal mesothelioma: radiologic appearances correlated with histology. *Acta Radiol*. 1991;32:355–358.
- Sheth S, Horton KM, Garland MR, et al. Mesenteric neoplasms: CT appearances of primary and secondary tumors and differential diagnosis. *Radiographics* 2003;23:457–473.
- Singh AK, Gervais DA, Hahn PF, Rhea J, Mueller PR. CT Appearance of acute appendagitis. *Am J Roentgenol* 2004;183:1303–1307.
- Stoupis C, Ros PR, Abbitt PL, et al. Bubbles in the belly: imaging of cystic mesenteric or omental masses. *Radiographics* 1994;14:729–737.
- Sulkin TV, O'Neill H, Amin AI, et al. CT in pseudomyxoma peritonei: a review of 17 cases. *Clin Radiol*. 2002;57:608–613.
- Suzuki S, Furui S, Kohtake H, et al. Isolated dissection of the superior mesenteric artery: CT findings in six cases. *Abdom Imaging*. 2004;29:153–157.
- van Breda Vriesman AC, Puylaert JBCM. Omental infarction: a self-limiting disease *Am J Roentgenol*. 2005;185:280–281.
- Walensky RP, Venbrux AC, Prescott CA, et al. Pseudomyxoma peritonei *Am J Roentgenol*. 1996;167:471–474.
- Wong WL, Johns TA, Herlihy WG, et al. Best cases from the AFIP: multicystic mesothelioma. *Radiographics* 2004;24:247–250.
- Yang ZG, Min PQ, Sone S, et al. Tuberculosis versus lymphoma in the abdominal lymph nodes: evaluation with contrast-enhanced CT. *Am J Roentgenol*. 1999;172:619–623.
- Yeh HC, Chahinan AP. Ultrasonography and computed tomography of peritoneal mesothelioma. *Radiology* 1980;135:705–712.

KIDNEY, URETER, AND BLADDER

NEOPLASMS

- Bosniak MA. The small (less than or equal to 3.0 cm) renal parenchymal tumor: detection, diagnosis, and controversies. *Radiology* 1991;179:307–317.
- Browne RFJ, Meehan CP, Colville J, et al. Transitional cell carcinoma of the upper urinary tract: spectrum of imaging findings. *Radiographics* 2005;25:1609–1627.
- Cardone G, D'Andrea A, Piscioli I, Scialpi M. Fat-poor angiomyolipoma and renal cell carcinoma: differentiation with MR imaging and accuracy of histopathologic evaluation. *Radiology*. 2012;265(3):979–980.
- Choyke PL, White EM, Zeman RK, et al. Renal metastases: clinicopathologic and radiologic correlation. *Radiology* 1987; 162:359–363.
- Ergen FB, Hussain HK, Caoili EM, et al. MRI for preoperative staging of renal cell carcinoma using the 1997 TNM classification: comparison with surgical and pathologic staging. *Am J Roentgenol*. 2004;182:217–225.
- Hasegawa T, Matsuno Y, Shinoda T, et al. Extrathoracic solitary fibrous tumors: their histological variability and potentially aggressive behavior. *Hum Pathol*. 1999;30:1464–1473.
- Hopkins JK, Giles HW Jr, Wyatt-Ashmead J, et al. Best cases from the AFIP: cystic nephroma. *Radiographics* 2004;24:589–593.
- Israel GM, Bosniak MA. How I do it: evaluating renal masses. *Radiology* 2005;236:441–450.
- Israel GM, Hindman N, Bosniak MA. Evaluation of cystic renal masses: comparison of CT and MR imaging by using the Bosniak classification system. *Radiology* 2004;231:365–371.
- Jinzaki M, McTavish JD, Zou KH, et al. Evaluation of small (</= 3 cm) renal masses with MDCT: benefits of thin overlapping reconstructions. *Am J Roentgenol*. 2004;183:223–228.
- Jinzaki M, Tanimoto A, Narimatsu Y, et al. Angiomyolipoma: imaging findings in lesions with minimal fat. *Radiology* 1997;205:497–502.
- Kim JK, Kim TK, Ahn HJ, et al. Differentiation of subtypes of renal cell carcinoma on helical CT scans. *Am J Roentgenol*. 2002;178:1499–1506.
- Kundra V, Silverman PM. Imaging in the diagnosis, staging, and follow-up of cancer of the urinary bladder. *Am J Roentgenol*. 2003;180:1045–1054.
- Kurl S, Rytkonen H, Farin P, et al. A primary carcinoid tumor of the kidney: a case report and review of the literature. *Abdom Imaging*. 1996;21:464–467.
- Laperriere J, Lafortune M. Case of the day. General. Oncocytoma of the right kidney. *Radiographics* 1990;10: 1105–1107.
- Liu H, Cooke K, Frager D. Bilateral massive renal angiomyolipomatosis in tuberous sclerosis. *Am J Roentgenol*. 2005;185:1085–1086.
- Logue LG, Acker RE, Sienko AE. Best cases from the AFIP: angiomyolipomas in tuberous sclerosis. *Radiographics* 2003;23:241–246.
- Lowe LH, Isuani BH, Heller RM, et al. Pediatric renal masses: Wilms tumor and beyond. *Radiographics* 2000;20:1585–1603.
- Mariscal A, Mate JL, Guasch I, et al. Cystic transformation of a fibroepithelial polyp of the renal pelvis: radiologic and pathologic findings. *Am J Roentgenol*. 1995;164:1445–1446.
- Pickhardt PJ, Lonergan GJ, Davis CJ Jr, et al. From the archives of the AFIP: infiltrative renal lesions: radiologic-pathologic correlation. *Radiographics* 2000;20:215–243.
- Rafal RB, Markisz JA. Urachal carcinoma: the role of magnetic resonance imaging. *Urol Radiol*. 1991;12:184–187.
- Remer EM, Weinberg EJ, Oto A, et al. MR imaging of the kidneys after laparoscopic cryoablation. *Am J Roentgenol*. 2000;174:635–640.
- Scatarige JC, Sheth S, Corl FM, et al. Patterns of recurrence in renal cell carcinoma: manifestations on helical CT. *Am J Roentgenol*. 2001;177:653–658.
- Sheth S, Scatarige JC, Horton KM, et al. Current concepts in the diagnosis and management of renal cell carcinoma: role of multidetector CT and three-dimensional CT. *Radiographics* 2001;21:S237–S254.
- Silverman SG, Lee BY, Seltzer SE, et al. Small (< or = 3 cm) renal masses: correlation of spiral CT features and pathologic findings. *Am J Roentgenol*. 1994;163:597–605.
- Tekes A, Kamel I, Imam K, et al. Dynamic MRI of bladder cancer: evaluation of staging accuracy. *Am J Roentgenol*. 2005;184:121–127.
- Urban BA, Fishman EK. Renal lymphoma: CT patterns with emphasis on helical CT. *Radiographics* 2000;20:197–212.
- Winalski CS, Lipman JC, Tumeh SS. Ureteral neoplasms. *Radiographics* 1990;10:271–283.
- Wong-You-Cheong JJ, Wagner BJ, Davis CJ Jr. Transitional cell carcinoma of the urinary tract: radiologic-pathologic correlation. *Radiographics* 1998;18:123–142.
- Zotalis G, Hicks DG. Solitary fibrous tumor of the soft tissues. *Arch Hellenic Pathol*. 1997;11:122–131.

INFECTION/INFLAMMATION

- Day DL, Carpenter DL. Abdominal complications in pediatric bone marrow transplant recipients. *Radiographics* 1993;13:1101–1112.
- Fan CM, Whitman GJ, Chew FS. Xanthogranulomatous pyelonephritis. *Am J Roentgenol*. 1995;165:1008.
- Kalantari BN, Mortelé KJ, Cantisani V, et al. CT features with pathologic correlation of acute gastrointestinal graft-versus-host disease after bone marrow transplantation in adults. *Am J Roentgenol*. 2003;181:1621–1625.
- Kawashima A, Sandler CM, Goldman SM, et al. CT of renal inflammatory disease. *Radiographics* 1997;17:851–866.
- Kuhlman JE, Fishman EK. CT evaluation of enterovaginal and vesicovaginal fistulas. *J Comput Assist Tomogr*. 1990;14:390–394.
- Slaughter A, Pandey T, Jambhekar K. MRI findings in chronic lithium nephropathy: a case report. *J Radiol Case Rep.* 2010;4(8):15–21.
- Soulen MC, Fishman EK, Goldman SM. Sequelae of acute renal infections: CT evaluation. *Radiology* 1989;173:423–426.
- Talner L, Vaughan M. Nonobstructive renal causes of flank pain: findings on noncontrast helical CT (CT KUB). *Abdom Imaging*. 2003;28:210–216.

CONGENITAL/DEVELOPMENTAL ANOMALIES

- Berrocal T, López-Pereira P, Arjonilla A, et al. Anomalies of the distal ureter, bladder, and urethra in children: embryologic, radiologic, and pathologic features. *Radiographics* 2002;22:1139–1164.
- Gay SB, Armistead JP, Weber ME, et al. Left infrarenal region: anatomic variants, pathologic conditions, and diagnostic pitfalls. *Radiographics* 1991;11:549–570.
- Hilpert PL, Friedman AC, Radecki PD, et al. MRI of hemorrhagic renal cysts in polycystic kidney disease. *Am J Roentgenol*. 1986;146:1167–1172.
- Lonergan GJ, Rice RR, Suarez ES. Autosomal recessive polycystic kidney disease: radiologic-pathologic correlation. *Radiographics* 2000;20:837–855.
- Oliva MR, Hsing J, Rybicki FJ, Fennessy F, Mortelé KJ, Ros PR. Glomerulocystic kidney disease: MRI findings. *Abdom Imaging*. 2003;28:889–892.
- Segal AJ, Spataro RF. Computed tomography of adult polycystic disease. *J Comput Assist Tomogr*. 1982;6:777–780.
- Yu JS, Kim KW, Lee HJ, et al. Urachal remnant diseases: spectrum of CT and US findings. *Radiographics* 2001;21:451–461.

MISCELLANEOUS

- Dyer RB, Chen MY, Zagoria RJ. Abnormal calcifications in the urinary tract. *Radiographics* 1998;18:1405–1424.
- Farres MT, Ronco P, Saadoun D, et al. Chronic lithium nephropathy: MR imaging for diagnosis. *Radiology* 2003; 229:570–574.
- Guest AR, Cohan RH, Korobkin M, et al. Assessment of the clinical utility of the rim and comet-tail signs in differentiating ureteral stones from phleboliths. *Am J Roentgenol*. 2001; 177:1285–1291.
- Hann L, Pfister RC. Renal subcapsular rim sign: new etiologies and pathogenesis. *Am J Roentgenol*. 1982;138:51–54.
- Harris AC, Zwirewich CV, Lyburn ID, et al. CT findings in blunt renal trauma. *Radiographics* 2001;21:S201–S214.
- Hodson CJ. Neuhauser lecture. Reflux nephropathy: a personal historical review. *Am J Roentgenol*. 1981;137:451–462.
- Joseph RC, Amendola MA, Artze ME, et al. Genitourinary tract gas: imaging evaluation. *Radiographics* 1996;16:295–308.
- Katz DS, Lane MJ, Sommer FG. Unenhanced helical CT of ureteral stones: incidence of associated urinary tract findings. *Am J Roentgenol*. 1996;166:1319–1322.
- Kawashima A, Sandler CM, Ernst RD, et al. CT evaluation of renovascular disease. *Radiographics* 2000;20:1321–1340.
- Lawler LP, Jarret TW, Corl FM, et al. Adult ureteropelvic junction obstruction: insights with three-dimensional multi–detector row CT. *Radiographics* 2005;25:121–134.
- Oliva MRB, Hsing J, Rybicki FJ, et al. Glomerulocystic kidney disease: MRI findings. *Abdom Imaging*. 2003;28:889–892.
- Rathaus V, Konen O, Werner M, et al. Pyelocalyceal diverticulum: the imaging spectrum with emphasis on the ultrasound features. *Br J Radiol*. 2001;74:595–601.
- Sallomi DF, Yaqoob M, White E, et al. Case report: the diagnostic value of contrast-enhanced computed tomography in acute bilateral renal cortical necrosis. *Clin Radiol*. 1995; 50:126–127.
- Sebastià C, Quiroga S, Boyé R, et al. Helical CT in renal transplantation: normal findings and early and late complications. *Radiographics* 2001;21:1103–1117.
- Vaccaro JP, Brody JM. CT cystography in the evaluation of major bladder trauma. *Radiographics* 2000;20:1373–1381.

PELVIS

NEOPLASMS

- Akbar SA, Sayyed TA, Jafri SZH, et al. Multimodality imaging of paratesticular neoplasms and their rare mimics. *Radiographics* 2003;23:1461–1476.
- Ascher SM, Jha RC, Reinhold C. Benign myometrial conditions: leiomyomas and adenomyosis. *Top Magn Reson Imaging*. 2003;14:281–304.
- Baeyens K, Fennessy F, Bleday R, et al. CT features of a tubal lipoma associated with an ipsilateral dermoid cyst. *Eur Radiol*. 2004;14:1720–1722.
- Baloglu H, Turken O, Levent T, et al. 24-year-old female with amenorrhea: bilateral primary ovarian Burkitt lymphoma. *Gynecol Oncol*. 2003;91:449–451.
- Bostwick DG, Grignon DJ, Hammond EL, et al. Prognostic factors in prostate cancer. *Arc Pathol Lab Med.* 2000; 124:995–1000.
- Bozaci EA, Atabekoglu C, Sertçelik A, et al. Metachronous metastases from renal cell carcinoma to uterine cervix and vagina: case report and review of literature. *Gynecol Oncol*. 2005;99:232–235.
- Cantisani V, Mortele KJ, Kalantari BN, et al. Vaginal metastasis from uterine leiomyosarcoma: magnetic resonance imaging features with pathological correlation. *J Comput Assist Tomogr*. 2003;27:805–809.
- Cornud F, Hamida K, Flam T, et al. Endorectal color Doppler sonography and endorectal MR imaging features of nonpalpable prostate cancer. *Am J Roentgenol.* 2000;175:1161–1168.
- Coumbaras M, Validire P, Strauss C, et al. Uterine lipoma: MRI features with pathologic correlation. *Abdom Imaging*. 2005;30:239–241.
- Covens A, Rosen B, Murphy J, et al. Changes in the demographics and perioperative care of stage IA-B cervical cancer over the past 16 years. *Gynecol Oncol.* 2001;81:133–137.
- Creasman WT. Vaginal cancers. *Curr Opin Obstet Gynecol*. 2005;17:71–76.
- D'Amico AV, Whittington R, Malkowicz SB, et al. Clinical utility of the percentage of positive prostate biopsies in defining biochemical outcome after radical prostatectomy for

patients with clinically localized prostate cancer. *J Clin Oncol.* 2000;18:1164–1172.
- Daya D, Young RH. Florid deep glands of the uterine cervix: another mimic of adenoma malignum. *Am J Clin Pathol.* 1995;103:614–617.
- DeSimone CP, Lele SM, Modesitt SC. Malignant struma ovarii: a case report and analysis of cases reported in the literature with focus on survival and I^{131} therapy. *Gynecol Oncol.* 2003;89: 543–548.
- Freedland SJ, Aronson WJ, Csathy GS, et al. Comparison of percentage of total prostate needle biopsy tissue with cancer to percentage of cores with cancer for predicting PSA recurrence after radical prostatectomy: results from the SEARCH database. *Urology* 2003;61:742–747.
- Grasel RP, Outwater EK, Siegelman ES, et al. Endometrial polyps: MR imaging features and distinction from endometrial carcinoma. *Radiology* 2000;214:47–52.
- Ha HK, Baek SY, Kim SH, et al. Krukenberg's tumor of the ovary: MR imaging features. *Am J Roentgenol.* 1995;164:1435–1439.
- Hoeks CMA, Barentsz JO, Hambrock T, et al. Prostate cancer: multiparametric MR imaging for detection, localization and staging. *Radiology* 2011;261(1):46–66.
- Jung SE, Lee JM, Rha SE, et al. CT and MR imaging of ovarian tumors with emphasis on differential diagnosis. *Radiographics* 2002;22:1305–1325.
- Kattan MW, Eastham JA, Stapleton AMF, et al. A preoperative nomogram for disease recurrence following radical prostatectomy for prostate cancer. *J Nal Cancer Inst.* 1998;10:766–771.
- Lau LU, Thoeni RF. Uterine lipoma: advantage of MRI over ultrasound. *Br J Radiol.* 2005;78:72–74.
- Li H, Sugimura K, Okizuka H, et al. Markedly high-signal intensity lesions in the uterine cervix on T2-weighted imaging: differentiation between mucin-producing carcinomas and Nabothian cysts. *Radiat Med.* 1999;17:137–143.
- Lilly MC, Arregui ME. Lipomas of the cord and round ligament. *Ann Surg.* 2002;4:586–590.
- Makani S, Kim W, Gaba AR. Struma ovarii with a focus of papillary thyroid cancer: a case report and review of the literature. *Gynecol Oncol.* 2004;94:835–839.
- Manfredi R, Mirk P, Maresca G, et al. Local-regional staging of endometrial carcinoma: role of MR imaging in surgical planning. *Radiology* 2004;231:372–378.
- Mayr NA, Yuh WT, Zheng J, et al. Prediction of tumor control in patients with cervical cancer: analysis of combined volume and dynamic enhancement pattern by MR imaging. *Am J Roentgenol.* 1998;170:177–182.
- Mercer SE, Ewton DZ, Shah S, et al. Mirk/Dyrk1b mediates cell survival in rhabdomyosarcomas. *Cancer Res.* 2006;66: 5143–5150.
- Mittl RL, Yeh I, Kressel HY. High-signal-intensity rim surrounding uterine leiomyomas on MR imaging: pathologic correlation. *Radiology* 1991;180:81–83.
- Murase E, Siegelman ES, Outwater EK, et al. Uterine leiomyomas: histopathologic features, MR imaging findings, differential diagnosis, and treatment. *Radiographics* 1999;19:1179–1197.
- Neary B, Young SB, Reuter KL, et al. Ovarian Burkitt lymphoma: pelvic pain in woman with AIDS. *Obstet Gynecol.* 1996;88:706–708.
- Outwater EK, Wagner BJ, Mannion C, et al. Sex cord stromal and steroid cell tumors of the ovary. *Radiographics* 1998;18:1523–1546.
- Parazzini F, Vecchia CL, Negri E, et al. Risk factors for uterine fibroids: reduced risk associated with oral contraceptives. *Br Med J.* 1988;72:853–857.
- Pellerito JS, McCarthy SM, Doyle MB, et al. Diagnosis of uterine anomalies: Relative accuracy of MR imaging, endovaginal ultrasound, and hysterosalpingography. *Radiology* 1992;183:795–800.
- Perlman S, Ben-Arie A, Feldberg E, et al. Non-Hodgkin's lymphoma presenting as advanced ovarian cancer—a case report and review of literature. *Int J Gynecol Cancer.* 2005;15:554–557.
- Propst AM, Hill JA. Anatomic factors associated with recurrent pregnancy loss. *Semin Reprod Med.* 2000;18:341–350.
- Rha SE, Byun JY, Jung SE, et al. Atypical CT and MRI manifestations of mature ovarian cystic teratomas. *Am J Roentgenol.* 2004;183:743–750.
- Shadbolt CL, Coakley FV, Qayym A, et al. MRI of vaginal leiomyomas. *J Comput Assist Tomogr.* 2001;25:355–357.
- Singh AK, Saokar A, Hahn PF, et al. Imaging of penile neoplasms. *Radiographics* 2005;25:1629–1638.
- Stevens SK, Hricak H, Campos Z. Teratomas versus cystic hemorrhagic adnexal lesions: differentiation with proton-selective fat-saturation MR imaging. *Radiology* 1993;186: 481–488.
- Stevens SK, Hricak H, Stern JL. Ovarian lesions: detection and characterization with gadolinium-enhanced MR imaging at 1.5T. *Radiology* 1991;181:481–488.
- Stewart ST, McCarthy SM. Case 77: aggressive angiomyxoma. *Radiology* 2004;233:697–700.
- Szklaruk J, Tamm EP, Choi H, et al. MR imaging of common and uncommon large pelvic masses. *Radiographics* 2003;23:403–424.
- Troiano RN, Lazzarini KM, Scoutt LM, et al. Fibroma and fibrothecoma of the ovary: MR findings. *Radiology* 1997;204:795–798.
- Ueda H, Togashi K, Ikuo K, et al. Unusual appearances of uterine leiomyomas: MR imaging findings and their histopathologic backgrounds. *Radiographics* 1999;19:S131–S145.
- Vargas HA, Barrett T, Sala E.J Magn Reson Imaging. MRI of ovarian masses. 2013;37(2):265–281.
- Yamashita Y, Torashima M, Takahashi M. Hyperintense uterine leiomyoma at T2- weighted MR imaging: differentiation with dynamic enhanced MR imaging and clinical implications. *Radiology* 1993;189:721–725.

CONGENITAL

- Candiani GB, Federle L, Zamberletti D, et al. Endometrial patterns in malformed uteri. *Acta Europ Fertil.* 1983;14:311–318.
- Carrington BM, Hricak H, Nuruddin RN, et al. Mullerian duct anomalies: MR imaging evaluation. *Radiology* 1990;176: 715–720.
- Fedele L, Bianchi S, Marchini M, et al. Residual uterine septum less than 1 cm after hysteroscopic metroplasty does not impair reproductive outcome. *Hum Reprod.* 1996;11:727–729.
- Fedele L, Dorta M, Brioschi D, et al. Magnetic resonance evaluation of double uteri. *Obstet Gynecol.* 1989;74:844–847.
- Homer HA, Li TC, Cooke ID. The septate uterus: a review of management and reproductive outcome. *Fertil Steril.* 2000; 73:1–14.
- Kupesic S, Kurjak A. Septate uterus: detection and prediction of obstetrical complications by different forms of ultrasonography. *J Ultrasound Med.* 1998;17:631–636.
- Raziel A, Arieli S, Bukovsky I, et al. Investigation of the uterine cavity in recurrent aborters. *Fertil Steril.* 1994;62:1080–1082.

MISCELLANEOUS

- Ananth CV, Smulian JC, Vintzileos AM. The association of placenta previa with history of cesarean delivery and abortion: a metaanalysis. *Am J Obstet Gynecol*. 1997;177:1071–1078.
- Bohyun K, Hricak H, Tanagho EA. Diagnosis of urethral diverticula in women: value of MR imaging. *Am J Roentgenol*. 1993;161:809–815.
- Dannecker C, Lienemann A, Fischer T, et al. Influence of spontaneous and instrumental vaginal delivery on objective measures of pelvic organ support: assessment with the pelvic organ prolapse quantification (POPQ) technique and functional cine magnetic resonance imaging. *Eur J Obstet Gyn Rep Biol*. 2004;104:32–38.
- Finberg HJ, Williams JW. Placenta accreta: prospective sonographic diagnosis in patients with placenta previa and prior cesarean section. *J Ultrasound Med*. 1992;11:333–343.
- Hann LE, Giess CS, Bach AM, et al. Endometrial thickness in tamoxifen-treated patients: correlation with clinical and pathologic findings. *Am J Roentgenol.* 1997;168:657–661.
- Hricak H, Alpers C, Crooks LE, et al. Magnetic resonance of the female pelvis: initial experience. *Am J Roentgenol.* 1983;141:1119–1128.
- Kido A, Nishiura M, Togashi K, et al. A semiautomated technique for evaluation of uterine peristalsis. *J Magn Reson Imaging*. 2005;21:249–257.
- Kido A, Togashi A, Nakai A, et al. Oral contraceptives and uterine peristalsis: evaluation with MRI. *J Magn Reson Imaging*. 2005;22:265–270.
- Kido A, Togashi K, Koyama T, et al. Diffusely enlarged uterus: evaluation with MRI. *Radiographics* 2003;23:1423–1439.
- Kido A, Togashi K, Koyama T, et al. Retained products of conception masquerading as acquired arteriovenous malformation. *J Comput Assist Tomogr*. 2003;27:88–92.
- Kuligowska E, Deeds L III, Lu K III. Pelvic pain: overlooked and underdiagnosed gynecologic conditions. *Radiographics* 2005;25:3–20.
- Lauria MR, Smith RS, Treadwell MC, et al. The use of second-trimester transvaginal sonography to predict placenta previa. *Ultrasound Obstet Gynecol*. 1996;8:337–340.
- Levine D, Hulka CA, Ludmir J, et al. Placenta accreta: evaluation with color Doppler, power Doppler and fast MR imaging. *Radiology* 1997;205:773–776.
- Lopez C, Balogun M, Ganesan R, et al. MRI of vaginal conditions: pictorial review. *Clin Radiol*. 2005;60:648–662.
- Mitchell DG. Chemical shift magnetic resonance imaging: applications in the abdomen and pelvis. *Top Magn Reson Imaging*. 1992;4:46–63.
- Nagayama M, Watanabe Y, Okumura A, et al. Fast MR imaging in obstetrics. *Radiographics* 2002;22:563–582.
- Noonan JB, Coackley FV, Qayyum A, et al. MR imaging of retained products of conception. *Am J Roentgenol.* 2003;181:435–439.
- Outwater EK, Siegelman ES, Chiowanich P, et al. Dilated fallopian tubes: MR imaging characteristics. *Radiology* 1998;208:436–439.
- Outwater EK, Siegelman ES, Van Deerlin V. Adenomyosis: current concepts and imaging considerations. *Am J Roentgenol.* 1998;170:437–441.
- Pannu HK, Kaufman HS, Cundiff GW, et al. Dynamic MR imaging of pelvic organ prolapse: spectrum of abnormalities. *Radiographics* 2000;20:1567–1582.
- Rajan DK, Scharer KA. Radiology of Fournier's gangrene. *Am J Roentgenol*. 1998;170:163–168.
- Rha SE, Byun JY, Jung SE, et al. CT and MR imaging features of adnexal torsion. *Radiographics* 2002;22:283–294.
- Rozenblit AM, Ricci ZJ, Tuvia J, et al. Incompetent and dilated ovarian veins: a common CT finding in asymptomatic parous women. *Am J Roentgenol*. 2001;176:119–122.
- Saxena AK, Castellani C, Ruttenstock EM, Höllwarth ME. Testicular torsion: a 15-year single-centre clinical and histological analysis. *Acta Paediatr*. 2012;101(7):e282–6.
- Scoutt LM, McCauley TR, Flynn SD, et al. Zonal anatomy of the cervix: correlation of MR imaging and histological examination of hysterectomy specimens. *Radiology* 1993;186:159–162.
- Siegelman ES, Outwater EK. Tissue characterization in the female pelvis by means of MR imaging. *Radiology* 1999; 212:5–18.
- Siegelman ES, Outwater EK, Wang T, et al. Solid pelvic masses caused by endometriosis: MR features. *Am J Roentgenol.* 1994;163:357–361.
- Taipale P, Tarjanne H, Ylostalo P. Transvaginal sonography in suspected pelvic inflammatory disease. *Ultrasound Obstet Gynecol* 1995;6:430–434.
- Togashi K, Kawakami S, Kimura I, et al. Uterine contractions: possible diagnostic pitfall at MR imaging. *J Magn Reson Imaging*. 1993;3:889–893.
- Twickler DM, Setiawan AT, Evans RS, et al. Imaging of puerperal septic thrombophlebitis: prospective comparison of MR imaging, CT, and sonography. *Am J Roentgenol.* 1997;169:1039–1043.
- Yigit H, Tuncbilek I, Fitoz S, et al. Cyst of the canal of Nuck with demonstration of proximal canal. *J Ultrasound Med.* 2006;25:123–125.

RETROPERITONEUM AND ADRENAL GLANDS

NEOPLASMS

- Agrons GA, Lonergan GJ, Dickey GE, et al. From the archives of the AFIP: adrenocortical neoplasms in children: radiologic-pathologic correlation. *Radiographics* 1999;19:989–1008.
- Alfuhaid TR, Khalili K, Kirpalani A, et al. Neoplasms of the inferior vena cava—pictorial essay. *Can Assoc Radiol J*. 2005;56:140–147.
- Apter S, Avigdor A, Gayer G, et al. Calcification in lymphoma occurring before therapy: CT features and clinical correlation. *Am J Roentgenol*. 2002;178:935–938.
- Beaman FD, Kransdorf MJ, Menke DM. Schwannoma: radiologic-pathologic correlation. *Radiographics* 2004;24: 1477–1481.
- Caoili EM, Korobkin M, Francis IR, et al. Adrenal masses: characterization with combined unenhanced and delayed enhanced CT. *Radiology* 2002;222:629–633.
- Cyran KM, Kenney PJ, Memel DS, et al. Adrenal myelolipoma. *Am J Roentgenol*. 1996;166:395–400.
- Dunnick NR, Korobkin M. Imaging of adrenal incidentalomas: current status. *Am J Roentgenol*. 2002;179:559–568.
- Elsayes KM, Mukundan G, Narra VR, et al. Adrenal masses: MR imaging features with pathologic correlation. *Radiographics* 2004;24:S73–S86.
- Elsayes KM, Narra VR, Leyendecker JR, et al. MRI of adrenal and extraadrenal pheochromocytoma. *Am J Roentgenol.* 2005;184:860–867.
- Faria SC, Iyer RB, Rashid A, et al. Desmoid tumor of the small bowel and the mesentery. *Am J Roentgenol*. 2004;183:118.
- Getachew MM, Whitman GJ, Chew FS. Retroperitoneal schwannoma. *Am J Roentgenol.* 1994;163:1356.

- Guermazi A, Feger C, Rousselot P, et al. Granulocytic sarcoma (chloroma): imaging findings in adults and children. *Am J Roentgenol*. 2002;178:319–325.
- Hartman DS, Hayes WS, Choyke PL, et al. From the archives of the AFIP. Leiomyosarcoma of the retroperitoneum and inferior vena cava: radiologic-pathologic correlation. *Radiographics* 1992;12:1203–1220.
- Hrehorovich PA, Franke HR, Maximin S, et al. Malignant peripheral nerve sheath tumor. *Radiographics* 2003;23:790–794.
- Israel GM, Bosniak MA, Slywotzky CM, et al. CT differentiation of large exophytic renal angiomyolipomas and perirenal liposarcomas. *Am J Roentgenol*. 2002;179:769–773.
- Israel GM, Korobkin M, Wang C, et al. Comparison of unenhanced CT and chemical shift MRI in evaluating lipid-rich adrenal adenomas. *Am J Roentgenol*. 2004;183:215–219.
- Jee WH, Oh SN, McCauley T, et al. Extraaxial neurofibromas versus neurilemmomas: discrimination with MRI. *Am J Roentgenol*. 2004;183:629–633.
- Korobkin M. CT characterization of adrenal masses: the time has come. *Radiology* 2000;217:629–632.
- Lane RH, Stephens DH, Reiman HM. Primary retroperitoneal neoplasms: CT findings in 90 cases with clinical and pathologic correlation. *Am J Roentgenol*. 1989;152:83–89.
- Lonergan GJ, Schwab CM, Suarez ES, et al. From the archives of the AFIP: neuroblastoma, ganglioneuroblastoma, and ganglioneuroma: radiologic-pathologic correlation. *Radiographics* 2002;22:911–934.
- Meyer JS, Harty MP, Mahboubi S, et al. Langerhans cell histiocytosis: presentation and evolution of radiologic findings with clinical correlation. *Radiographics* 1995;15:1135–1146.
- Mortelé K, Lemmerling M, Defreyne L, et al. Ossified retroperitoneal malignant schwannoma with spinal leptomeningeal metastases. *Neuroradiology* 1998;40:48–50.
- Mourad K, Katz D, Paradinas FJ. Extravisceral diffuse infiltration of adult histiocytosis X demonstrated by CT. *Br J Radiol.* 1983;56:879–881.
- Murphey MD, Arcara LK, Fanburg-Smith J. From the archives of the AFIP: imaging of musculoskeletal liposarcoma with radiologic-pathologic correlation. *Radiographics* 2005; 25:1371–1395.
- Murphey MD, Smith WS, Smith SE, et al. From the archives of the AFIP: imaging of musculoskeletal neurogenic tumors: radiologic-pathologic correlation. *Radiographics* 1999; 19:1253–1280.
- Pomeranz SJ, Hawkins HH, Towbin R, et al. Granulocytic sarcoma (chloroma): CT manifestations. *Radiology* 1985;155:167–170.
- Radin R, David CL, Goldfarb H, et al. Adrenal and extra-adrenal retroperitoneal ganglioneuroma: imaging findings in 13 adults. *Radiology* 1997;202:703–707.
- Saurborn DS, Kruskal JB, Stillman IE, et al. Best cases from the AFIP: paraganglioma of the organs of Zuckerkandl. *Radiographics* 2003;23:1279–1286.
- Scatarige JC, Fishman EK, Kuhajda FP, et al. Low attenuation nodal metastases in testicular carcinoma. *J Comput Assist Tomogr*. 1982;7:682–687.
- Siegelman SS. Taking the X out of histiocytosis X. *Radiology* 1997;204:322–324.
- Smets A, Mortelé K, De Wever N, et al. Coexistence of an adrenocortical carcinoma with an abdominal ganglioneuroma in a child. *Pediatr Radiol*. 1998;28:329–331.
- Urban BA, Fishman EK. Renal lymphoma: CT patterns with emphasis on helical CT. *Radiographics* 2000;20:197–212.
- Westphalen A, Yeh B, Qayyum A, et al. Differential diagnosis of perinephric masses on CT and MRI. *Am J Roentgenol*. 2004;183:1697–1702.
- Yang DA, Jung DH, Kim H, et al. Retroperitoneal cystic masses: CT, clinical, and pathologic findings and literature review. *Radiographics* 2004;24:1353–1365.
- Yang ZG, Min PQ, Sone S, et al. Tuberculosis versus lymphoma in the abdominal lymph nodes: evaluation with contrast-enhanced CT. *Am J Roentgenol*. 1999;172:619–623.

INFECTION/INFLAMMATION

- Amis ES Jr. Retroperitoneal fibrosis. *Am J Roentgenol*. 1991;157:321–329.
- Arrive L, Correas JM, Leseche G, et al. Inflammatory aneurysms of the abdominal aorta: CT findings. *Am J Roentgenol*. 1995;165:1481–1484.
- De Backer AI, Mortelé KJ, Deeren D, et al. Abdominal tuberculous lymphadenopathy: MRI features. *Eur Radiol*. 2005;15:2104–2109.
- De Backer AI, Mortelé KJ, Vanhoenacker FM, et al. Imaging of extraspinal musculoskeletal tuberculosis. *Eur J Radiol*. 2006;57:119–130.
- De Backer AI, Mortelé KJ, Vanschoubroeck IJ, et al. Tuberculosis of the spine: CT and MR imaging features. *JBR-BTR*. 2005;88:92–97.
- Macedo TA, Stanson AW, Oderich GS, et al. Infected aortic aneurysms: imaging findings. *Radiology* 2004;231:250–257.

CONGENITAL/DEVELOPMENTAL ANOMALIES

- Bass JC, Korobkin M, Francis IR, et al. Retroperitoneal plexiform neurofibromas: CT findings. *Am J Roentgenol*. 1994;163:617–620.
- Bass JE, Redwine MD, Kramer LA, et al. Spectrum of congenital anomalies of the inferior vena cava: cross-sectional imaging findings. *Radiographics* 2000;20:639–652.
- Dahan H, Arrivé L, Wendum D, et al. Retrorectal developmental cysts in adults: clinical and radiologic-histopathologic review, differential diagnosis, and treatment. *Radiographics* 2001;21:575–584.
- Fortman BJ, Kuszyk BS, Urban BA, et al. Neurofibromatosis type 1: a diagnostic mimicker at CT. *Radiographics* 2001;21:601–612.

MISCELLANEOUS

- Bechtold RE, Dyer RB, Zagoria RJ, et al. The perirenal space: relationship of pathologic processes to normal retroperitoneal anatomy. *Radiographics* 1996;16:841–854.
- Cirillo RL Jr, Bennett WF, Vitellas KM, et al. Pathology of the adrenal gland: imaging features. *Am J Roentgenol*. 1998;170:429–435.
- Delfaut EM, Beltran J, Johnson G, et al. Fat suppression in MR imaging: techniques and pitfalls. *Radiographics* 1999; 19:373–382.
- Doppman JL, Miller DL, Dwyer AJ, et al. Macronodular adrenal hyperplasia in Cushing disease. *Radiology* 1988;166:347–352.
- Dorfman RE, Alpern MB, Gross BH, et al. Upper abdominal lymph nodes: criteria for normal size determined with CT. *Radiology* 1991;180:319–322.
- Einstein DM, Singer, AA, Chilcote, WA, et al. Abdominal lymphadenopathy: spectrum of CT findings. *Radiographics* 1991;11:457–472.
- Garg K, Mao J. Deep venous thrombosis: spectrum of findings and pitfalls in interpretation on CT venography. *Am J Roentgenol*. 2001;177:319–323.

- Gore RM, Balfe DM, Aizenstein RI, et al. The great escape: interfascial decompression planes of the retroperitoneum. *Am J Roentgenol*. 2000;175:363–370.
- Kawashima A, Sandler CM, Ernst RD, et al. CT evaluation of renovascular disease. *Radiographics* 2000;20:1321–1340.
- Kawashima A, Sandler CM, Fishman EK, et al. Spectrum of CT findings in nonmalignant disease of the adrenal gland. *Radiographics* 1998;18:393–412.
- Krebs TL, Wagner BJ. MR imaging of the adrenal gland: radiologic-pathologic correlation. *Radiographics* 1998; 18:1425–1440.
- Mesurolle B, Sayag E, Meingan P, et al. Retroperitoneal extramedullary hematopoiesis: sonographic, CT, and MR imaging appearance. *Am J Roentgenol*. 1996;167:1139–1140.
- O'Hara SM, Donnelly LF. Intense contrast enhancement of the adrenal glands: another abdominal CT finding associated with hypoperfusion complex in children. *Am J Roentgenol*. 1999;173:995–997.
- Premkumar A, Chow CK, Choyke PL, et al. Stress-induced adrenal hyperplasia simulating metastatic disease: CT and MR findings. *Am J Roentgenol*. 1992;159:675–676.
- Siegel CL, Cohan RH. CT of abdominal aortic aneurysms. *Am J Roentgenol*. 1994;163:17–29.
- Siegel CL, Cohan RH, Korobkin M, et al. Abdominal aortic aneurysm morphology: CT features in patients with ruptured and nonruptured aneurysms. *Am J Roentgenol*. 1994;163:1123–1129.
- Spritzer CE. Progress in MR imaging of the venous system. *Perspect Vasc Surg Endovasc Ther*. 2009;21(2):105–16.
- Torres GM, Cernigliaro JG, Abbitt PL, et al. Iliopsoas compartment: normal anatomy and pathologic processes. *Radiographics* 1995;15:1285–1297.
- Yamauchi T, Furui S, Katoh R, et al. Acute thrombosis of the inferior vena cava: treatment with saline-jet aspiration thrombectomy catheter. *Am J Roentgenol*. 1993;161: 405–407.

ABDOMINAL WALL

NEOPLASMS

- Dunnick NR, Shaner EG, Doppman JL. Detection of subcutaneous metastasis by computed tomography. *J Comput Assist Tomogr*. 1978;2:275–279.
- Krathen RA, Orengo IF, Rosen T. Cutaneous metastasis: a meta-analysis of data. *South Med J*. 2003;96:164–167.
- Murphey MD, Carroll JF, Flemming DJ, et al. From the archives of the AFIP: benign musculoskeletal lipomatous lesions. *Radiographics* 2004;24:1433–1466.
- Patten RM, Shuman WP, Teefey S. Subcutaneous metastases from malignant melanoma: prevalence and findings on CT. *Am J Roentgenol*. 1989;152:1009–1012.
- Spencer PS, Helm TN. Skin metastases in cancer patients. *Cutis* 1987;39:119–121.

INFECTION/INFLAMMATION

- Blane CE, White SJ, Braunstein EM, et al. Patterns of calcification in childhood dermatomyositis. *Am J Roentgenol*. 1984;142:397–400.
- Chan LP, Gee R, Keogh C, et al. Imaging features of fat necrosis. *Am J Roentgenol*. 2003;181:955–959.
- Gastrointestinal Case of the day. Acute nontraumatic rhabdomyolysis. *Am J Roentgenol*. 1994;162:1451.
- Hui GC, Amaral J, Stephens D, et al. Gas distribution in intraabdominal and pelvic abscesses on CT is associated with drainability. *Am J Roentgenol*. 2005;184:915–919.
- Johnston C, Keogan MT. Imaging features of soft-tissue infections and other complications in drug users after direct subcutaneous injection ("skin popping"). *Am J Roentgenol*. 2004;182:1195–1202.
- Malzberg MS, Rogg JM, Tate CA, et al. Poliomyelitis: hyperintensity of the anterior horn cells on MR images of the spinal cord. *Am J Roentgenol*. 1993;161:863–865.
- Russ PD, Dillingham M. Demonstration of CT hyperdensity in patients with acute renal failure associated with rhabdomyolysis. *J Comput Assist Tomogr*. 1991;15:458–463.

CONGENITAL/DEVELOPMENTAL ANOMALIES

- Das Narla L, Doherty RD, Hingsbergen EA, et al. Pediatric Case of the day. Prune-belly syndrome (Eagle-Barrett syndrome, triad syndrome). *Radiographics* 1998;18:1318–1322.
- Fortman BJ, Kuszyk BS, Urban BA, et al. Neurofibromatosis type 1: a diagnostic mimicker at CT. *Radiographics* 2001;21:601–612.
- Levy AD, Patel N, Dow N, et al. From the archives of the AFIP: abdominal neoplasms in patients with neurofibromatosis type 1: radiologic-pathologic correlation. *Radiographics* 2005;25:455–480.

MISCELLANEOUS

- Aguirre DA, Casola G, Sirlin C. Abdominal wall hernias: MDCT findings. *Am J Roentgenol*. 2004;183:681–690.
- Aguirre DA, Santosa AC, Casola G, et al. Abdominal wall hernias: imaging features, complications, and diagnostic pitfalls at multi–detector row CT. *Radiographics* 2005;25:1501–1520.
- Breen DJ, Rutherford EE, Stedman B, et al. Intrahepatic arterioportal shunting and anomalous venous drainage: understanding the CT features in the liver. *Eur Radiol*. 2004;14:2249–2260.
- Burkhardt JH, Arshanskiy Y, Munson JL, Scholz FJ. Diagnosis of inguinal region hernias with axial CT: the lateral crescent sign and other key findings. *Radiographics* 2011;31(2):E1–E12.
- Faro SH, Racette CD, Lally JF, et al. Traumatic lumbar hernia: CT diagnosis. *Am J Roentgenol*. 1990;154:757–759.
- Goeser CD, McLeary MS, Young LW. Diagnostic imaging of ventriculoperitoneal shunt malfunctions and complications. *Radiographics* 1998;18:635–651.
- Goodman P, Raval B. CT of the abdominal wall. *Am J Roentgenol*. 1990;154:1207–1211.
- Hadar H, Gadoth N, Heifetz M. Fatty replacement of lower paraspinal muscles: normal and neuromuscular disorders. *Am J Roentgenol*. 1983;141:895–898.
- Herbener TE, Basile V, Nakamoto D, et al. Abdominal Case of the day. Focal liver enhancement on contrast-enhanced CT scan caused by obstruction of the superior vena cava (SVC). *Am J Roentgenol*. 1997;169:250–254.
- Hickey NA, Ryan MF, Hamilton PA, et al. Computed tomography of traumatic abdominal wall hernia and associated deceleration injuries. *Can Assoc Radiol J*. 2002;53:153–159.
- Khati NJ, Enquist EG, Javitt MC. Imaging of the umbilicus and periumbilical region. *Radiographics* 1998;18:413–431.
- Lassandro F, Iasiello F, Pizza NL, et al. Abdominal hernias: Radiological features. *World J Gastrointest Endosc*. 2011;3(6): 110–7.
- Miller PA, Mezwa DG, Feczko PJ, et al. Imaging of abdominal hernias. *Radiographics* 1995;15:333–347.